12-2014

ESTIMATING FIELD AT-REST LATERAL STRESS COEFFICIENT AND LIQUEFACTION RESISTANCE OF AGED SANDS

MD Hossian
Clemson University, mhossai@g.clemson.edu

ESTIMATING FIELD AT-REST LATERAL STRESS COEFFICIENT AND LIQUEFACTION RESISTANCE OF AGED SANDS

A Dissertation
Presented to
the Graduate School of
Clemson University

In Partial Fulfillment
of the Requirements for the Degree
Doctor of Philosophy
Civil Engineering

---

by
Md Akhter Hossain
December 2014

Accepted by:
Dr. Ronald D. Andrus, Committee Chair
Dr. C. Hsein Juang
Dr. Nadarajah Ravichandran
Dr. WeiChiang Pang

ABSTRACT

Published results of laboratory tests to evaluate the influence of the at-rest lateral stress coefficient (K_0) and the overconsoildation ratio (*OCR*) on liquefaction resistance of sands are reviewed in this dissertation. It is found that significant increase in liquefaction resistance can occur with high K_0 and/or high *OCR*. A unique relationship between liquefaction resistance of isotropic and anisotropic normally consolidated sands exists based on the published laboratory data. Relationships between liquefaction resistance of overconsolidated sands and normally consolidated sands also have been shown in previous laboratory studies. Based on the previous studies, expressions for K_0 and *OCR* correction factors (K_{K0} and K_{OCR}, respectively) are recommended.

Methods of estimating in situ K_0 in sands are reviewed. An improved relationship for estimating K_0 is derived based on results of dilatometer tests (DMT), cone penetration tests (CPT) and *OCR* using published calibration chamber test data. Values of K_0 estimated from DMT-CPT-*OCR* in natural and man-made sand deposits are compiled and compared with values of K_0 calculated from self-boring pressuremeter test (SBPMT) results. Estimates of K_0 based on both DMT-CPT-*OCR* and SBPMT increased at about 4 to 5% per log cycle of time based on the geologic age of the sand deposits.

Methods of estimating K_0 based on the ratio of horizontally to vertically polarized shear wave velocities propagating in the horizontal directions (V_{sHH}/V_{sHV}) are reviewed. When plotted versus the geologic age or the time since the last liquefaction event, values of V_{sHH}/V_{sHV} do not exhibit an increasing trend, but a slight decreasing trend. These results suggest that both V_{sHH} and V_{sHV} increase at similar rates with time, and thus the

influence of age is cancelled out in the ratio. An improved relationship for estimating K_0 from V_{sHH}/V_{sHV} is suggested by adding the age term and assuming average values of the fabric anisotropic ratio and the stress exponent.

Because K_0 increases with age, it is reasoned that much of the K_0 correction on liquefaction resistance of aged sands is captured by the age or diagenesis correction factor K_{DR} that has been proposed by various researchers. Hence, it is recommended that the K_{K0} factor not be used with the K_{DR} factor, unless there is clear evidence that K_{K0} is not captured by K_{DR}. The entire effect of *OCR* is not captured by K_{DR}, however. Therefore, it is suggested that the K_{OCR} factor be used in field liquefaction evaluations of aged sands.

Values of K_0 are estimated from DMT-CPT-*OCR* information in natural sand deposits at eight geotechnical investigation sites in the South Carolina Coastal Plain (SCCP). Estimates of K_0 for the eight sites fall in the typical range for natural sands. A gentle increasing trend in K_0 with age is observed in these data, similar to the previously published data. A weaker trend is observed in K_0 with the time since initial deposition or the time since the last liquefaction event, which indicates that K_0 decreases little, if any, because of liquefaction.

Based on the V_S profiles from the SCCP sites, the crosshole V_{sHV} (velocity of vertically polarized shear waves propagating in the horizontal direction) and the SCPT V_{sVH} (velocity of horizontally polarized shear waves propagating in near vertical direction) measurements are in good general agreement with each other. Ratios of V_{sHH} to V_{sHV} at six crosshole sites indicate greater overall stress stiffness in the vertical

direction than in the horizontal direction. Values of K_0 estimated from ratios of V_{sHH} to V_{sHV} at the SCCP sites fall in the typical range for natural sands when the age term is added to the predictive relationship.

Profiles of compression wave velocities (V_P) suggest existence of unsaturated (i.e., V_P < 1,400 m/s) zones extending from 0.2 to 1.3 m below the groundwater tables at five of six crosshole sites in the SCCP.

The liquefaction potential of sand deposits in the SCCP is evaluated based on both penetration resistances and V_S, assuming the ground shaking levels during the 1886 Charleston earthquake. Five of the eight sites are no liquefaction sites. The other three are paleoliquefaction sites, with only one site exhibiting surface manifestations of liquefaction in 1886. Geological ages of the sand deposits at the eight sites range from 70,000 to over 1,000,000 years. Overconsolidation ratios range from 1.0 to 2.4 in the critical sand layers. The behavior at six of the eight sites during the 1886 Charleston earthquake is correctly predicted when corrections for diagenesis, unsaturated conditions and *OCR* are made. One of the no liquefaction sites and one of the paleoliquefaction sites are incorrectly predicted to liquefy in 1886. It is possible that liquefaction, or at least pore pressure build up occurred at these two sites in 1886, but the capping non-liquefiable layer was thick enough to prevent noticeable surface manifestations. The results support the use of diagenesis, unsaturation, and *OCR* corrections, as well as the need to assess the capping layer and the critical layer thicknesses in liquefaction assessment of aged sand deposits.

DEDICATION

This dissertation is dedicated to my parents in recognition of their love and inspiration

ACKNOWLEDGMENTS

I would like to express my sincere gratitude to my advisor Dr. Ronald Andrus for his valuable guidance, sound technical insights and constant support throughout this study. His consistent positive personality and motivation helped me attain my academic and research goal. I feel privileged having the opportunity to work with him and attend his classes. I hope to maintain his level of professional integrity and ethics in my future career.

I also would like to thank my committee members Dr. C. Hsein Juang, Dr. Nadarajah Ravichandran and Dr. WeiChiang Pang for their kind support and for taking the time to review my dissertation.

I am grateful to my friend Shimelies Aboye, for his gracious company throughout my stay in Clemson. I would like to thank many current and former graduate students, especially Michael Esposito, Shimelies Aboye, Lawrence Simonson and Aaron Geiger for their assistance in field data collection.

I give thanks to Mr. William (Billy) M. Camp at S&ME for assisting with the drilling and cone testing services, and for providing the inclinometer test equipment. I thank Mr. Michael Hasek and Dr. Sarah Gassman of the University of South Carolina for overseeing installation of and arranging access to the crosshole arrays at the three paleoliquefaction sites. I would also like to thank Mr. Mike Arnold of Red Mountain Timber, Mr. Mark Muckenfuss of Oakridge Landfill, and Mr. Ed Hollen, the Hollywood Town Planner for their allowing us to access the three paleoliquefaction sites.

I would like to thank Mr. George Askew and Mr. Jeff Vernon of Clemson's Baruch Institute of Coastal Ecology and Forest Science, Mr. Hal Hanvey of Clemson's Research and Education Center, and Mr. Charles Byrd of the SCDOT Waterboro office for allowing us access to the five no liquefaction field sites.

Finally, this research was supported in part by the National Science Foundation, under the NSF grant number CMS–0556006 which is greatly appreciated. Any opinions, findings, conclusions, or recommendations are made by the author of this dissertation and do not necessarily reflect the views of the National Science Foundation.

TABLE OF CONTENTS

Table of Contents (Continued)

Page

Table of Contents (Continued)

Page

Table of Contents (Continued)

Page

Table of Contents (Continued)

Page

LIST OF TABLES

Table Page

List of Tables (Continued)

Table Page

List of Tables (Continued)

Table Page

List of Tables (Continued)

Table Page

List of Tables (Continued)

Table Page

List of Tables (Continued)

Table Page

List of Tables (Continued)

Table Page

List of Tables (Continued)

Table Page

List of Tables (Continued)

Table Page

List of Tables (Continued)

Table Page

LIST OF FIGURES

Figure Page

List of Figures (Continued)

Figure Page

List of Figures (Continued)

Figure Page

List of Figures (Continued)

Figure Page

List of Figures (Continued)

Figure Page

List of Figures (Continued)

Figure Page

List of Figures (Continued)

Figure Page

List of Figures (Continued)

Figure Page

List of Figures (Continued)

Figure Page

List of Figures (Continued)

Figure Page

CHAPTER 1

INTRODUCTION

1.1 Background

Since the massive liquefaction-induced ground failures during the two disastrous earthquakes in Alaska, USA and Niigata, Japan in 1964, evaluating soil liquefaction potential has been a major area of research in the field of geotechnical engineering worldwide. Seed and Idriss (1971) developed the commonly used simplified procedure for evaluating liquefaction potential of soil, which has been modified and improved periodically since that time by numerous researchers. In 1985 and 1996, two workshops were convened, participated by many of the experts in the field, to review the state-of-knowledge and the state-of-the-art for assessing liquefaction hazard and to update the simplified procedure based on new findings. A summary of the 1885 workshop was reported by NRC Committee on Earthquake Engineering (1985). Recommendations made in the 1996 workshop were summarized by Youd et al. (2001).

The simplified procedure, as stated by Youd et al. (2001), involves estimation of "the seismic demand on a soil layer, expressed in terms of the cyclic stress ratio (*CSR*) and the capacity of the soil to resist liquefaction, expressed in terms of the cyclic resistance ratio (*CRR*)." The ratio of *CRR* to *CSR* is called the factor of safety against liquefaction. Various field tests including the standard penetration test (SPT), the cone penetration test (CPT), various shear wave velocity (V_S) tests, and the Becker penetration test (BPT) have been used for liquefaction investigations because of the complexities

associated with sampling and laboratory testing. *CRR* is commonly estimated using field test results and charts developed from case histories of liquefaction and no liquefaction.

Various factors can influence the accuracy of the simplified procedure, particularly when the conditions at the sites being evaluated differ from the case history sites. A listing of such factors is as follows:

(1) As stated by Youd et al. (2001), "the simplified procedure was developed and validated only for level to gently sloping sites (low static shear stress) and depths less than about 15 m (low overburden pressure)".

(2) The *CRR* charts were developed from case histories involving soils less than a few thousand years old (Youd et al. 2001), while a number of researchers have concluded that aged soils often exhibits significantly higher resistance against liquefaction compared to young soils due to various diagenetic processes that can occur over time (Youd and Perkins 1978; Seed 1979; Troncoso et al. 1988; Arango and Migues 1996; Lewis et al. 1999, 2004; Arango et al. 2000; Robertson et al. 2000; Leon et al. 2006; Hayati and Andrus 2008; Andrus et al. 2009).

(3) In the field case histories, the soils below the groundwater table were assumed that to be saturated, which may not be true in all cases. In fact, unsaturated conditions often exist below the groundwater table (Barrow 1883, Andrus et al. 1992; Kokusho 2000; Fourie et al. 2001; Ishihara et al. 2001; Holzer and Bennett 2003) which can significantly increase the liquefaction resistance of soils (Sherif et al. 1977; Yoshimi et al. 1989; Ishihara et al. 1998; Grozic et al. 2000; Tsukamoto et al. 2002; Nakazawa et al. 2004; Okamura and Soga 2006; Okamura

et al. 2006; Seid-Karbasi and Byrne 2006; Hatanaka and Masuda 2008; Hossain et al. 2013).

(4) The *CRR* charts are mostly based on case histories of normally consolidated soils with at rest lateral stress coefficient (K_0) of about 0.5. Moreover, the simplified procedure implicitly assumes that the *CRR* charts are independent of K_0, which has not been validated with empirical results (Salgado et al. 1997). However, based on laboratory test results on sands with varying K_0 conditions and overconsoildation ratio (*OCR*), researchers have demonstrated that liquefaction resistance increases with an increase in K_0 and *OCR* (Ishibashi and Sherif 1974; Ishihara et al. 1977; Ishihara and Takatsu 1979; Bhatia 1982; Ishihara et al. 1985; Yamashita and Toki 1993).

Based on the above listing, various correction factors might be needed to extrapolate the *CRR* curves to conditions different from the case history database as follows (modified from Youd et al. 2001):

$$CRR_{\text{corrected}} = CRR\ K_\sigma\ K_\alpha\ (K_{DR} \text{ or } K_{K0})\ K_S\ K_{OCR} \quad (1.1)$$

where K_σ is the correction factor for high effective overburden pressure, K_α is the correction factor to incorporate the effect of static shear stresses, K_{DR} is the correction factor to capture the influence of aging processes or diagenesis, K_{K0} is the factor to account for K_0 much greater than 0.5, K_S is the factor to correct for unsaturated conditions and K_{OCR} is the factor to capture the effects of overconsolidated conditions. It will be shown in this report that K_0 generally increases with the age of the deposit. Thus, the use of both K_{DR} and K_{K0} may not be appropriate in many cases.

1.2 Scope and Objectives

The overall scope of the research presented in this dissertation is to better quantify the influence of K_0 conditions and *OCR* on liquefaction resistance of natural sand deposits. To do so, the specific objectives of this dissertation are to:

1. Review existing relationships and establish new relationships, if needed, for estimating in-situ K_0 of sands based on (a) flat plate dilatometer test (DMT), CPT and *OCR* information, and (b) the ratio of horizontally to vertically polarized shear wave velocities propagating in horizontal directions (V_{sHH}/V_{sHV}) from seismic crosshole tests.
2. Compile databases of in-situ K_0 estimates in natural and man-made sand deposits from self-boring pressuremeter test, DMT-CPT-*OCR* and crosshole V_{sHH}/V_{sHV} along with the soil age and liquefaction history information.
3. Analyze the variation in K_0 with age and seismicity.
4. Review literature for expressions for K_{K0} and K_{OCR}.
5. Apply the DMT-CPT-*OCR*- and the V_{sHH}/V_{sHV}-based procedures to estimate K_0 in eight aged sand deposits in the South Carolina Coastal Plain (SCCP).
6. Assess liquefaction potential of eight SCCP sites using penetration resistance- and shear wave velocity-based *CRR* charts, while examining the significance of K_{DR}, K_S, K_{K0} and K_{OCR} corrections.

1.3 Organization

This dissertation is organized in eight chapters. The introduction is presented in the current chapter, Chapter 1. Reviewed in Chapter 2 are proposed selected methods of

estimating K_0 in sand deposits from in-situ tests. Based on the review, two new relationships for estimating K_0 based on DMT-CPT-*OCR* and V_{sHH}/V_{sHV} ratios are proposed. Presented in Chapter 3 is a database of in situ K_0 in sands at sites around the world along with the information of geologic age and time since last liquefaction event. The database of K_0 is analyzed with respect to age. Discussed in Chapter 4 are the effects of fabric anisotropy, K_0 conditions and *OCR* on liquefaction resistance of sands based on a review of the literature. Presented in Chapter 5 are estimates of K_0 from DMT-CPT-*OCR* at eight geotechnical investigation sites in the SCCP. Presented in Chapter 6 are the seismic wave velocity characterizations of the eight sites in SCCP from seismic CPT and crosshole tests, and estimates of K_0 based on V_{sHH}/V_{sHV} ratios. In Chapter 7, penetration resistance- and shear wave velocity-based liquefaction evaluations of the eight SCCP sites are presented. Finally, the major conclusions of this dissertation and the recommendations for future research are summarized in Chapter 8.

CHAPTER 2

REVIEW OF IN SITU TESTS FOR DETERMINING K_0 IN SANDS

2.1 Introduction

Estimation of the initial geostatic state of stress in the ground is frequently coupled with the coefficient of lateral stress at rest (K_0). Donath (1891) was one of the first to express K_0 as the ratio of effective horizontal stress ($\sigma_h^{'}$) to effective vertical stress ($\sigma_v^{'}$). K_0 is an important input parameter in the design and analysis of many geotechnical engineering problems (e.g., selecting initial consolidation stresses for laboratory tests, design of earth retaining structures and excavation walls, assessing shaft friction on piles and piers, numerical simulations in finite element method and liquefaction studies).

Despite its importance, reliable estimation of K_0 remains a great challenge in geotechnical engineering. Estimation of K_0 from laboratory tests which requires high quality undisturbed sample, and sophisticated and time-consuming procedures is generally not applicable for granular soils (Fioravante et al. 1998). The following expression derived by Jaky (1944) is widely used to estimate K_0 of normally consolidated soils:

$$K_0 = 1 - \sin\varphi' \tag{2.1}$$

where φ' is the effective friction angle of soil. For overconsolidated soils, the following expression suggested by Mayne and Kulhawy (1982) is often used to estimate K_0:

$$K_0 = (1 - \sin\varphi')OCR^{\sin\varphi'} \quad (2.2)$$

where *OCR* is the overconsolidation ratio of soil.

Because K_0 is dependent on many factors, the use of simple correlations such as Equations 2.1 and 2.2 can lead to significant error. Hanna and Ghaly (1992) reported that, in addition to φ', K_0 is affected by shape and interlocking of soil particles, amount of fines in the soil, porosity, crushing, modulus of elasticity of the mineral particles, elastic and sliding strains, aging, dilation, densification, compacting method, stress history, and applied stress level.

Presented in this chapter is a review of in situ tests for estimating K_0 in sands. Based on the review, relationships for estimating K_0 in sands from common in situ tests are recommended.

2.2 Estimating K_0 from In Situ Tests

Several researchers have classified different methods of estimating K_0 from in situ tests into two broad categories (Mayne and Kulhawy 1990; Sully and Campanella 1990; Hamouche et al. 1995; Lunne and Mayne 1998; Cai et al. 2011; Ku and Mayne 2013) – 1) direct, and 2) semi-direct or indirect methods. Direct in situ methods include self-boring pressuremeter test (SBPMT) (Baguelin et al. 1972; Wroth and Hughes 1973), total stress cell (TSC, also known as Glötzl cell or push-in spade cell) (Massarsch 1975; Tavenas et al. 1975), hydraulic fracture (HF) (Bjerrum and Anderson 1972; Bozozuk 1974), self-boring load cell (SBLC) (Dalton and Hawkins 1982; Tedd and Charles 1983) and suction probe (Ridley and Burland 1993). K_0 obtained from direct methods are often used as reference benchmark values in assessing the usefulness of other methods. Direct

methods often suffer from large effects of even small degrees of disturbance, the consequences of which become more important as the soil stiffness increases. Because of large disturbance to soil, pre-bored (Menard) pressuremeter (MPMT) and full displacement (cone/seismic cone) pressuremeter (FDPMT) failed to achieve high degree of success in estimating K_0 using a direct approach (Powell 1990; Sully 1991).

Commonly used in-direct field methods include the flat plate dilatometer test (DMT) (Marchetti 1980), the cone penetration test (CPT or CPTu) (Mayne and Kulhawy 1990) and the Iowa stepped blade (ISB) test (Handy et al. 1982). Indirect methods generally involve either some interpretation effort and back extrapolation or empirical inference from different penetration indices. Other attempts to estimate K_0 from field tests include the piezo lateral stress cell (PSLC) (Baligh et al. 1985), the field vane (Schmertmann 1975), and electrical methods (Meegoda and Arulanandan 1986).

In situ methods can be either intrusive or non-intrusive based on the nature of the test and the degree of caution practiced for avoiding disturbance during insertion of probes into the soil. All intrusive methods cause changes of various degrees to the state of stress in soil. In this respect, Hamouche et al. (1995) described SBPMT as a non-intrusive or less intrusive method. A truly non-intrusive method, however, involves geophysical measurements such as seismic shear wave velocity (V_S). During seismic measurements, although the soil adjacent to the boreholes is in a semi-disturbed condition, the readings are representative of a large mass of undisturbed soil.

Figure 2.1 displays a comparison of the expected conceptual change in stress state in soil caused by various in-situ tests originally presented by Sully and Campanella

(1990) and modified by Ku and Mayne (2013). Figure 2.1 indicates that SBPMT and geophysical methods impart the minimum disturbance in soil and at least in theory, can give the most reliable field estimation of K_0.

Published data of in situ K_0 from numerous geotechnical studies have shown that some of the field test methods can be applied with reasonable success to both sands and clays (e.g., SBPMT, DMT, V_S test, CPT or CPTu), while others are mostly applicable to only clayey soils (e. g., TSC, HF, SBLC, ISB). Because the in situ K_0 of sands is the topic of this dissertation study, only the procedures of estimating K_0 using SBPMT, DMT and V_S tests are discussed in detail in the following sections.

2.2.1 K_0 from SBPMT

The self-boring pressuremeter is a cylindrical probe with an expandable membrane close to its mid-section. During testing, a cutting shoe and a drilling or jetting mechanism at the bottom the pressuremeter allows it to be advanced in the soil with minimal disturbance. After the self-boring pressuremeter cuts/drills to desired depth, the membrane is pressurized and expanded by injecting air or water. The membrane movement is measured by strain arms (usually 3 arms at 120° or 6 arms at 60°) around the mid-section of the pressuremeter module. A diagram showing the details of a British type SBPM is presented in Figure 2.2.

SBPMT in sand is assumed to be drained (Clarke 1995). Generally, $\sigma_h^{'}$ in sand is evaluated using the lift-off method which involves visual determination of lift-off pressure at each of the strain arms. The lift off pressure is defined as the pressure at which a break or substantial change of slope occurs in the early stages of cavity pressure

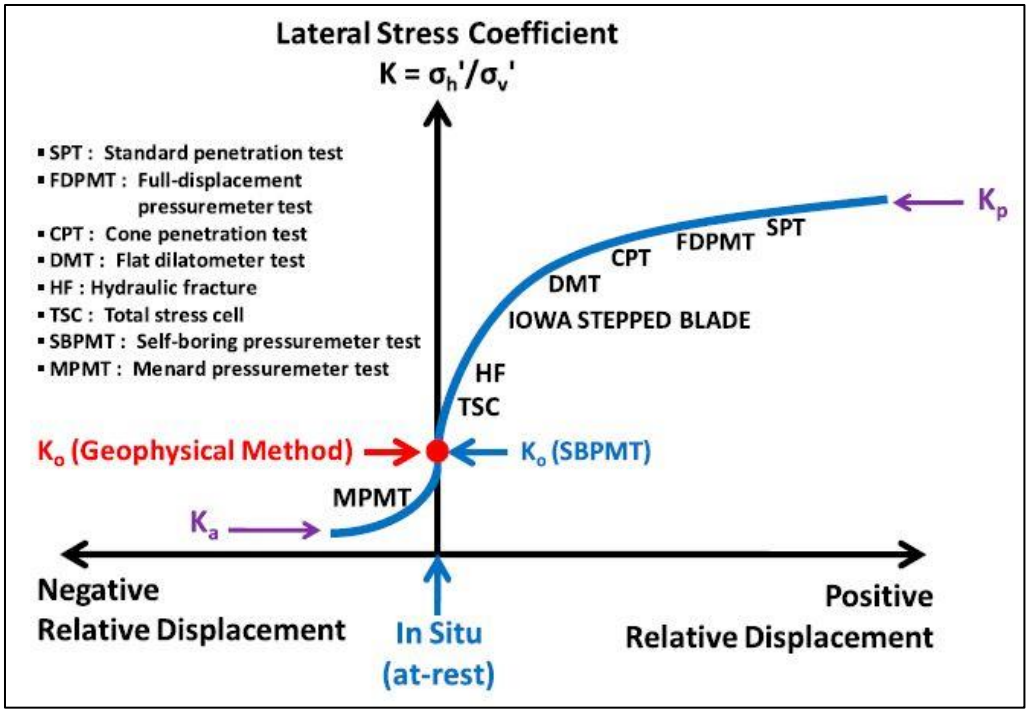

Figure 2.1: Conceptual change of lateral stress coefficient (*K*) state caused by insertion of various in situ devices (modified after Sully and Campanella 1990) as presented by Ku and Mayne (2013).

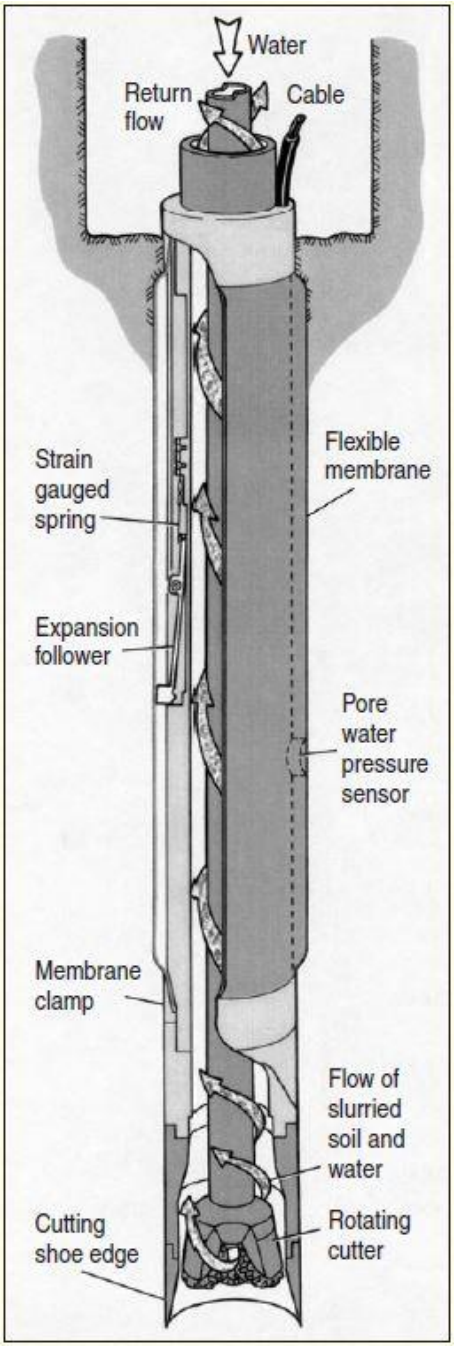

Figure 2.2: Details of a British type self-boring pressuremeter manufactured by Cambridge Insitu Ltd. (https://www.cambridge-insitu.com/system/files/files_trackable/pressuremeters_web.pdf).

behind the membrane versus the strain arm displacement curve. Figure 2.3 shows a SBMPT testing curve measured in a natural sand deposit. K_0 for each elevation of the strain arms is determined by dividing $\sigma_h^{'}$ by the calculated $\sigma_v^{'}$.

2.2.2 K_0 from DMT

Flat plate dilatometer is a tapered steel blade with a thin circular calibrated steel membrane mounted on one face (Marchetti 1980). A diagram showing the steel blade and membrane of a dilatometer is presented in Figure 2.4. As described in ASTM D6635 01, during testing the blade is pushed to the desired depth and the membrane is expanded using nitrogen gas pressure. The pressures at membrane deformation of 0.05 mm and 1.1 mm are recorded, which are called the lift-off pressure (A) and expansive pressure (B), respectively. The membrane is depressurized and the pressure reading at the point of zero deformation is taken which is referred as the closing pressure (C). The pressure readings are all taken within a 15 to 20 second time interval.

Membrane stiffness correction factors ΔA and ΔB are determined prior to testing. To find ΔA, a vacuum pressure is applied to the membrane using a syringe. A buzzer alerts the operator that the pressure needed to collapse the membrane is reached and is recorded as ΔA. The membrane is then expanded from the collapsed position to a deformation of 1.1 mm. At this deformation, the buzzer sounds and ΔB is recorded. The same procedures are followed to calculate ΔA and ΔB at the end of testing. The two ΔA and ΔB values are averaged together and the correction is applied to the values A and B to find the contact stress, P_0 and the expansion stress, P_1. The values of P_0 and P_1 are determined using the following equations presented by Marchetti (1980):

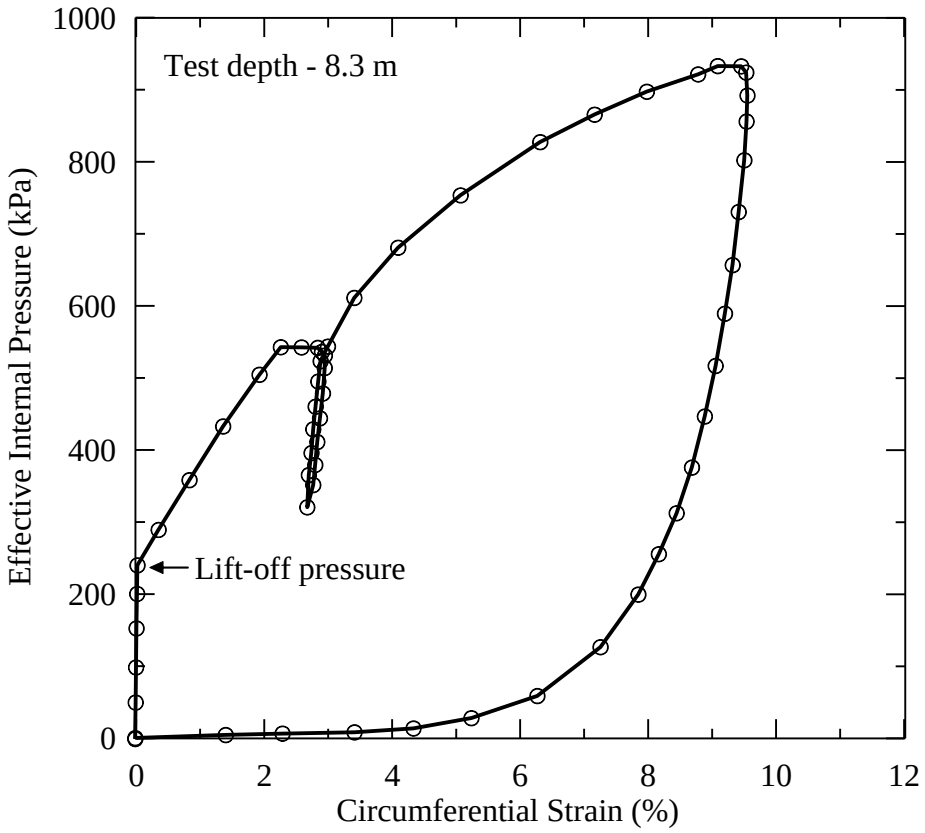

Figure 2.3: Testing curve measured by SBPM at Laing Bridge site in British Columbia, Canada reproduced from Cunha (1994).

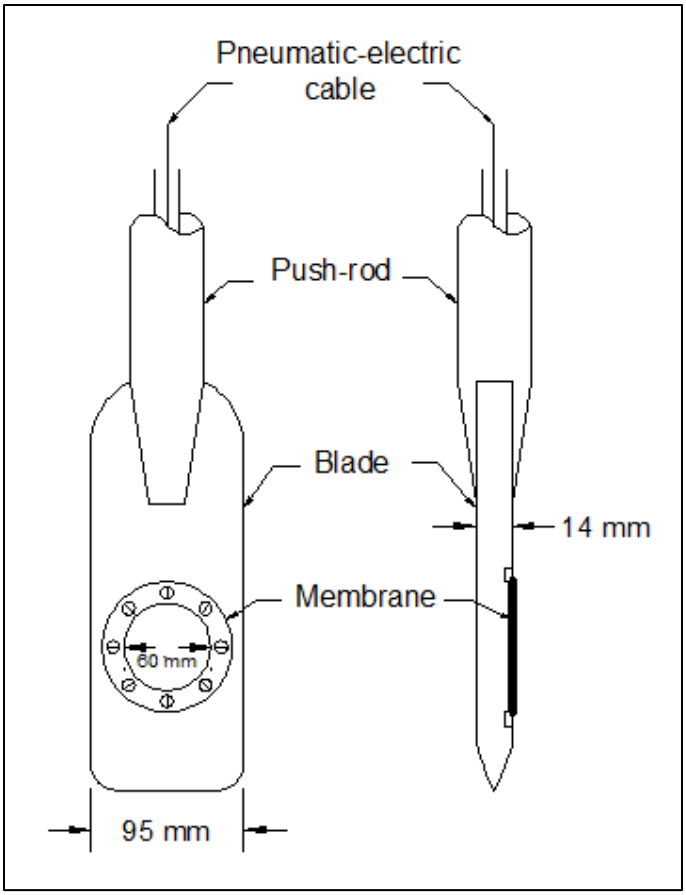

Figure 2.4: Flat dilatometer blade and membrane.

$$P_0 = 1.05(A + \Delta A - Z_m) - 0.05(B - \Delta B - Z_m) \quad (2.3)$$

$$P_1 = B - \Delta B - Z_m \quad (2.4)$$

where Z_m is the reading of the gauge for zero pressure. The DMT material index (I_D) and horizontal stress index (K_D) are obtained using the following equations recommended by Marchetti (1980):

$$I_D = (P_1 - P_0)/(P_0 - u_0) \quad (2.5)$$

$$K_D = (P_0 - u_0)/\sigma_v' \quad (2.6)$$

where u_0 is the hydrostatic pore water pressure.

Marchetti (1980) made the first attempt to estimate K_0 from K_D and suggested the following empirical relationship:

$$K_0 = (K_D/1.5)^{0.47} - 0.6 \quad (2.7)$$

Equation 2.7 was derived mostly from data available for clays, with only a few data for sands. Moreover, Equation 2.7 overpredicts K_0 both in natural sands and in calibration chamber (CC) test sand specimens (Baldi et al. 1986). To improve the estimate of K_0 in sands, Schmertmann proposed a procedure based on limited CC testing during a 1983 DMT workshop, which was later summarized by Jamiolkowski et al. (1985). The correlation is expressed by:

$$K_0 = \frac{40 + 23K_D - 86K_D(1 - \sin\varphi'_{tr}) + 152(1 - \sin\varphi'_{tr}) - 717(1 - \sin\varphi'_{tr})^2}{192 - 717(1 - \sin\varphi'_{tr})} \quad (2.8)$$

where φ'_{tr} is the triaxial friction angle of the soil determined from CPT or DMT data.

Because the Schmertmann method is complex, Marchetti (1985) suggested the use of the dimensionless parameter, q_t/σ'_v (where q_t is the cone tip resistance) rather than φ'. Marchetti (1985) also found that the Schmertmann method overestimates K_0 for the Po River sand deposit, a well-documented case history from Italy. Based on the bearing capacity theory of Durgunoglu and Mitchell (1975), Marchetti (1985) produced a graphical form where both K_D and q_t/σ'_v are functions of K_0 and φ'. Robertson et al. (1986) modified the graphical form by Marchetti (1985) using the Campanella and Robertson (1983) q_t-φ' empirical relationship, which is presented in Figure 2.5. As seen from Figure 2.5, the modified graphical form still noticeably overestimates K_0 in Po river sand.

To evaluate $K_0 = f(K_D, q_t/\sigma'_v)$ as suggested by Marchetti (1985), Baldi et al. (1986) performed a series of DMTs in a large calibration chamber on two widely used reference sands. The specimens were prepared by pluvial deposition using a gravity mass sand spreader. For each DMT test, corresponding q_t was computed from mean octahedral consolidation stress and relative density using empirical relationship by Baldi et al. (1985). Due to boundary condition effects on DMT results, only test data with constant σ'_v and σ'_h were considered. Results of such 27 tests are summarized in Table 2.1. These test results led to the following relationship (Baldi et al. 1986):

$$K_0 = 0.376 + 0.095K_D - 0.00172(q_t/\sigma'_v) \qquad (2.9)$$

with a coefficient of determination (R^2) of 0.64. Because Equation 2.9 seemed to over-

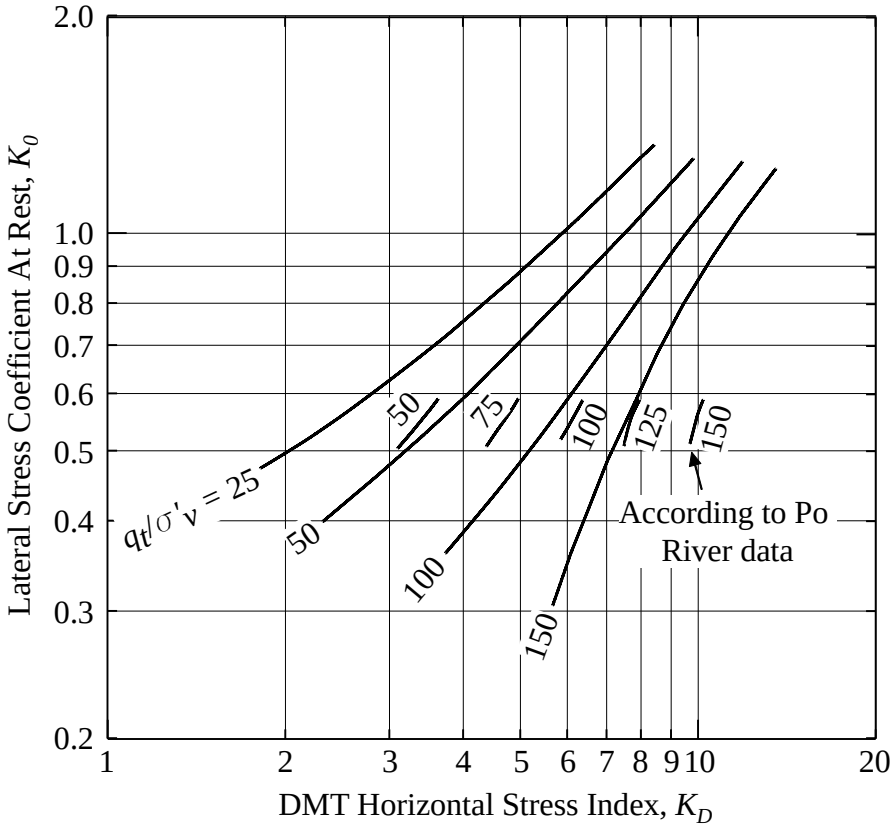

Figure 2.5: Marchetti (1985) graphical form for K_D-K_0-q_t / σ'_v relationship modified using Robertson and Campanella (1983) q_t-φ' correlation (after Robertson et al. 1986) reproduced from Sully (1991).

Table 2.1: Summary of DMT test results with constant boundary stress (i.e., σ'_v = constant and σ'_h = constant) in calibration chamber by Baldi et al. (1986).

Test ID	σ'_v **(kPa)**	σ'_h **(kPa)**	D_r **(%)**	***OCR***	K_0	I_D	K_D	E_D **(MPa)**	q_t **(MPa)**
Ticino sand									
43	112.78	45.11	77.3	1.00	0.40	2.08	4.19	61.73	13.76
44	212.81	88.26	79.3	1.00	0.41	1.80	4.28	102.99	20.96
47	63.74	24.52	77.6	1.00	0.39	2.70	4.23	46.82	10.01
97	113.76	50.99	79.4	1.00	0.45	2.53	3.00	42.44	15.09
98	114.74	50.01	91.4	1.00	0.44	2.11	5.06	79.62	21.05
102	111.80	58.84	39.9	1.00	0.53	2.26	3.38	44.66	5.19
105	312.83	152.98	52.8	1.00	0.49	1.66	2.41	49.72	12.98
117	112.78	51.98	72.0	1.00	0.46	2.45	2.79	35.89	12.31
118	111.80	51.98	45.0	1.00	0.46	3.54	1.47	17.16	5.79
119	111.80	51.98	45.0	1.00	0.46	3.02	1.50	15.04	5.79
45	112.78	97.09	81.0	5.50	0.86	1.67	8.50	139.35	19.23
46	113.76	82.38	77.3	2.80	0.73	1.81	6.73	108.80	16.45
49	110.82	106.89	79.6	5.60	0.96	1.63	8.91	142.00	19.07
99	112.78	84.34	93.3	2.80	0.75	1.53	8.84	125.94	25.82
100	111.80	84.34	79.9	2.82	0.75	1.79	5.39	71.56	17.73
101	110.82	60.80	79.3	1.47	0.55	2.06	4.09	54.17	15.69
103	110.82	64.72	51.2	1.46	0.58	2.37	2.66	31.30	7.30
104	111.80	88.26	50.5	2.80	0.79	2.23	3.41	44.55	7.93
115	112.78	127.49	97.9	8.08	1.13	1.57	11.46	185.03	34.12
Hokksund sand									
123	311.85	134.35	64.7	1.00	0.43	1.90	1.67	29.07	17.88
199	61.78	27.45	71.0	1.00	0.44	3.31	3.98	47.95	8.88
203	62.76	28.44	71.0	1.00	0.45	3.08	5.11	65.74	9.01
204	112.77	49.03	46.0	1.00	0.43	3.62	1.82	26.21	5.98
200	60.80	42.17	70.0	1.58	0.69	2.49	8.44	103.97	9.73
202	61.78	54.92	70.0	7.44	0.89	3.31	6.38	95.34	10.67
205	111.79	94.14	50.0	8.30	0.84	5.68	4.66	188.68	8.15
206	108.85	71.59	50.5	3.30	0.66	3.50	2.47	42.03	7.51

predict K_0 in Po River sand, Baldi et al. (1986) suggested the following modified relationship:

$$K_0 = 0.376 + 0.095K_D - 0.00461(q_t/\sigma'_v) \quad (2.10)$$

as the 'best available tentative procedure for estimating K_0 from DMT's in natural, predominantly quartz uncemented sand deposit'.

Difficulties arise, however, when using Equation 2.10 to predict K_0 for other field case histories of natural sand deposits, as shown in this dissertation study. Equation 2.10 seems to predict unreasonably low values of K_0 in cases with relatively high q_t and low K_D values. Therefore, the 27 test data from Baldi et al. (1986) are reviewed and reanalyzed in this study to find a relationship which can make a better prediction of K_0 and is applicable for both laboratory and field conditions.

Figure 2.6 presents the residuals of K_0 from Equations 2.9 and 2.10 for the calibration chamber (CC) data plotted against *OCR*. Both Figure 2.6(a) and 2.6(b) show a strong increasing trend in residual with *OCR*. Thus, the Baldi et al. (1986) K_D-K_0 relationship can be improved by adding an *OCR* term.

Adding an *OCR* term and redoing the regression leads to a new relationship for estimating K_0 expressed by:

$$K_0 = 0.359 + 0.045K_D - 0.00085(q_t/\sigma'_v) + 0.056OCR \quad (2.11)$$

where q_t is cone tip resistance corrected for pore pressure if a piezocone is used. R^2 associated with Equation 2.11 is 0.88 which indicates a significant improvement with the addition of *OCR*. Figure 2.7 presents a comparison between the predicted K_0 using Equation 2.11 and the measured K_0 in CC tests, which also reflects a very good fit to the

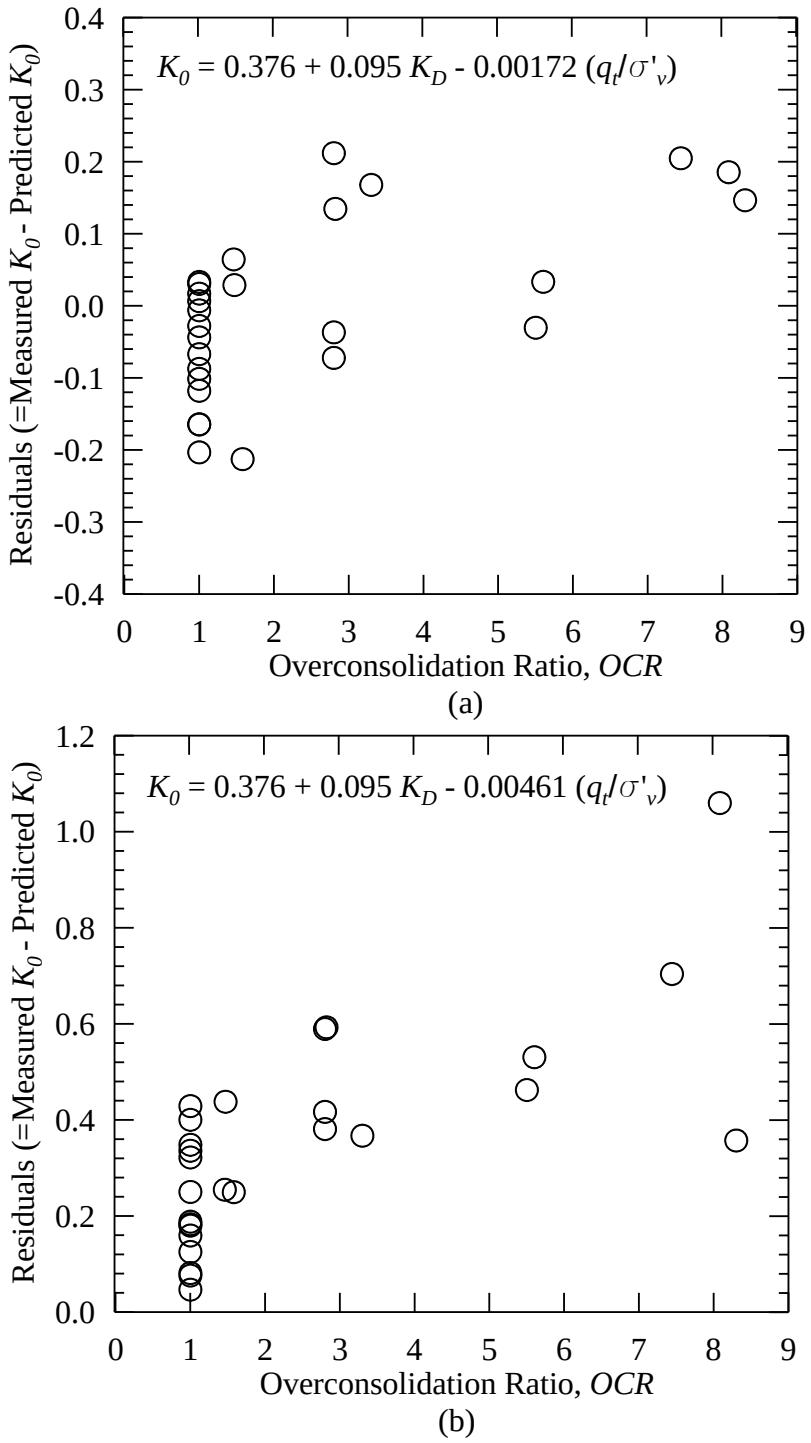

Figure 2.6: Residuals of K_0 from Baldi et al. (1986) calibration chamber test data plotted against overconsoildation ratio using (a) Equation 2.9 and (b) Equation 2.10.

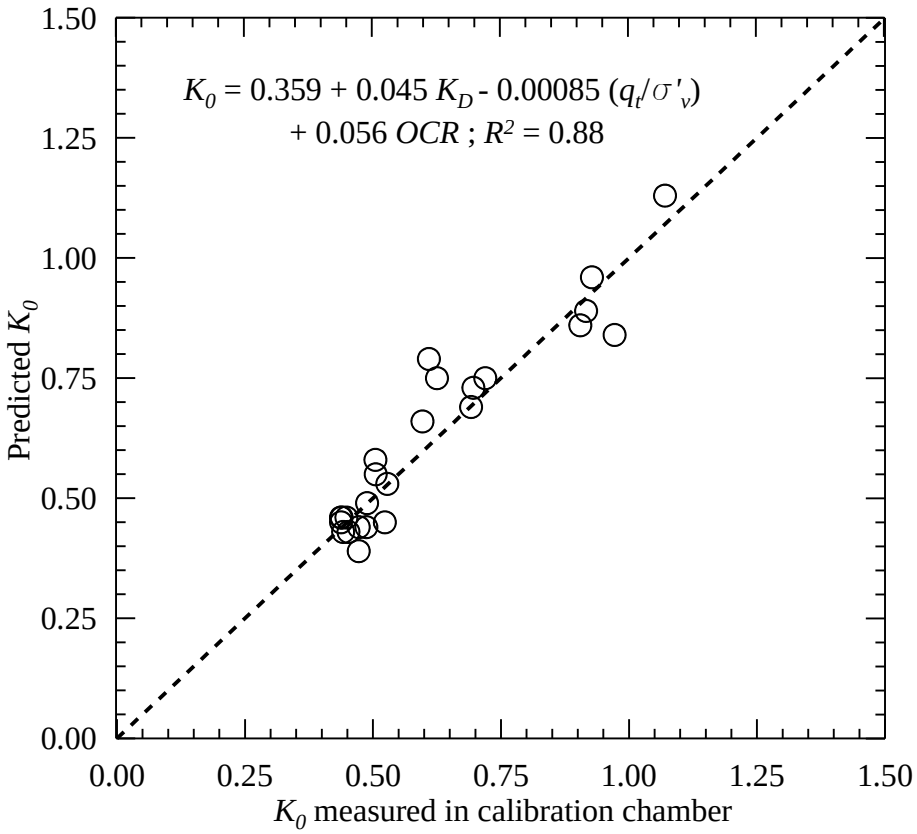

Figure 2.7: Predicted values of K_0 using Equation 2.11 plotted against measured values of K_0 for the calibration chamber test data reported by Baldi et al. (1986).

data. In addition, Equation 2.11 correctly predicts K_0 for Po River sand which will be presented later in Chapter 3.

2.2.3 K_0 from V_S Tests

Stress-dependency of low amplitude V_S in dry sand has been investigated and recognized in numerous laboratory studies both independently (Lawrence 1965; Schmertmann 1978; Roesler 1979; Allen and Stokoe 1982; Knox et al. 1982; Yu and Richart 1984; Lee and Stokoe 1985; Stokoe et al. 1985; Stokoe and Ni 1985; Thormann and Hryciw 1990; Yan and Byrne 1990; Lee 1993; Bellotti et al. 1996) and in terms of small strain shear modulus, G_0 or G_{max} (Hardin 1961; Hardin and Richart 1963; Gardner et al. 1964; Hardin and Black 1966; Hardin and Drnevich 1972; Kuribayashi et al. 1975; Iwasaki et al. 1978; Tatsuoka et al. 1979; Uchida et al. 1980). Most of the earlier studies were conducted under isotropic loading conditions and the mean effective confining pressure was considered to be the major factor affecting V_S. Subsequently, other researchers conducted studies under anisotropic loading conditions (biaxial and triaxial confinement) and demonstrated that V_S depends about equally on the principal stresses in the direction of wave propagation and polarization and is relatively independent of the principal stress in the out-of-plane direction (Roesler 1979; Knox et al. 1982; Lee and Stokoe 1985; Lee 1993; Yan and Byrne 1990). In more recent studies, the scope of these findings has been expanded to estimate the in situ geostatic state of stress.

Based on the works by Lee and Stokoe (1985) and Stokoe et al. (1985), several researchers formulated simple correlations between K_0 and the paired sets of directional V_S from in situ seismic tests (Sully 1991; Andrus 1994; Sully and Campanella 1995;

Fioravante et al. 1998). These correlations have been used to estimate the in situ K_0 in soil deposits with some success (Andrus 1994; Sully and Campanella 1995; Fioravante et al. 1998; Cai et al. 2011; Ku and Mayne 2013; Tong et al. 2013).

Figure 2.8 illustrates the three modes of shear wave through soil during in situ seismic tests. These three modes are (Fioravante et al. 1998; Cai et al. 2011; Ku and Mayne 2013):

(a) V_{sVH} is velocity of shear wave propagating in the near vertical (at depths >> distance from downhole source to hole) direction with particle motion in the horizontal direction. V_{sVH} can be measured in downhole or seismic CPT test. Measurement procedure in seismic CPT is identical to downhole test except that no borehole is required and the receiver(s) is built into the cone rod.

(b) V_{sHV} is velocity of shear wave propagating in the horizontal direction with particle motion in the vertical direction. V_{sHV} is measured in the conventional crosshole test.

(c) V_{sHH} is velocity of shear wave propagating in the horizontal direction with particle motion in the complementary horizontal direction. V_{sHH} can be measured using a special type of crosshole test, sometimes referred as rotary crosshole, where the wave source and the receivers are rotated perpendicular to the direction of wave propagation.

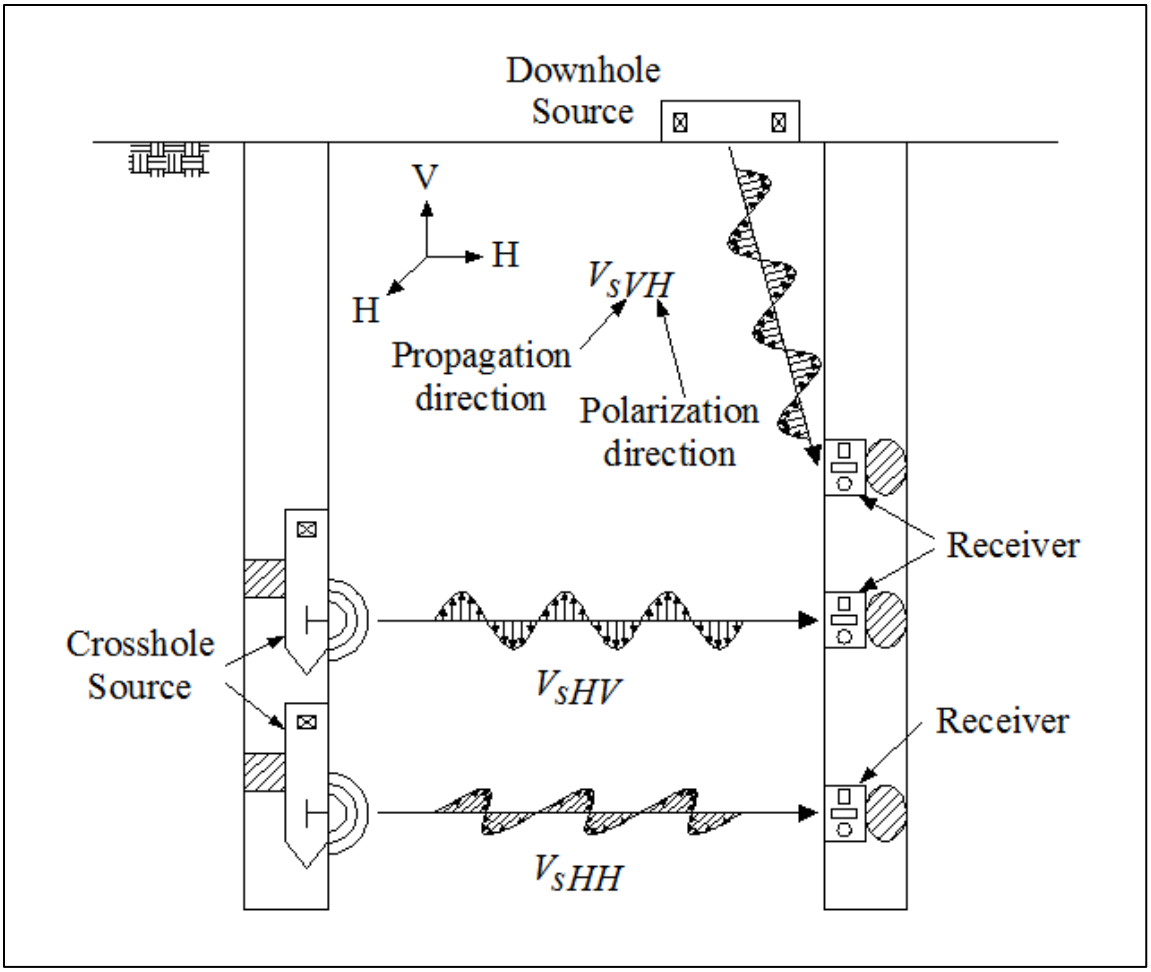

Figure 2.8: Methods of estimating V_S with different direction of wave propagation and particle polarization.

For level ground and anisotropic soil structure, two correlations between in situ K_0 and pairs of V_S modes can be derived:

(a) Individual stress method

$$V_{sVH} = C_{VH}(\sigma'_v)^n(\sigma'_h)^n = C_{VH}(\sigma'_v)^{2n}(K_0)^n \quad \text{or}$$

$$V_{sHV} = C_{HV}(\sigma'_h)^n(\sigma'_v)^n = C_{HV}(\sigma'_v)^{2n}(K_0)^n \tag{2.12}$$

$$V_{sHH} = C_{HH}(\sigma'_h)^n(\sigma'_h)^n = C_{HH}(\sigma'_v)^{2n}(K_0)^{2n} \tag{2.13}$$

Dividing Equation 2.13 by Equation 2.12 and after rearrangement,

$$K_0 = \left(\frac{C_{VH}}{C_{HH}}\frac{V_{sHH}}{V_{sVH}}\right)^{(1/n)} \quad \text{or} \quad K_0 = \left(\frac{C_{HV}}{C_{HH}}\frac{V_{sHH}}{V_{sHV}}\right)^{(1/n)} \tag{2.14}$$

(b) Average stress method

$$V_{sVH} = C_{VH}\left(\frac{\sigma'_v+\sigma'_h}{2}\right)^{2n} = C_{VH}(\sigma'_v)^{2n}\left(\frac{1+K_0}{2}\right)^{2n} \quad \text{or}$$

$$V_{sHV} = C_{HV}\left(\frac{\sigma'_h+\sigma'_v}{2}\right)^{2n} = C_{HV}(\sigma'_v)^{2n}\left(\frac{1+K_0}{2}\right)^{2n} \tag{2.15}$$

$$V_{sHH} = C_{HH}\left(\frac{\sigma'_h+\sigma'_h}{2}\right)^{2n} = C_{HH}(\sigma'_v)^{2n}(K_0)^{2n} \tag{2.16}$$

Dividing Equation 2.16 by Equation 2.15 and after rearrangement,

$$\frac{2K_0}{1+K_0} = \left(\frac{C_{VH}}{C_{HH}}\frac{V_{sHH}}{V_{sVH}}\right)^{(1/2n)} \quad \text{or} \quad \frac{2K_0}{1+K_0} = \left(\frac{C_{HV}}{C_{HH}}\frac{V_{sHH}}{V_{sHV}}\right)^{(1/2n)} \tag{2.17}$$

where the stress exponent n is an empirically fitted parameter and C_{VH}/C_{HH} or C_{HV}/C_{HH} is referred to as the fabric anisotropic ratio for the soil skeleton which is independent of stress conditions (Andrus 1994; Sully and Campanella 1995; Fioravante et al. 1998).

Table 2.2 summarizes estimated average values of the fabric anisotropic ratio and the exponent n in four laboratory studies conducted on six different sands under controlled stress conditions. General test procedure in these studies involved the following steps: (1) reconstituting specimens to desired density by air pluviation or in "quick sand" technique; (2) instrumentations for V_S measurement at the desired elevations by stopping the filling process at those elevations and carefully placing the instruments; and (3) performing wave propagation measurements under various stress state. As seen from Table 2.2, values of the fabric anisotropic ratio from laboratory tests show significant variability ranging between 0.78 and 1.10. Values of the stress exponent n, however, fall within a narrow range and an average value for n is often taken as 0.125.

Table 2.2: Estimated values of anisotropic ratio and exponent n from laboratory studies.

Study	Sand type	Average C_{VH}/C_{HH} or C_{HV}/C_{HH}	Average n	Note
Stokoe et al. (1985)	Washed mortar sand	1.00-1.10	0.09-0.11	Pulse test
Yan and Byrne (1990)	Ottawa sand	1.00-1.10	0.12	Hydraulic gradient similitude
Bellotti et al. (1996)	Ticino sand	0.82-0.98	0.11-0.12	Pulse test
Fioravante et al. (1998)	Ticino sand	0.94-0.95	0.11-0.12	Pulse test
	Kenya sand	0.90-0.95	0.12-0.13	
	HK-TC sand	0.78-0.89	0.13-0.15	
	HK-CLK sand	0.91-0.92	0.12-0.13	

Researchers have used both the individual and average stress methods to estimate K_0 in natural sand deposits and found that both methods provide similar K_0, indicating that the type of stress attribute used in both formulations has low influence on the predictions (Fioravante et al. 1998; Cai et al. 2011). Thus, for simplicity, only the individual stress method in considered in this study.

Using an average anisotropic ratio of 0.95 and n of 0.125, Equation 2.14 can be re-written as:

$$K_0 = \left(0.95\frac{V_{sHH}}{V_{sHV}}\right)^{(1/0.125)} = 0.66\left(\frac{V_{sHH}}{V_{sHV}}\right)^{8.0} \quad (2.18)$$

Applicability of Equation 2.18 to estimate the in situ K_0 of sands will be evaluated in Chapter 3.

2.3 Summary

Various in situ methods of estimating K_0 in sands were discussed in this chapter. Based on the literature, self-boring pressuremeter is considered the most reliable in-situ test to estimate K_0 in sands. A new relationship to estimate K_0 from DMT, CPT, and *OCR* data was derived from previously published calibration chamber test data. The new relationship (Equation 2.11) proved to be a better fit to the test data of Baldi et al. (1986) than previously proposed relationships without *OCR*. Methods for estimating K_0 based on shear wave velocity was also reviewed and a relationship was derived (Equation 2.18), assuming average values of the fabric anisotropic ratio and the stress exponent from published laboratory data. Equations 2.11 will be used in subsequent chapters for estimating K_0 from DMT-CPT-*OCR*. Applicability of Equation 2.18 for estimating K_0 from V_S tests will be evaluated in Chapter 3.

CHAPTER 3

LATERAL STRESS COEFFICIENT IN SAND DEPOSITS

3.1 Introduction

As discussed in Chapter 2, the lateral stress coefficient (K_0) in sands can be estimated directly from the self-boring pressuremeter test (SBPMT), and indirectly from the flat plate dilatometer test (DMT) and from the geophysical method using seismic waves. In this chapter, a database of K_0 obtained from these three methods is compiled after reviewing numerous studies involving geotechnical site characterizations of natural and man-made sand deposits. Geologic age of the sand deposits and time since the occurrence of last critical disturbance (i.e., liquefaction) are also included in the database. With the compiled database, the change in K_0 with age of the sand deposits is analyzed.

3.2 Database

Summary information from seventeen studies (including this dissertation study) conducted at twenty-five sites in the United States, Canada, Italy and Japan are compiled in the database. The database includes eighteen natural and eight man-made deposits (one of the sites has two distinct sand layers) of soils ranging from predominantly quartz clean fine sands to fine silty sands. Properties of the natural and the man-made sand deposits are summarized in Tables 3.1 and 3.2, respectively. Thickness of the sand layers at the sites ranges from 0.9 to 11.0 m. Median grain size (D_{50}) of the sands ranges between 0.05 and 0.50 mm. Fines content (FC) in the sand deposits range from 0 to 15%. For two

of the sites where FC data are not available, apparent fines content values were calculated based on CPT data using the method developed by Robertson and Wride (1998).

Total unit weight (γ_t) of sands at the sites range between 16.4 and 19.6 kN/m^3. For the sites where γ_t data were not available, one of the following relationships was used to estimate γ_t (Mayne 2013):

$$\gamma_t = 8.32\log(V_S) - 1.61(z) \tag{3.1}$$

$$\gamma_t = 26 - \frac{14}{1 + [0.50\log(f_s + 1)]^2} \tag{3.2}$$

where z is the depth to the middle of the sand layer in meters and FS is the CPT sleeve friction in kPa. It can be seen from the available void ratio (e) and relative density (D_r) data in Tables 3.1 and 3.2 that values of e range from 0.51 to 0.85; and values D_r range from 20 to 75% at the sites. Values of specific gravity (G_S) of the sands fall within the typical range of 2.62 to 2.80.

As seen from Tables 3.1 and 3.2, the groundwater table was above the sand layer(s) at the time of geotechnical investigations at twenty sites. At the other five sites, the groundwater table was either in the middle or below the sand layers.

Table 3.1: Summary of soil properties of the natural sand deposits.

Study	Site	Location	GWT (m)	Depth range (m)	Sand description	Average $.D_{50}$ (mm)	FC (%)	γ_t (kN/m^3)	G_S	e	D_r (%)
Bruzzi et al. (1986); Bellotti et al. (1989); Fioravante et al. (1998)	Po River valley	Mantova, Italy	2.0	4.0-15.0	Predominantly quartz clean or slightly silty sand	0.30	0-12	18.5	NA*	NA	67± 7.6
Thormann (1990)	University of Michigan biological station	Cheboygan County, Michigan	Below test depth	2.0-4.6	Medium dense, medium to fine, poorly graded sand (SP)	NA	<5	17.1	2.65	e_{min} = 0.54, e_{max} = 0.82	NA
				4.6-6.6				17.2			
Fuhriman (1993); Pass (1994)	Treasure Island	San Francisco Bay, California	1.4	9.1-11.6	Grey silty fine sand (shoal material, SW-SM)	0.11	15	18.8	2.80	0.67	NA
Cunha (1994)	Laing bridge south approach embankment	Fraser River Delta, British Columbia, Canada	1.5	4.1-15.0	Predominantly (67.3%) quartz fine sand	0.31	<5	19.6	2.67	e_{min} = 0.51, e_{max} = 0.84	40-60
Ricceri and Simonini (1998); Ricceri et al. (2002)	Malamocco inlet	Venice, Italy	0.0	34.2-38.1	Fine sand	0.20	<5	18.6	NA	~0.70	NA
Benoit and Lutenegger (2000)	TAMU sand site	TAMU Riverside Campus, Texas	7.5	4.0-8.0	Very uniform fine grained clean sand	0.25	4	17.0	NA	NA	NA
Robertson et al. (2000)	Massey	Fraser River Delta, British Columbia, Canada	1.5	8.0-13.0	Clean quartz sand with small amount of mica and feldspar	0.20	<5	18.5	2.68	0.97	32.5
	Kidd		1.5	12.0-17.0		0.20	<5		2.72	0.98	29.4

Table 3.1: Summary of soil properties of the natural sand deposits (continued).

Study	Site	Location	GWT (m)	Depth range (m)	Sand description	Average D_{50} (mm)	FC (%)	γ_t (kN/m^3)	G_S	e	D_r (%)
Williamson (2013)	Gapway	South Carolina Coastal Plain	1.4	1.2-2.1	SP-SM/SC	0.20	2.3-6.9	16.4	NA	NA	NA
	Fort Dorchester		5.2	2.4-4.9	SC-SM	0.21	15	18.0	NA	NA	NA
Williamson and Gassman (2014); This study	Hollywood Dtich	South Carolina Coastal Plain	2.0	2.4-3.7	SP-SM	0.11	11	18.9	2.67	NA	NA
	Sampit		1.9	2.4-6.4	SP	0.18	4	18.9	2.65	NA	NA
	Four Hole Swamp		2.2	2.8-4.8	SP-SC	0.20	10	18.9	2.65	NA	NA
Boller (2008); Geiger (2010); This study	CREC	South Carolina Coastal Plain	1.0	2.7-3.4	SP-SM to SP	0.20	5	18.1	NA	NA	NA
	Hobcaw Borrow Pit		2.0	6.0-8.6	SP-SM to SP	0.23	3	19.2	NA	NA	NA
	Walterboro Rest Area		2.3	2.4-4.6	SP to SP-SM	0.18	7	18.9	NA	NA	NA
	Hobcaw Beach Ridge		0.4	2.6-4.6	NA	NA	9[†]	18.9	NA	NA	NA
	Walterboro Lowcountry		1.4	2.9-4.2	Sand to Silty sand	NA	5[†]	18.9	NA	NA	NA

[*]Not available.
[†]Apparent fines content.

Table 3.2: Summary of soil properties of the man-made sand deposits.

Study	Site	Location	GWT (m)	Depth range (m)	Sand description	Average D_{50} (mm)	FC (%)	γ_t (kN/m^3)	G_S	e	D_r
Hughes et al. (1977)	Tidal defence embankment	England	1.4	2.0-8.0	Loose, becoming medium dense to dense sand with occasional pockets and partings of organic silt	0.13	<5	19.0	NA*	NA	NA
Mitchell et al. (1994)	The Port of Oakland	San Francisco Bay, California	3.0	4.0-8.0	Poorly graded sand (SP) to sand with silt binder (SPSM)	0.30	<5	19.0	NA	NA	NA
	NGES at Northwestern University		3.0	2.0-8.8	Poorly graded clean sand (SP)	0.23	<5	18.9	2.66	NA	NA
Tanaka and Tanaka (1998)	Ohgishima	Kawasaki, Japan	2.0	4.0-11.0	Loose sand	0.25	<5	18.2	NA	NA	~20
Robertson et al. (2000)	Mildred lake	Alberta, Canada	21.0	27.0-37.0	Tailings sand (primarily quartz material)	0.16	10	18.5	2.66	0.77	43.6
	J-pit		0.5	3.0-7.0		0.17	15		2.62	0.76	42.7
	LL dam	British Columbia, Canada	2.1	6.0-10.0	Tailings sand (primarily quartz material)	0.20	8		2.66	0.85	40.3
	Highmont dam		4.0	8.0-12.0		0.25	10		2.66	0.83	37.4

*Not available.

3.3 Estimates of K_0

Summarized in Tables 3.3 and 3.4 are estimates of K_0 for the twenty-six natural and man-made sand deposits, along with age and stress history information. Overconsolidation ratio (*OCR*) data are mostly based on geologic history of the deposits and in some cases, from laboratory oedometer test results. As seen in Tables 3.3 and 3.4, most of the sand deposits are normally consolidated. The maximum value of *OCR* in any deposit is 4.0.

Values of K_0 in the sand layers are obtained from SBPMT, DMT-CPT-*OCR* and V_s test results by following the procedures discussed in Chapter 2. K_0 from SBPMT are available in eleven of the total twenty-six sand layers. Average K_0 from SBPMT varies between 0.40 and 0.80. DMT-CPT-*OCR* data are available for nineteen of the twenty-six sand layers. Horizontal stress index (K_D) varies between 1.6 and 15.8 and cone tip resistance (q_t) varies between 1.5 and 21.6 MPa in these layers. Estimates of K_0 from the DMT-CPT-*OCR* information using Equation 2.11 vary between 0.28 and 0.97. For nine sand layers values of V_{sHH}/V_{sHV} are available from crosshole V_s tests. Estimates of K_0 using Equation 2.18 and the V_s test results vary between 0.07 and 0.52, which are significantly lower than the estimates from SBPMT and DMT-CPT-*OCR* approach.

Table 3.3: Summary of soil age information and K_0 estimates from different methods in natural sand deposits.

Site	Depth range (m)	Approx. average geologic age (years)	Approx. average time since last liquefaction (years)	$(q_{t1N})_{cs}$	$(V_{S1})_{cs}$ (m/s)	*MEVR*	K_0 from SBPMT	K_D	*OCR*	q_t (Mpa)	K_0 from DMT-CPT-*OCR*[a]	V_{sHH}/V_{sHV}	K_0 from V_{sHH}/V_{sHV}[b]
Po River valley	4.0-15.0	<10,000	360[c]	90	177	1.01	0.65	8.0	1.50 (1.0-2.0)	9.0	0.73	0.96	0.48
University of Michigan biological station	2.0-4.6	9,700 (8,000-11,400)	No known liquefaction	75	204	1.20	NA*	6.8	2.1	4.5	0.72	NA	NA
	4.6-6.6			107	220			7.0	2.7	8.9	0.75		
Treasure Island	9.1-11.6	<8,000	2[d]	57	179	1.12	0.73	3.0	1.0	3.4	0.52	0.97	0.52
Laing bridge south approach embankment	4.1-15.0	<5,500	3,500[e]	73	170	1.01	0.80	NA	1.0	7.0	NA	NA	NA
Malamocco inlet	34.2-38.1	6,500[f]	1000[g]	111	235	1.27	0.46	3.0	2.50 (1.0-4.0)	19.3	0.58	NA	NA
TAMU sand site	4.0-8.0	50,000	No known liquefaction	117	222	1.18	NA	8.3	1.0	9.0	0.71	NA	NA
Massey	8.0-13.0	200[h]	No known liquefaction	66	177	1.02	0.40	NA	1.0	5.8	NA	NA	NA
Kidd	12.0-17.0	4,000[h]		77	158	1.04	0.64			8.5			

Table 3.3: Summary of soil age information and K_0 estimates from different methods in natural sand deposits (continued).

Site	Depth range (m)	Approx. average geologic age (years)	Approx. average time since last liquefaction (years)	$(q_{t1N})_{cs}$	$(V_{S1})_{cs}$ (m/s)	*MEVR*	K_0 from SBPMT	K_D	*OCR*	q_t (Mpa)	K_0 from DMT-CPT-*OCR*[a]	V_{sHH}/V_{sHV}	K_0 from V_{sHH}/V_{sHV}[b]
Gapway	1.2-2.1	450,000	1,660	84	194	1.11	NA	11.3	1.0	3.6	0.82	NA	NA
Fort Dorchester	2.4-4.9	200,000	5,000	135	NA	NA	NA	15.8	1.0	9.6	0.97	NA	NA
Hollywood Dtich	2.4-3.7	120,000-130,000[i]	126[j]	97	183	1.04	NA	6.9	1.0	7.5	0.61	0.79	0.10
Sampit	2.4-6.4	450,000[k,l]	500[m]	130	319	1.76	NA	10.0	1.0	6.6	0.83	0.88	0.24
Four Hole Swamp	2.8-4.8	≥1,000,000[n]	1,660[m]	48	189	1.14	NA	3.7	1.4	1.6	0.58	0.87	0.22
CREC	2.7-3.4	70,000-130,000[n]	No known liquefaction	108	223	1.20	NA	6.4	1.0	7.7	0.51	0.87	0.22
Hobcaw Borrow Pit	6.0-8.7	100,000-200,000[k,o]	No known liquefaction	81	194	1.10	NA	3.2	2.4	7.0	0.57	0.83	0.15
Walterboro Rest Area	2.4-4.6	≥1,000,000[n]	No known liquefaction	101	204	1.14	NA	9.8	1.6	7.1	0.79	0.75	0.07
Hobcaw Beach Ridge	2.6-4.6	59,000[k]	No known liquefaction	94	237	1.35	NA	6.6	1.0	5.3	0.59	NA	NA
Walterboro Lowcountry	2.9-4.2	450,000[n]	No known liquefaction	330	259	1.20	NA	6.3	2.3	21.6	0.32	NA	NA

[a]Equation 2.11; [b]Equation 2.18.
[c]Caputo et al. (2012); [d]Egan and Wang (1991); [e]Clague et al. (1992); [f]Brambati et al. (2003); [g]Carminati et al. (2007); [h]Wride et al. (2000); [i]Weems et al. (1986); [j]Obermeier et al. (1986, 1987); [k]Owens (1989); [l]Leon et al. (2006); [m]Talwani and Schaeffer (2001); [n]McCartan et al. (1984); [o]May (1978).
[*]Not available.

Table 3.4: Summary of soil age and K_0 from different methods in man-made sand deposits.

Site	Depth range (m)	Approx. average time since deposition (years)	Approx. average time since last liquefaction (years)	$(q_{t1N})_{cs}$	$(V_{S1})_{cs}$ (m/s)	*MEVR*	K_0 from SBPMT	K_D	*OCR*	q_t (Mpa)	K_0 from DMT-CPT-*OCR*[a]	V_{sHH}/V_{sHV}	K_0 from V_{sHH}/V_{sHV}[b]
Tidal defence embankment	2.0-8.0	<10	No known liquefaction	NA[*]	NA	NA	0.50	NA	1.0	NA	NA	NA	NA
The Port of Oakland	4.0-8.0	65	2	221	186	0.85	NA	5.6	1.0	9.0	0.58	0.90	0.29
NGES at Northwestern University	2.0-8.8	23	No known liquefaction	210	198	0.92	NA	1.6	1.0	17.4	0.28	NA	NA
Ohgishima	4.0-11.0	25	5	37	177	1.21	NA	1.8	1.0	3.6	0.46	NA	NA
Mildred lake	27-37	12[c]	No known liquefaction	92	158	0.89	0.40	NA	1.0	16.5	NA	NA	NA
J-pit	3-7	0.17[c]		56	131	0.82	0.50		1.0	1.5			
LL dam	6-10	5[c]		56	155	0.98	0.55		1.0	3.9			
Highmont dam	8-12	15[c]		58	143	0.89	0.62		1.0	5.1			

[a]Equation 2.11.
[b]Equation 2.18.
[c]Wride et al. (2000).
[*]Not available.

3.4 Variation of K_0 with Time

Tables 3.3 and 3.4 include the geologic age (or time since deposition) and the time since last known liquefaction event in the natural and man-made sand deposits, respectively. Values of geologic age for the compiled data range from 0.17 to over 1,000,000 years. For the eleven sites with known liquefaction, time since the occurrence of last liquefaction event range from 2 to 5,000 years.

Presented in Figure 3.1 are values of K_0 from SBPMT plotted against the average geologic age or time since deposition (t_1). Linear regression is used to fit relationship to all K_0-t_1 data pairs. The regression line can be expressed by:

$$K_0 = 0.041\log(t_1) + 0.477 \tag{3.3}$$

The coefficient of determination (r^2) associated with Equation 3.3 is 0.27. This moderately low value of r^2 reflects significant scatter in the data. Equation 3.3 indicates about a 4% increase in K_0 over one log cycle of time.

Figure 3.2 presents values of K_0 from DMT-CPT-*OCR* plotted against t_1. The regression line for all K_0-t_1 data pairs can be expressed by:

$$K_0 = 0.054\log(t_1) + 0.390 \tag{3.4}$$

r^2 associated with Equation 3.4 is 0.21, reflecting an even greater scatter in the DMT-CPT-*OCR* estimates of K_0 than in the SBPMT estimates of K_0. Equations 3.4 indicate about 5% increase in K_0 over one log cycle of time. Comparing the regression lines plotted in Figures 3.1 and 3.2, the line based on DMT-CPT-*OCR* provides slightly higher estimates of K_0 than the line based on SBPMT.

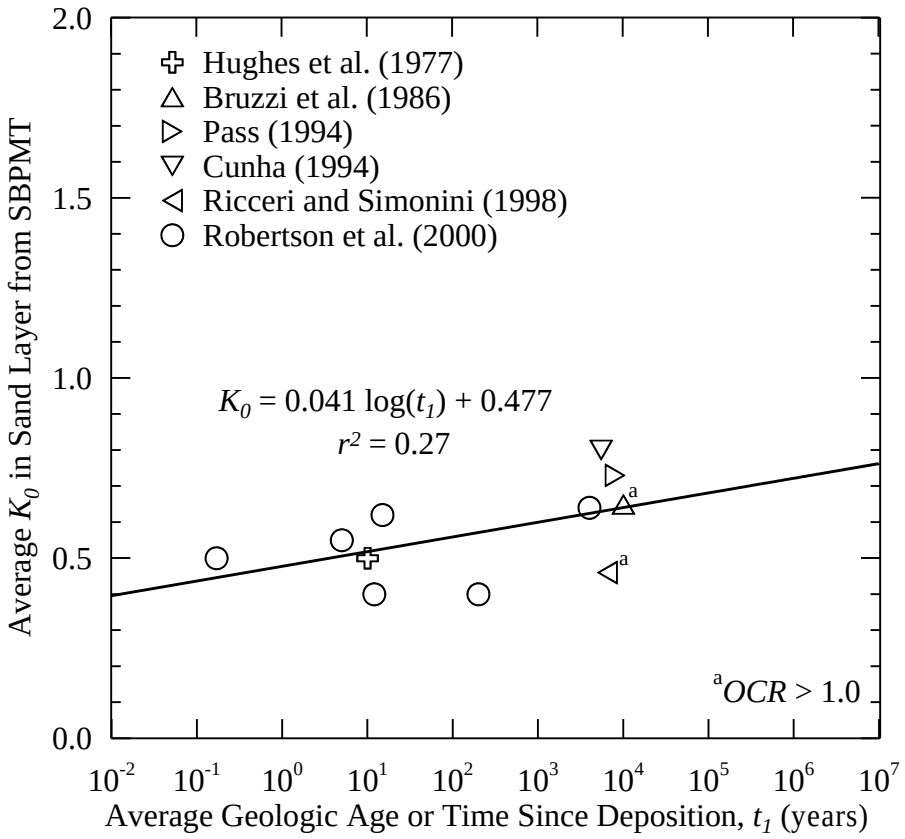

Figure 3.1: Variation of K_0 from SBPMT with the geologic age or time since deposition of sand deposits.

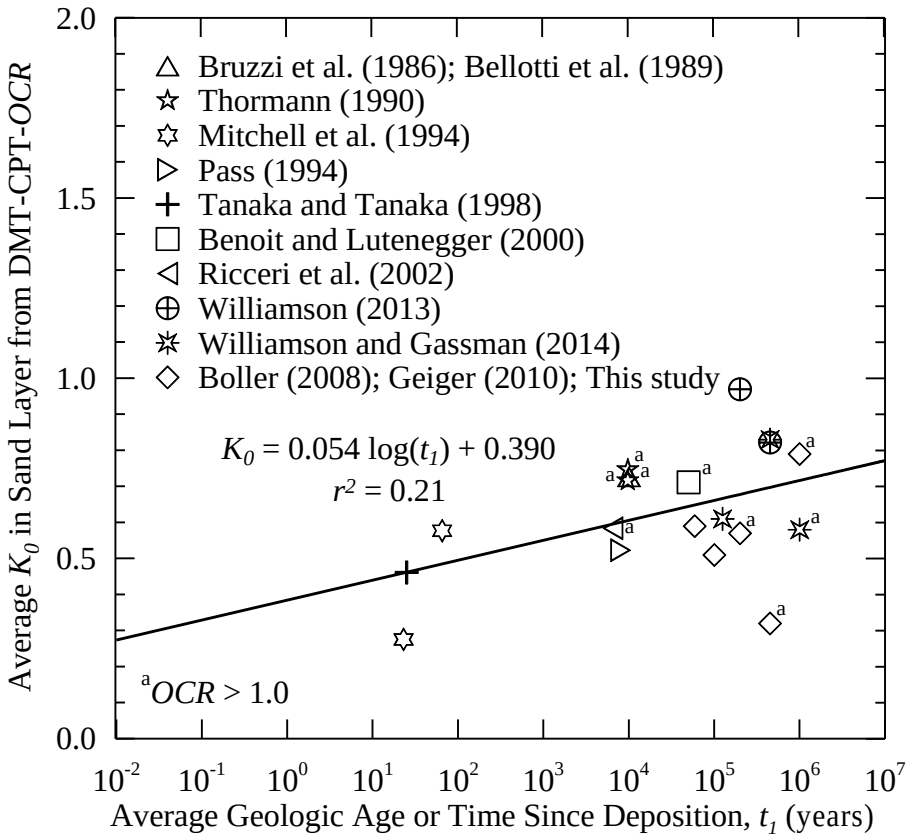

Figure 3.2: Variation of K_0 from DMT-CPT-*OCR* with the geologic age or time since deposition of sand deposits.

As mentioned earlier, K_0 is influenced by the stress history of soil. Thus, part of the scatter in the K_0-time plots in Figures 3.1 and 3.2 may be due to the difference in *OCR*. However, more data is needed to determine the influence of stress history on the in situ K_0 in sands.

Figure 3.3 presents the estimates of K_0 from V_s tests using Equation 2.18 plotted against t_1. As seen from Figure 3.3, the values of K_0 are significantly lower than the typical K_0 in sands.

The ratios of V_{sHH} to V_{sHV} in the sand layers are plotted against t_1 and t_2 in Figures 3.4a and b, respectively. As seen from both Figures 3.4a and b, V_{sHH}/V_{sHV} exhibits a slight decreasing trend with time. These results suggest that both V_{sHH} and V_{sHV} increase at similar rates with time and therefore, the influence of age is cancelled out in the ratio. Thus, Equation 2.18 gives the K_0 estimates in freshly deposited sands. For estimating K_0 in aged sands, an age term is needed in the predictive relationship. Assuming the rate of increase in K_0 with age from the SBPMT data, and an average anisotropic ratio of 1.0 and n of 0.125 based on the nine field cases with available V_{sHH}/V_{sHV} data, Equation 2.18 can be rewritten as:

$$K_0 = 0.041\log(t_1) + \left(1.0\frac{V_{sHH}}{V_{sHV}}\right)^{(1/0.125)} = 0.041\log(t_1) + \left(\frac{V_{sHH}}{V_{sHV}}\right)^{8.0} \qquad (3.5)$$

Presented in Figure 3.5 are the estimates of K_0 using Equation 3.5 plotted against t_1. As seen from Figure 3.5, the values of K_0 vary from 0.35 to 0.94, which are within the typical range for natural sands. Henceforth, Equation 3.5 will be used for estimating K_0 from V_S tests in this report.

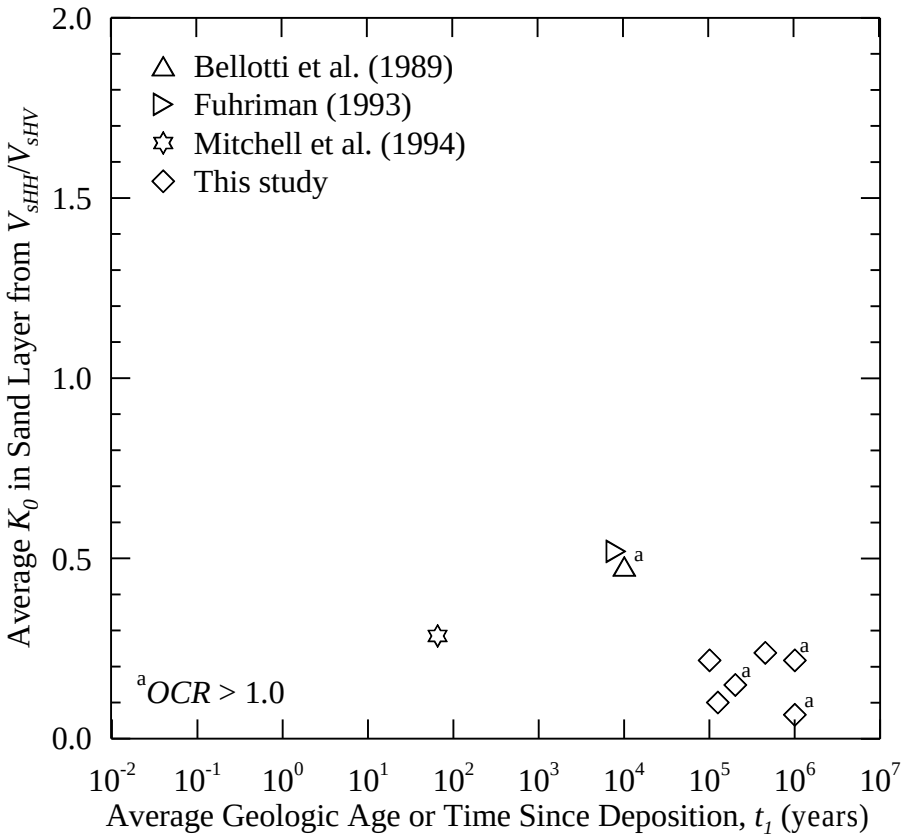

Figure 3.3: Variation of K_0 from V_S tests using Equation 2.18 with the geologic age or time since deposition of sand deposits.

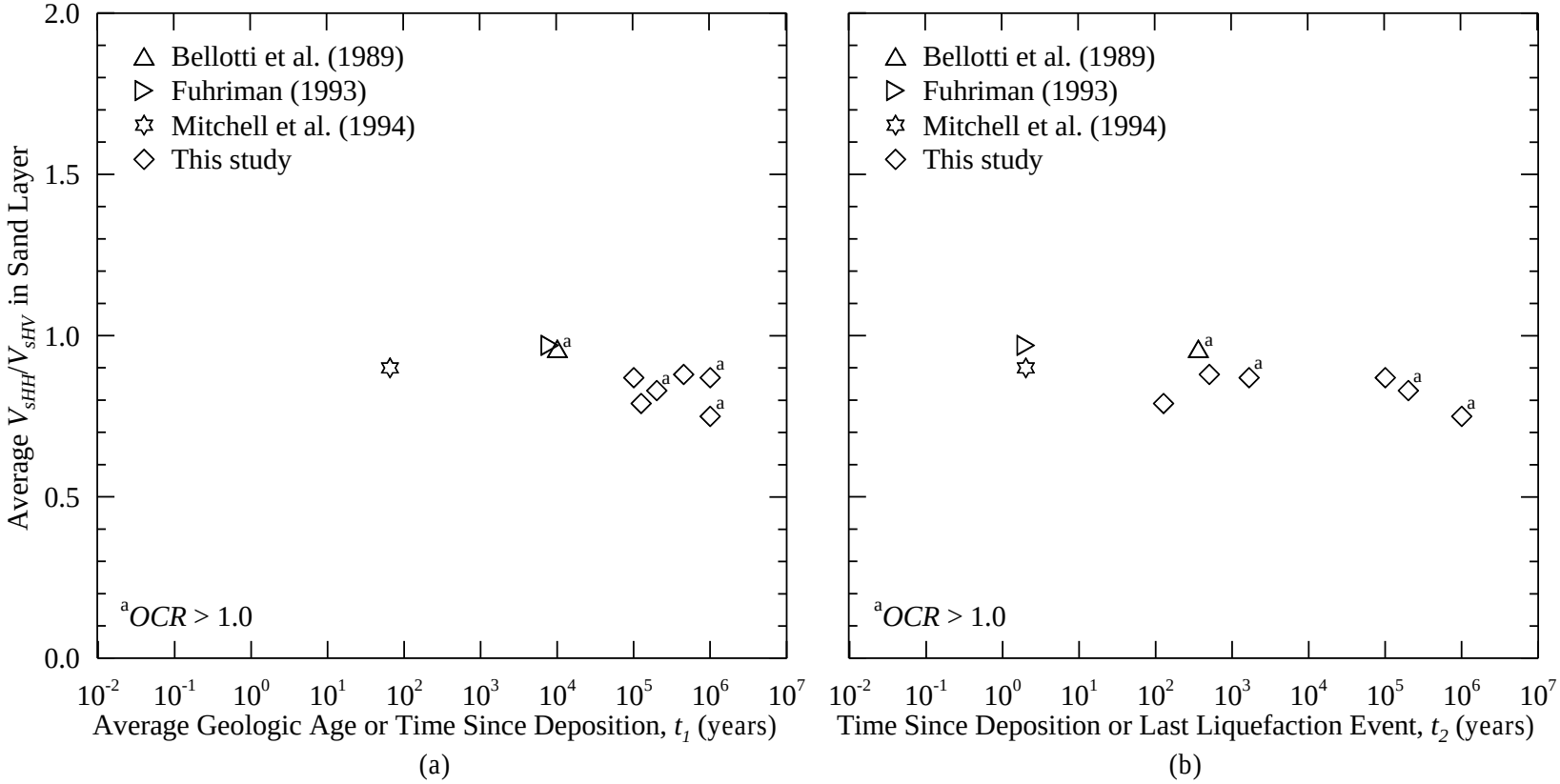

Figure 3.4: Variation of V_{sHH}/V_{sHV} in sand layers with (a) geologic age, and (b) time since deposition or last liquefaction event.

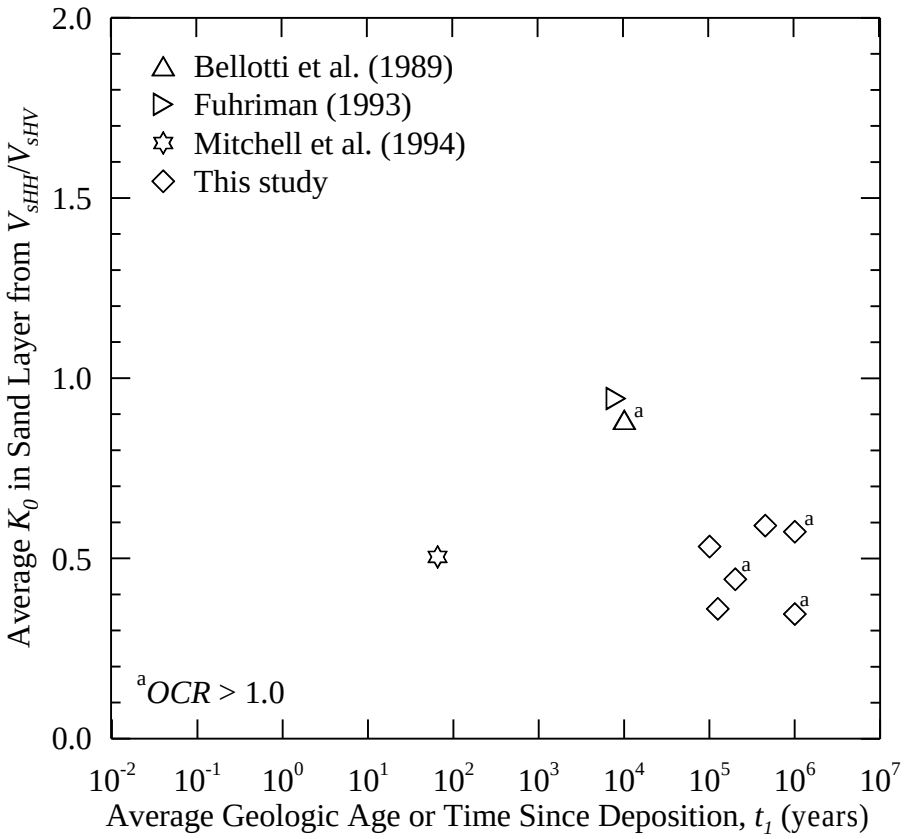

Figure 3.5: Variation of K_0 from V_S tests using Equation 3.5 with the geologic age or time since deposition of sand deposits.

In Figure 3.6, values of K_0 from SBPMT are plotted against the time since deposition at sites with no evidence of liquefaction or time since last liquefaction event at sites where liquefaction occurred in the past(t_2). The regression line for all K_0-t_2 data pairs can be expressed by:

$$K_0 = 0.024 \log(t_2) + 0.528 \quad (3.6)$$

r^2 associated with Equation 3.6 is 0.06, which is very low and suggests major scatter in the data.

In Figure 3.7, values of K_0 from DMT-CPT-*OCR* are plotted against t_2. The regression line for all K_0-t_2 data pairs can be expressed by:

$$K_0 = 0.024 \log(t_2) + 0.538 \quad (3.7)$$

r^2 associated with Equation 3.7 is 0.07, reflecting about equal scatter in the DMT-CPT-*OCR* estimates of K_0. Comparing the regression lines plotted in Figures 3.6 and 3.7, the lines based on DMT-CPT-*OCR* and SBPMT provide very similar estimates of K_0; and increase about 2% per log cycle of time.

Part of the scatter in the K_0-time plots in Figures 3.6 to 3.7 may be due to the difference in *OCR*. However, more data with varying *OCR* values is needed to determine the influence of stress history on the in situ K_0 in sands.

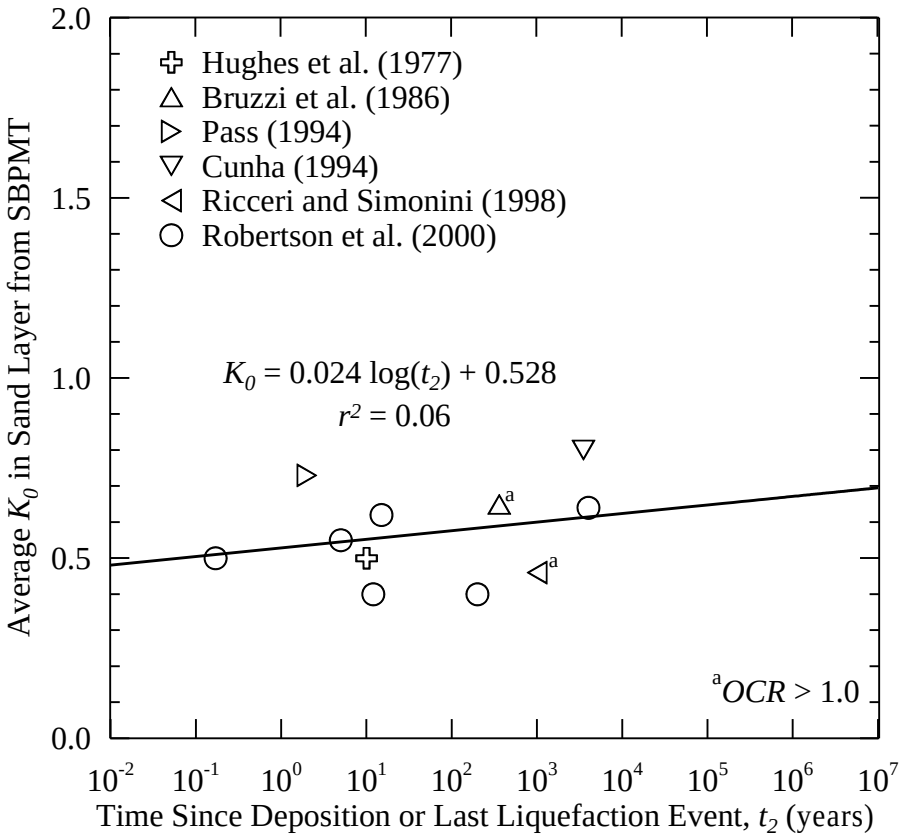

Figure 3.6: Variation of K_0 from SBPMT with the time since deposition or last liquefaction event in sand deposits.

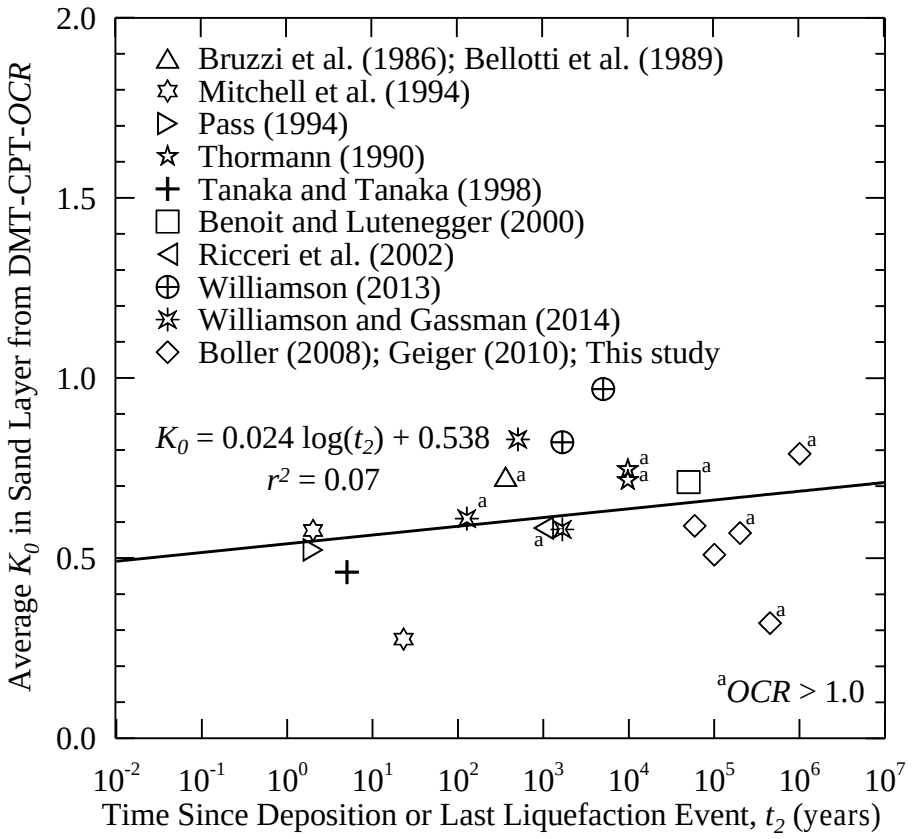

Figure 3.7: Variation of K_0 from DMT-CPT-*OCR* with the time since deposition or last liquefaction event in sand deposits.

3.5 Measure to Estimated Velocity Ratio

The measured to estimated velocity ratio (*MEVR*) is defined as the ratio of measured V_S to estimated V_S based on relationships with penetration (CPT or SPT) resistances. *MEVR* was proposed by Andrus et al. (2009) as a proxy physical measure of degree of aging (or diagenesis) in sands where the geologic age or time since the occurrence of last liquefaction event is not readily available. Based on 91 penetration resistance-V_S data pairs from Holocene, Pleistocene and Tertiary sand deposits, Andrus et al. (2009) suggested the following *MEVR*-t_2 relationship:

$$MEVR = 0.0820 \log_{10}(t_2) + 0.935 \tag{3.8}$$

Values of *MEVR* are calculated using available V_S and cone tip resistance data for the sand deposits compiled in the database. Measured V_S data are from seismic crosshole, or downhole, or seismic CPT tests. Estimated V_S data are obtained using the following relationship developed by Andrus et al. (2004):

$$(V_{S1})_{cs} = 62.6\left[(q_{t1N})_{cs}\right]^{0.231} \tag{3.9}$$

where, $(V_{S1})_{cs}$ and $(q_{t1N})_{cs}$ are normalized V_S and CPT tip resistance corrected to equivalent clean sand value, respectively. As seen in Tables 3.3 and 3.4, values of $(q_{t1N})_{cs}$ range from 37 to 221; and $(V_{S1})_{cs}$ range from 131 to 319 m/s in the sand layers. Values of *MEVR* for the sand layers vary between 0.82 and 1.76.

The *MEVR*-t_2 data pairs from Tables 3.3 and 3.4 (except the data pairs common with Andrus et al. (2009) dataset) are plotted in Figure 3.8 along with the relationship expressed in Equation 3.8. As seen in Figure 3.8, most of the new data points plot within one standard deviation from the mean curve expressed by Equation 3.8.

In Figure 3.9, values of K_0 from SBPMT are plotted against *MEVR*. The regression line for all K_0-*MEVR* data pairs can be expressed by:

$$K_0 = 0.128MEVR + 0.447 \tag{3.10}$$

r^2 associated with Equation 3.10 is 0.01, which reflects major scatter in the data.

In Figure 3.10, values of K_0 from DMT-CPT-*OCR* are plotted against *MEVR*. The regression line for all K_0-*MEVR* data pairs can be expressed by:

$$K_0 = 0.252\log MEVR + 0.317 \tag{3.11}$$

r^2 associated with Equation 3.11 is 0.10, reflecting major scatter in the DMT-CPT-*OCR* estimates of K_0. Comparing the regression lines plotted in Figures 3.9 and 3.10, the line based on DMT-CPT-*OCR* provides higher estimates of K_0 than the line based on SBPMT.

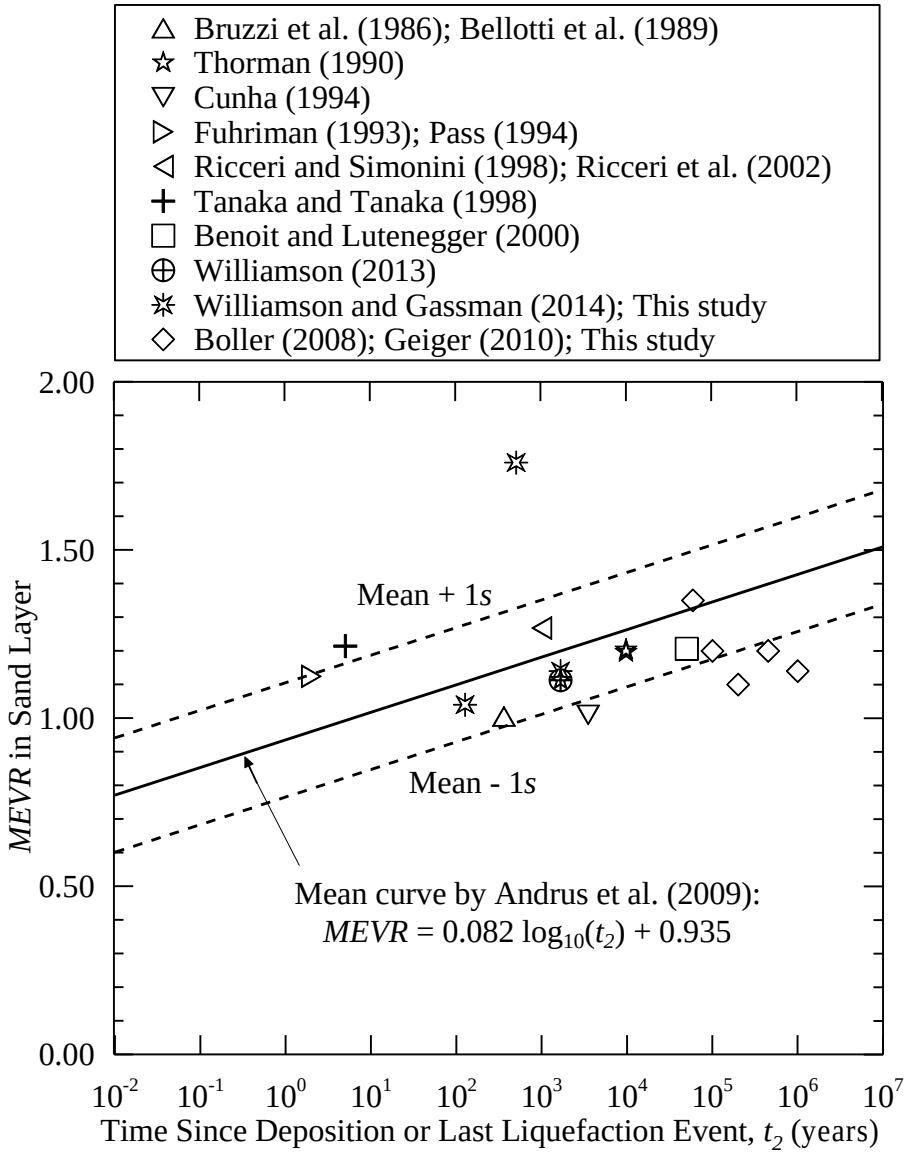

Figure 3.8: Variation of *MEVR* with time.

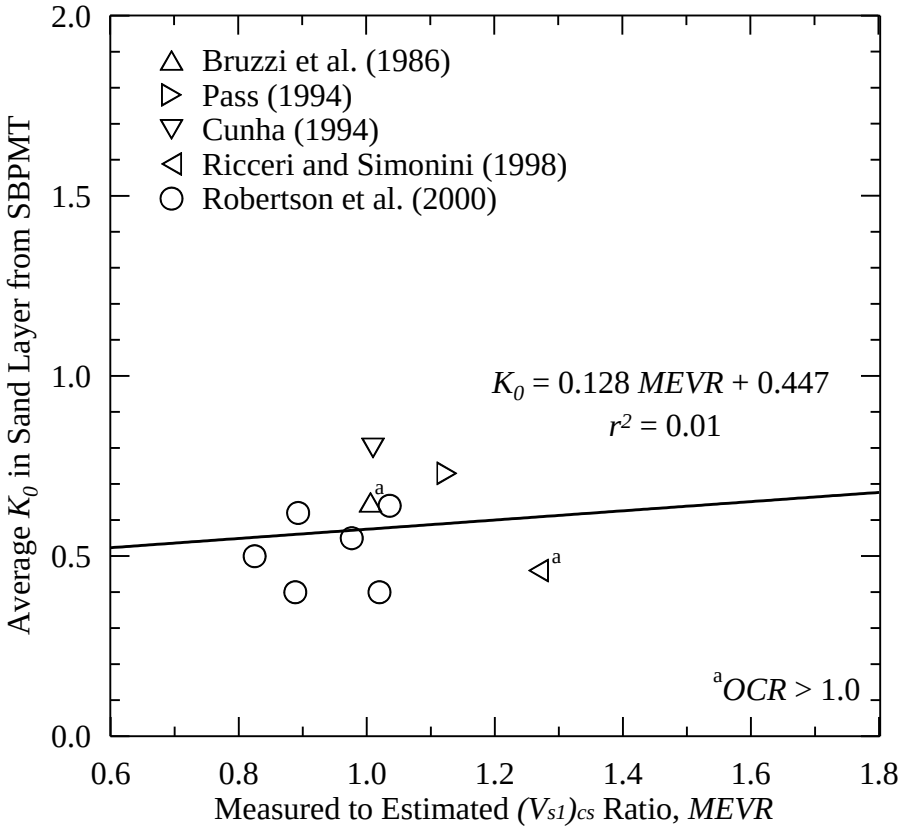

Figure 3.9: Variation of K_0 from SBPMT with measured to estimated $(V_{s1})_{cs}$ ratio in sand deposits.

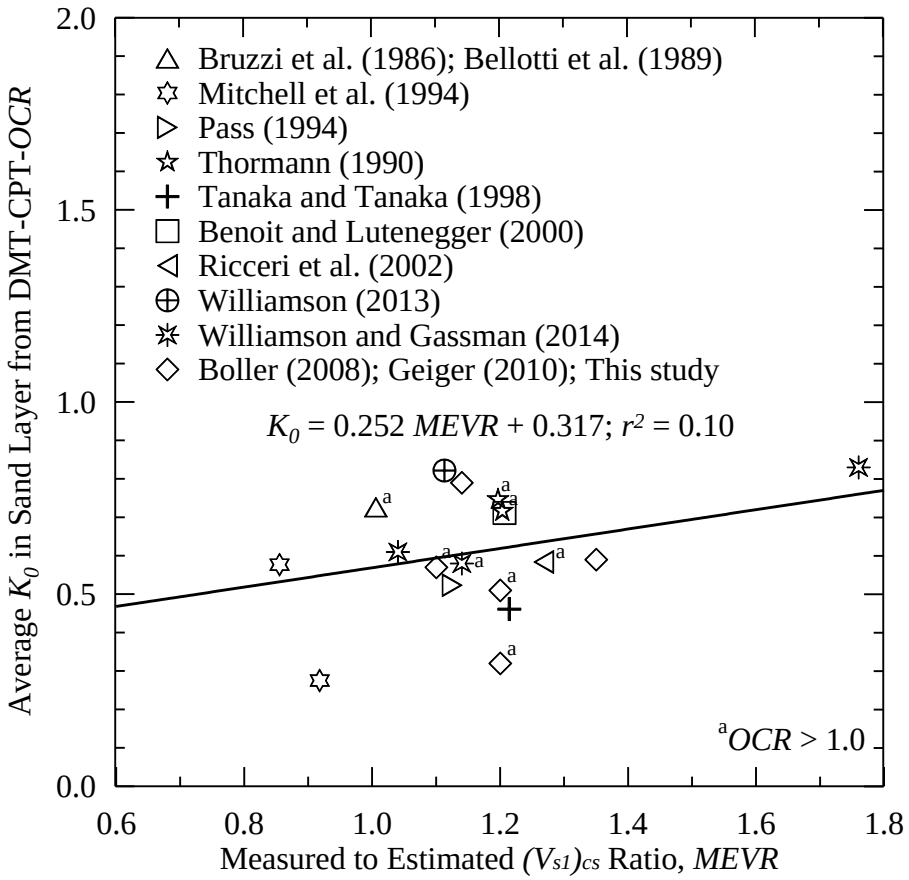

Figure 3.10: Variation of K_0 from DMT-CPT-*OCR* with measured to estimated $(V_{s1})_{cs}$ ratio in sand deposits.

3.6 Effect of Seismicity on K_0

In order to evaluate the possible effect of seismicity on K_0 in the sand layers, average estimates of K_0 based on SBPMT and DMT-CPT-*OCR* are plotted in Figure 3.11 versus peak ground acceleration (*PGA*) for soft rock outcropping condition and 10% probability of exceedence in 50 years for sites in North America. The values of *PGA* for sites in the United States are estimated using US Geological Survey 2002 deaggregation map (accessed June, 2014). *PGA*s for sites in Canada are estimated based on 2010 National Building Code of Canada seismic hazard calculator (accessed June, 2014). *PGA*s at these sites range from 0.10 to 0.50 g.

As can be seen in Figure 3.11, K_0 values are equally scattered over the range of *PGA*s showing no distinct trend in the data. Thus the data does not support higher K_0 values in sand deposits in region of greater seismicity.

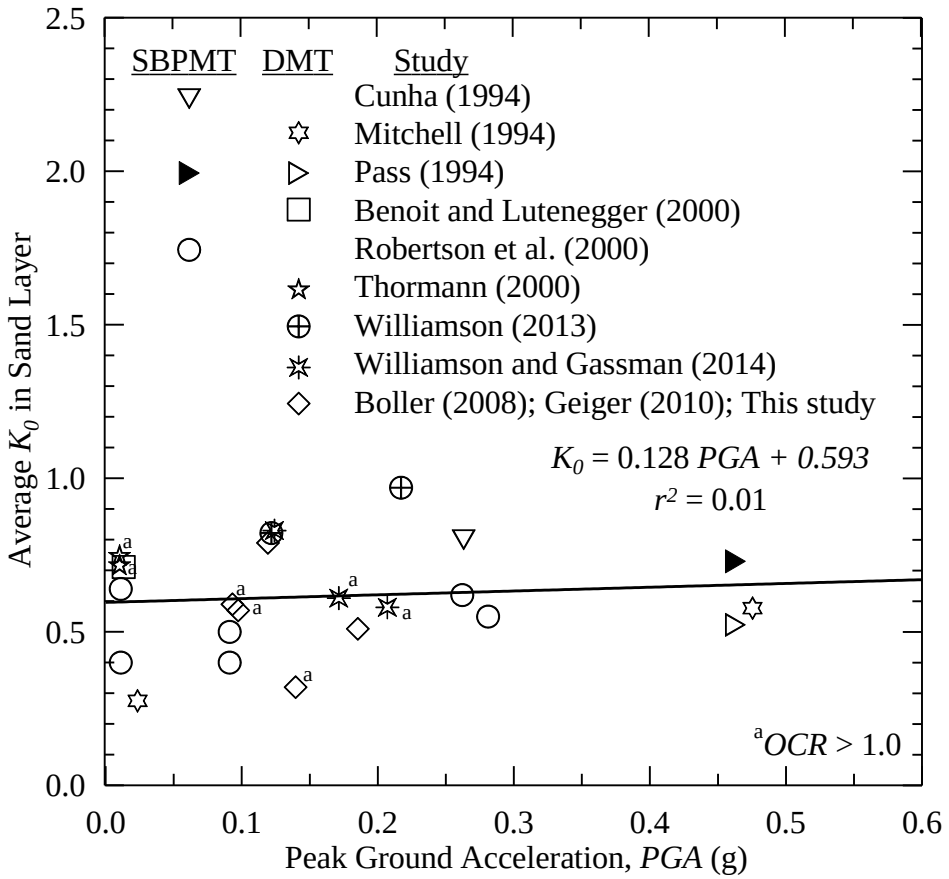

Figure 3.11: Variation of K_0 with *PGA* for 10% probability of exceedance in 50 years at sites in North America.

3.7 Summary

K_0 calculated from SBPMT, DMT-CPT-*OCR* and V_S test results in natural and man-made sand deposits are compared in this chapter. The following conclusions can be made based on the finding from this chapter:

- Estimates of K_0 based on SBPMT and DMT-CPT-*OCR* increase at about the same rate – 2 to 5% per log cycle of time. Estimates of K_0 based on SBPMT and DMT-CPT-*OCR* exhibit similar significant scatter.
- Scatter in the plotted K_0-time data appeared to increase when time since last liquefaction event was used.
- An improved relationship for estimating in situ K_0 from V_S tests was suggested by adding an age term.
- Data compiled in this study provided independent support for the time versus *MEVR* relationship proposed by Andrus et al. (2009).
- Estimates of K_0 based on SBPMT and DMT-CPT-*OCR* increase at a similar rate with *MEVR*, but exhibit just as much scatter as K_0 data plotted versus time since last liquefaction event.
- Some of the scatter of K_0 estimates versus time plots may be explained by difference in *OCR*, but there was insufficient data to quantify its influence.
- Estimates of K_0 do not exhibit any increase with regional seismicity.

CHAPTER 4

REVIEW OF STUDIES ON EFFECTS OF ANISOTROPY ON LIQUEFACTION RESISTANCE

4.1 Introduction

Sand is an anisotropic material. The study by Casagrande and Carillo (1944) was one of the first to distinguish anisotropy in sand into two categories – (1) fabric anisotropy and (2) stress-induced anisotropy. Fabric anisotropy is also commonly referred as the structural or inherent anisotropy. The term 'fabric' is used to describe the spatial arrangement of soil particles and pores in soil which is determined by the particle shape, contact orientation, granular packing, roughness of particles, and depositional history and pattern (Brewer 1964; Johansson 1965; Phillips and May 1967; Parkin et al. 1968; Arthur and Menzies 1972; Oda 1972; Mahmood and Mitchell 1974; Santamarina 2004).

Stress-induced anisotropy is due to the strain caused by an applied stress and therefore, a function of stress history (Arthur et al. 1977; Oda et al. 1985; Wong and Arthur 1985; Zeng and Ni 1999; Hu et al. 2010). Anisotropic consolidation and overconsoildation ratio (*OCR*) are two important factors that contribute to the stress-induced anisotropy in soil (Zeng and Ni 1999; Yamashita et al. 2005).

In this chapter, previous studies to characterize the effects of fabric anisotropy, anisotropic consolidation and *OCR* on the liquefaction resistance of sands are reviewed.

4.2 Effects of Fabric Anisotropy

The effect of fabric anisotropy on static behavior of sands such as shear strength, bearing capacity, and other elastic and plastic properties has long been recognized by numerous researchers using simple shear test (Philip and May 1967; El-Sohby and Andrawes 1973; Mahmood and Mitchell 1974; Guo 2008), conventional triaxial test (Oda 1972a & b; Arthur and Menzies 1972; El-Sohby and Andrawes 1973; Arthur and Philips 1975; Oda and Koshikawa 1977) and true triaxial test (Kjellman 1936; Ramumurthy 1970; Miyamori 1976). Studies involving seismic wave measurement in horizontal and vertical plains provide insights into the effect of fabric anisotropy on small strain dynamic properties of sands as discussed in Chapter 2.

Subsequently, many researchers investigated the effect of fabric anisotropy on large strain behavior such as liquefaction resistance of sands (Mitchell et al. 1978; Mulilis et al. 1977; Nemat-Nasser and Tobita 1982; Yu et al. 2013). Mitchell et al. (1978) and Mulilis et al. (1977) performed undrained stress controlled cyclic triaxial tests and showed that the orientation and arrangement of the contacts between sand grains caused significant change in liquefaction resistance. Nemat-Nasser and Tobita (1982) performed a series of tests in a cyclic simple shear device and showed that liquefaction resistance increases with increasing angles between the sliding and the microscopic shearing directions. Yu et al. (2013) performed a series of earthquake centrifuge tests on samples prepared with different deposition angles (angle between longest axes of particles and vertical axis, θ) and showed that samples with $\theta = 90^{\circ}$ had high liquefaction resistance, while samples with $\theta = 0^{\circ}$ were highly unstable.

4.3 Effects of Anisotropic Consolidation

Salgado et al. (1997) provided a comprehensive review of laboratory studies investigating effects of anisotropic consolidations on liquefaction resistance of both normally consolidated and overconsolidated sands. Table 4.1 summarizes four laboratory studies on three different types of normally consolidated sands. General test procedures in these studies involved (1) preparing specimens with varying relative density (D_r) by pluviation of dry sand through air from different heights, (2) permeating de-aired water through the specimen and regulating the back pressure to obtain saturation, (3) application of vacuum or circulation of carbon dioxide gas through the specimen to aid the saturation process, (4) consolidating the specimen to desired K_0, and (5) cyclic torsional shear testing under undrained condition to determine cyclic strength of soil. As seen from Table 4.1, D_r of sand specimens tested in the studies ranged from 27 to 95% and K_0 ranged from 0.6 to 2.0.

Table 4.1: Summary of laboratory studies on liquefaction resistance of anisotropically consolidated sands after Salgado et al. (1997).

Study	Sand type	D_r (%)	K_0	Test type
Ishibashi and Sherif (1974)	Ottawa sand	27, 41	0.6, 0.75, 1.0	Torsional simple shear
Ishihara et al. (1977)	Fuji river sand	55	0.5, 1.0, 1.5	Triaxial torsional shear
Ishihara et al. (1985)	Toyoura sand	43-95	0.5, 0.75, 1.0	Triaxial torsional shear
Yamashita and Toki (1993)	Toyoura sand	80	0.5, 1.0, 2.0	Triaxial torsional shear

In the studies listed in Table 4.1, cyclic torsional shear testing was carried out with designated cyclic stress ratio (τ/σ'_{v0}) and sinusoidal cycles of 0.1 to 2.0 Hz, where τ is maximum single amplitude of horizontal cyclic shear stress, σ'_{v0} is initial effective vertical confining pressure. Ishibashi and Sherif (1974) considered cyclic strength as τ/σ'_{v0} at the first point where pore water pressure (u_0) decreases while shear stress remains nearly constant. Ishihara et al. (1977) referred to cyclic strength as τ/σ'_{v0} required to induce u_0 equal vertical stress. Ishihara et al. (1985) and Yamashita and Toki (1993) referred to cyclic strength as τ/σ'_{v0} required to induce a double amplitude shear strain of 5% and 7.5%, respectively. Because this cyclic strength represents the liquefaction resistance of soil, it is henceforth referred as cyclic resistance ratio (*CRR*).

Figure 4.1 presents the results of cyclic torsional shear tests on Fuji river sand by Ishihara et al. (1977). In Figure 4.1(a), *CRR* values are plotted against number of cycles to cause initial liquefaction for both isotropically and anisotropically consolidated specimens. As seen from the trend lines plotted in Figure 4.1(a), *CRR* of soil increases as K_0 increases. However, when the *CRR* values are normalized by the factor [$(1+2K_0)/3$] as shown in Figure 4.1(b), a single trend line can capture the variation in all of the test data. The same conclusion was made in all four studies listed in Table 4.1, which led to the following unique relationship between *CRR* of anisotropically consolidated sand (CRR_A) and *CRR* of isotropically consolidated sand (CRR_I) (Ishihara et al. 1977):

$$CRR_A = \frac{1+2K_0}{3} CRR_I \qquad (3.1)$$

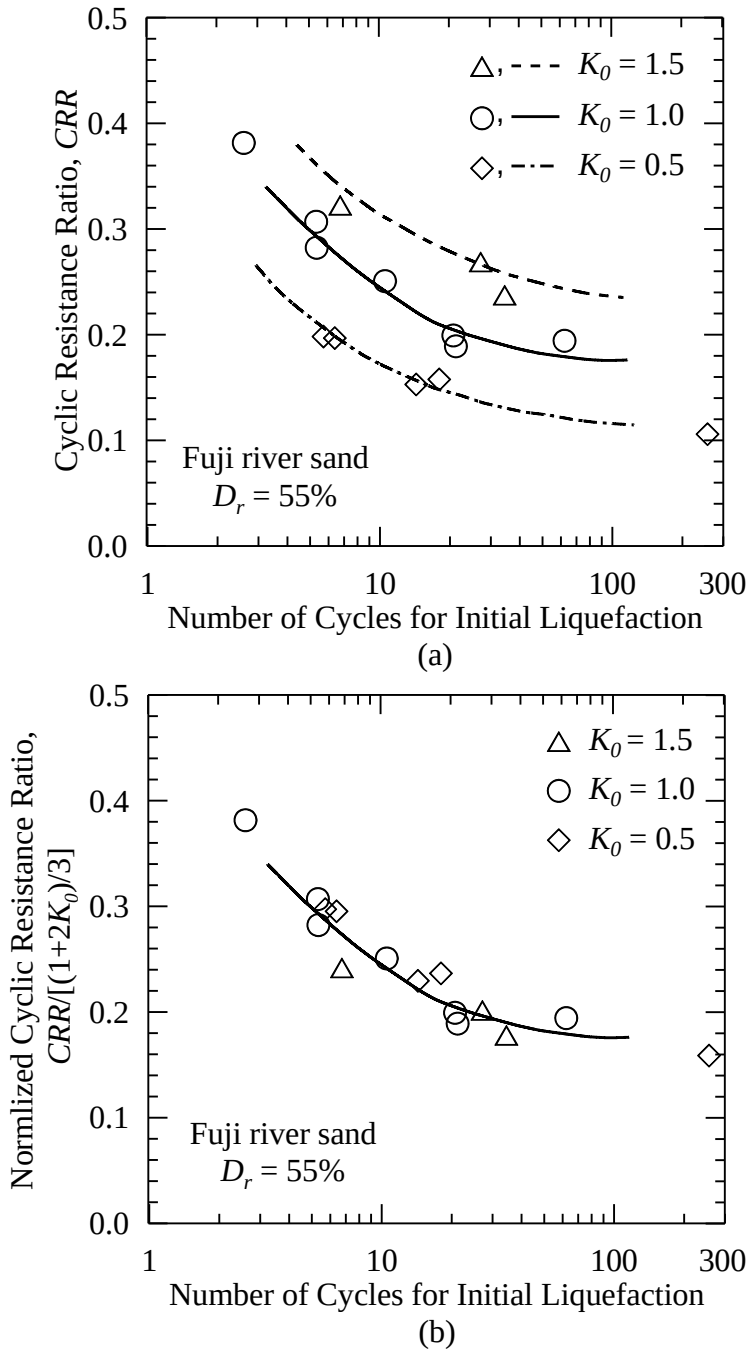

Figure 4.1: Results of cyclic triaxial torsional shear tests on hollow cylindrical specimens of Fuji river sand: (a) cyclic resistance ratio versus number of cycles and (b) cyclic resistance ratio normalized by $[(1+2K_0)/3]$ versus number of cycles reproduced from Ishihara et al. (1977).

Salgado et al. (1997) developed a systematic procedure to correct the CPT-based liquefaction charts by considering separately the effects of K_0 on *CRR* and q_t, which can be can be summarized as follows:

(1) Estimate or measure the in situ K_0 and the expected value of K_0 at normally consolidated state or a stress state similar to the case history conditions for liquefaction charts, denoted as $K_{0,NC}$.

(2) Estimate the in situ D_r using the $\sigma_h^{'}/P_a$ - q_t/P_a -D_r relationships based on the results from about 400 calibration chamber tests and a numerical code called 'CONPOINT'.

(3) Using the value of D_r, obtain the normalization factors for $\sigma_v^{'}$ and $\sigma_h^{'}$ (C_{NV} and C_{NH}, respectively) from the charts developed using 'CONPOINT' and calculate the normalized tip resistance ($q_{t1K_{0,NC}}$) as:

$$q_{t1K_{0,NC}} = C_{NV} C_{NH} q_t \tag{3.2}$$

(4) Using the value of $q_{t1K_{0,NC}}$, obtain the corresponding value of $CRR_{K_{0,NC}}$ from CPT-based liquefaction chart.

(5) Estimate the *CRR* corrected for K_0 (CRR_{K_0}) as:

$$CRR_{K_0} = \frac{1+2K_0}{1+2K_{0,NC}} CRR_{K_{0,NC}} \tag{3.3}$$

Because the charts are mostly based on case histories of normally consolidated soils with K_0 of about 0.5 (i.e., $K_{0,NC}$ = 0.5), Equation 3.3 can be re-written as :

$$CRR_{K_0} = \left(\frac{1+2K_0}{2}\right) CRR_{0.5} = K_{K0} CRR_{0.5} \tag{3.4}$$

where K_{K0} is the correction factor for K_0 conditions.

4.4 Effects of Overconsoildation Ratio

Laboratory studies were conducted by several researchers (Sherif et al. 1974; Ishihara and Takatsu 1979; Bhatia 1982) to investigate the increase in K_0 due to overconsoildation. These studies involved (1) producing an initial K_0 condition in the sample, (2) consolidating the sample to desired *OCR* while preventing any lateral displacement from occurring, and (3) determining the final K_0 from the value of lateral stress after overconsoildation. The following relationship between the K_0 of the normally consolidated sample (the initial K_0) and the overconsolidated sample (K_0^*) has been suggested from these studies:

$$K_0^* = OCR^a K_0 \tag{3.5}$$

where the value of exponent *a* can vary between 0.68 and 0.84.

Several researchers investigated the combined effects of *OCR* and K_0 on cyclic resistance of sands (Seed and Peacock 1971; Ishihara and Takatsu 1979; Finn 1981; Bhatia 1982). These studies indicated that the entire effect of overconsolidation cannot be explained simply in terms K_0 (or K_0^*) expressed by Equation 3.1. Table 4.2 summarizes two such studies on two types of sands.

Figure 4.2 presents the results of constant-volume cyclic simple shear tests on Ottawa sand by Bhatia (1982) where the values of *OCR* ranged from 1 to 4 and the corresponding values of K_0^* ranged from 0.39 to 0.93. In Figure 4.2 (a), *CRR* values are

plotted against number of cycles to cause initial liquefaction for both normally consolidated and overconsolidated specimens. When the *CRR* values are normalized by the factor [(1+2 K_0^*)/3] as shown in Figure 4.2 (b), separate trend lines for test data with different *OCR* values indicate the additional increase in liquefaction resistance due to overconsolidation. This additional increase ranges from 10 to 40 % at an *OCR* of 2 and from 25 to 100% at an *OCR* of 4, which can be attributed to a more stable rearrangement in particle structures during the process of overconsoildation (Bhatia 1982).

Figure 4.3 presents the ratio of *CRR*/[(1+2 K_0^*)/3] causing initial liquefaction in 20 cycles for overconsolidated specimens to that for normally consolidated specimens (CRR_{OC}/CRR_{NC}) plotted versus the values of *OCR*. The results of cyclic torsional shear tests on Fuji river sand by Ishihara and Takatsu (1979) are included in Figure 4.3 along with the test results by Bhatia (1982). As mentioned in Table 4.2, Ishihara and Takatsu (1979) prepared the overconsolidated specimens while keeping the values of K_0 constant during the overconsolidation (i.e., $K_0^* = K_0$), where the values of *OCR* ranged from 1 to 4 and the values of K_0^* (= K_0) ranged from 0.5 to 1.5. From Figure 4.3, the following approximate relationship between CRR_{OC}/CRR_{NC} and *OCR* after the K_0 correction is found representing an array of curves:

$$CRR_{OC} = OCR^m CRR_{NC} = K_{OCR} CRR_{NC} \tag{3.6}$$

where the exponent *m* is equal to 0.25 for the Bhatia (1982) data and varies from 0.50 to 0.75 for the Ishihara and Takatsu (1979) data. Alternatively, Salgado et al. (1997) suggested the following relationship between CRR_{OC}, CRR_{NC} and *OCR* after the K_0

Table 4.2: Summary of laboratory studies on liquefaction resistance of overconsolidated sands.

Study	Test method	Sand tested	Mean diameter D_{50} (mm)	Consolidation process	Duration of overcon-solidation	K_0 before overcon-solidation	K_0 after overcon-solidation (K_0^*)	Conditions during testing	Range of *OCR*	Exponent *m*
Ishihara and Takatsu (1979)	Cyclic torsional shear	Fuji river sand	0.40	Effective confining pressure was increased and then, decreased to achieve the desired *OCR*. K_0 was kept constant throughout the process.	2 days	0.5	0.5	Stress controlled, constant volume and no lateral displacement allowed	1 to 4	0.75
						1.0	1.0		1 to 4	0.50
						1.5	1.5		1 to 4	0.50
Bhatia (1982)	Cyclic simple shear	Ottawa sand	0.40	Effective vertical pressure was increased and then, decreased to achieve the desired *OCR*. Change in Lateral stress was monitored throughout the process.	NA*	0.416	0.39	Stress controlled and constant volume	1	0.25
						0.412	0.67		2	
						0.406	0.83		3	
						0.398	0.93		4	

*Not available

correction:

$$CRR_{OC} = CRR_{NC} + bCRR_{NC}(OCR^{0.50} - 1) \quad (3.7)$$

with *b* being between 0.25 and 1.0.

Because the laboratory test condition (increased K_0 due to overconsolidation) adopted in Bhatia (1982) is a more realistic representation of in situ cases, it is appropriate to use Equation 3.6 with *m* equals 0.25 for correcting liquefaction resistance due to overconsoildation. Moreover, values of CRR_{OC} using Equation 3.6 with *m* equals 0.25 agree with the lower bound values from Equation 3.6, giving the most conservative estimates. Thus, the relationship for K_{OCR} recommended in this study is as follows:

$$K_{OCR} = OCR^{0.25} \quad (3.8)$$

As a final note, Salgado et al. (1997) concluded that no modification is necessary to the normalized cone tip resistance ($q_{t1K_{0,NC}}$) due to overconsoildation because calibration chamber studies (Baldi et al. 1983, Baldi 1985) have shown that q_t is essentially independent of *OCR* other than through its effect on K_0.

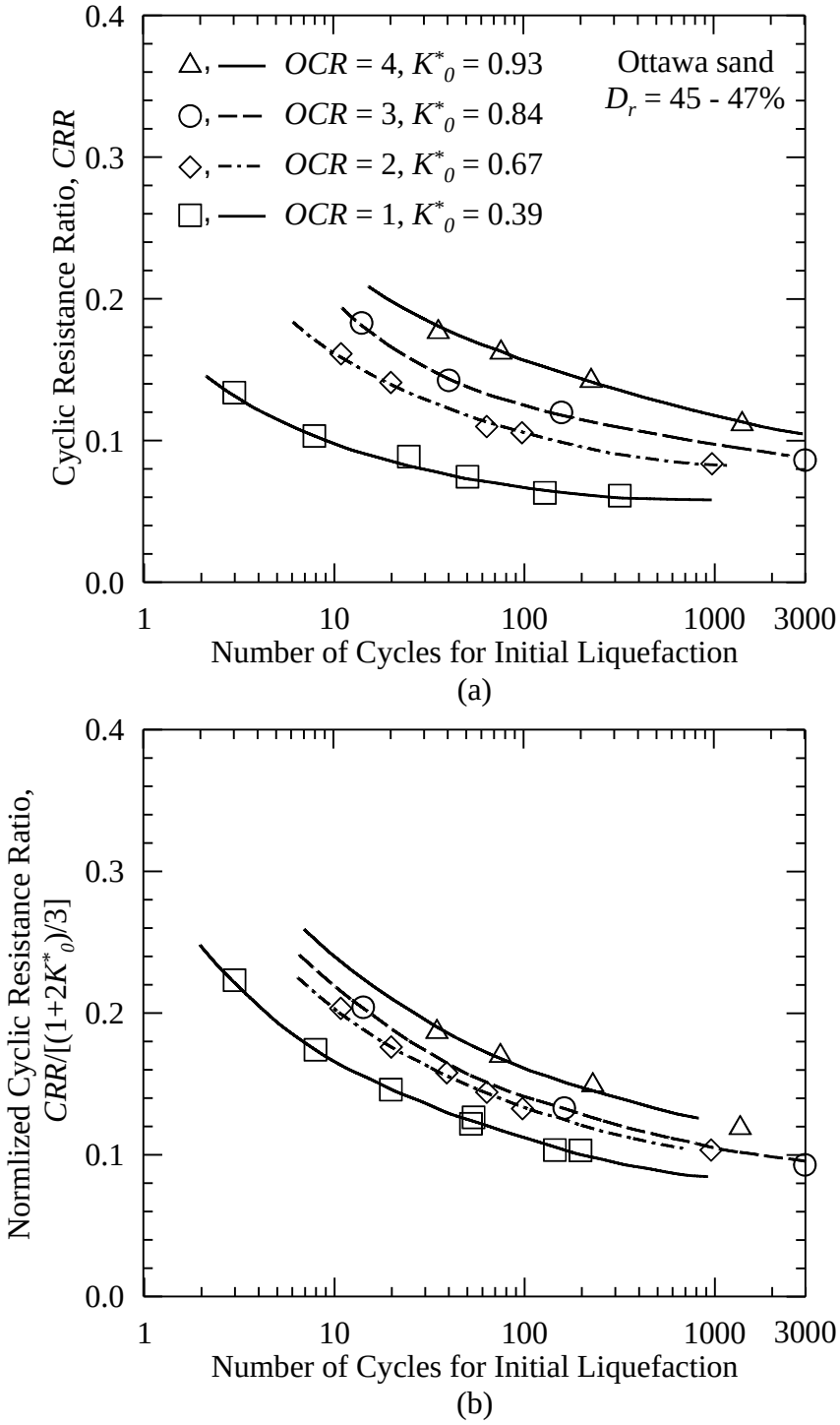

Figure 4.2: Results of cyclic simple shear tests on Ottawa sand: (a) cyclic resistance ratio versus number of cycles and (b) cyclic resistance ratio normalized by $[(1+2\,K_0^*)/3]$ versus number of cycles reproduced from Bhatia (1982).

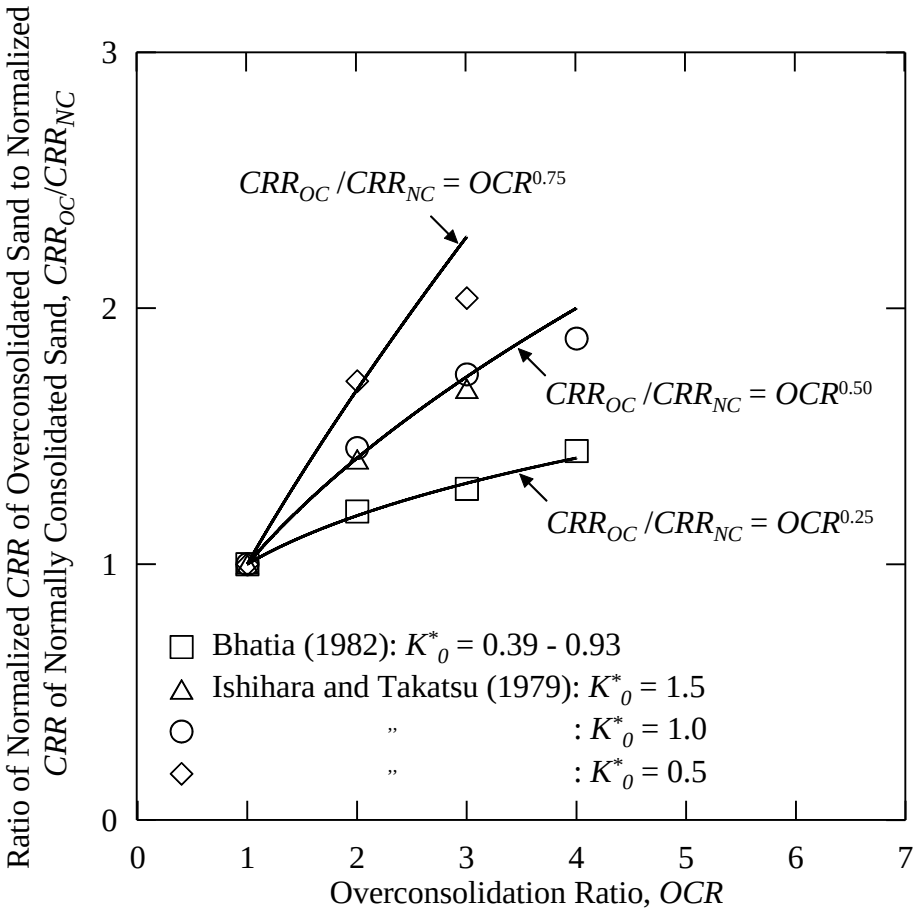

Figure 4.3: Ratio of normalized *CRR* of overconsolidated sand to normalized *CRR* of normally consolidated sand versus overconsolidation ratio modified from Ishihara and Takatsu (1979).

4.5 Summary

Effects of fabric anisotropy, K_0 conditions and *OCR* on liquefaction resistance of sands were reviewed in this chapter. The following conclusions can be made based on the discussions from this chapter:

- Liquefaction resistance of sands changes significantly with changes in the angles between the sliding and the microscopic shearing directions, and the angles between longest axes of particles and the vertical axis.
- A unique relationship between liquefaction resistance of isotropic and anisotropic normally consolidated sands exists (represented in Equations 3.1 and 3.4) as suggested by several researchers from cyclic torsional shear tests results.
- An approximate relationship between liquefaction resistance of overconsolidated sands and normally consolidated sands (after the correction for K_0 being applied) have been suggested (Equation 3.8) based on results from previous studies.

CHAPTER 5

AT-REST LATERAL STRESS COEFFICIENT FOR SANDS IN THE SOUTH CAROLINA COASTAL PLAIN BASED ON DMT AND CPT

5.1 Introduction

In this chapter, the at-rest lateral stress coefficient (K_0) is estimated for eight geotechnical investigation sites in the South Carolina Coastal Plain (SCCP) from the results of DMT and the nearest CPT measurements, and using a relationship established in Chapter 2 for predominantly quartz, uncemented, clean sands. The relationship for estimating K_0 is expressed by:

$$K_0 = 0.359 + 0.045K_D - 0.00085(q_t/\sigma'_v) + 0.056OCR \quad (5.1)$$

Equation 5.1 is used in this chapter to calculate K_0 only in sand with fines content (FC) ≤ 15%. For sites where FC information is not available, the CPT soil behavior type index (I_c) value less than 2.07 is used as an indicator of FC ≤ 15% (Robertson and Wride 1998). Values of *OCR* are assumed based on the geologic history of the deposits or obtained from the results of laboratory consolidation tests.

Locations of the eight test sites are plotted on the geologic map of the SCCP near Charleston by McCartan et al. (1984) shown in Figure 5.1. The eight sites can be divided into two groups: 1) sites of no known liquefaction, here in called "no liquefaction sites" (i.e., CREC, Hobcaw Borrow Pit, Walterboro Rest Area, Hobcaw Beach Ridge, and Walterboro Lowcountry); and 2) sites where paleoliquefaction features have been discovered, here in called "paleoliquefaction sites" (i.e., Hollywood Ditch, Sampit, and

Four Hole Swamp). A summary of the geologic ages of the surficial beach deposits and the time since the last known liquefaction event at these eight sites is presented in Table 5.1.

5.2 Coastal Research and Education Center Site

The Coastal Research and Education Center (CREC) site is located about 15 km west of Charleston, just off of Highway U.S. 17. CREC is mainly an agricultural research facility owned by Clemson University with multiple level fields. The surficial sand deposits at CREC are in a similar geomorphic position as the Wando Formation mapped by Weems and Lemon (1993) in Charleston. No surface manifestations of liquefaction due to the 1886 Charleston earthquake were reported in the general area (Dutton 1889; Martin and Clough 1990).

An area of about 0.4 acres at CREC was made available for geotechnical and geophysical testing (Boller 2008; Boller et al. 2008; Hayati 2009; Esposito et al. 2014; Hossain et al. 2014). Figure 5.2 presents the CPT, DMT and K_0 profiles for the top 10 m of soil at the CREC site. The locations of DMT (D1) and SCPT (SC6) are 4 m apart. As seen from Figure 5.2a, four distinct soil layers (A, B, C, and D) exist at this site, with layers A and B divided into two sub-layers (A1 and A2, and B1 and B2). Sub-layers A1, B1 and B2 are predominantly sands with average FC of 1, 5 and 4%, respectively (Boller 2008).

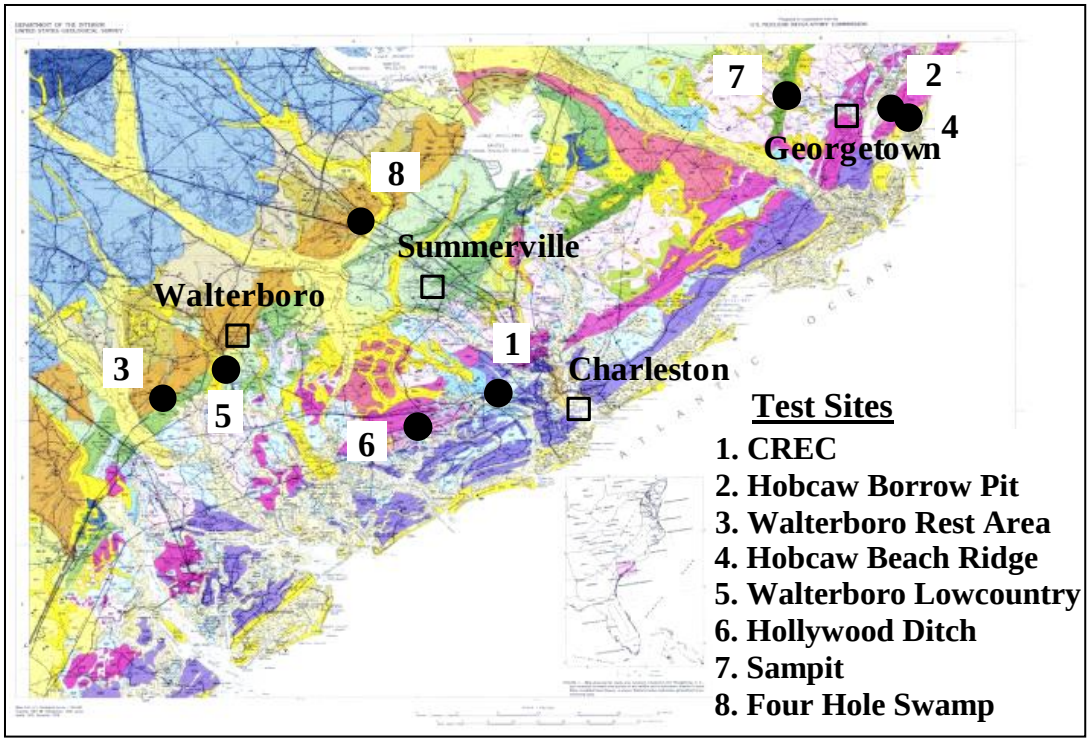

Figure 5.1: Geologic map of the South Carolina Coastal Plain near Charleston by McCartan et al. (1984) with locations of the eight test sites.

Table 5.1: Summary of age information for eight surficial beach sand deposits.

Site	Geologic age (years)	Time since last liquefaction event (years)
No liquefaction sites		
1. CREC	70,000 - 130,000[a]	Not a site of known liquefaction
2. Hobcaw Borrow Pit	100,000 - 200,000[b,c]	Not a site of known liquefaction
3. Walterboro Rest Area	≥ 1,000,000[a]	Not a site of known liquefaction
4. Hobcaw Beach Ridge	59,000[c]	Not a site of known liquefaction
5. Walterboro Lowcountry	450,000[a]	Not a site of known liquefaction
Paleoliquefaction sites		
6. Hollywood Ditch	120,000 - 130,000[d]	126[f]
7. Sampit	450,000[c,e]	~ 500[g]
8. Four Hole Swamp	≥ 1,000,000[a]	~ 1,660[g]

[a]McCartan et al. (1984); [b]May (1978); [c]Owens (1989); [d]Weems et al. (1986); [e]Leon et al. (2006); [f]Obermeier et al. (1986, 1987); [g]Talwani and Schaeffer (2001)

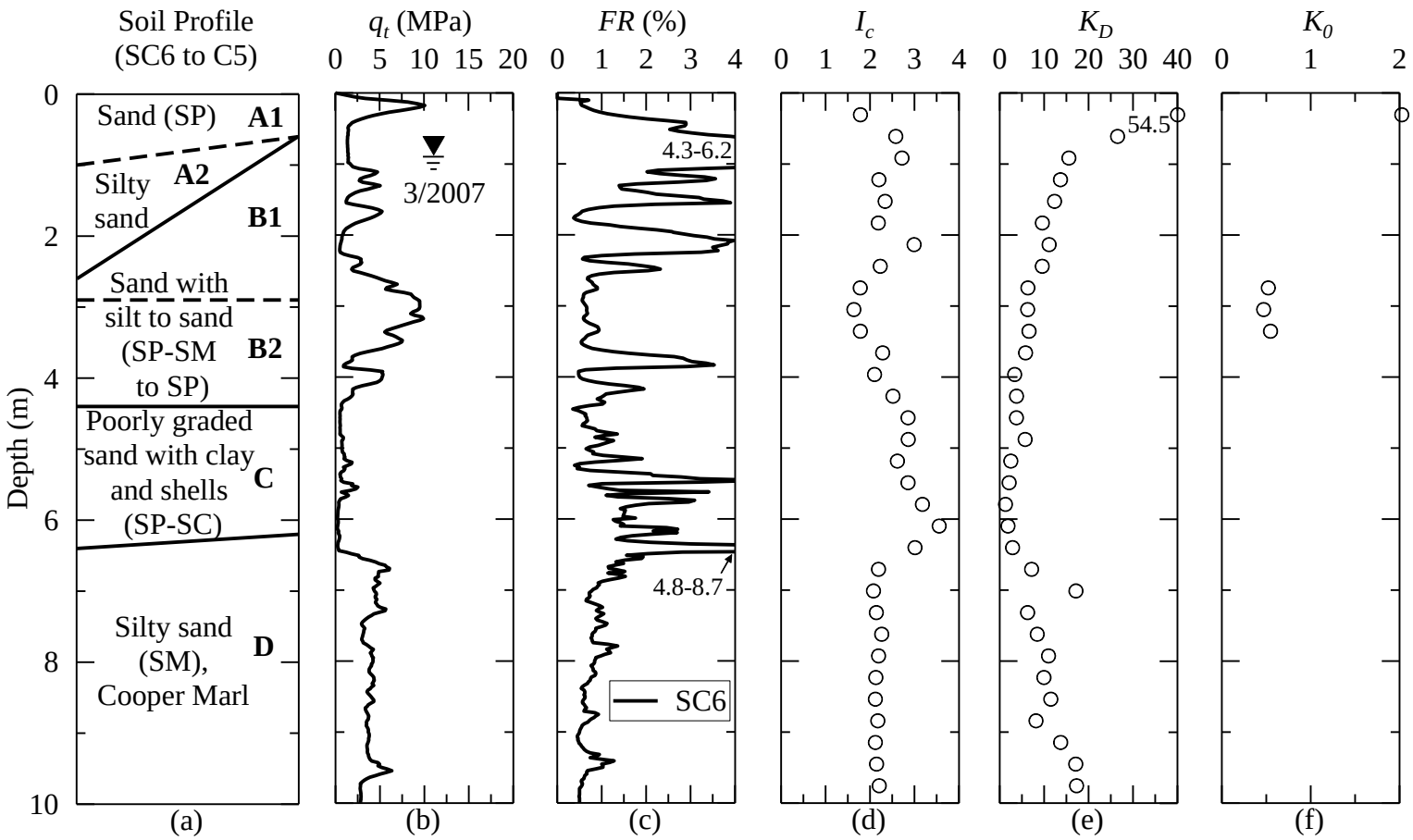

Figure 5.2: CPT, DMT and K_0 profiles from the CREC site based on information reported in Boller (2008).

Presented in Figure 5.2f are values of K_0 estimated using Equation 5.1 for layers that consist of sands with FC ≤ 15%. *OCR* for these sands is assumed to be 1.0. Computed values of K_0 in Layer B range between 0.47 and 0.55, with an average of 0.51.

5.3 Hobcaw Borrow Pit Site

The Hobcaw Borrow Pit site is located east of Georgetown off of Highway U.S. 17. It is part of an area called Hobcaw Barony, a 17,500-acre outdoor laboratory owned and managed by the Belle W. Baruch Foundation. Hobcaw Barony is covered by sand beach ridges that were formed by waves and seaward growth of the coastline (May 1978). The thick surficial sand deposits at Hobcaw Barony are part of the Socastee Formation (Owens 1989). Martin and Clough (1990) and Lewis et al. (1999) reviewed earthquake reports and found no evidence that liquefaction occurred in the Hobcaw Barony area during the 1886 Charleston earthquake.

Geotechnical and geophysical investigations at Hobcaw Barony included testing near an active borrow pit area (Boller 2008; Geiger 2010; Geiger et al. 2010; Hossain 2010; Hossain et al. 2014). Figure 5.3 presents the CPT, DMT and K_0 profiles for the top 10 m of soil at the Hobcaw Borrow Pit site. The locations of DMT (D1) and SCPT (SC1) are 2 m apart. As seen from Figure 5.3a, two distinct soil layers (A and B) exist at this site. Layer A is divided into three sub-layers (A1, A2 and A3) based mainly on variation in the q_t and K_D profiles. Sub-layers A1, A2 and A3 consist predominantly of poorly graded sands with average FC of 6, 8 and 3%, respectively (Geiger 2010). Geiger (2010)

conducted a consolidation test on a fixed piston sample collected from a depth of 8.7 m and estimated the *OCR* of layer B to be 2.4. The same *OCR* is assumed for sub-layer A3.

Presented in Figure 5.3f are values of K_0 estimated using Equation 5.1 for layers that consist of sands with FC $\leq$ 15%. Computed values of K_0 in Sub-layer A3 range between 0.52 and 0.64, with an average of 0.57.

5.4 Walterboro Rest Area Site

The Walterboro Rest Area site is located behind a rest area on Interstate-95 northbound at mile marker 47 near Walterboro. The South Carolina Department of Transportation made available an area adjacent to two sewage treatment ponds for investigations. The site lies in an area mapped by McCartan et al. (1984) of beach deposit with age of at least 100,000 years old, and well outside the zone of major craterlets generated by the 1886 Charleston earthquake reported by Dutton (1889, Plate XXVIII) as well as outside areas of liquefaction reported in Martin and Clough (1990) and Lewis et al. (1999).

Geotechnical and geophysical investigations at the Walterboro Rest Area site were reported by Geiger (2010), Hossain (2010) and Hossain et al. (2014). Figure 5.4 presents the CPT, DMT and K_0 profiles for the top 10 m of soil at the site. The locations of DMT (D1) and SCPT (SC3) are 3.7 m apart. As seen from Figure 5.4a, four distinct soil layers (A B, C and D) exist at this site. Layers A, B and C are predominantly sands with average FC of 10, 11 and 7%, respectively (Geiger 2010). Geiger (2010) conducted a consolidation test on a fixed piston sample collected from a depth of 8.2 m and

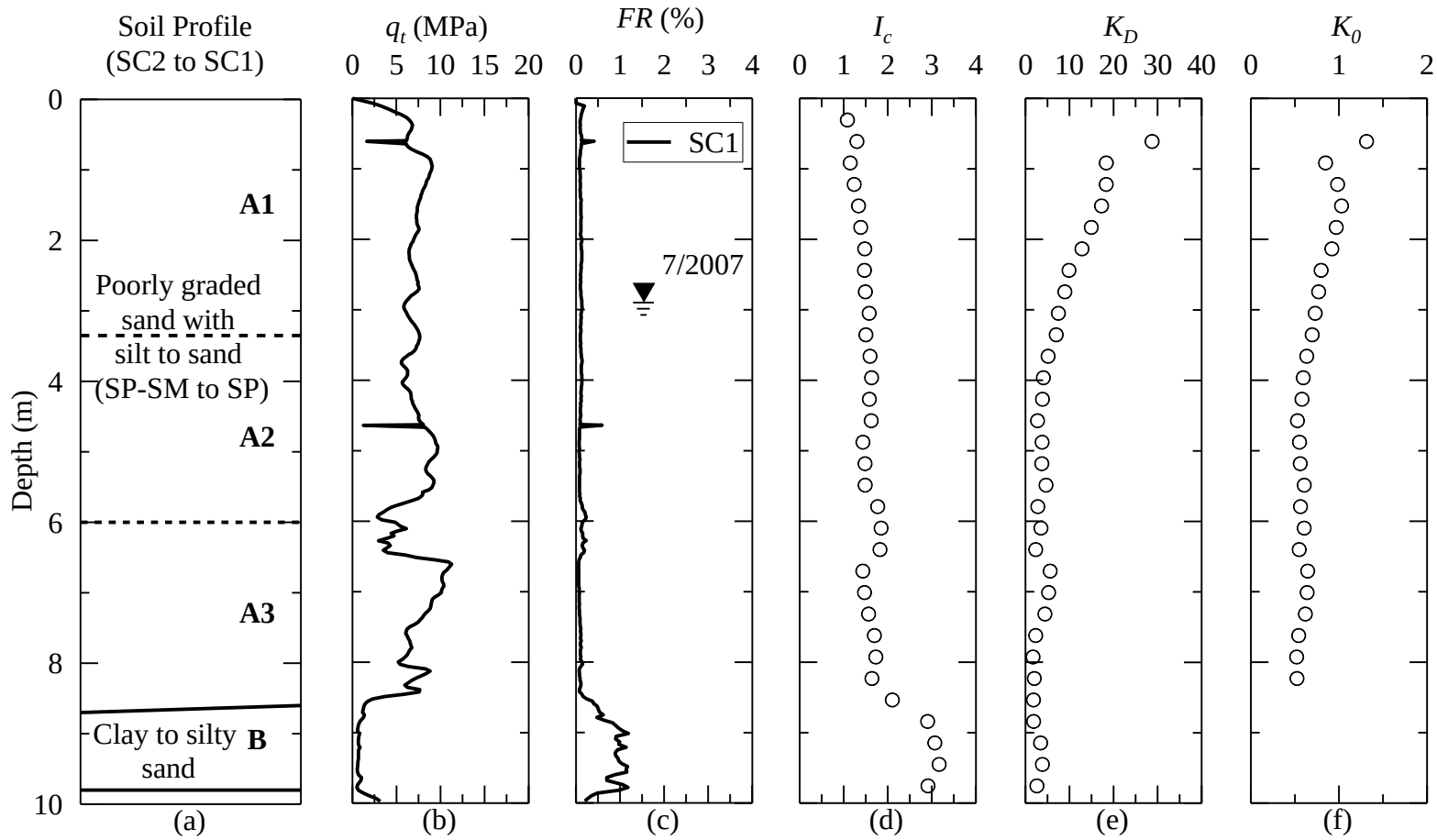

Figure 5.3: CPT, DMT and K_0 profiles from the Hobcaw Borrow Pit site based on information reported in Boller (2008) and Geiger (2010).

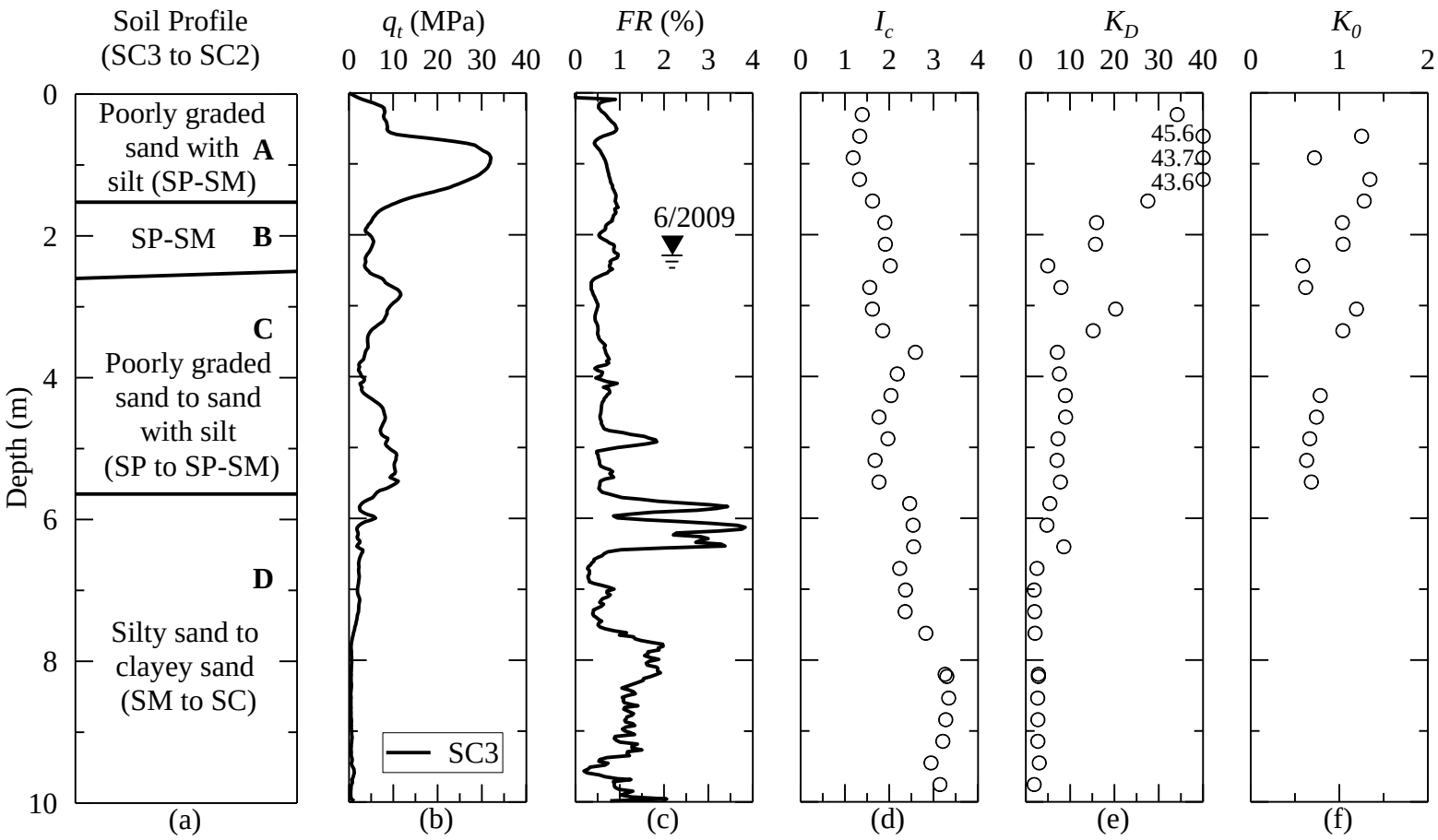

Figure 5.4: CPT, DMT and K_0 profiles from the Walterboro Rest Area site based on information reported in Geiger (2010).

estimated the *OCR* to be 1.6. Same *OCR* is assumed for Layer C.

Presented in Figure 5.4f are values of K_0 estimated using Equation 5.1 for layers that consist of sands with FC ≤ 15%. Computed values of K_0 in Layer C range between 0.63 and 1.19, with an average of 0.79.

5.5 Hobcaw Beach Ridge Site

The Hobcaw Beach Ridge site is located near the Hobcaw Borrow Pit site within Hobcaw Barony. As seen in Figure 5.5, Hobcaw Barony lies southeast of Georgetown and is located on a peninsula set between the Waccamaw River and the Atlantic Ocean. As discussed by May (1978), Hobcaw Barony is formed on the east by beach barriers and tidal flats. Inland, the area is covered by beach ridges formed by deposition of sand by waves. Figure 5.6 presents the depositional trends of the beach ridges, as interpreted by May (1978), and the location of the investigation site. The beach ridges are labeled from oldest to youngest (number 1 to 7). The Hobcaw Beach Ridge site is located on ridge 6. Based on the geomorphic position, the surficial sand deposit at this site is estimated to be 59,000 years old (Owens 1989). No evidence of liquefaction in the Hobcaw Barony area was reported following the 1886 earthquake (Martin and Clough 1990; Lewis et al. 1999).

One SCPT, one DMT and one hand-auger sample hole were conducted at the Hobcaw Beach Ridge site on March 9, 2012 by S&ME. Figure 5.7 presents a photograph

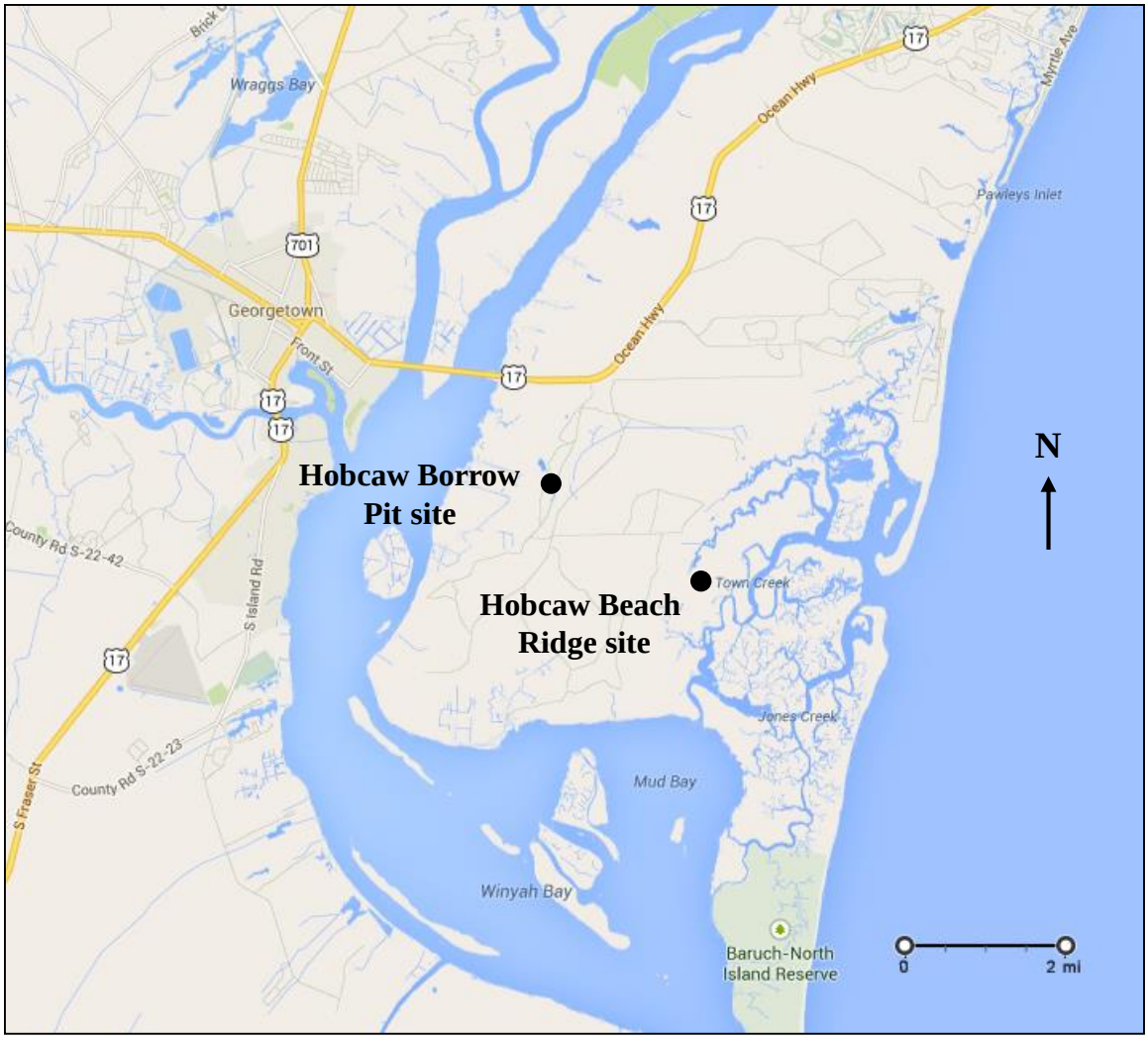

Figure 5.5: Map showing the Hobcaw Beach Ridge and Borrow Pit sites.

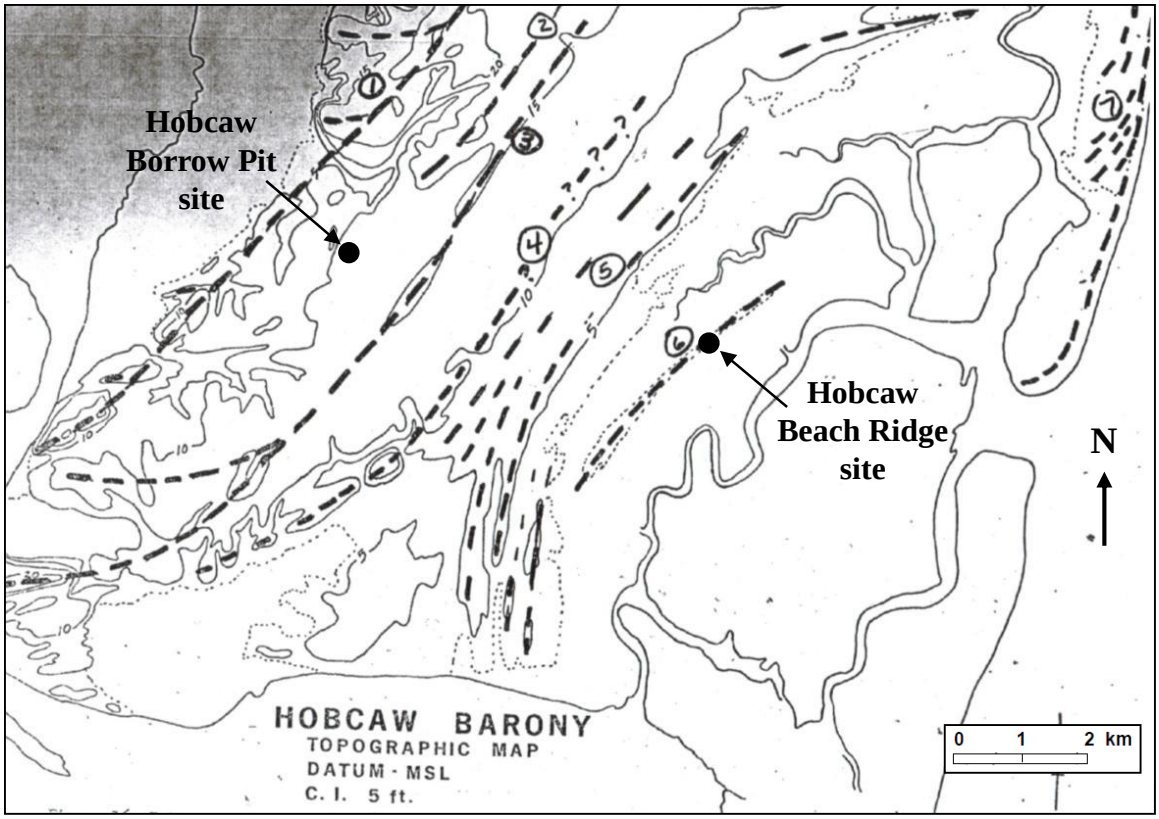

Figure 5.6: Topographic map showing beach ridges and the location of Hobcaw Borrow Pit and Beach Ridge sites (May 1978).

showing the cone truck at the site. The SCPT was conducted pushing the cone until refusal at a depth of 12 m below the ground surface. The DMT was conducted to a depth of 7.0 m. Because the groundwater table was found at a depth of 0.4 m, hand augering was not possible below a depth of 0.6 m due to caving in of the borehole.

Figure 5.8 presents the CPT, DMT and K_0 profiles for the top 10 m of soil at the Hobcaw Beach Ridge site. The locations of the DMT and SCPT are separated by a distance of 1.5 m. As seen from Figure 5.8a, four distinct soil layers (A, B, C and D) exist at this site. Layers A and B are predominantly sands, based on the CPT and DMT results.

Presented in Figure 5.8f are values of K_0 estimated using Equation 5.1 for layers that consist of sands with FC $\leq$ about 15%. *OCR* for these sands is assumed to be 1.0. Computed values of K_0 in Layer B range between 0.52 and 0.68, with an average of 0.59.

5.6 Walterboro Lowcountry Site

The Walterboro Lowcountry site is located about 5.6 km (3.5 mi) southeast of Walterboro, just off of Route 303. The site is owned by Lowcountry Sand & Gravel, Inc. The coarse sands being mined at the site are fluvial in origin, unlike the beach sands at the seven other sites. The Walterboro Lowcountry site lies well outside the zone of craterlets generated by the 1886 Charleston earthquake reported by Dutton (1889, Plate XXVIII) and outside areas of liquefaction reported in Martin and Clough (1990) and Lewis et al. (1999).

Figure 5.7: Photograph of the cone truck at the Hobcaw Beach Ridge site (by Ariful Bhuiyan 2012).

The results of geotechnical testing at the Walterboro Rest Area site were reported by Geiger (2010). Figure 5.9 presents the CPT, DMT and K_0 profiles for the top 10 m of soil at the Walterboro Lowcountry site. The locations of DMT (D1) and SCPT (SC1) are 5.6 m apart. As seen from Figure 5.9a, 5 distinct soil layers (A B, C, D and F) exist at this site. Layers A and C are predominantly sands based on CPT and DMT results.

Over the years, mining operations at the site have consisted of stripping off of finer grained soils above the groundwater table and dredging coarse sand deposits that lie below the groundwater table. Based on mining operations at the time of the geotechnical investigations, the site was graded down from its original elevation by about 3.4 m (11 ft). Thus, the surficial sand deposits at Walterboro are overconsolidated, with Layer C having an *OCR* of at least 2.3.

Presented in Figure 5.9f are values of K_0 estimated using Equation 5.1 for layers that consist of sands with FC $\leq$ 15%. Computed values of K_0 in Layer C range between 0.22 and 0.40, with an average of 0.32.

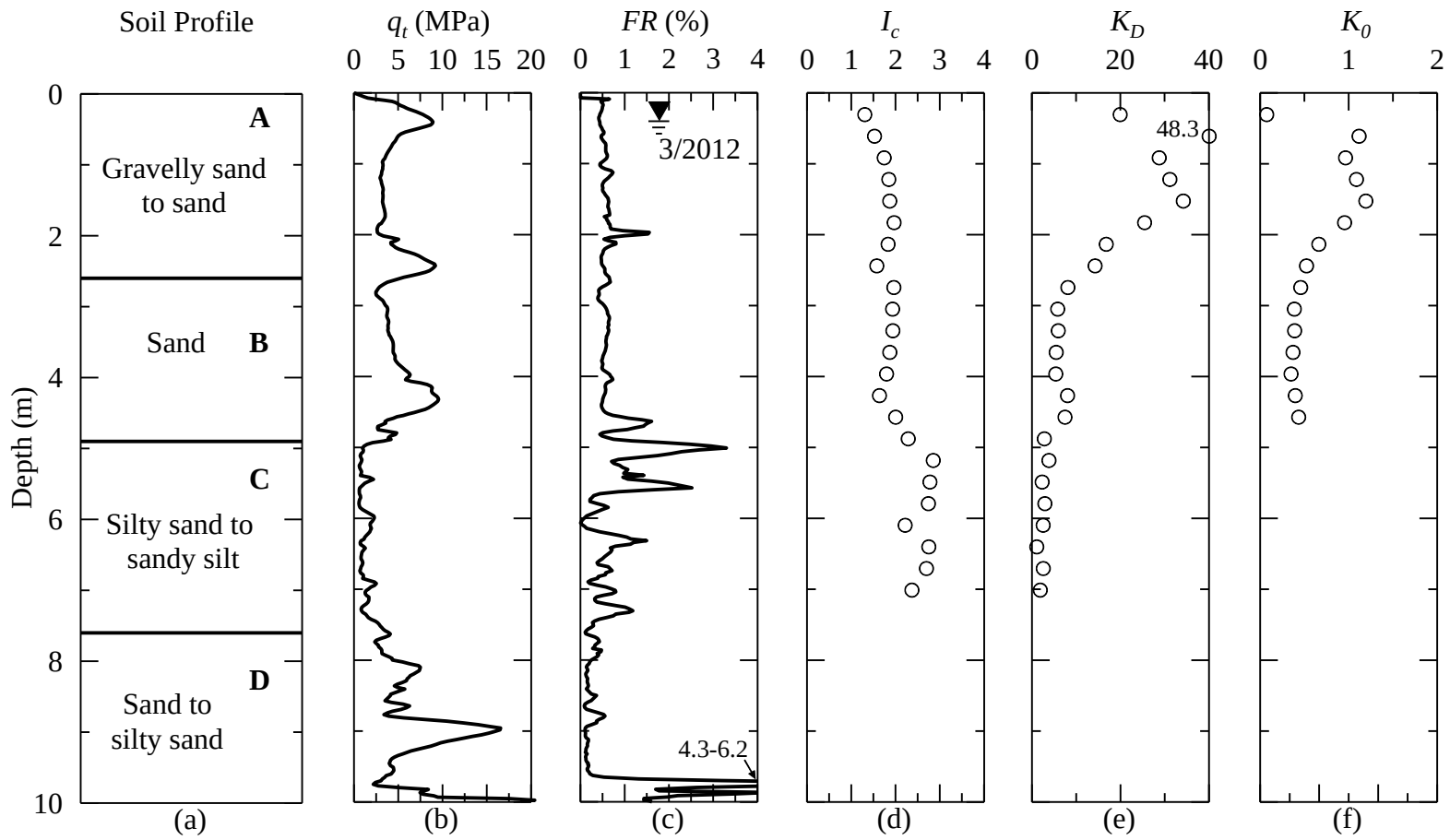

Figure 5.8: CPT, DMT and K_0 profiles from the Hobcaw Beach Ridge site.

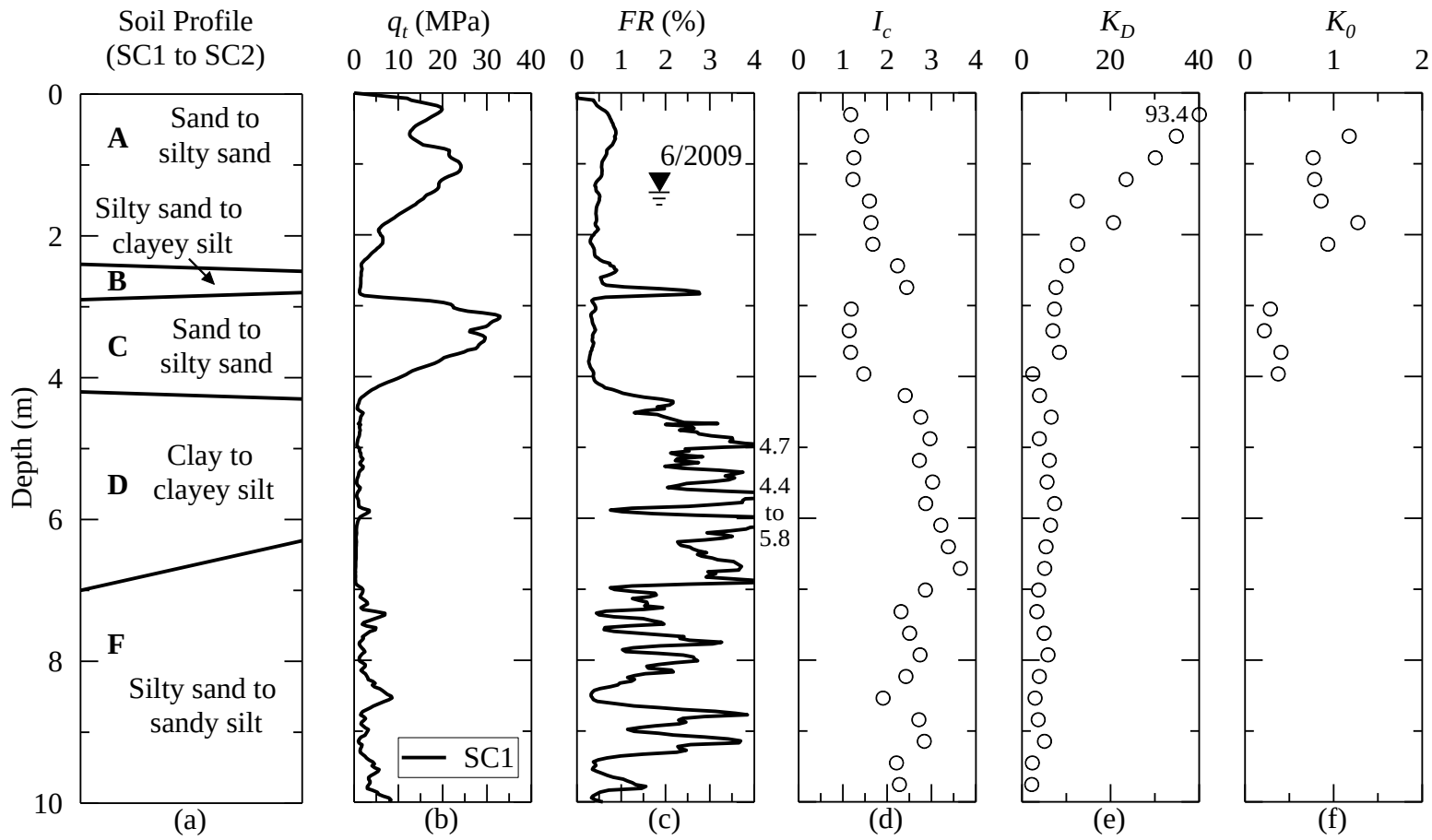

Figure 5.9: CPT, DMT and K_0 profiles from the Walterboro Lowcountry site based on information reported in Geiger (2010).

5.7 Hollywood Ditch Site

The Hollywood Ditch site is located close to the town of Hollywood, along a drainage ditch that is 3.7 m wide and 2.4 m deep. Surficial soils in the area are part of Ten Mile Hill beds (Weems et al. 1986). The drainage ditch, as well as another ditch in the area, offers some of the most extensive exposures of relic liquefaction features that have been observed in South Carolina (Obermeir et al. 1986, 1987; Martin and Clough 1990). Obermeier et al. (1986, 1987) found some 162 liquefaction features representing five separate episodes of soil liquefaction. Of the 162 liquefaction features, only 24 were attributed to the 1886 event. These 24 features were mostly minor expressions forming thin cracks in the overburden, while the formation of sand craters as large as 2.5 m in diameter were common in prehistoric events.

A number of geotechnical and geophysical investigations have been conducted along the Hollywood Ditch (Martin and Clough 1990; Talwani and Schaffer 2001; Hossain 2010; Hossain et al. 2014; Williamson and Gassman 2014). Figure 5.10 presents the CPT, DMT and K_0 profiles for the top 10 m of soil. The locations of DMT (D1) and SCPT (SC2) are 7.3 m apart. As seen from Figure 5.10a, four distinct soil layers (A, B, C, and D) exist at this site, with layer B divided into two sub-layers (B1 and B2). Sub-layer B2 consists of sand with an average FC of 11% (Williamson et al. 2014).

Presented in Figure 5.10f are values of K_0 estimated using Equation 5.1 for layers that consist of sands with FC $\leq$ 15%. *OCR* for the sands of sub-layer B2 is assumed to be 1.0. Computed values of K_0 in Sub-layer B2 range between 0.52 and 0.77, with an average of 0.61.

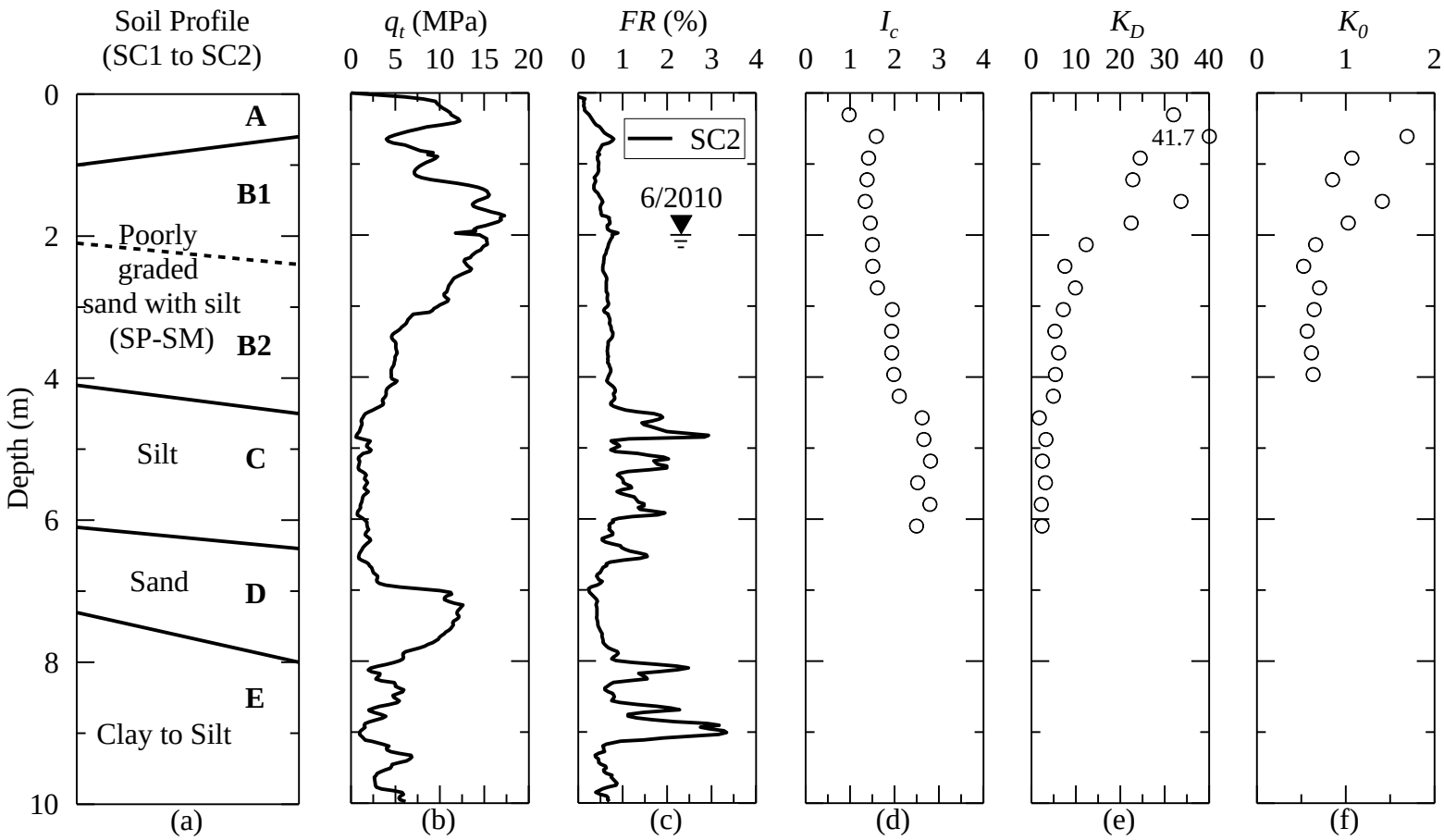

Figure 5.10: CPT, DMT and K_0 profiles from the Hollywood Ditch site based on information reported in Williamson and Gassman (2014).

5.8 Sampit Site

The Sampit site is located about 20 km west of Georgetown on the eastern flank of a mid-Pleistocene-age beach ridge (Leon et al. 2006). There is a northwest-southeast trending drainage ditch about 500 m long, and ranging in depth from 2 to 3.5 m. Talwani and Schaeffer (2001) studied the paleoliquefaction features exposed in the ditch and found six sand boils. They concluded that these sand boils were associated with three different earthquakes that occurred about 500, 1,000 and 1,560 years ago.

A number of geotechnical and geophysical investigations have been conducted at the Sampit site (Hu et al. 2002; Hossain 2010; Hossain et al. 2014; Williamson and Gassman 2014). Figure 5.11 presents the CPT, DMT and K_0 profiles for the top 10 m of soil at the site. The locations of DMT (D1) and SCPT (SC1) are 6.8 m apart. As seen from Figure 5.11a, two distinct soil layers (A and B) exist at this site, with layer A divided into two sub-layers (A1 and A2). Sub-layer A2 is predominantly sands with average FC of 4% (Williamson and Gassman 2014).

Presented in Figure 5.11f are values of K_0 estimated using Equation 5.1 for layers that consist of sands with FC $\leq$ 15%. *OCR* for the sands of sub-layer A2 is assumed to be 1.0. Computed values of K_0 in Sub-layer A3 range between 0.63 and 1.14, with an average of 0.83.

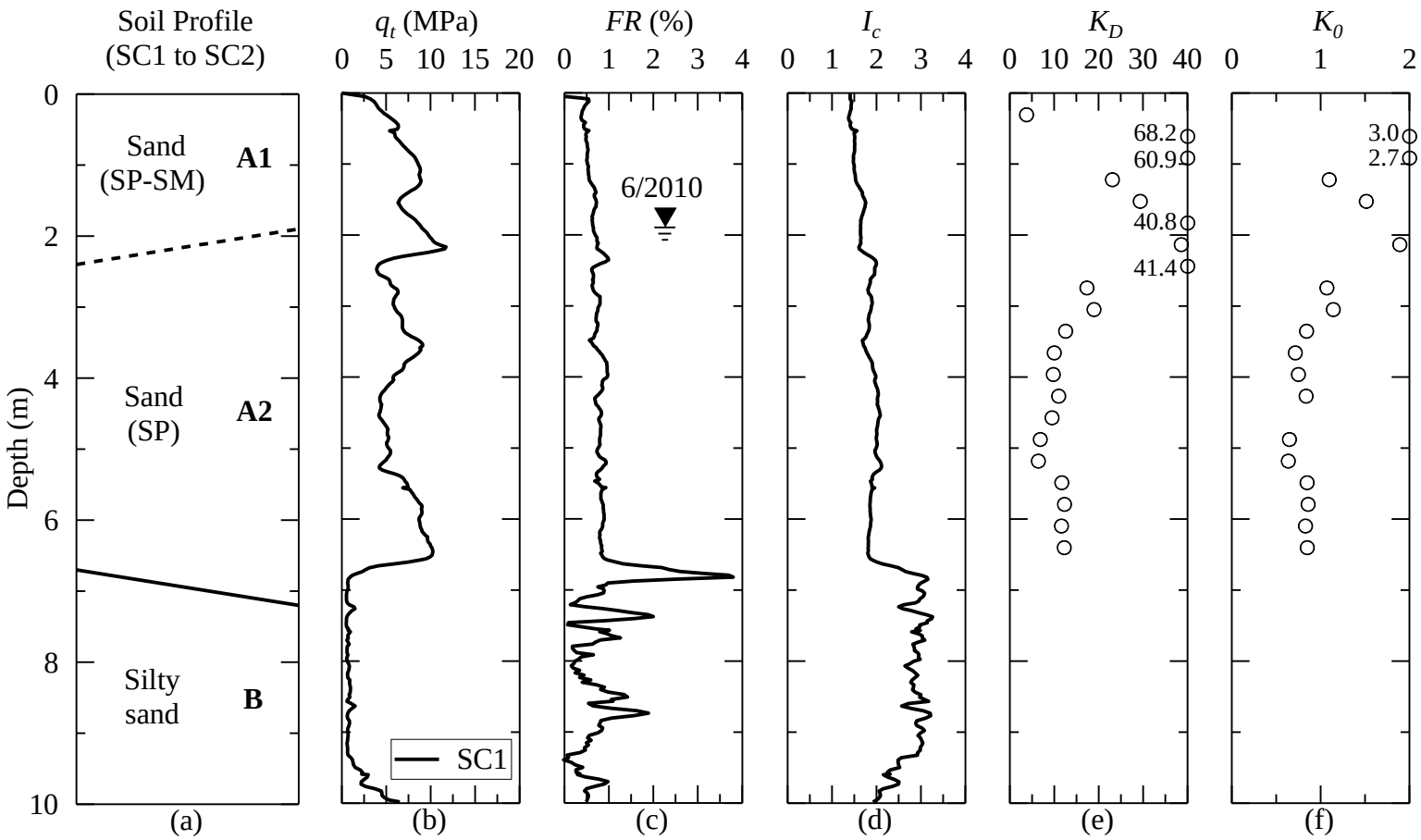

Figure 5.11: CPT, DMT and K_0 profiles from the Sampit site based on information reported in Williamson and Gassman (2014).

5.9 Four Hole Swamp Site

The Four Hole Swamp site is located near the Y-intersection of U.S. Highways 178 and 78, which becomes Highway 78 when heading east. This area was mapped by McCartan et al. (1984) as a beach sand deposit with age of at least 1,000,000 years. One paleoliquefaction feature (sand blow) was discovered at this site and has been attributed to an earthquake episode that occurred about 1,660 years ago (Talwani and Schaeffer 2001). The Four Hole Swamp site lies outside the zone of major liquefaction features generated by the 1886 Charleston earthquake shown in a map presented in Dutton (1889, Plate XXVIII).

Geotechnical and geophysical investigations at the Four Hole Swamp site have been reported by Hossain (2010), Hossain et al. (2014) and Williamson and Gassman (2014). Figure 5.12 presents the CPT, DMT and K_0 profiles for the top 10 m of soil. The locations of DMT (D1) and SCPT (SC1) are separated by a distance of 3.2 m. As seen from Figure 5.12a, two distinct soil layers (A and B) exist at this site, with Layer A divided into two sub-layers (A1 and A2). Layer A2 consists of sand with an average FC of 10% (Williamson and Gassman 2014). The test site has been eroded about 1.2 m (4 ft). Thus, the surficial sand deposits at this site are overconsolidated, with Sub-layer A2 having an estimated *OCR* of 1.4.

Presented in Figure 5.12f are values of K_0 estimated using Equation 5.1 for layers that consist of sands with FC $\leq$ 15%. Computed values of K_0 in Sub-layer A2 range between 0.48 and 0.74, with an average of 0.58.

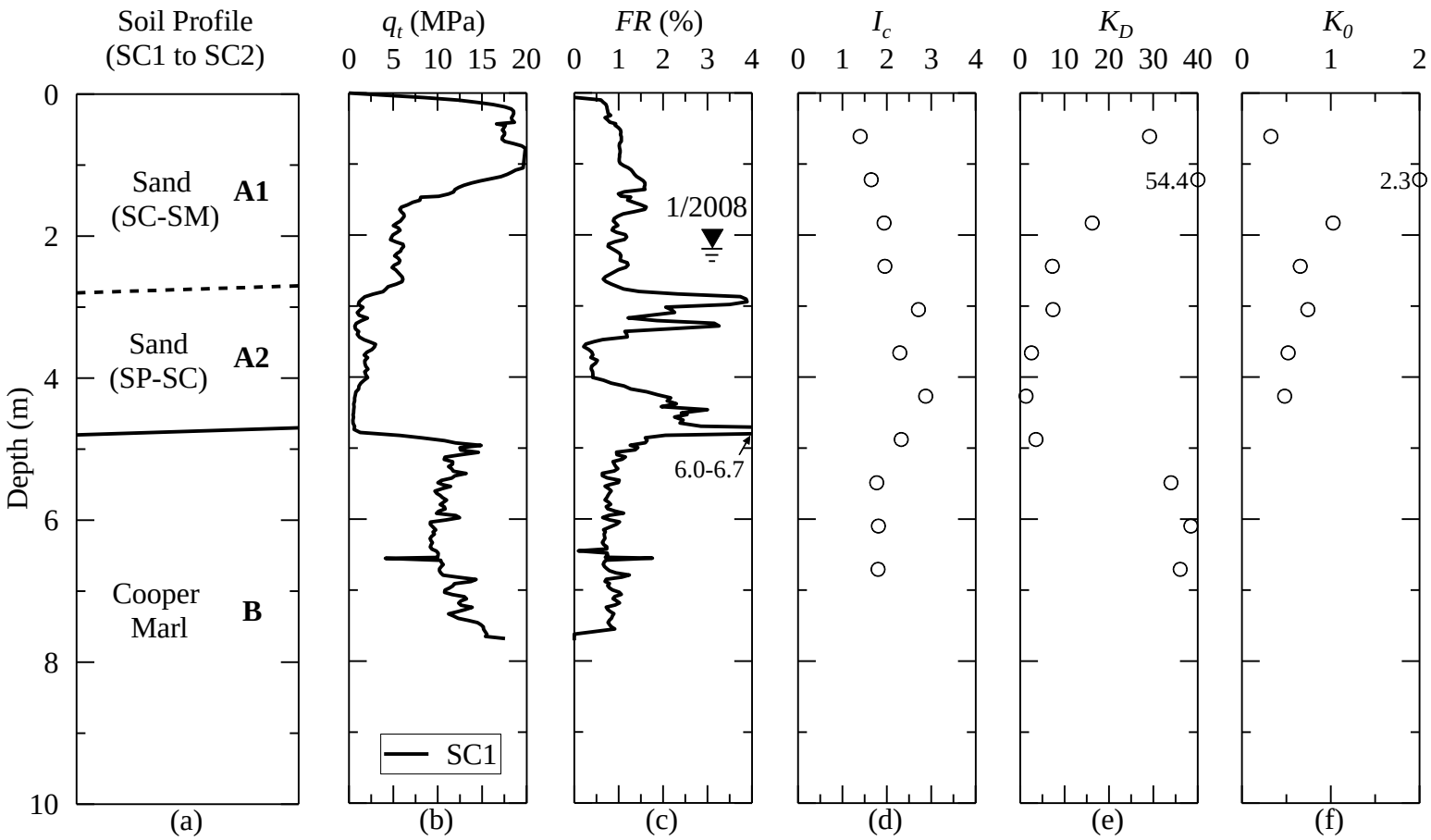

Figure 5.12: CPT, DMT and K_0 profiles from the Four Hole Swamp site based on information reported in Williamson and Gassman (2014).

5.10 Summary

Profiles of K_0 from DMT-CPT-*OCR* for eight sites in the SCCP were presented in this chapter. A summary of estimates of K_0 and key information for the critical sand layers below the groundwater table at the eight sites is presented in Table 5.2. As seen in Table 5.2, values of K_D ranges from 3.7 to 10.0 and values of q_t ranges from 1.6 to 21.6 MPa in the sand layers. At four of the sites, the estimated *OCR* of the sand layers is greater than 1.0. Estimates of K_0 for the sites fall in the typical range for natural sands.

Presented in Figure 5.13a are estimates of K_0 plotted against the average geologic age or time since deposition (t_1). A gentle increasing trend in K_0 with t_1 can be observed in Figure 5.13a. In Figure 5.13b, estimates of K_0 are plotted against the time since deposition at sites with no evidence of liquefaction or the time since last liquefaction event at sites where liquefaction occurred in the past (t_2). No distinct trend in K_0 with t_2 is observed from Figure 5.13b, indicating that K_0 does not decrease because of liquefaction.

Table 5.2: Summary of information for calculating K_0 from DMT-CPT-*OCR* at eight sites in the South Carolina Coastal Plain.

Site	Depth (m)	USCS classification of sand	Average D_{50} (mm)	Average FC (%)	Average K_D	Average q_t (MPa)	Average σ'_v (MPa)	Estimated average *OCR*	Average K_0
CREC	2.7-3.4	SP-SM to SP	0.20	5	6.4	7.7	0.0345	1.0	0.51
Hobcaw Borrow Pit	6.0-8.6	SP-SM to SP	0.23	3	3.2	7.0	0.0940	2.4	0.57
Walterboro Rest Area	2.6-5.6	SP-SM	0.18	7	9.8	7.1	0.0680	1.6	0.79
Hobcaw Beach Ridge	2.6-4.6	NA[a]	NA	9[b]	6.6	5.3	0.0367	1.0	0.59
Walterboro Lowcountry	2.9-4.2	NA	NA	1[b]	6.3	21.6	0.0433	2.3	0.32
Hollywood Ditch	2.4-3.7	SP-SM	0.11	11	6.9	7.5	0.0481	1.0	0.61
Sampit	2.4-6.4	SP	0.18	4	10.0	6.6	0.0603	1.0	0.83
Four Hole Swamp	2.8-4.8	SP-SC	0.20	10	3.7	1.6	0.0518	1.4	0.58

[a]Not available.

[b]Apparent fines content (AFC). AFC (%) = 0, if $I_c < 1.26$; AFC (%) = $1.75I_c^{3.25} - 3.7$, if $1.26 \leq I_c \leq 3.5$; where I_C is the soil behavior type index (Robertson and Wride 1998).

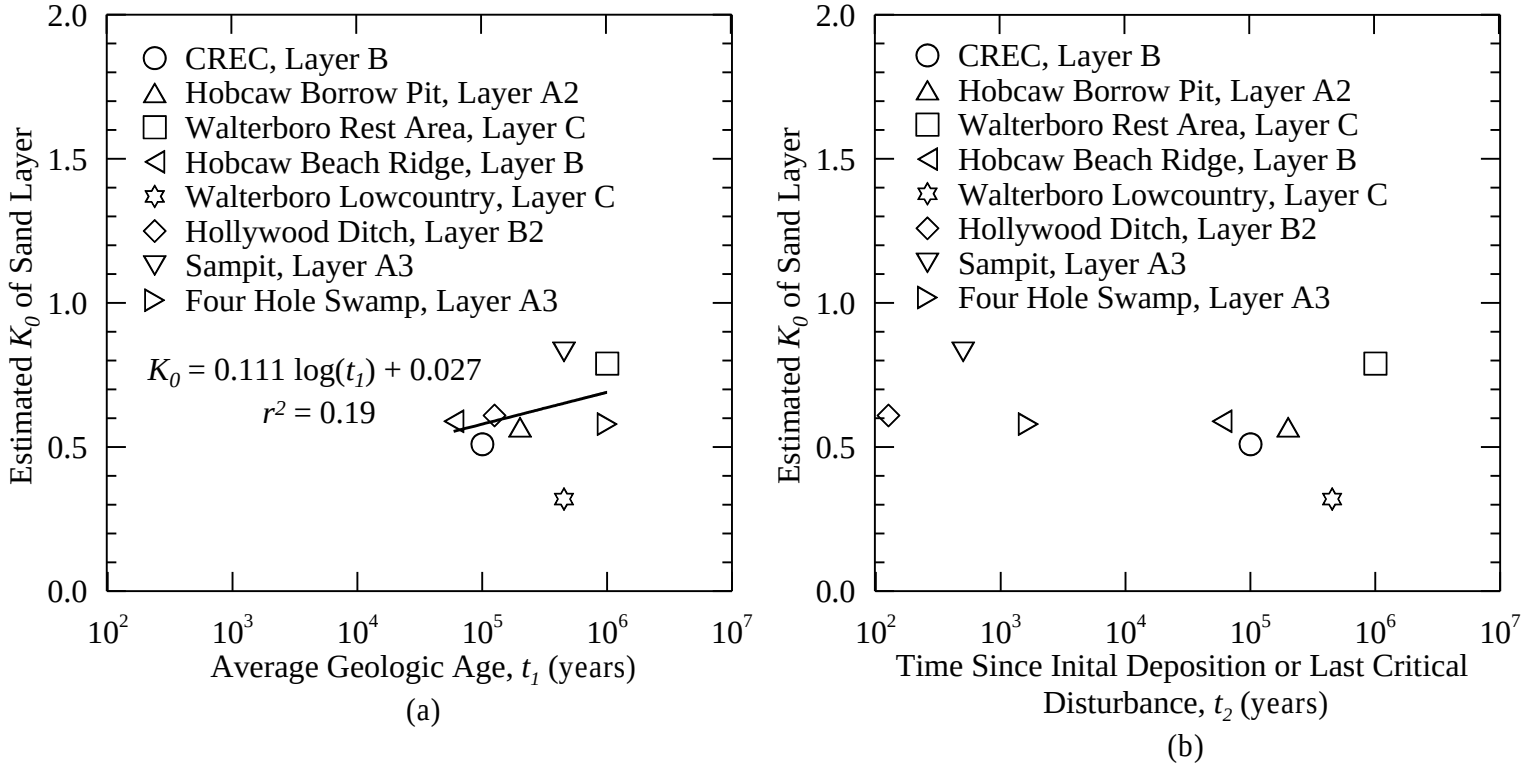

Figure 5.13: Variation of K_0 estimated from DMT-CPT-*OCR* for eight sand sites in the South Carolina Coastal Plain with (a) geologic age, and (b) time since deposition or last liquefaction event.

CHAPTER 6

IN SITU SEISMIC WAVE VELOCITY MEASUREMENTS AND ESTIMATES OF K_0 FROM EIGHT SITES IN THE SOUTH CAROLINA COASTAL PLAIN

6.1 Introduction

Presented in this chapter are the results of seismic wave velocity test from 5 no liquefaction sites (i.e., CREC, Hobcaw Borrow Pit, Walterboro Rest Area, Hobcaw Beach Ridge, and Walterboro Lowcountry) and 3 paleoliquefaction sites (i.e., Hollywood Ditch, Sampit, and Four Hole Swamp) in the SCCP. The results include compression wave velocity (V_P), vertically and horizontally polarized shear wave velocities propagating in horizontal direction (V_{sHV} and V_{sHH}, respectively) from crosshole testing at 6 of the 8 sites. The crosshole V_P and V_{sHV} measurements are obtained using two types of stress-wave sources – 1) a solenoid hammer, and 2) a portable dynamic cone. The results also include horizontally polarized shear wave velocity propagating in near-vertical direction (V_{sVH}) from SCPT at 8 sites.

The SCPT results from 4 of the 5 no liquefaction sites were initially documented in the thesis research reports by Boller (2008) and Geiger (2010). The results from crosshole testing with the solenoid hammer source at 2 of the 5 no liquefaction sites were documented in the dissertation research report by Hayati (2009) and the thesis report by Geiger (2010). Results from V_P-crosshole testing with the solenoid hammer source at 4 sites and the dynamic cone source at 6 sites were documented in the thesis research report

by Hossain (2010). A summary of all V_P- and V_{sHV}-crosshole test results was published in the conference paper by Hossain et al. (2014). The V_{sHH}-crosshole results at 4 sites and the SCPT results at the Hobcaw Beach Ridge site are presented in this dissertation study for the first time. Also presented for the first time are estimates of at-rest lateral earth pressure coefficients (K_0) based on crosshole V_{sHH} and V_{sHV} results.

6.2 Test Procedures

Presented in this section is information about the testing procedures employed in SCPT and seismic crosshole wave velocity measurements at the eight sites in the SCCP.

6.2.1 Seismic Cone Penetration Testing

The SCPTs were conducted according to ASTM D 5778. The seismic wave energy produced for the SCPTs came from an automatic solenoid hammer source that doubled as the cone truck's front hydraulic leveling jacks. The solenoid hammer was controlled by the operator inside of the cone truck. At about 1 m depth intervals, the operator stopped the push of the rods and activated the hammer. The solenoid hammer made one horizontal strike from the left (forward hit) followed by one horizontal strike from the right (reverse hit). The horizontal strikes were parallel to the ground surface and shear waves were captured by one geophone (pseudo interval) at the CREC site and two geophones (true interval) at the other seven sites. A combined time history plot of geophone voltage versus time was produced from the left and right strikes.

SCPT values of V_{sVH} are calculated by the following equation:

$$V_{sVH} = \frac{d_2 - d_1}{t_2 - t_1} \quad (6.1)$$

where d_2 and d_1 are the shear wave travel distances at consecutive depths assuming straight ray paths; and t_2 and t_1 are the corresponding average first arrival times of the shear waves for both strikes at consecutive depths. Based on the ease in determining the pick of arrival times, the records were classified as excellent, very good, good, fair, and poor.

6.2.2 Seismic Crosshole Test

6.2.2.1 Equipment and Set Up

Seismic crosshole tests were performed at the CREC, Hobcaw Borrow Pit, Walterboro Rest Area, Hollywood Ditch, Sampit and Four Hole Swamp sites. At each site, three boreholes designated as BH1, BH2 and BH3 were mud-rotary drilled into the ground about 2.7 to 3.3 m apart and in a straight line. Depths of boreholes at the six sites ranged from 7.3 to 11.0 m. Sixty-mm inside diameter inclinometer casing with four grooves at 90° intervals on the inside was installed in each borehole and grouted in place. The inclinometer casing was inserted in such a way that one set of grooves was in line with the three boreholes. The inclinometer casing grooves were used as tracks for spring-loaded wheel assemblies which helped orient the solenoid source and the receivers.

Piezometer standpipes were also installed into the ground at the Hobcaw Borrow Pit, Walterboro Rest Area, Hollywood Ditch, Sampit and Four Hole Swamp sites. The standpipes were installed by augering at a distance of 2.4 - 2.8 m from the nearest boreholes in the crosshole array to record the depth of groundwater table with time.

The solenoid hammer source contained three electro-mechanical solenoids that hit in the up, down and horizontal directions, as well as one accelerometer for determining the time of hammer impact. A photograph of crosshole testing equipment, including the solenoid hammer source and the receivers manufactured by Olsen Instruments is presented in Figure 6.1.

The dynamic cone source, as specified in ASTM SPT 399, consisted of a 38-mm diameter, 45-degree cone tip attached to E-rods which was driven into the ground using a 6.8 kg steel ring weight (Sower and Hedges 1966). A photograph of the dynamic cone penetrometer source is showed in Figure 6.2.

Each of the two receivers contained three velocity transducers (or geophones) in the radial, vertical, and transverse directions. During testing, the receivers were inserted into two adjacent casings at the same depth with the solenoid hammer source in the other casing or the dynamic cone source driven into the ground at a distance of 2.1-2.7 m away from the nearest borehole. Shown in Figure 6.3 is a schematic diagram of the crosshole test set up.

A dynamic signal analyzer manufactured by Agilent Technologies shown in Figure 6.4 was used to record the signals. The cables from the source and the two receivers were connected to the analyzer for both direct and interval measurements during testing with the solenoid hammer source. During testing with the dynamic cone source, only the cables from the two receivers were connected for interval measurements.

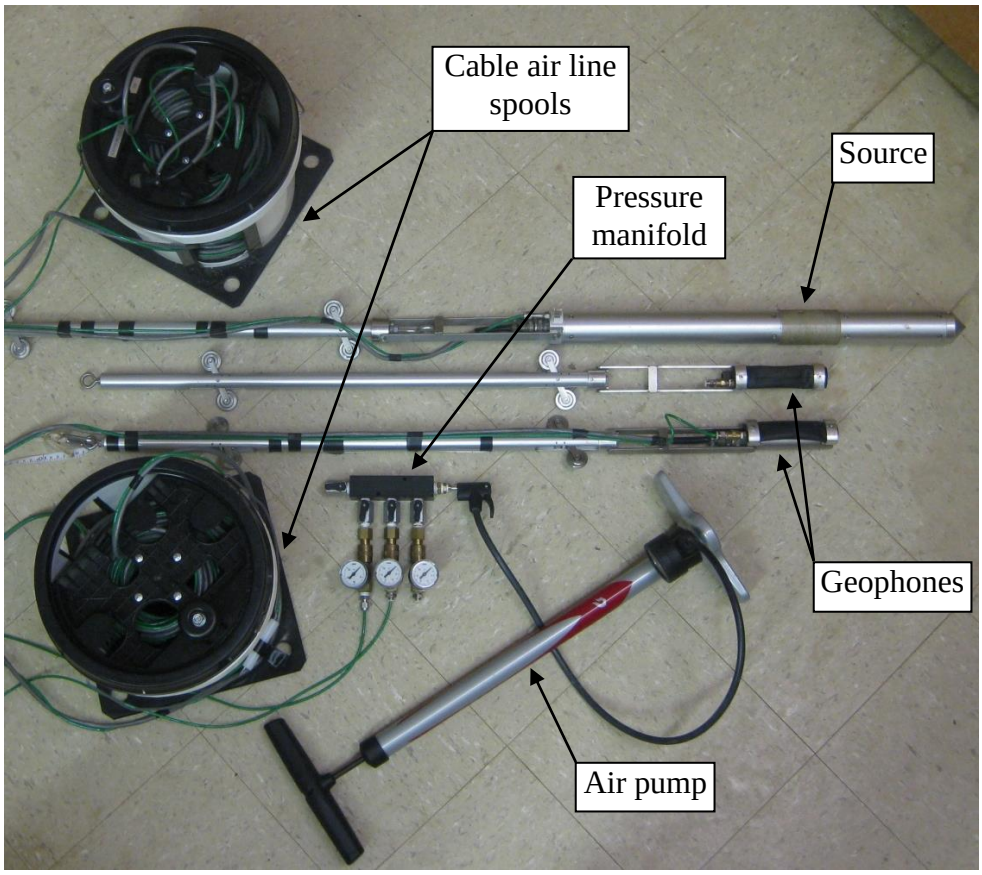

Figure 6.1: Photograph of crosshole testing equipment including the solenoid hammer source and the two three-component geophones (Hossain 2010).

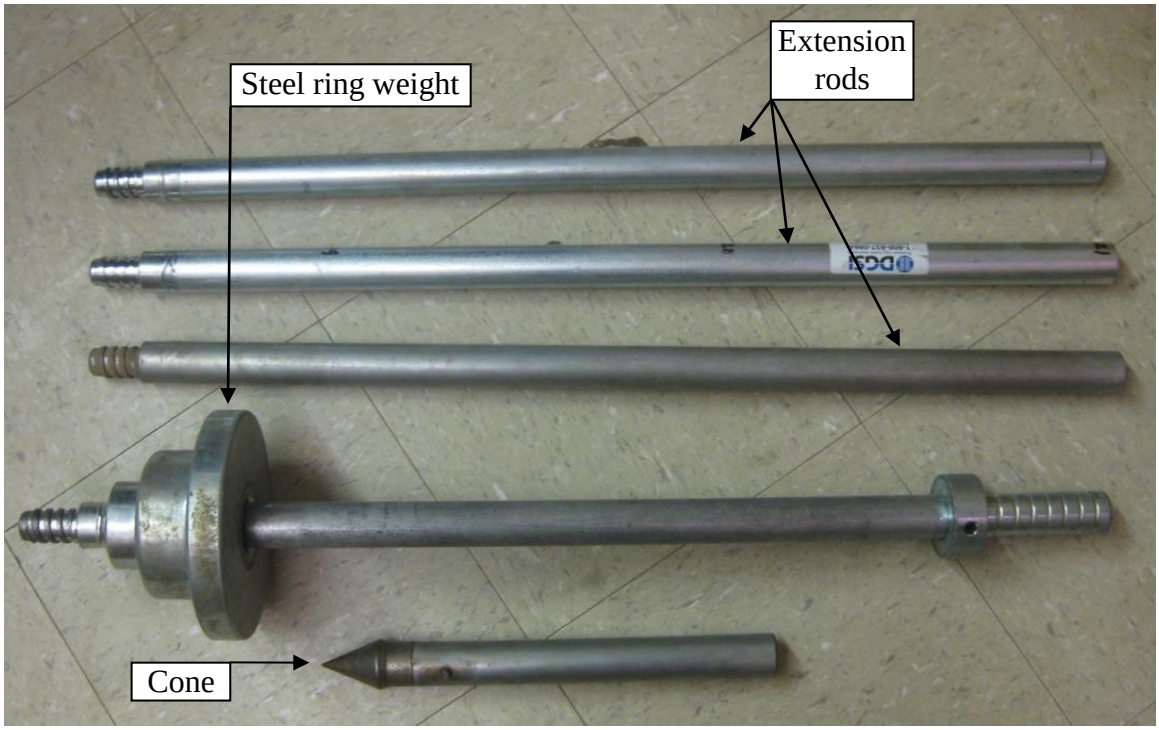

Figure 6.2: Photograph of the dynamic portable cone penetrometer (Hossain 2010).

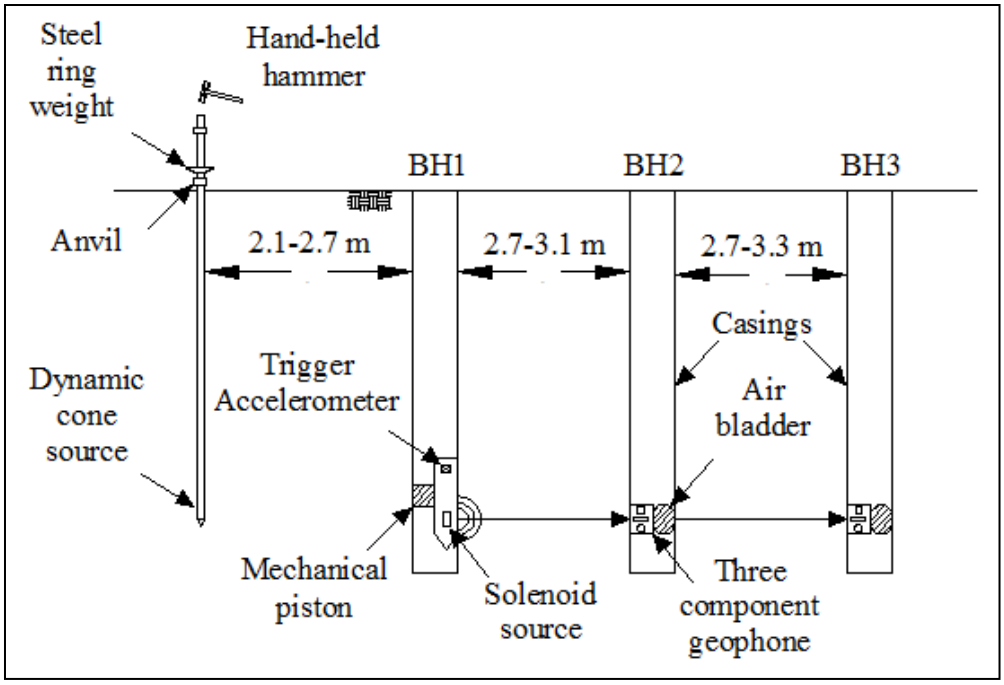

Figure 6.3: Schematic diagram of the crosshole test set up with solenoid hammer and dynamic cone sources.

Figure 6.4: Agilent Technologies dynamic signal analyzer used for recording and analyzing crosshole measurements (Hossain 2010).

6.2.2.2 Procedures

General procedures outlined in ASTM D 4428 were followed to perform the crosshole tests. During testing with the solenoid hammer source, the source was connected to the signal analyzer via the control box shown in Figure 6.5. The control box had a switch for selecting the solenoid that would hit and another switch for initiating the hit. Both of the receivers were connected to the analyzer directly with the cables. The air bladders attached to the receivers were connected to the pressure manifold and then to the air pump.

For testing with the solenoid hammer source, the source and the receiver probes were lowered into the casings down to the test depth. To keep the source and the receivers firmly held against the casing wall, the air bladders attached to the receiver probes and the piston part of the source were pressurized using the air pump. The pressure was controlled through the pressure manifold. Compression (P) waves were produced using the horizontally hitting solenoid oriented directly towards the receivers. Vertically polarized shear (sHV) waves were produced using the downward and upward hitting solenoids. For horizontally polarized (sHH) waves, the source was rotated 90° both clockwise and counterclockwise so that the horizontal solenoid was hitting transverse to the borehole array. The trigger signal from the source accelerometer and the signals received by the geophones were recorded by the signal analyzer. The procedure was repeated at each test depth. Testing with the solenoid hammer source was conducted at depth intervals of 0.6 m to a maximum depth of 11 m. Often multiple hits were conducted to ensure the best possible record for a given depth.

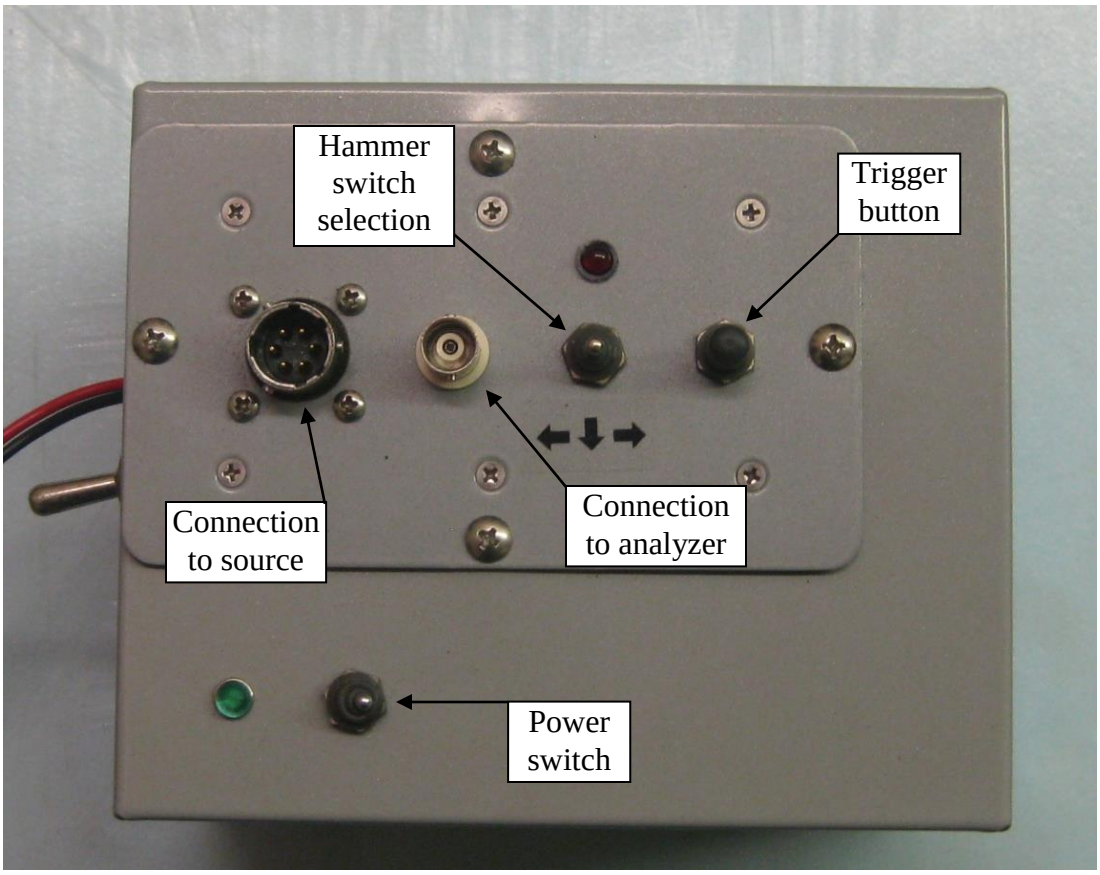

Figure 6.5: Solenoid hammer control box used in crosshole testing (Hossain 2010).

For testing with the dynamic cone source, the cone was driven into the ground in alignment with the boreholes to the selected test depth. To create stress waves rich in P or sHV energy, the top of the cone rod was hit manually either with a hand-held hammer or by lifting and dropping the steel ring weight onto the anvil. The falling steel ring weight seemed to generate better signals than the hand-held hammer. The vertically oriented receivers at the same depth as the cone tip were used to record wave forms. True interval measurements were obtained by recording the receiver signals in two boreholes generated from one hit with the dynamic cone source. Tests were carried out at depth intervals of 0.3 m or 0.6 m down to a maximum depth of 5.5 m. The recording and analysis procedures were the same as used in interval testing with the solenoid hammer source.

Figure 6.6 is a photograph taken during crosshole testing at the Hollywood Ditch site. As seen in Figure 6.6, the top of the rod attached to the dynamic cone source is being hit by a hand-held hammer to create waves rich in P and sHV energy. The fastest wave path is assumed to be down the steel rod and horizontally across to the two nearest boreholes where geophones are placed inside to record the wave signals.

Figure 6.6: Photograph of seismic crosshole testing at the Hollywood Ditch site.

6.2.2.3 Inclination Survey

The following is a description of the inclination survey conducted at the six crosshole sites as presented in Hossain (2010):

"The distance between casings was measured at the ground surface. Below the ground surface, an inclination survey was conducted to determine the deviation of casings from the vertical position. The inclination surveys were conducted at each site following the general procedures outlined in ASTM D4428-D4428M. A Slope Indicator system manufactured by Durham Geo Slope Indicator (DGSI) was used for the survey. The apparatus consisted of an inclinometer probe and a digital data collection device, as shown in Figure [6.7]

"The A_0A_{180} direction was considered along the borehole alignment, and the B_0B_{180} at 90° with the borehole alignment. The inclinometer probe was lowered to the bottom of the casing keeping the upper wheels in the A_0 groove, and readings of A_0 and B_0 were taken at 0.6 m depth intervals with the data collection device. A_{180} and B_{180} readings were obtained repeating the procedure keeping the upper wheels of inclinometer probe in A_{180} groove. The algebraic sum of A_0 and A_{180} gives the combined A reading at any depth.

"The readings obtained from the data collection device are in specific 'reading units' which must be converted to lateral displacement values. The following equation is provided by DGSI to convert the readings into displacements for every 0.6 m (2 ft) depth interval:

Figure 6.7: Digitilt Slope Inclinometer system manufactured by DGSI (Geiger 2010).

Displacement (in.) = 24 (Current combined reading - initial combined reading) / (2 × 20000) (6.2)

Displacements in both A and B directions were estimated for each borehole casing. Because the lateral displacements in the B direction were not significant in velocity calculations, only the A direction data were used for correcting the distances between casings."

Plots of the displacements of each borehole casing at the six crosshole sites are presented in Appendix B. The maximum correction on the horizontal distance between casings was 129 mm at a depth of 11 m at the Hobcaw Borrow Pit site.

6.2.2.4 Data Reduction

In testing with the solenoid hammer source, the three borehole arrangement allowed for direct and interval stress wave travel time measurements. Interval measurements are considered more reliable because the effects of grout and soil disturbance caused by drilling cancel out in the travel time calculation. Both direct and interval measurements are useful for identifying refracted waves. However, the energy of the solenoid hammer used in this study was often too weak for good, reliable wave form recordings in the far borehole to complete the interval measurements. In testing with the dynamic cone source, both of the measurements were interval measurements as the source was positioned at some distance from the boreholes and no trigger accelerometer was attached to the dynamic cone rod. So, in the case of testing with the solenoid hammer source, one trigger and two receiver signals were obtained, while in the case of testing with the dynamic cone source, two receiver signals were obtained.

Back in the laboratory, the trigger and receiver signals were recalled using the dynamic signal analyzer. The trigger or first arrival points of waves were carefully identified. The first high frequency movement in the record was considered as the arrival point. The travel time was corrected for the grout thickness and an accelerometer source-to-geophone receiver travel calibration factor for the direct measurements. No travel time correction was necessary for the interval measurements.

A sample set of trigger and first receiver P-wave signals using the solenoid hammer source at the Hollywood Ditch site is presented in Figure 6.8; and a sample set of first and second receiver P-wave signals using the dynamic cone source at the Hollywood Ditch site and testing the same interval is presented in Figure 6.9. The signal-to-noise ratio was much higher in the receiver records using the dynamic cone source, than in the receiver records using the solenoid hammer source. As can be seen in the sample records presented in Figures 6.8 and 6.9, values of V_P (1,607 m/s and 1,516 m/s) obtained from both set ups are within 6%.

A sample set of trigger and first receiver sHV-wave signals using the solenoid hammer source at the Hollywood Ditch site is presented in Figure 6.10; and a sample set of first and second receiver sHV-wave signals using the dynamic cone source at the Hollywood Ditch site and testing the same interval is presented in Figure 6.11. As can be seen in Figures 6.10 and 6.11, values of V_{sHV} (176 m/s and 185 m/s) obtained from both set ups are within 7%.

Sample sets of trigger and first receiver sHH-wave signals using the solenoid hammer source rotated 90° clockwise and 90° counterclockwise with respect to the

borehole alignment at the Hollywood Ditch site are presented in Figure 6.12 and 6.13, respectively. As can be seen in Figures 6.12 and 6.13, values of V_{sHH} (124 m/s and 121 m/s) obtained from both hits are within 3%.

The records were classified as excellent, very good, good, fair, and poor depending on the relative amount of noise in the signal and the level of ease in picking the arrival points. Poor records were not used in to calculate velocities. The P-wave recordings presented in Figure 6.8 are classified as very good and the P-wave recordings presented in Figure 6.9 are classified as excellent. The sHV-wave recordings presented in Figures 6.10 and 6.11 are classified as very good and excellent, respectively. The sHH-wave recording presented in both Figures 6.12 and 6.13 are classified as very good.

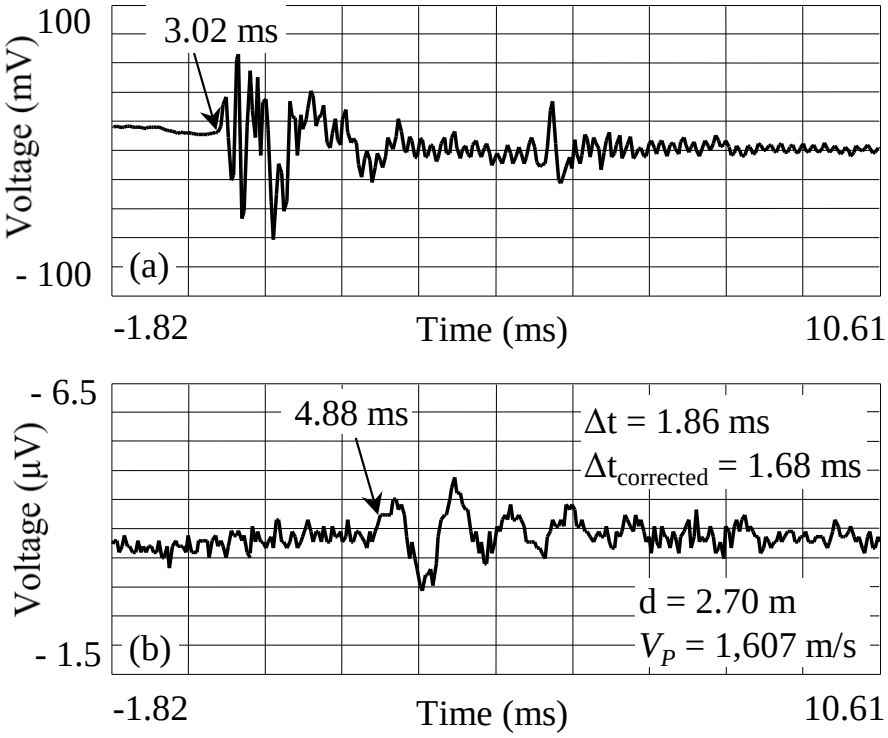

Figure 6.8: P-wave records from the Hollywood Ditch site with the solenoid hammer source at depth of 3.7 m − (a) signal from trigger accelerometer in BH3, and (b) signal from first receiver in BH2.

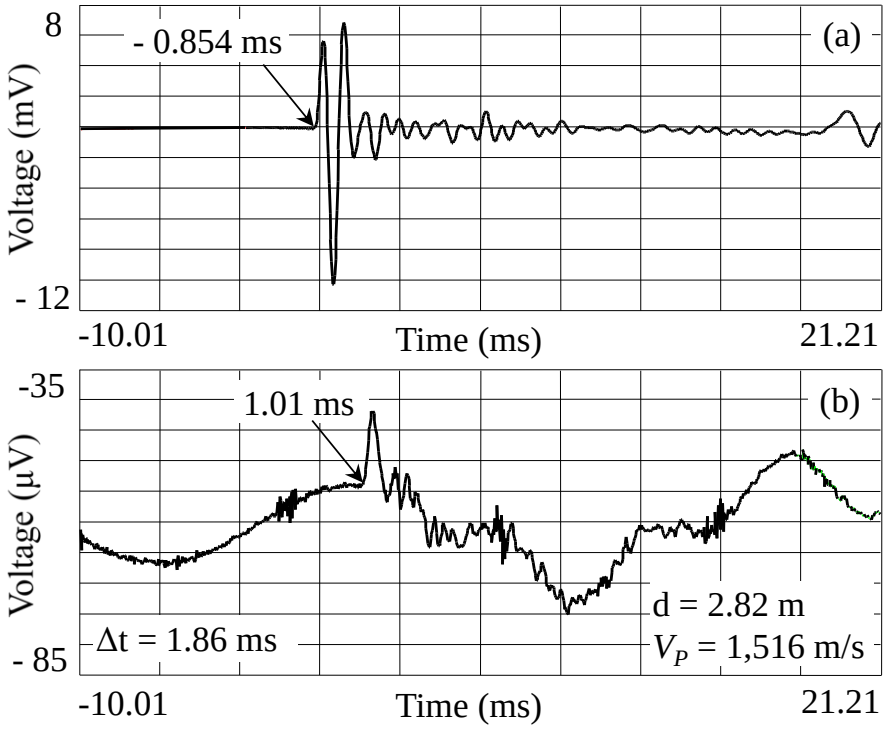

Figure 6.9: P-wave records from the Hollywood Ditch site with the dynamic cone source at depth of 3.7 m − (a) signal from first receiver in BH3, and (b) signal from second receiver in BH2.

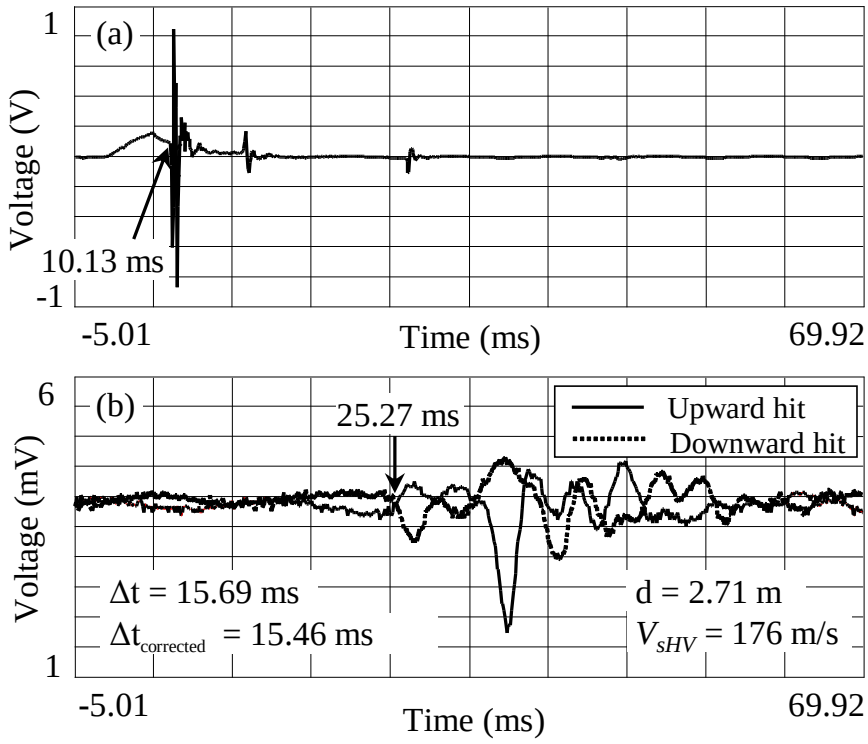

Figure 6.10: sHV-wave records from the Hollywood Ditch site with the solenoid hammer source at depth of 3.0 m − (a) signal from trigger accelerometer in BH3, and (b) signals from first receiver in BH2.

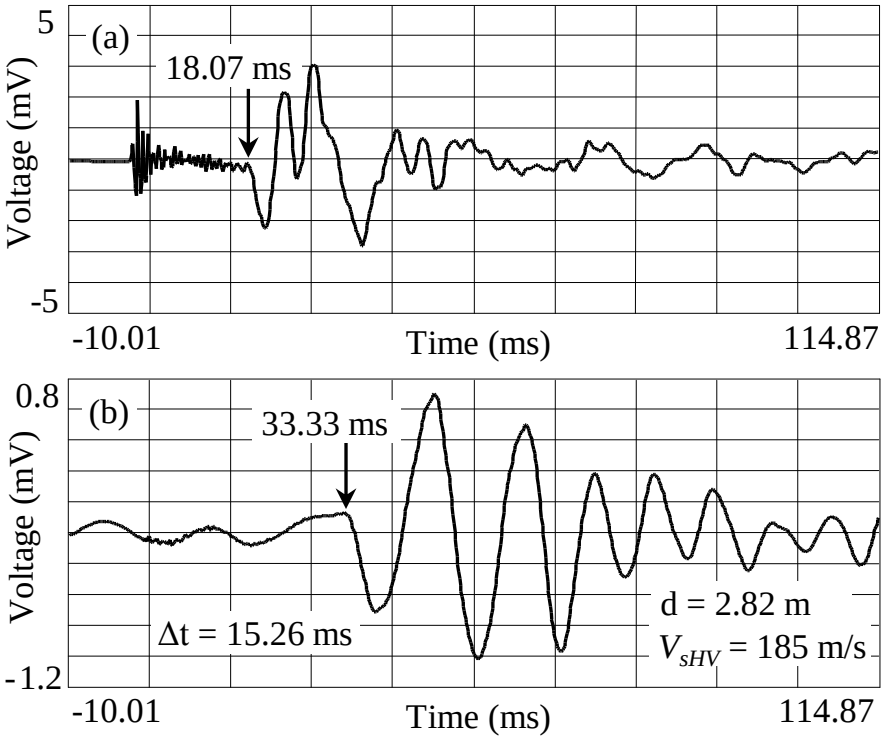

Figure 6.11: sHV-wave records from the Hollywood Ditch site with the dynamic cone source at depth of 3.0 m − (a) signal from first receiver in BH3, and (b) signal from second receiver in BH2.

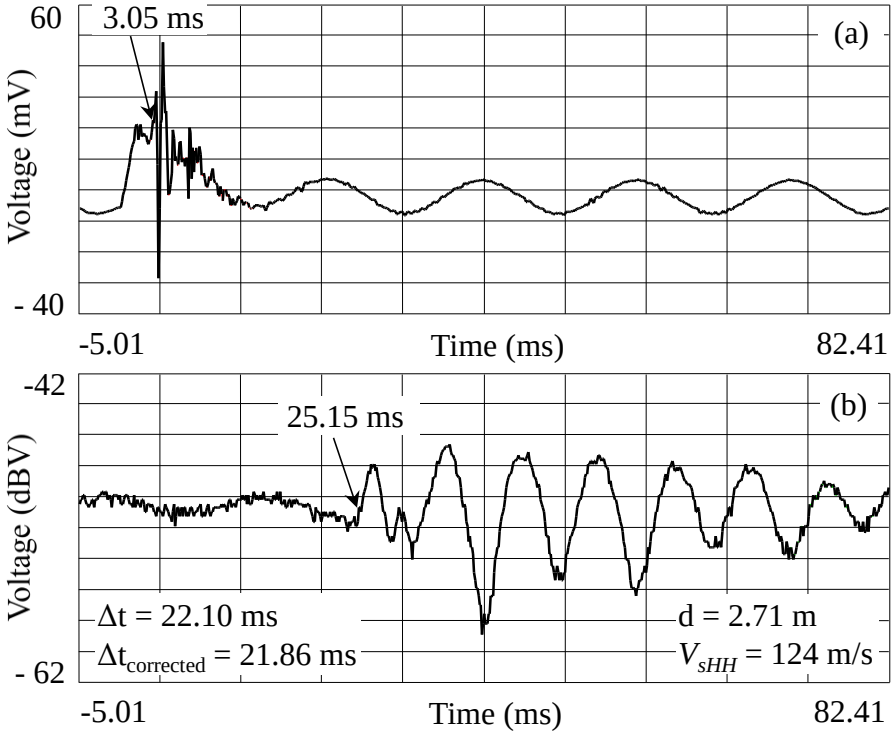

Figure 6.12: sHH-wave records from the Hollywood Ditch site with the solenoid hammer source rotated 90° clockwise at depth of 3.0 m − (a) signal from trigger accelerometer in BH3, and (b) signal from first receiver in BH2.

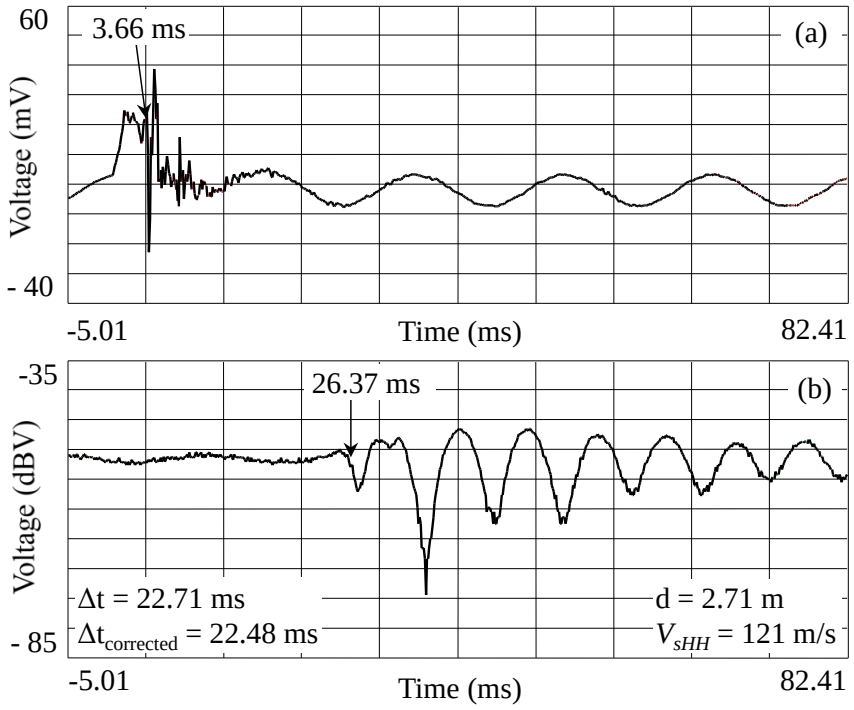

Figure 6.13: sHH-wave records from the Hollywood Ditch site with the solenoid hammer source rotated 90° counterclockwise at depth of 3.0 m − (a) signal from trigger accelerometer in BH3, and (b) signal from first receiver in BH2.

6.3 Results

Shown in Figures 6.14-6.21 are the profiles of wave velocity and K_0 estimated from V_{sHH}/V_{sHV} ratios at the eight sites. Also shown in Figures 6.14-6.21 are the layouts of boreholes associated with the crosshole tests, the seismic cone (SC) soundings, and the piezometer standpipe (P1) installations. The velocity data from SCPT are plotted at the average of top and bottom geophone depths. The velocity data from crosshole are plotted at the measurement depths and grouped by the test interval, with the first borehole designation for the location of the source or the near receiver and the second borehole designation for the location of the near or the far receiver, and by the stress-wave source (SH = solenoid hammer, DC = dynamic cone) used. The designations D, I, N, and F represent direct measurement, interval measurement, near interval and far interval, respectively. For example, in Figure 6.14, "BH2-BH3, DC-I,F" is the designation for a far interval measurement between boreholes BH2 and BH3 with the dynamic cone source positioned to the left of borehole BH1.

Measured groundwater table depths at the eight sites range from 0.4 to 2.8 m below the ground surface, depending on the site and the time of year. Summer groundwater table depths are typically 0.3 to 0.8 m lower than spring groundwater table depths.

At the time of crosshole testing, estimated depths to the tops of saturated ($V_P \geq$ 1,400 m/s) zones range from 2.1 to 3 m at the six crosshole sites. Thus, as discussed in Hossain (2010), unsaturated (i.e., V_P < 1,400 m/s) zones extended from 0.2 to 1.3 m below the groundwater tables at these six sites. The unsaturated zones below the

groundwater tables appear to be due to the seasonal fluctuations in the groundwater tables.

Values of K_0 are estimated using the following equation derived in Section 3.4:

$$K_0 = 0.041\log(t_1) + \left(\frac{V_{sHH}}{V_{sHV}}\right)^{8.0} \quad (6.3)$$

Because Equation (6.3) was derived based on results from laboratory and in-situ tests on clean sands, Figures 6.14-6.21 only includes the K_0 estimates for the sand layers with a fines content ≤ 15%.

6.3.1 Coastal Research and Education Center Site

Presented in Figure 6.14 are the wave velocity profiles from three SCPTs (i.e., SC1, SC3 and SC6) and one crosshole test array in the top 10 m of soil at the CREC site. SC6 is the SCPT nearest the crosshole test array, located 7.6 m away.

The groundwater table during testing in March 2008 was measured in a hand-augured hole at a depth of 1.0 m. During testing in April 2011, the groundwater table was measured in another hand-augured hole at a depth of 1.3 m.

The V_P profiles determined by the crosshole test are presented in Figure 6.14b. The V_P values of 706 and 560 m/s at depths of 1.5 and 1.8 m, respectively indicate unsaturated zone below the groundwater table and possibly refracted waves off of the lower saturated zone. Thus, the unsaturated zone at CREC exists above the depth of 2.1 m.

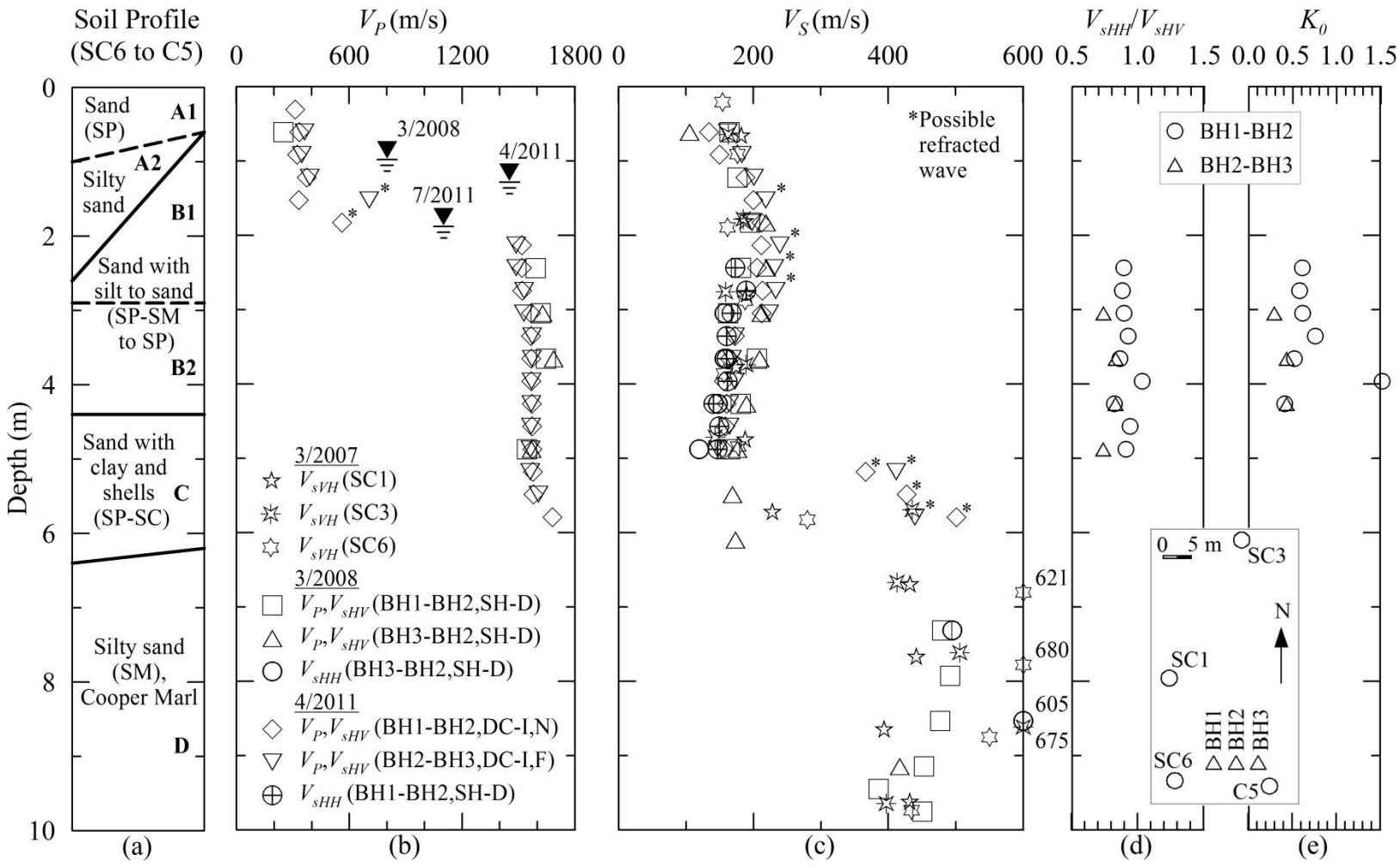

Figure 6.14: Profiles of seismic wave velocities and velocity-based K_0 estimates from the CREC site.

The V_S profiles are presented in Figure 6.14c. The layer most susceptible to liquefaction (or critical layer) is defined as the layer of saturated non-plastic soil having generally the lower values of stress-corrected V_S and penetration resistances, and the greatest cyclic stress ratio. At CREC, the critical layer is Sub-layer B2, as will be shown in Chapter 7. The average value of V_{sHV} from crosshole testing in Sub-layer B2 is 180 m/s, while the average V_{sVH} from SC6 is 156 m/s. The high average V_{sHV} and V_{sVH} of 451 and 498 m/s, respectively, measured in Layer D are common at the top of the Cooper Marl. The results indicate good general agreement between crosshole and SCPT V_S measurements. The average value of V_{sHH} in Sub-layer B2 is 156 m/s.

The profiles of the V_{sHH}/V_{sHV} ratios are presented in Figure 6.14d. The average value of V_{sHH}/V_{sHV} in Sub-layer B2 is 0.87. The average estimated K_0 from V_{sHH}/V_{sHV} measurements in Sub-layer B2 is 0.53, which agrees with the average K_0 (0.51) estimated from the DMT-CPT-*OCR* approach as discussed in Chapter 5.

6.3.2 Hobcaw Borrow Pit Site

Presented in Figure 6.15 are the wave velocity profiles from three SCPTs (i.e., SC1, SC2 and SC3) and one crosshole test array in the top 10 m of soil at the Hobcaw Borrow Pit site. SC2 is the SCPT nearest the crosshole test array, located 2.8 m away.

The groundwater table during testing in November 2008 was measured at a depth of 2.0 m in the piezometer standpipe. During testing in June 2010, the groundwater table was measured at a depth of 2.8 m in the piezometer standpipe.

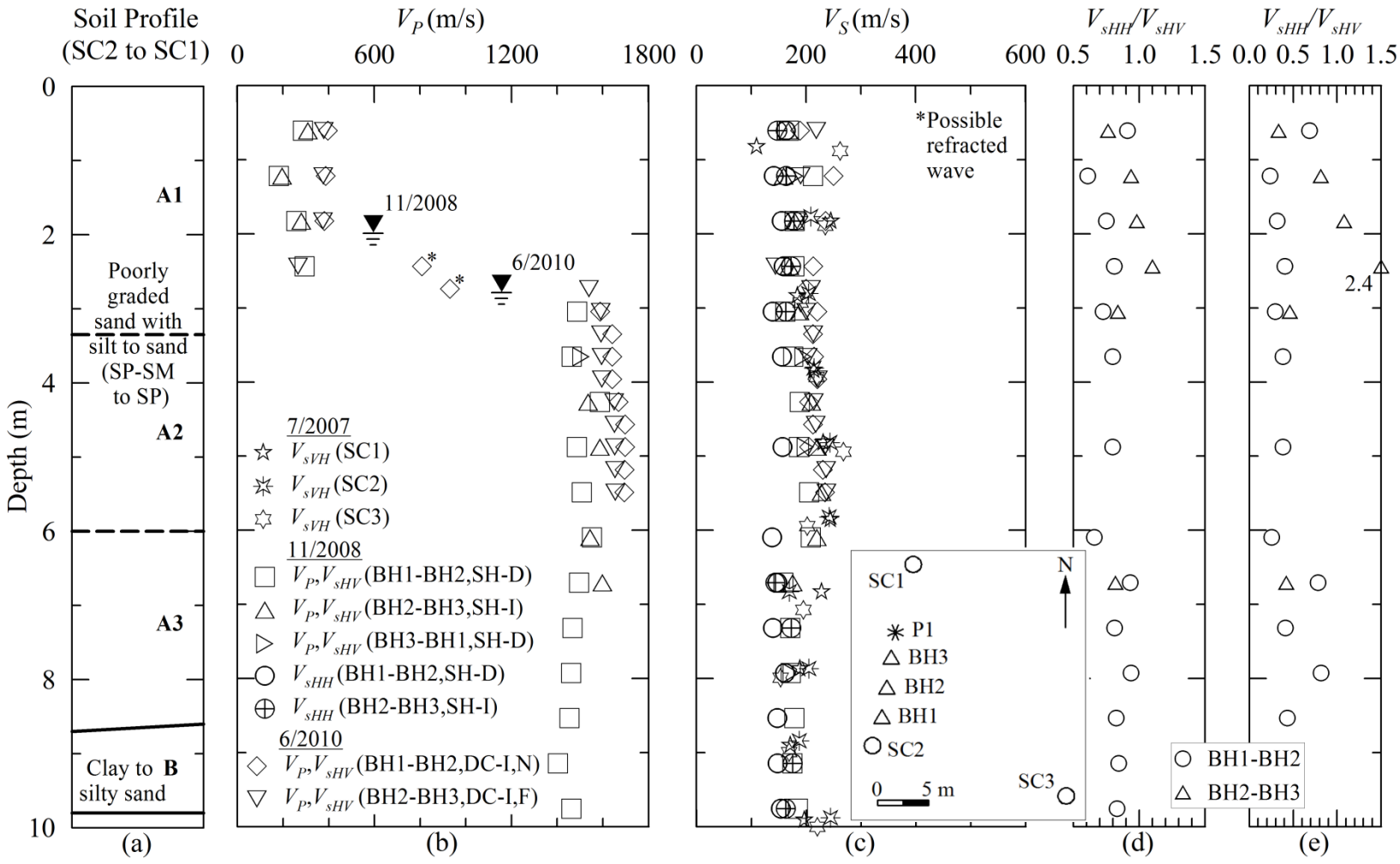

Figure 6.15: Profiles of seismic wave velocities and velocity-based K_0 estimates from the Hobcaw Borrow Pit site.

The V_P profiles are presented in Figure 6.15b. The June 2010 measurements suggest refraction of P-waves for measurements at 2.4 and 2.7 m. Thus, the unsaturated zone exists above the depth of 2.7 m at the Hobcaw Borrow Pit site.

The V_S profiles are presented in Figure 6.15c. Sub-layer A3 is the critical layer at the site, as will be shown in Chapter 7. The average value of V_{sHV} from crosshole in Sub-layer A3 is 180 m/s, while the average V_{sVH} from SC2 is 186 m/s. These results indicate very good agreement between crosshole and SCPT V_S measurements. The average value of V_{sHH} in Sub-layer A3 is 150 m/s.

The profiles of the V_{sHH}/V_{sHV} ratios are presented in Figure 6.15d. The average value of V_{sHH}/V_{sHV} in Sub-layer A3 is 0.83. The average estimated K_0 from V_{sHH}/V_{sHV} measurements in Sub-layer A3 is 0.44, which is lower than the average K_0 (0.57) estimated from the DMT-CPT-*OCR* approach.

6.3.3 Walterboro Rest Area Site

Presented in Figure 6.16 are the wave velocity profiles from three SCPTs (i.e., SC1, SC2 and SC3) and one crosshole test array in the top 10 m of soil at the Walterboro Rest Area site. SC3 is the SCPT nearest the crosshole test array, located 3.5 m away.

The groundwater table measured in the piezometer standpipe was at depths of 1.7 and 2.3 m during testing in January and June 2010, respectively.

The V_P profiles are presented in Figure 6.16b. The V_P values of 319 - 1182 m/s between 2.3 and 2.7 m provide strong evidence of unsaturated zone below the groundwater table. Thus, the unsaturated zone exists above the depth of 3.0 m at the

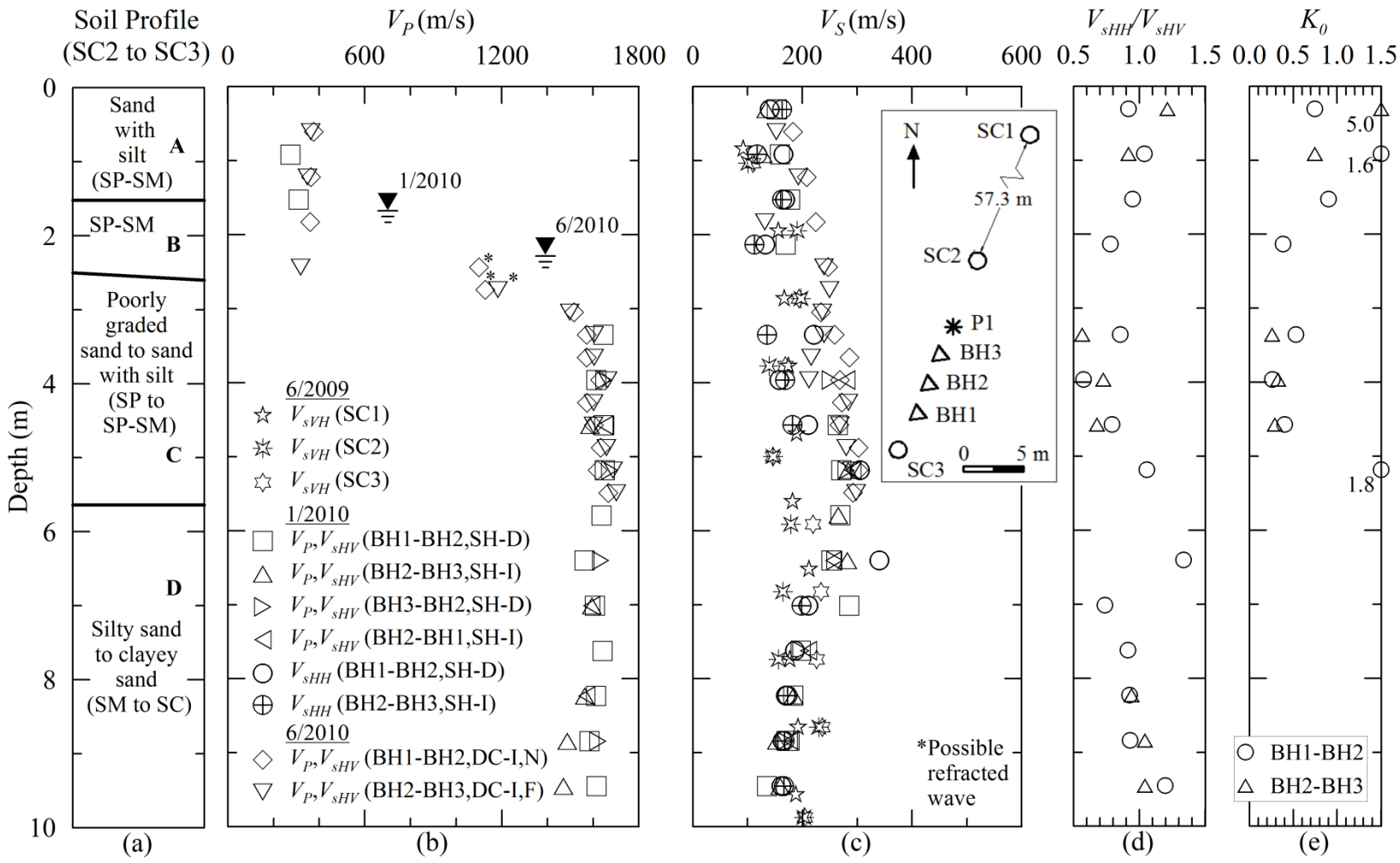

Figure 6.16: Profiles of seismic wave velocities and velocity-based K_0 estimates from the Walterboro Rest Area site.

Walterboro Rest site.

The V_S profiles are presented in Figure 6.16c. Layer C is the critical layer at the site, as will be shown in Chapter 7. The average value of V_{sHV} from crosshole in Layer C is 269 m/s, while the average V_{sVH} from SC3 is 157 m/s. These results indicate a large difference between crosshole and SCPT V_S measurements, and suggest sufficient lateral variation in soil properties. The average value of V_{sHH} in Layer C is 197m/s.

The profiles of V_{sHH}/V_{sHV} ratios are presented in Figure 6.16d. The average value of V_{sHH}/V_{sHV} in Layer C is 0.75. The average estimated K_0 from V_{sHH}/V_{sHV} in Layer C is 0.35, which is significantly lower than the average K_0 (0.79) estimated from the DMT-CPT-*OCR* approach.

6.3.4 Hobcaw Beach Ridge Site

Presented in Figure 6.17 is the shear wave velocity profile from the SCPT in the top 10 m of soil at the Hobcaw Beach Ridge site. The groundwater table was found at a depth of 0.4 m in the hand-auger sample hole during testing in March 2012.

As seen in Figure 6.17b, the average values of V_{sVH} in Layers A, B, C and D are 208, 177, 156 and 251 m/s, respectively.

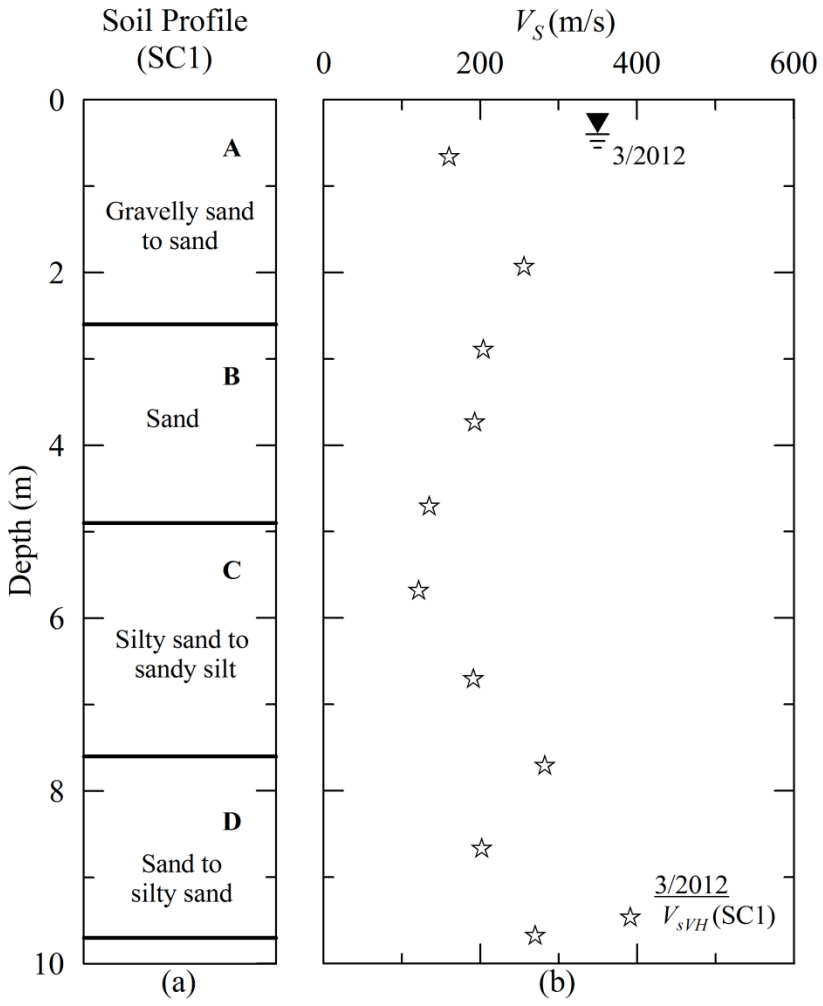

Figure 6.17: Profiles of shear wave velocitiey from the Hobcaw Beach Ridge site.

6.3.5 Walterboro Lowcountry Site

Presented in Figure 6.18 are the shear wave velocity profiles from three SCPTs (i.e., SC1, SC2 and SC3) in the top 10 m of soil at the Walterboro Lowcountry site. As seen from the site layout shown in Figure 6.18, the locations of SCPTs are within a distance of 47.7 m. The groundwater table was estimated to be at a depth of 1.5 m during testing in June 2009 based on the water level in the adjacent lake.

As seen in Figure 6.18b, the shear wave velocity is fairly constant with depth. In Layer C, the critical layer, the average value of V_{sVH} is 213 m/s.

6.3.6 Hollywood Ditch Site

Presented in Figure 6.19 are the wave velocity profiles from three SCPTs (i.e., SC1, SC2 and SC3) and one crosshole test array in the top 10 m of soil at the Hollywood Ditch site. SC1 is the SCPT nearest the crosshole test array, located 7.2 m away.

The groundwater table measured in a piezometer standpipe was at a depth of 2.0 m during testing in June 2010.

The V_P profiles are presented in Figure 6.19b. The V_P value of 1,253 m/s at a depth of 2.4 m indicates unsaturated zone below the groundwater table and possibly a refracted wave. Thus, the unsaturated zone at Hollywood Ditch exists above the depth of about 2.8 m.

The V_S profiles are presented in Figure 6.19c. The critical layer is Sub-layer B2. The average value of V_{sHV} from crosshole testing in Sub-layer B2 is 157 m/s, while the average V_{sVH} from SC1 is 152 m/s. These results indicate excellent agreement between

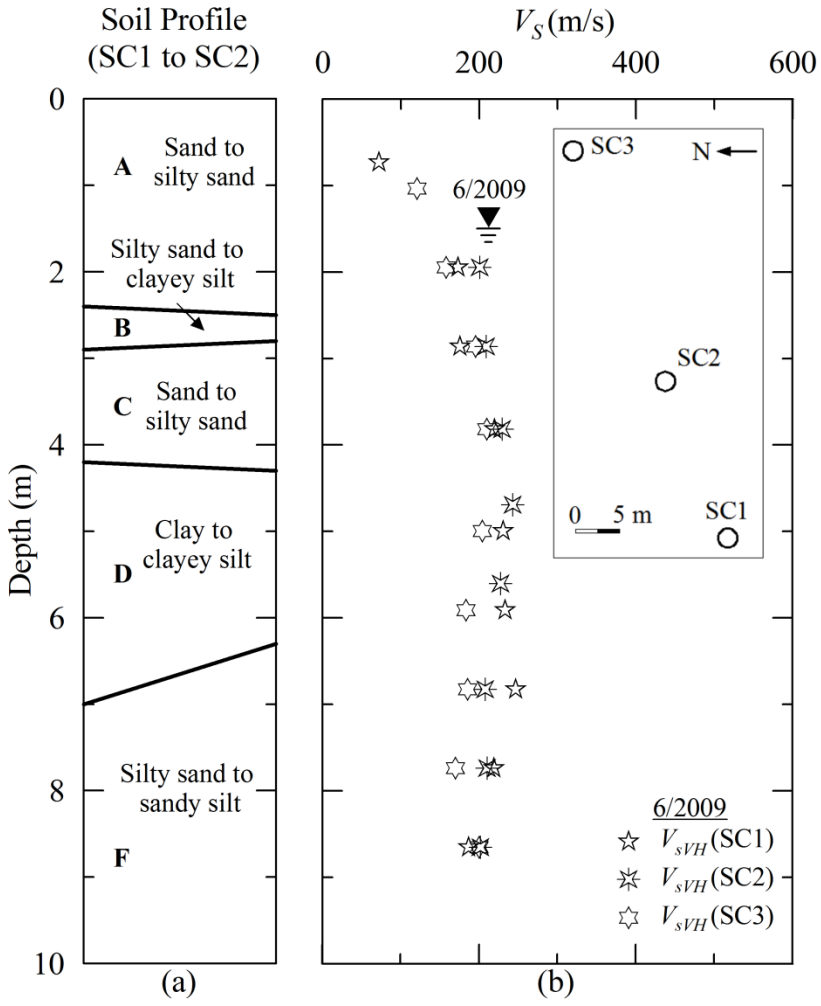

Figure 6.18: Profiles of shear wave velocitiy from the Walterboro Lowcountry site.

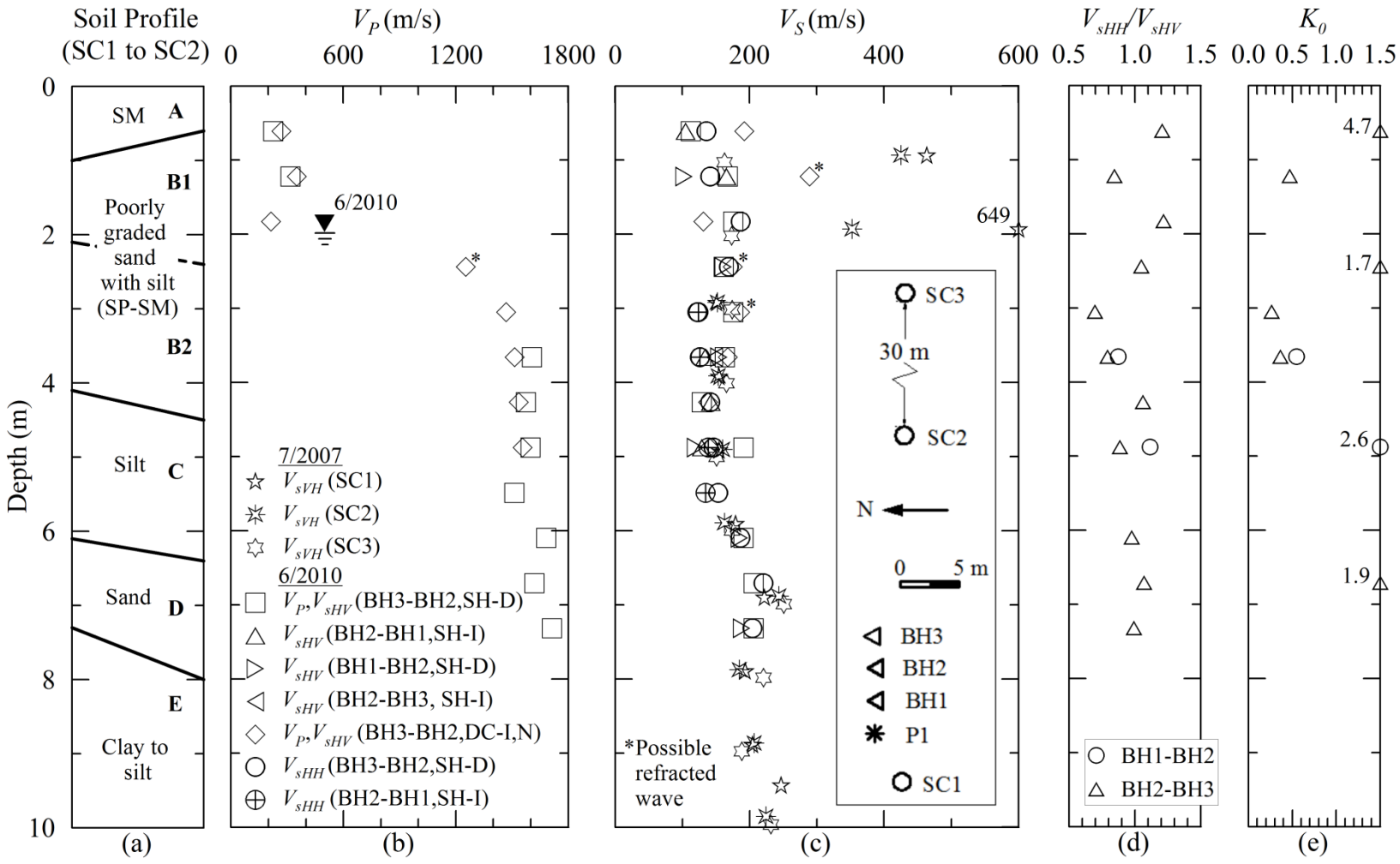

Figure 6.19: Profiles of seismic wave velocities and velocity-based K_0 estimates from the Hollywood Ditch site.

crosshole and SCPT V_S measurements. The average value of V_{sHH} in Sub-layer B2 is 124 m/s.

The profiles of the V_{sHH}/V_{sHV} ratios are presented in Figure 6.19d. The average value of V_{sHH}/V_{sHV} in Sub-layer B2 is 0.79. The average estimated K_0 from V_{sHH}/V_{sHV} in Sub-layer B2 is 0.36, which is significantly lower than the average K_0 (0.61) estimated from the DMT-CPT-*OCR* approach.

6.3.7 Sampit Site

Presented in Figure 6.20 are the wave velocity profiles from three SCPTs (i.e., SC1, SC2 and SC3) and one crosshole test array in the top 10 m of soil at the Sampit site. SC1 is the SCPT nearest the crosshole test array, located 2.7 m away.

The groundwater table measured in a piezometer standpipe was at a depth of 1.9 m during testing in June 2010.

The V_P profiles are presented in Figure 6.20b. The V_P value of 881 m/s at a depth of 1.8 m indicates unsaturated zone below the groundwater table and/or a refracted wave. Thus, the unsaturated zone exists at Sampit above the depth of about 2.4 m.

The V_S profiles are presented in Figure 6.20c. Sub-layer A2 is the critical layer at the site. The average value of V_{sHV} from crosshole in Sub-layer A2 is 236 m/s, while the average V_{sVH} from SC1 is 271 m/s. These results indicate some variation between crosshole and SCPT V_S measurements. The average value of V_{sHH} in Sub-layer A2 is 196 m/s.

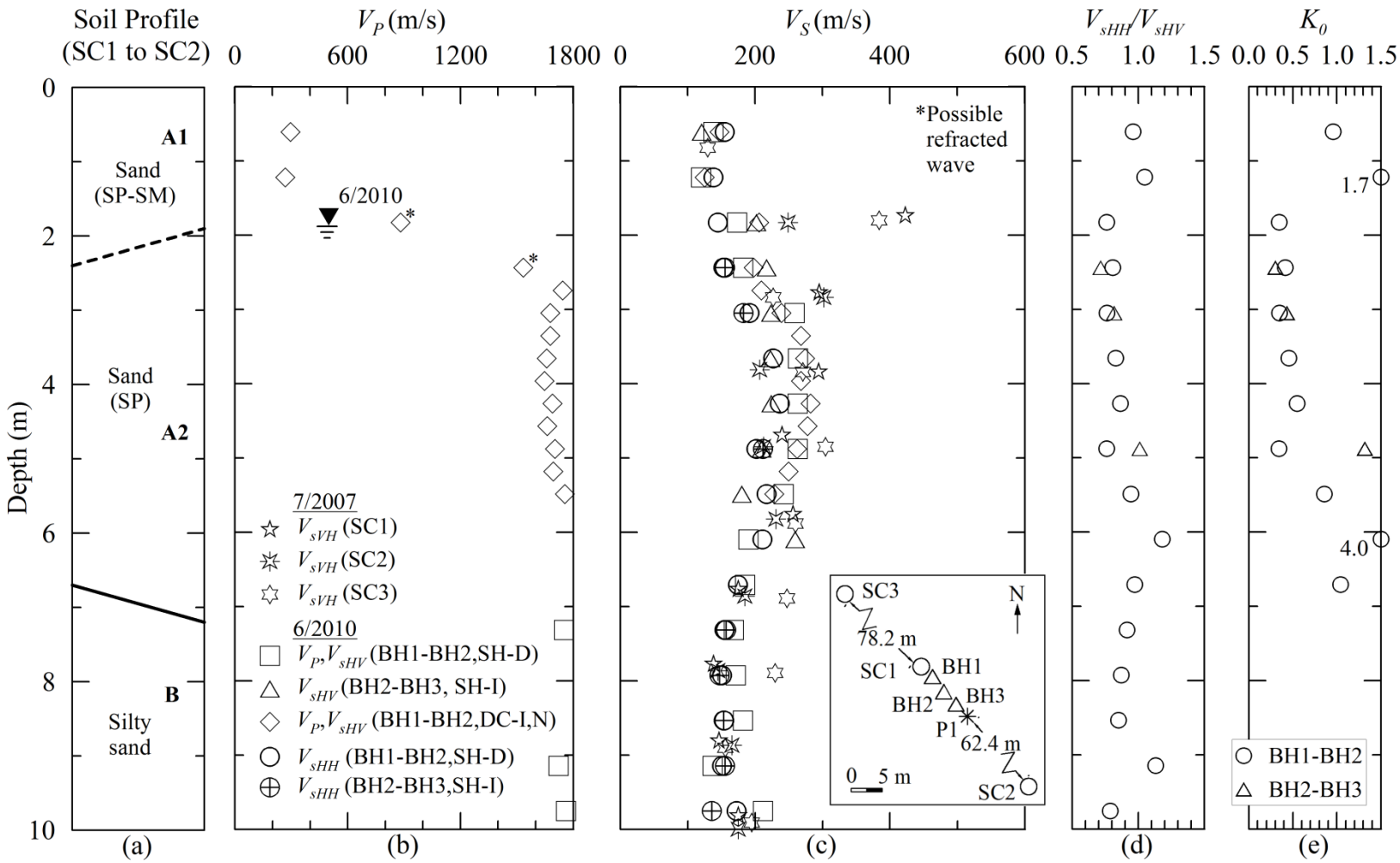

Figure 6.20: Profiles of seismic wave velocities and velocity-based K_0 estimates from the Sampit site.

The profiles of the V_{sHH}/V_{sHV} ratios are presented in Figure 6.20d. The average value of V_{sHH}/V_{sHV} in Sub-layer A2 is 0.88. The average estimated K_0 from V_{sHH}/V_{sHV} in Sub-layer A2 is 0.59, which is significantly lower than the average K_0 (0.83) estimated from DMT- CPT-*OCR*.

6.3.8 Four Hole Swamp Site

Presented in Figure 6.21 are the wave velocity profiles from three SCPTs (i.e., SC1, SC2 and SC3) and one crosshole test array in the top 10 m of soil at the Four Hole Swamp site. SC1 is the SCPT nearest the crosshole test array, located 2.7 m away.

The groundwater table measured in a piezometer standpipe was at depth of 2.2 m during testing in June 2010. The V_P profiles are presented in Figure 6.21b. The unsaturated zone at Four Hole Swamp exists above the depth of 2.4 m.

The V_S profiles are presented in Figure 6.21c. The critical layer is Sub-layer A2. The average value of V_{sHV} from crosshole in Sub-layer A2 is 153 m/s, while the average V_{sVH} from SC1 is 166 m/s. The average value of V_{sHH} in Sub-layer A3 is 139 m/s. The high average V_{sHV} and V_{sVH} of 485 and 632 m/s, respectively, measured in Layer B are common at the top of the Cooper Marl. These results indicate good agreement between crosshole and SCPT V_S measurements.

The profile of the V_{sHH}/V_{sHV} ratios is presented in Figure 6.21d. The average value of V_{sHH}/V_{sHV} in Sub-layer A2 is 0.87. The average estimated K_0 from V_{sHH}/V_{sHV} in Sub-layer A2 is 0.57, which agrees with the average K_0 (0.58) estimated from the CPT-DMT-*OCR* approach.

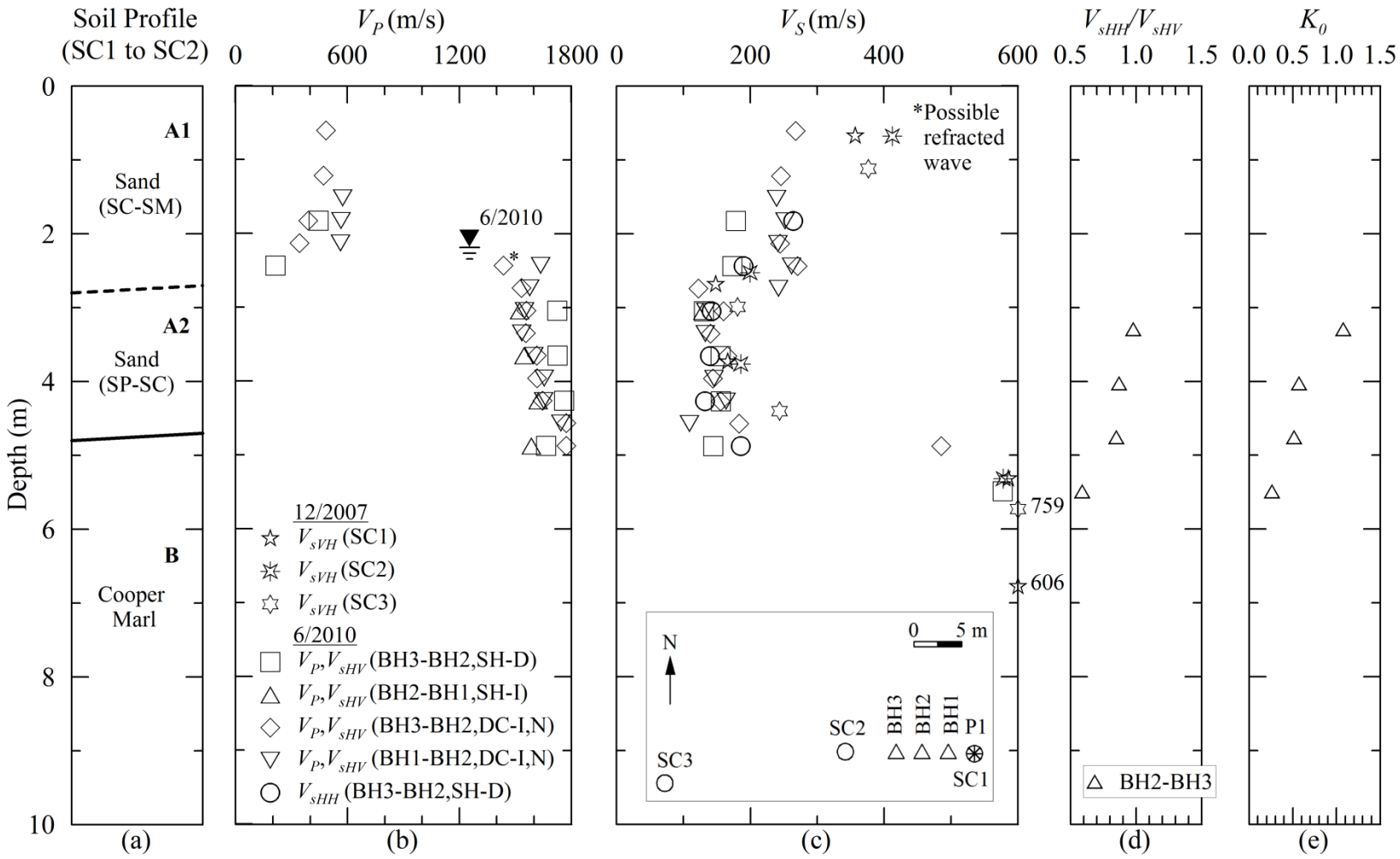

Figure 6.21: Profiles of seismic wave velocities and velocity-based K_0 estimates from the Four Hole Swamp site.

6.4 Summary

Profiles of seismic wave velocities from cone and crossohole testing at eight sites in the SCCP were presented in this chapter. A summary of the results from the critical sand layers at each site is presented in Table 6.1. As seen from Table 6.1, values of V_P in the critical layer at the six crosshole sites are greater than 1,400 m/s indicating these sand layers are saturated. The average V_{sVH} values from seismic cone at the eight sites (based on only the cone test nearest to crosshole location at the crosshole sites) range between 152 and 241 m/s. The V_{sHV} and V_{sVH} values at the crosshole sites are in general agreement with each other.

Average values of V_{sHV} range from 153 to 269 m/s and average values of V_{sHH} range from 124 to 197 m/s in the critical layers. Average ratio of V_{sHH} to V_{sHV} at the six crosshole sites ranges between 0.75 and 0.88, indicating greater overall stress (and may be structural stiffness) in the vertical direction than in the horizontal direction. The average values of K_0 estimated from these ratios of V_{sHH} to V_{sHV} range from 0.35 to 0.59. At two of the six sites, the velocity-based K_0 estimates agree with the estimates based on DMT-CPT-*OCR* presented in Chapter 5. At the other four sites, K_0 estimates from the velocity-based method are lower than the estimates based on the DMT-CPT-*OCR* approach.

Table 6.1: Summary of seismic wave velocities and velocity based K_0 estimates for the critical layers at eight sites in the South Carolina Coastal Plain.

Site	Depth	SCPT	Crosshole				Average K_0 from V_{sHH}/V_{sHV}
		Average V_{sVH} (m/s)	Average V_P (m/s)	Average V_{sHV} (m/s)	Average V_{sHH} (m/s)	Average V_{sHH}/V_{sHV}	
CREC	2.9-4.4	156	1,587	180	156	0.87	0.53
Hobcaw Borrow Pit	6.0-8.7	169	1,510	180	150	0.83	0.44
Walterboro Rest Area	3.0-5.6	157	1,620	269	197	0.75	0.35
Hobcaw Beach Ridge	2.6-4.9	177	NA[a]	NA	NA	NA	NA
Walterboro Lowcountry	2.9-4.2	213	NA	NA	NA	NA	NA
Hollywood Ditch	2.8-4.1	152	1,529	157	124	0.79	0.36
Sampit	2.4-6.7	241	1,676	236	196	0.88	0.59
Four Hole Swamp	3.4-4.1	166	1,626	153	139	0.87	0.57

[a]Not available

CHAPTER 7

LIQUEFACTION EVALUATION OF EIGHT SITES IN THE SOUTH CAROLINA COASTAL PLAIN[1]

7.1 Introduction

Older sands often exhibit liquefaction resistance greater than younger sands because of various diagenetic processes that can occur over time, such as cementation at particle contacts, particle rearrangement and interlocking, densification due to seismic shaking, weathering, and contact force homogenation (Mitchell and Solymar 1984; Mesri et al. 1990; Schmertmann 1991; Gao et al. 2013). On the other hand, old natural sand can be just as liquefiable as freshly deposited sand, if the older sand experiences a disturbance that results in a loose structure or if dissolution of minerals occurs (Olson et al. 2001; Heidari and Andrus 2012). For example, Heidari and Andrus (2012) described 200,000-year-old sand deposits near Charleston, SC that have liquefaction resistances as low as loose Holocene sand, likely due to liquefaction and rearrangement of soil particles during the 1886 Charleston earthquake. The effect of diagenesis (often referred collectively as aging processes) must be taken into account to obtain accurate evaluations of liquefaction resistance.

[1]An earlier version of this chapter is published in the proceedings of ASCE's 2014Geocongress; Hossain, A. M., Geiger, A. J., Andrus, R. D., Hayati, H., Aboye, S. A., Esposito III, M. P., and Heidari, T. (2014). "In Situ Seismic Crosshole Testing of Six Natural Sand Deposits in the South Carolina Coastal Plain." *Proc., 2014 Geo-Congress: Geo-characterization and Modelling for Sustainability*, ASCE, Atlanta, GA, February 23-26, pp. 1142-1156.

During the 1886 Charleston earthquake with moment magnitude of ~7.0, significant liquefaction-induced ground failures occurred in the South Carolina Coastal Plain (SCCP), which included large sand blows as well as ground fissures (Dutton 1889). In addition, a number of researchers have discovered ground failures characteristic of liquefaction that pre-date the 1886 event at several locations in the SCCP (e.g., Weems et al. 1986; Obermeier et al. 1987; Amick et al. 1990; Talwani and Schaeffer 2001). Based on studies of these paleoliquefaction features, Talwani and Schaeffer (2001) suggested a recurrence rate between 500 and 600 years for magnitude 7+ earthquakes near Charleston.

In this chapter, the liquefaction potential of sand layers most susceptible to liquefaction at the five no liquefaction sites (i.e., CREC, Hobcaw Borrow Pit, Walterboro Rest Area, Hobcaw Beach Ridge, and Walterboro Lowcountry) and the three paleoliquefaction sites (i.e., Hollywood Ditch, Sampit, and Four Hole Swamp) in the SCCP is evaluated. Simplified liquefaction potential evaluation procedures are applied using the CPT tip resistance, SPT blow count, and V_s from seismic CPT and crosshole test results at the eight sites, assuming estimates of ground shaking during the 1886 earthquake.

7.2 Liquefaction Evaluation Procedures

The simplified liquefaction assessment procedure originally proposed by Seed and Idriss (1971) involves estimation of the seismic demand, expressed in terms of the cyclic stress ratio (*CSR*); and the capacity of the soil to resist liquefaction, expressed in

terms of the cyclic resistance ratio (*CRR*). *CSR* at a particular depth is a function of the horizontal peak ground acceleration (*PGA*), the total and effective vertical stresses at the depth of interest, and a shear stress-reduction coefficient. *CRR* is typically estimated using penetration resistance- or V_s-based charts developed from field case histories (Youd et al. 2001).

In CPT-based evaluation, the initial screening for liquefaction susceptibility of soils at the eight sites is conducted following the criteria by Robertson and Wride (1998) and modified by Hayati and Andrus (2008). According to the criteria, soils with the behavior type index (I_c) > 2.6 or the normalized cone pore pressure ratio, $B_q = (u_2 - u_0)/(q_t - \sigma_v)$ > 0.5 (where u_2 and u_0 are the pore pressure acting behind the cone tip and the hydrostatic pressure, respectively) are identified as non-susceptible to liquefaction. In SPT-based evaluation, soils with corrected blow count, $(N_1)_{60cs} \geq 30$ are considered too dense to liquefy (Youd et al. 2001). In V_S-based procedure, soils with *MEVR* corrected normalized V_S, $(V_{S1})_{cs}$ > 215 m/s are considered non-susceptible to liquefaction (Andrus et al. 2009). Thus, only the soils with $I_c \leq 2.6$ and $B_q \leq 0.5$, or $(N_1)_{60cs} < 30$, or corrected $(V_{S1})_{cs} \leq 215$ m/s and lie below the groundwater table are further evaluated using the simplified procedure.

Values of *CSR* are calculated for the SCCP sites assuming *PGA*s obtained from the simulated ground-motion map by Silva et al. (2003) for the 1886 earthquake. Vertical stresses are calculated using average unit weights determined from fixed-piston samples or estimated from penetration test results.

In the CPT-based evaluation, the values of *CRR* corresponding to an earthquake moment magnitude (M_w) of 7.5, $CRR_{7.5}$, are estimated from the clean-sand base curve by Robertson and Wride (1998) and recommended by Youd et al. (2001). In the SPT-based evaluation, the modified Seed et al. (1984) clean-sand base curve recommended by Youd et al. (2001) is used to estimate $CRR_{7.5}$. The clean-sand base curve by Andrus and Stokoe (2000) recommended by Youd et al. (2001) is used to estimate $CRR_{7.5}$ in the V_S-based evaluation. These CPT-, SPT- and V_S-based deterministic curves correspond to average probability of liquefaction (P_L) of about 50, 31, and 26%, respectively (Juang et al. 2002).

The *CSR* values are divided by a magnitude scaling factor (*MSF*) to obtain $CSR_{7.5}$. Values of *MSF* are calculated using the following equation (Youd et al. 2001):

$$MSF = \left(M_w/7.5\right)^{-2.56} \tag{7.1}$$

Three correction factors are applied to the values of $CSR_{7.5}$ when applicable – (a) diagenesis, K_{DR}, (b) overconsoildation, K_{OCR}, and (c) unsaturated conditions, K_S. These corrections are applied to the values of $CSR_{7.5}$ as follows:

$$CSR_{corrected} = \frac{CSR_{7.5}}{K_{DR} \times K_{OCR} \times K_S} \tag{7.2}$$

Values of K_{DR} are calculated using the following relationship with *MEVR* (Hayati and Andrus 2009):

$$K_{DR} = 1.08MEVR - 0.08 \tag{7.3}$$

Values of *MEVR* are computed using the measured V_S from SCPT or crosshole testing and estimated V_S using the following relationships developed by Andrus et al. (2004):

$$\left(V_{S1}\right)_{cs} = 62.6\left[\left(q_{t1N}\right)_{cs}\right]^{0.231} \tag{7.4}$$

$$(V_{S1})_{cs} = 87.8\left[(N_1)_{60cs}\right]^{0.253} \quad (7.5)$$

where $(q_{t1N})_{cs}$ and $(N_1)_{60cs}$ are CPT tip resistance and SPT blow count corrected to equivalent clean sand value, respectively. It should be noted that no correction for K_0 conditions (K_{K0}) different from about 0.5 is applied because it was shown in Chapter 2 that K_0 increases with age and its effect is believed to be captured by the K_{DR} factor. However, the K_{K0} correction can be of particular significance when the mechanism involved in lateral stress increase in soils is different from the natural field aging processes. For example, Salgado et al. (1997) suggested a K_0 correction while evaluating the ground improvement techniques that increase the lateral stress. In addition, K_{K0} correction can be important while evaluating dynamic lab test results where repeated shaking has induced lateral stress.

The correction factor, K_{OCR} recommended in Chapter 4 is expressed as:

$$K_{OCR} = OCR^{0.25} \quad (7.6)$$

As indicated in Chapter 4, *OCR* has an additional effect on liquefaction resistance other than through its effect on K_0. Thus, K_{OCR} is believed to be not a significant part of the K_{DR} correction and is also applied. K_{OCR} also can be significant in evaluating ground improvement techniques that induce overconsoildation through large prestressing effects (Salgado et al. 1997).

The correction factor for unsaturated conditions (V_P < 1,400 m/s) below the groundwater table (K_S) is calculated using the following equation (Hossain et al. 2013):

$$K_S = \left\{0.95 + e^{[2-1.95\ln(V_P/100-1.3)]}\right\}\left(M_w/8\right)^{(100-D_r)\Big/\left[\left(0.03D_r^2+1.31D_r\right)e^{2.85B}\right]} \quad (7.7)$$

where V_P is the compression wave velocity from crosshole testing, D_r is relative density expressed in percentage and B is Skempton's (Skempton 1954) pore-pressure coefficient. D_r is estimated based on the following relationship with $(N_1)_{60}$ suggested by Skempton (1986) for natural fine sand deposits:

$$D_r = \sqrt{(N_1)_{60}/55} \tag{7.8}$$

Skempton's B coefficient is estimated using the following relationship assuming a Poisson's ratio of the soil skeleton equals 0.3 (Kokusho 2000):

$$B = \frac{(V_P/V_S)^2 - 3.5}{(V_P/V_S)^2 - 4/3} \tag{7.9}$$

Because V_S is more sensitive to diagenesis than penetration resistances, an additional correction for diagenesis is applied to $(V_{S1})_{cs}$ as follows:

$$(V_{S1})_{cs,corrected} = (V_{S1})_{cs} / MEVR \tag{7.10}$$

Applying a correction to $(V_{S1})_{cs}$ for diagenesis and not penetration, assumes that the influence of diagenesis on penetration resistance is much smaller. This assumption makes sense because V_S is a small strain measurement, and penetration resistances are large strain measurements.

7.3 Results

7.3.1 Coastal Research and Education Center Site

Liquefaction evaluation of the CREC site is conducted using the results from three SCPT profiles (i.e., SC1, SC3 and SC6), one SPT profile and two sHV-crosshole

test profiles. The results of liquefaction evaluation for the top 10 m of soil at the CREC site based on the SC6 profile are presented in Figure 7.1. Results from the 5 other profiles are presented in Appendix F. Values of *CSR* are calculated based on an estimated *PGA* of 0.35 g at the site.

The groundwater table at the site lied at a depth of 0.9 m during testing in March 2007. Based on the V_P profile presented in Chapter 6, an unsaturated zone exists below the groundwater table from a depth of 0.9 to 2.1 m.

As seen in Figure 7.1f, the average *MEVR* in Layer B is 1.20 based on the SC6 data, which does support the classification of CREC as a no liquefaction site. The sands at CREC are assumed to be normally consolidated, as indicated in Chapter 5. Thus, no *OCR* correction is applied to the site data.

As seen in Figure 7.1h, the Sub-layers A2 and B1 have an average factor of safety (*FS*) of 1.6 and 1.3, respectively. With an average *FS* of 0.54, the Sub-layer B2 has the lowest *FS* and is identified as the critical layer with the greatest potential to liquefaction. Although *FS* of 0.54 suggests liquefaction during the 1886 Charleston earthquake, a thick capping layer may explain why surface manifestations were not observed.

Ishihara (1985) suggested that surface manifestations of liquefaction depend on the thickness of the liquefiable layer and the thickness of the non-liquefiable capping layer. Based on the criteria of Ishihara (1985), it is possible that liquefaction occurred in the 1.5-m-thick Sub-layer B2, but surface manifestations were prevented because of the overlaying 2.9 m of soil (Layers A and B1) and given *PGA* = 0.35g. Thus, the prediction

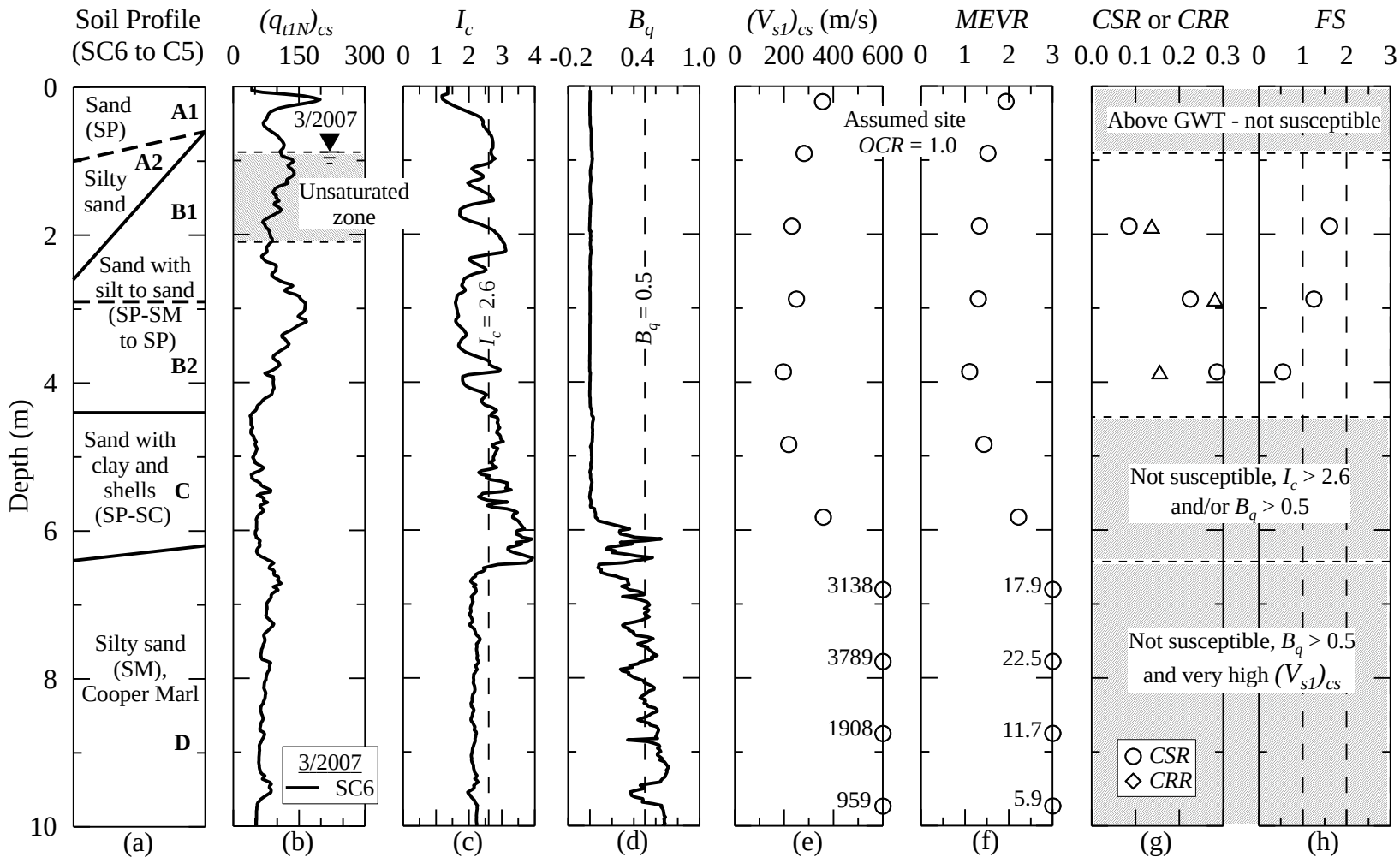

Figure 7.1: Liquefaction assessment of the CREC site based on seismic cone SC6 data reported in Boller (2008) and general CPT-based procedure recommended by Youd et al. (2001).

of liquefaction at CREC should not be considered as a false positive prediction just because surface manifestations were not reported in the area.

7.3.2 Hobcaw Borrow Pit Site

Liquefaction evaluation of the Hobcaw Borrow Pit site is conducted using the results from three SCPT profiles (i.e., SC1, SC2 and SC3), one SPT profile and two sHV-crosshole test profiles. Presented in Figure 7.2 are the results of liquefaction evaluation for the top 10 m of soil at the Hobcaw Borrow Pit site based on the SC2 profile. Results from the 5 other profiles are presented in Appendix F. Values of *CSR* are calculated based on an estimated *PGA* of 0.15 g at the site.

The groundwater table at the site lied at a depth of 2.7 m during testing in July 2007. The V_P profile shown in Chapter 6 suggests that soils are saturated below the groundwater table.

As seen in Figure 7.2f, the average *MEVR* in Sub-layers A2 and A3 are 1.49 and 1.10, respectively, based on the SC2 data. An *MEVR* of 1.49 suggests no liquefaction in 1886 earthquake, but an *MEVR* of 1.14 is characterized of a very young material and suggests possible liquefaction in 1886. As seen in Figure 7.2f, the average *OCR* of the sand layers at Hobcaw is about 2.4, based on a laboratory consolidation test on a specimen from Layer B. The K_{OCR} applied to Sub-layers A2 and A3 is equal 1.24, using Equation 7.6.

As seen in Figure 7.2h, the Sub-layer A2 has an average *FS* of 3.0. The Sub-layer A3 is identified as the critical layer with the lowest average *FS* of 1.8.

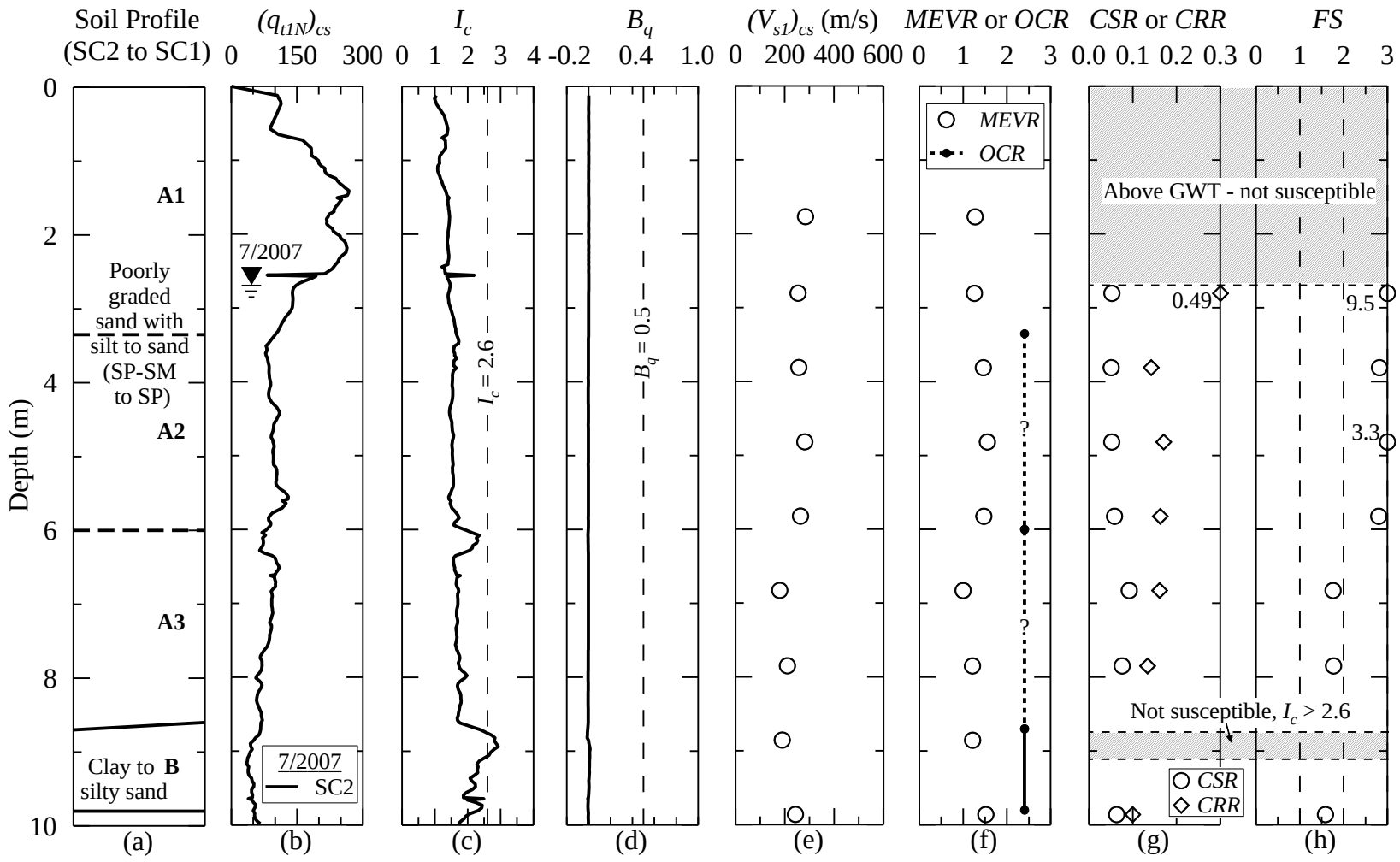

Figure 7.2: Liquefaction assessment of the Hobcaw Borrow Pit site based on seismic cone SC2 data reported in Boller (2008) and general CPT-based procedure recommended by Youd et al. (2001).

The prediction of no liquefaction in the critical layer at the site is consistent with the observations of no surface manifestations of liquefaction at Hobcaw in 1886.

7.3.3 Walterboro Rest Area Site

Liquefaction evaluation of the Walterboro Rest Area site is conducted using the results from three SCPT profiles (i.e., SC1, SC2 and SC3), one SPT profile and two sHV-crosshole test profiles. The results of liquefaction evaluation for the top 10 m of soil at the Walterboro Rest Area site based on the SC3 profile are presented in Figure 7.3. Results from the 5 other profiles are presented in Appendix F. Values of *CSR* are calculated based on an estimated *PGA* of 0.23g at the site.

The groundwater table at the site was measured in the piezometer standpipe at a depth of 2.3 m in June 2009. The V_P profile for the site indicates that the unsaturated zone extends from the ground surface to a depth of 3.0 m.

As seen in Figure 7.3f, the average *MEVR* in Layer C is 1.14, which is characteristic of a young material and suggests possible liquefaction in 1886. The average *OCR* of the sand layers at the site is about 1.6, based on a laboratory consolidation test on a specimen from Layer D. The *OCR* correction applied to Layer C is equal 1.12.

The soil at a depth from 3.0 to 5.6 m in Layer C exhibits the lowest average *FS* of 1.1. The *FS* from a depth of 6.4 to 7.6m in Layer D is 1.2. Thus, Layer C is identified as the critical layer. The prediction of no liquefaction in the critical layer is consistent with the observations of no surface manifestations of liquefaction at Walterboro in 1886.

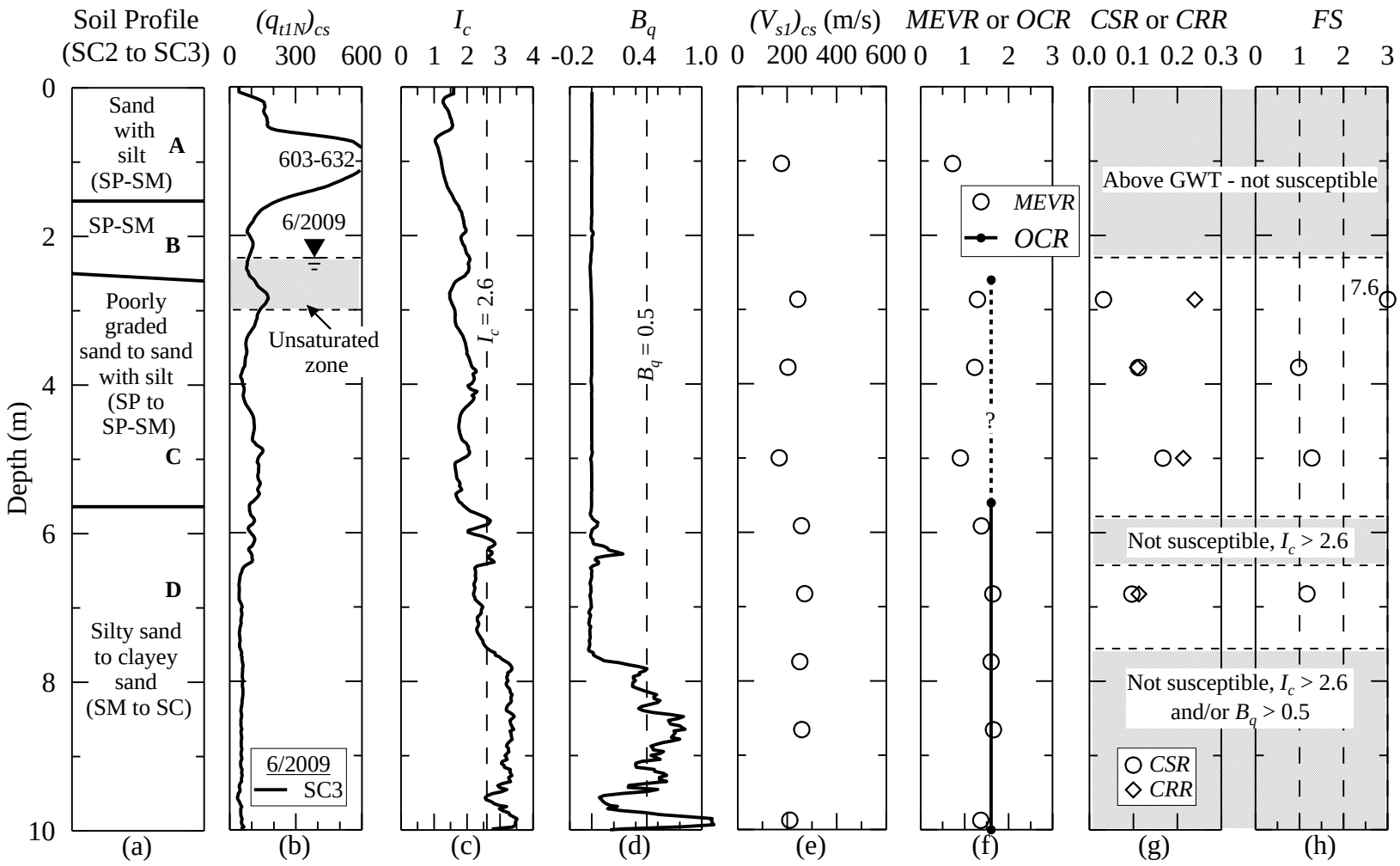

Figure 7.3: Liquefaction assessment of the Walterboro Rest Area site based on seismic cone SC3 data reported in Geiger (2010) and general CPT-based procedure recommended by Youd et al. (2001).

7.3.4 Hobcaw Beach Ridge Site

Liquefaction evaluation of the Hobcaw Beach Ridge site is conducted using the results from one SCPT profile. Presented in Figure 7.4 are the results of liquefaction evaluation for the top 10 m of soil at the Hobcaw Beach Ridge site. Values of *CSR* are calculated based on an estimated *PGA* of 0.15 g at the site.

At the time of testing in March 2012, the groundwater table lied at a depth of 0.4 m based on a hand-augured hole. Because no P-wave tests were conducted at the site, identifying an unsaturated zone below the groundwater table is not possible.

As seen in Figure 7.4f, the average *MEVR* in Layer B is 1.35, indicating that liquefaction did not occur in 1886. The soils at the Hobcaw Beach Ridge site are assumed to be normally consolidated. Thus, no *OCR* correction is applied.

As seen in Figure 7.4h, Layers A, B and D have an average *FS* of 2.9, 1.4 and 1.5, respectively. The Layer B is identified as the critical layer with the lowest average *FS*. The prediction of no liquefaction at the site is consistent with the observations of no surface manifestations of liquefaction in the Hobcaw area in 1886.

7.3.5 Walterboro Lowcountry Site

Liquefaction evaluation of the Walterboro Lowcountry site is conducted using the results from three SCPT profiles (i.e., SC1, SC2 and SC3). The results of liquefaction evaluation for the top 10 m of soil at the Walterboro Lowcountry site based on the SC2 profile are presented in Figure 7.5. Results from the 2 other profiles are presented in

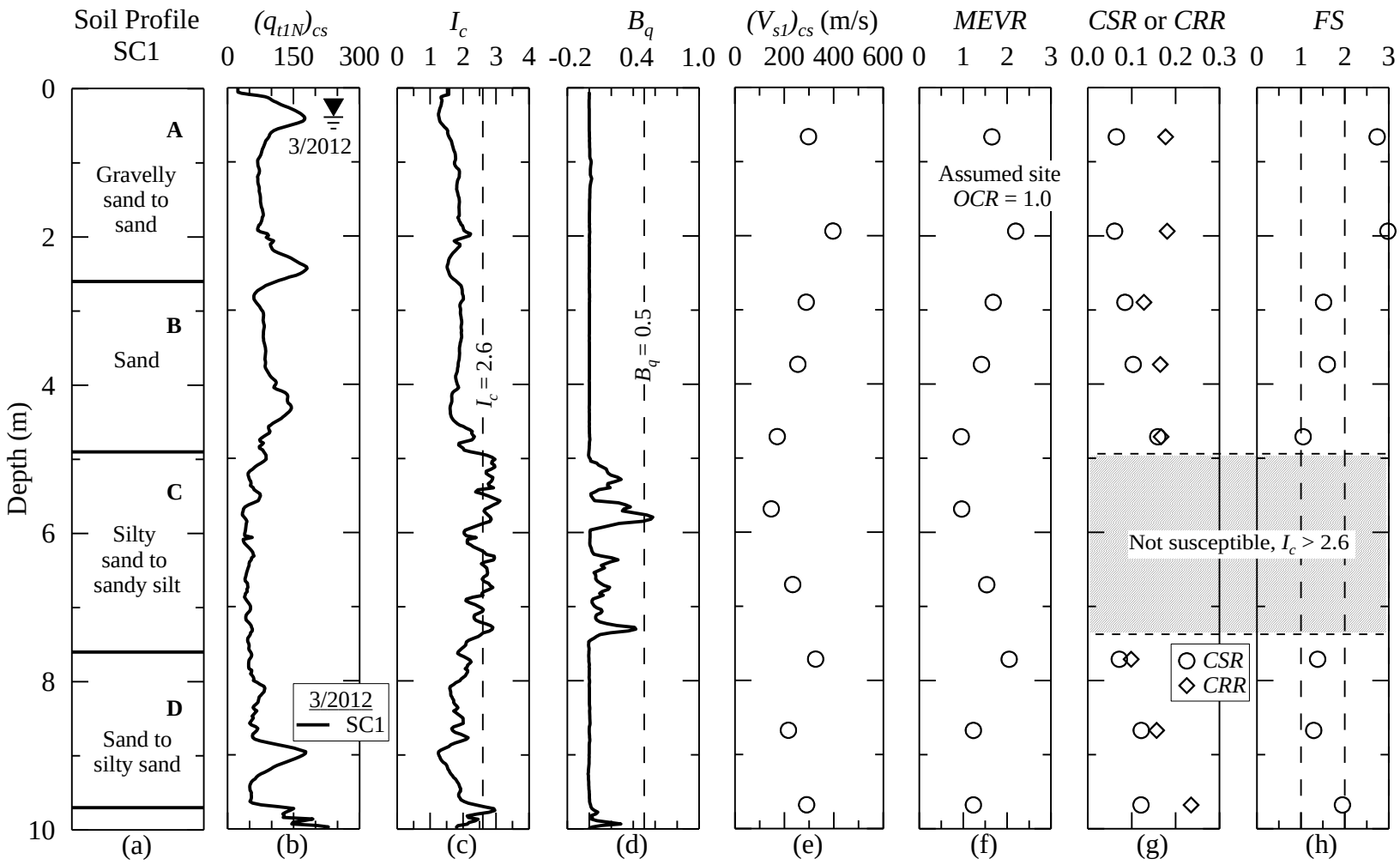

Figure 7.4: Liquefaction assessment of the Hobcaw Beach Ridge site based on seismic cone data and general CPT-based procedure recommended by Youd et al. (2001).

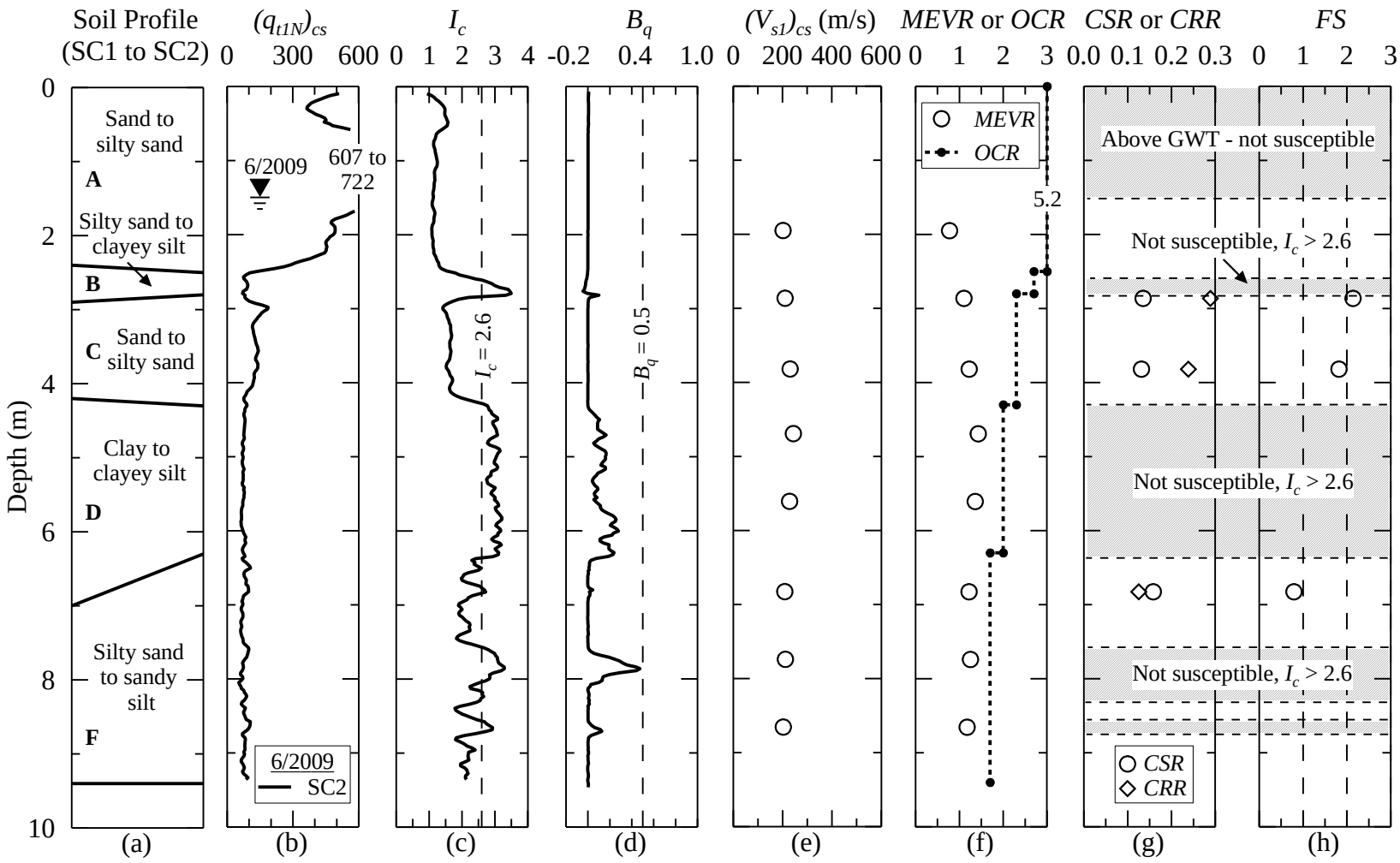

Figure 7.5: Liquefaction assessment of the Walterboro Lowcountry site based on seismic cone SC2 data reported in Geiger (2010) and general CPT-based procedure recommended by Youd et al. (2001).

Appendix F. Values of *CSR* are calculated based on an estimated *PGA* of 0.25 g at the site.

The groundwater table lied at a depth of 1.5 m during testing based on the adjacent lake level. P-wave tests were not conducted at the site and thus, identifying an unsaturated zone below the groundwater table is not possible.

As seen in Figure 7.5f, the average *MEVR* in Layer C is 1.44, suggesting an older deposit that did not liquefy in 1886. The site was graded down from its original elevation by about 3.4 m (11 ft) during mining operations, as discussed in Chapter 5. Thus, the average *OCR* of the soil layers range between 1.7 and 5.2. The *OCR* correction applied to Layer C is equal 1.18.

As seen in Figure 7.5h, the Layer C has an average *FS* of 2.5, predicting no liquefaction. Although Layer F has an *FS* of 0.9, the layer contains a number of locations with $I_C > 2.6$ and thus is not considered the critical layer. Therefore, Layer C is identified as the critical layer at the site. The prediction of no liquefaction in the critical layer is consistent with the observations of no surface manifestations of liquefaction at Walterboro in 1886.

7.3.6 Hollywood Ditch Site

Liquefaction evaluation of the Hollywood site is conducted using the results from three SCPT profiles (i.e., SC1, SC2 and SC3), one SPT profile and the sHV-crosshole test profiles. Presented in Figure 7.6 are the results of liquefaction evaluation for the top 10 m of soil at the Hollywood site based on the SC1 profile. Results from the 5 other

profiles are presented in Appendix F. Values of *CSR* are calculated based on an estimated *PGA* of 0.57 g at the site.

The depth to the groundwater table at the eight SCCP sites fluctuates between 0.4 and 2.8 m. For this assessment, the depth of 2.0 m is assumed at Hollywood Ditch. Based on the V_P profiles, the unsaturated zone extends to a depth of 2.8 m.

As seen in Figure 7.6f, the average *MEVR* in Sub-layer B2 is 1.05, is characterized of a very young soil and suggests liquefaction in 1886. The soils at the Hollywood Ditch site are assumed to be normally consolidated. Thus, no *OCR* correction is applied.

As seen in Figure 7.6h, the average *FS* in the soil layers range from 0.3 to 0.5. Layers C and E have soils with $I_C > 2.6$ at several locations. Thus, the soil at a depth from 2.8 to 4.1 m in Sub-layer A2 is identified as the critical layer at the site. The prediction of liquefaction agrees with the observation of liquefaction along the Hollywood Ditch during the 1886 Charleston earthquake.

7.3.7 Sampit Site

Liquefaction evaluation of the Sampit is conducted using the results from three SCPT profiles (i.e., SC1, SC2 and SC3), one SPT profile and two sHV-crosshole test profiles. The results of liquefaction evaluation for the top 10 m of soil at the Sampit site based on the SC1 profile are presented in Figure 7.7. Results from the 5 other profiles are presented in Appendix F. Values of *CSR* are calculated based on an estimated *PGA* of 0.17 g at the site.

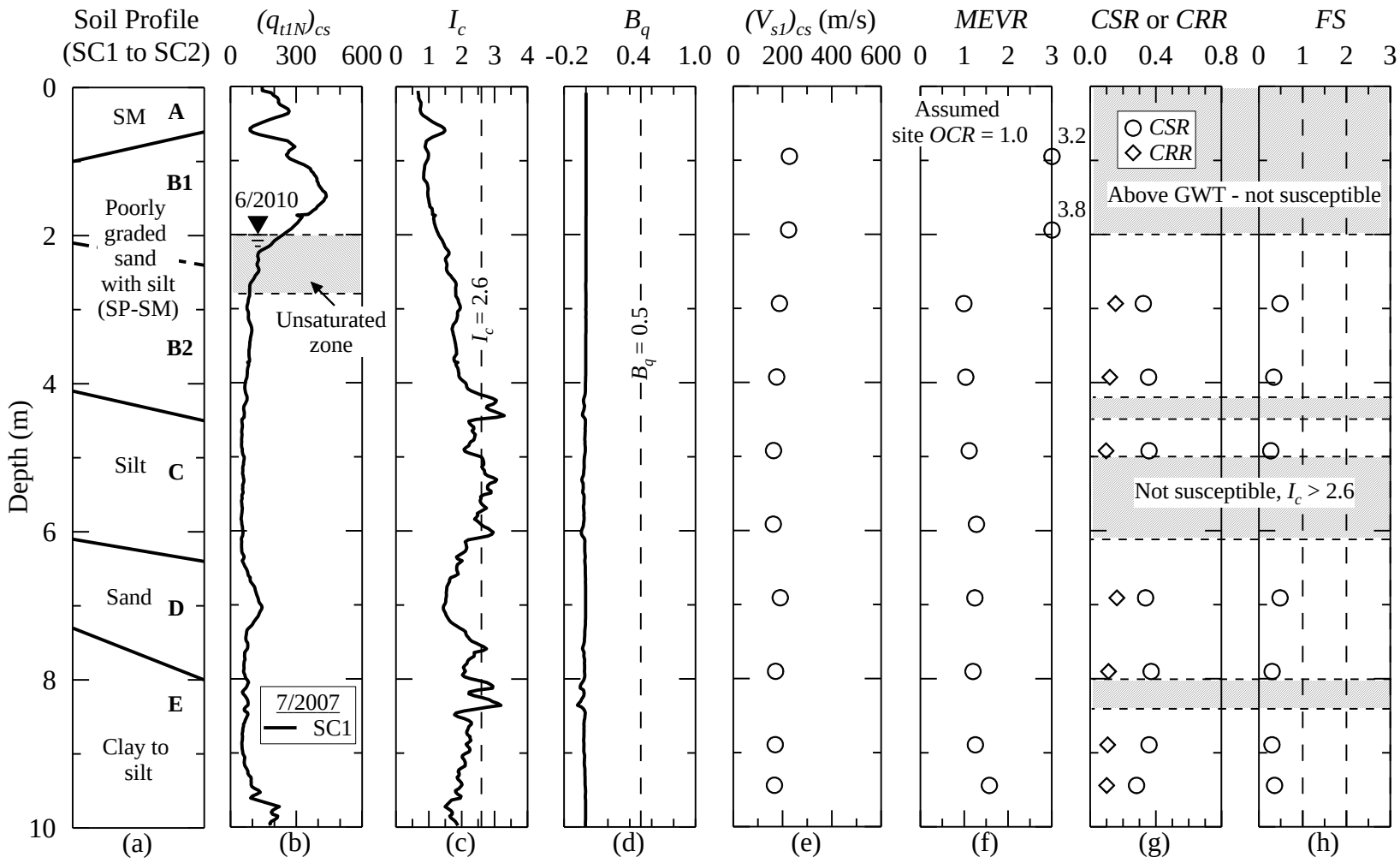

Figure 7.6: Liquefaction assessment of the Hollywood Ditch site based on seismic cone SC1 data and general CPT-based procedure recommended by Youd et al. (2001).

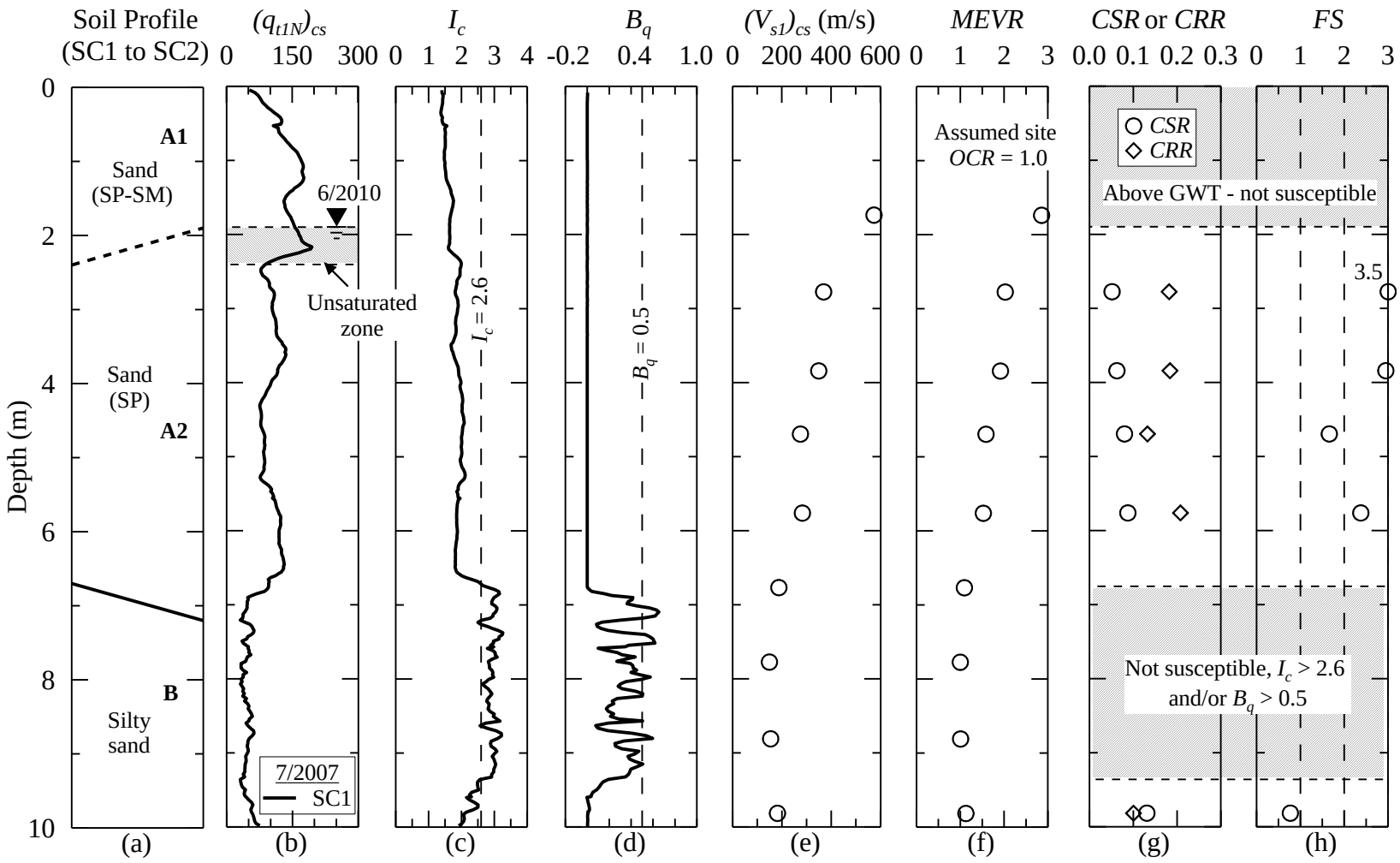

Figure 7.7: Liquefaction assessment of the Sampit site based on seismic cone SC1 data reported in Williamson and Gassman (2014) and general CPT-based procedure recommended by Youd et al. (2001).

For this assessment, the depth to the groundwater table is assumed to be at1.9 m. Based on the V_P profiles, the unsaturated zone extends to a depth of 2.4 m.

As seen in Figure 7.7f, the average *MEVR* in Sub-layer A2 is 1.76, which suggests no liquefaction in 1886 earthquake. No *OCR* correction is applied because the soils at the Sampit site are assumed to be normally consolidated.

The Sub-layer A2 is identified as the critical layer. As seen in Figure 7.7h, the Sub-layer A2 with an average *FS* of 2.6, predicting no liquefaction. The prediction of no liquefaction is consistent with the observation of no surface manifestations of liquefaction in the Sampit area in 1886.

7.3.8 Four Hole Swamp Site

Liquefaction evaluation of the Four Hole Swamp is conducted using the results from three SCPT profiles (i.e., SC1, SC2 and SC3), one SPT profile and two sHV-crosshole test profiles. Presented in Figure 7.8 are the results of liquefaction evaluation for the top 10 m of soil at the Four Hole Swamp site based on the SC1 profile. Results for the top 10 m of soil at the Four Hole Swamp site based on the SC1 profile. Results from the 5 other profiles are presented in Appendix F. Values of *CSR* are calculated based on an estimated *PGA* of 0.40 g at the site.

The groundwater table was measured in the standpipe at a depth of 2.2 m in January 2008 (Williamson and Gassman 2014). Based on the V_P profiles, the unsaturated zone extends to a depth of 2.4 m.

As seen in Figure 7.8f, the average *MEVR* in Sub-layer A2 is 1.14, is characterized of a very young soil and suggests liquefaction in 1886. The average *OCR* of the soil layers range between 1.3 and 2.0 at the site, assuming a 1.2 m erosion of the top soil. The *OCR* correction applied to Sub-layer A2 is equal 1.08.

As seen in Figure 7.8h, the soil between the depths of 2.4 and 2.9 m in Sub-layer A1 has an *FS* of 0.9. The soil at a depth from 3.4 to 4.1 m in Sub-layer A2 has an *FS* of 0.5, which is identified as the critical layer at the site.

The prediction of liquefaction does not agree with the report of no surface manifestations of liquefaction at Four Hole Swamp in 1886. Based on the criteria of Ishihara (1985), it is possible that liquefaction occurred in the 0.5 m thick soil in Sub-layer A1 or the 0.7-m-thick soil in Sub-layer A2, but surface manifestations were prevented because of the overlaying 2.4 m of soil (Sub-layer A1) and given *PGA* = 0.4 g. Thus, the prediction of liquefaction at Four Hole Swamp may not be a false positive prediction.

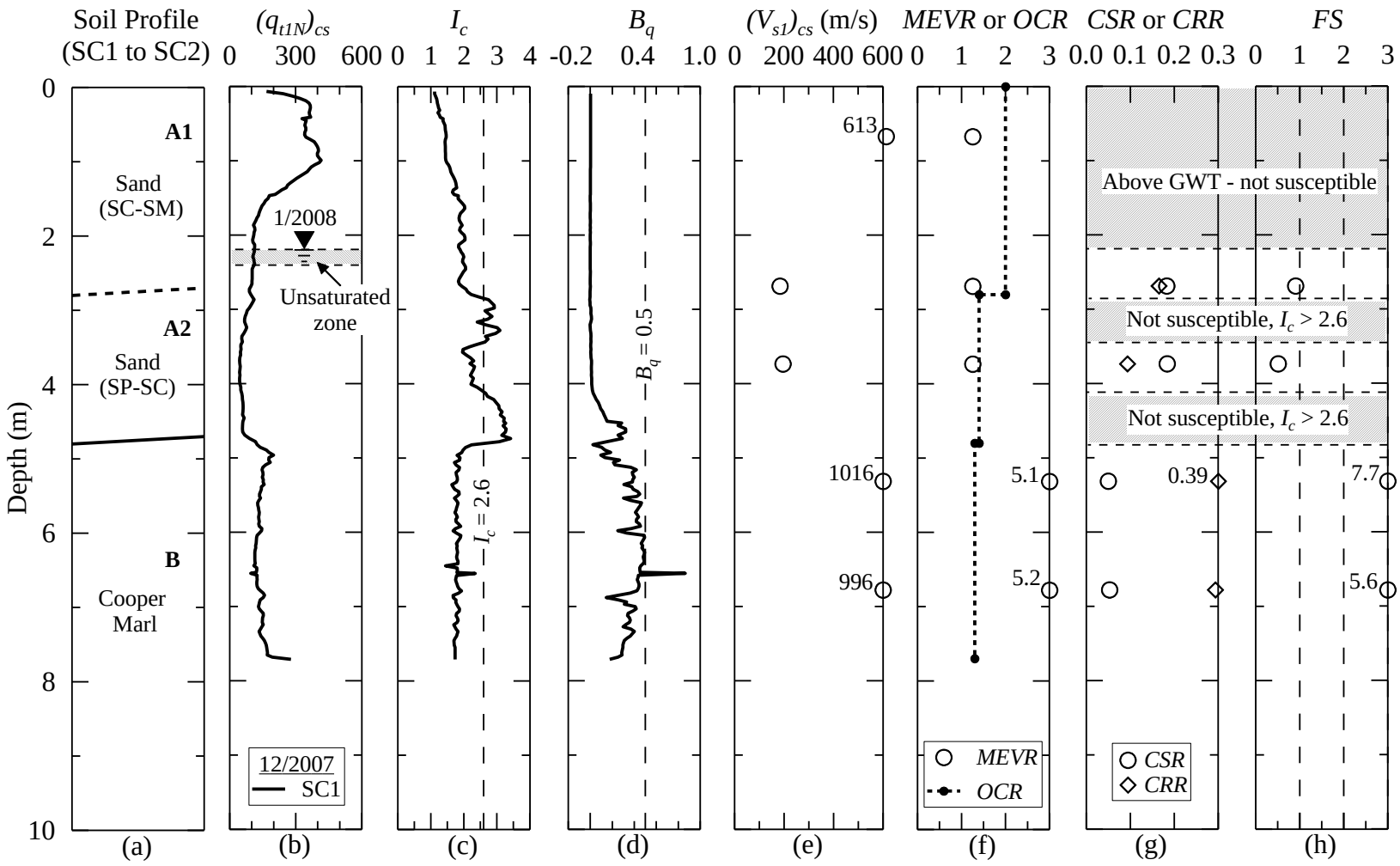

Figure 7.8: Liquefaction assessment of the Four Hole Swamp site based on seismic cone SC1 data reported in Williamson and Gassman (2014) and general CPT-based procedure recommended by Youd et al. (2001).

7.4 Summary

The liquefaction potential of natural sand deposits at five no liquefaction sites and three paleoliquefaction sites in the SCCP was evaluated in this chapter. Geological ages of the sand deposits at the eight sites range from 70,000 to over 1,000,000 years. A summary of the liquefaction evaluation calculations with diagenesis and *OCR* correction in the critical layers at the sites is presented in Table 7.1. Results of the CPT-, SPT- and V_S-based evaluations in the critical layers are plotted in Figures 7.9-7.11.

The behavior at six of the eight sites during the 1886 Charleston earthquake was correctly predicted. However, one of the no liquefaction sites and one of the paleoliquefaction sites were incorrectly predicted to liquefy in 1886. It is possible that liquefaction occurred at these two sites in 1886, but the capping non-liquefiable layer was thick enough to prevent surface manifestations, based on the criteria by Ishihara (1985). The results confirm the importance of diagenesis and *OCR* corrections in liquefaction assessment of aged sand deposits.

Table 7.1 Summary of liquefaction evaluation calculations for the critical layers at the eight sites in the South Carolina Coastal Plain.

Site – layer	Test Location	Depth range (m)	Average Overburden Corrected Penetration or Velocity	*MEVR*-Corrected $(V_{s1})_{cs}$ (m/s)	Average *MEVR* (*OCR*)	Average $CSR_{7.5}$	Corrected $CSR_{7.5}$
CREC – B2	SC1	2.9-4.7	$(q_{t1N})_{cs}$ = 120 $(V_{s1})_{cs}$= 222 m/s	196	1.13 (1.0)	0.328	0.228
	SC3	2.9-4.6	$(q_{t1N})_{cs}$ = 102 $(V_{s1})_{cs}$= 237 m/s	188	1.26 (1.0)	0.304	0.238
	SC6	2.9-4..4	$(q_{t1N})_{cs}$ = 108 $(V_{s1})_{cs}$= 223 m/s	186	1.20 (1.0)	0.308	0.255
	SPT (BH3)	2.9-4..4	$(N_1)_{60cs}$ = 8	NA[a]	1.56[b] (1.0)	0.306	0.190
	BH1-BH2	2.9-4..4	$(V_{s1})_{cs}$ = 228 m/s	146	1.56[b] (1.0)	0.306	0.190
	BH2-BH3	2.9-4..4	$(V_{s1})_{cs}$= 231 m/s	148	1.56[b] (1.0)	0.306	0.190
Hobcaw Borrow Pit – A3	SC1	6.0-8.6	$(q_{t1N})_{cs}$ = 75 $(V_{s1})_{cs}$= 215 m/s	172	1.25 (2.4)	0.110	0.070
	SC2	6.0-8.7	$(q_{t1N})_{cs}$ = 81 $(V_{s1})_{cs}$= 194 m/s	176	1.10 (2.4)	0.114	0.084
	SC3	6.0-8.2	$(q_{t1N})_{cs}$ = 70 $(V_{s1})_{cs}$= 180 m/s	164	1.10 (2.4)	0.114	0.084
	SPT (BH1)	6.0-8.7	$(N_1)_{60cs}$ = 9	NA	1.23[b] (2.4)	0.116	0.075
	BH1-BH2	6.0-8.7	$(V_{s1})_{cs}$ = 188 m/s	153	1.23[b] (2.4)	0.116	0.075
	BH2-BH3	6.0-8.7	$(V_{s1})_{cs}$= 214 m/s	174	1.23[b] (2.4)	0.116	0.075
Walterboro Rest Area – C	SC1	3.0-6.2	$(q_{t1N})_{cs}$ = 219 $(V_{s1})_{cs}$= 215 m/s	203	1.06 (1.6)	0.180	0.141
	SC2	3.0-5.6	$(q_{t1N})_{cs}$ = 132 $(V_{s1})_{cs}$= 195 m/s	189	1.03 (1.6)	0.168	0.176
	SC3	3.0-5.6	$(q_{t1N})_{cs}$ = 101 $(V_{s1})_{cs}$= 204 m/s	185	1.14 (1.6)	0.161	0.139
	SPT (BH3)	3.0-5.6	$(N_1)_{60cs}$ = 13	NA	1.83[b] (1.6)	0.160	0.075
	BH1-BH2	3.0-5.6	$(V_{s1})_{cs}$ = 329 m/s	180	1.83[b] (1.6)	0.160	0.075
	BH2-BH3	3.0-5.6	$(V_{s1})_{cs}$= 308 m/s	168	1.83[b] (1.6)	0.160	0.075
Hobcaw Beach Ridge	SC1	2.6-4.9	$(q_{t1N})_{cs}$ = 94 $(V_{s1})_{cs}$= 237 m/s	176	1.35 (1.0)	0.148	0.115

Table 7.1: Summary of liquefaction evaluation calculations for the critical layers at eight sites in the South Carolina Coastal Plain (continued).

Site – layer	Test Location	Depth range (m)	Average Overburden Corrected Penetration or Velocity	*MEVR*-Corrected $(V_{s1})_{cs}$ (m/s)	Average *MEVR*	Average $CSR_{7.5}$	Corrected $CSR_{7.5}$
Walterboro Lowcountry – C	SC1	2.9-4.2	$(q_{t1N})_{cs}$ = 330 $(V_{s1})_{cs}$= 259 m/s	216	1.20 (2.3)	0.192	0.128
	SC2	2.8-4.3	$(q_{t1N})_{cs}$ = 123 $(V_{s1})_{cs}$= 274 m/s	191	1.44 (2.3)	0.192	0.105
	SC3	2.6-4.1	$(q_{t1N})_{cs}$ = 146 $(V_{s1})_{cs}$= 253 m/s	190	1.33 (2.3)	0.191	0.116
Hollywood Ditch – B2	SC1	2.8-4.1	$(q_{t1N})_{cs}$ = 88 $(V_{s1})_{cs}$= 183 m/s	174	1.05 (1.0)	0.358	0.339
	SC2	2.8-4.5	$(q_{t1N})_{cs}$ = 97 $(V_{s1})_{cs}$= 183 m/s	176	1.04 (1.0)	0.357	0.344
	SC3	2.8-4.5	$(q_{t1N})_{cs}$ = 57 $(V_{s1})_{cs}$= 204 m/s	173	1.18 (1.0)	0.361	0.304
	SPT (BH1)	2.8-4.1	$(N_1)_{60cs}$ = 9	NA	1.28[b] (1.0)	0.400	0.307
	BH1-BH2	2.8-4.1	$(V_{s1})_{cs}$ = 186 m/s	162	1.28[b] (1.0)	0.400	0.307
	BH2-BH3	2.8-4.1	$(V_{s1})_{cs}$= 207 m/s	145	1.28[b] (1.0)	0.400	0.307
Sampit – A2	SC1	2.4-6.7	$(q_{t1N})_{cs}$ = 130 $(V_{s1})_{cs}$= 319 m/s	181	1.76 (1.0)	0.124	0.070
	SC2	2.4-7.2	$(q_{t1N})_{cs}$ = 120 $(V_{s1})_{cs}$= 263 m/s	191	1.38 (1.0)	0.128	0.094
	SC3	3.0-8.2	$(q_{t1N})_{cs}$ = 169 $(V_{s1})_{cs}$= 295 m/s	178	1.66 (1.0)	0.138	0.092
	SPT (BH2)	2.4-6.7	$(N_1)_{60cs}$ = 12	NA	1.69[b] (1.0)	0.126	0.072
	BH1-BH2	2.4-6.7	$(V_{s1})_{cs}$ = 293 m/s	173	1.69[b] (1.0)	0.126	0.072
	BH2-BH3	2.4-6.7	$(V_{s1})_{cs}$= 258 m/s	153	1.69[b] (1.0)	0.126	0.072
Four Hole Swamp – A2	SC1	3.4-4.1	$(q_{t1N})_{cs}$ = 48 $(V_{s1})_{cs}$= 189 m/s	166	1.14 (1.4)	0.254	0.184
	SC2	2.4-4.7	$(q_{t1N})_{cs}$ = 95 $(V_{s1})_{cs}$= 219 m/s	180	1.22 (1.4)	0.257	0.191
	SC3	2.4-4.3	$(q_{t1N})_{cs}$ = 107 $(V_{s1})_{cs}$= 221 m/s	183	1.21 (1.4)	0.230	0.172
	SPT (BH2)	3.4-4.1	$(N_1)_{60cs}$ = 5	NA	1.30[b] (1.4)	0.274	0.190
	BH1-BH2	3.4-4.1	$(V_{s1})_{cs}$ = 162 m/s	124	1.30[b] (1.4)	0.274	0.190
	BH2-BH3	3.4-4.1	$(V_{s1})_{cs}$= 189 m/s	145	1.30[b] (1.4)	0.274	0.190

[a]Not applicable; [b]Calculated based on average V_S measurements from both BH1-BH2 and BH2-BH3 profiles and estimated V_S from SPT blow counts.

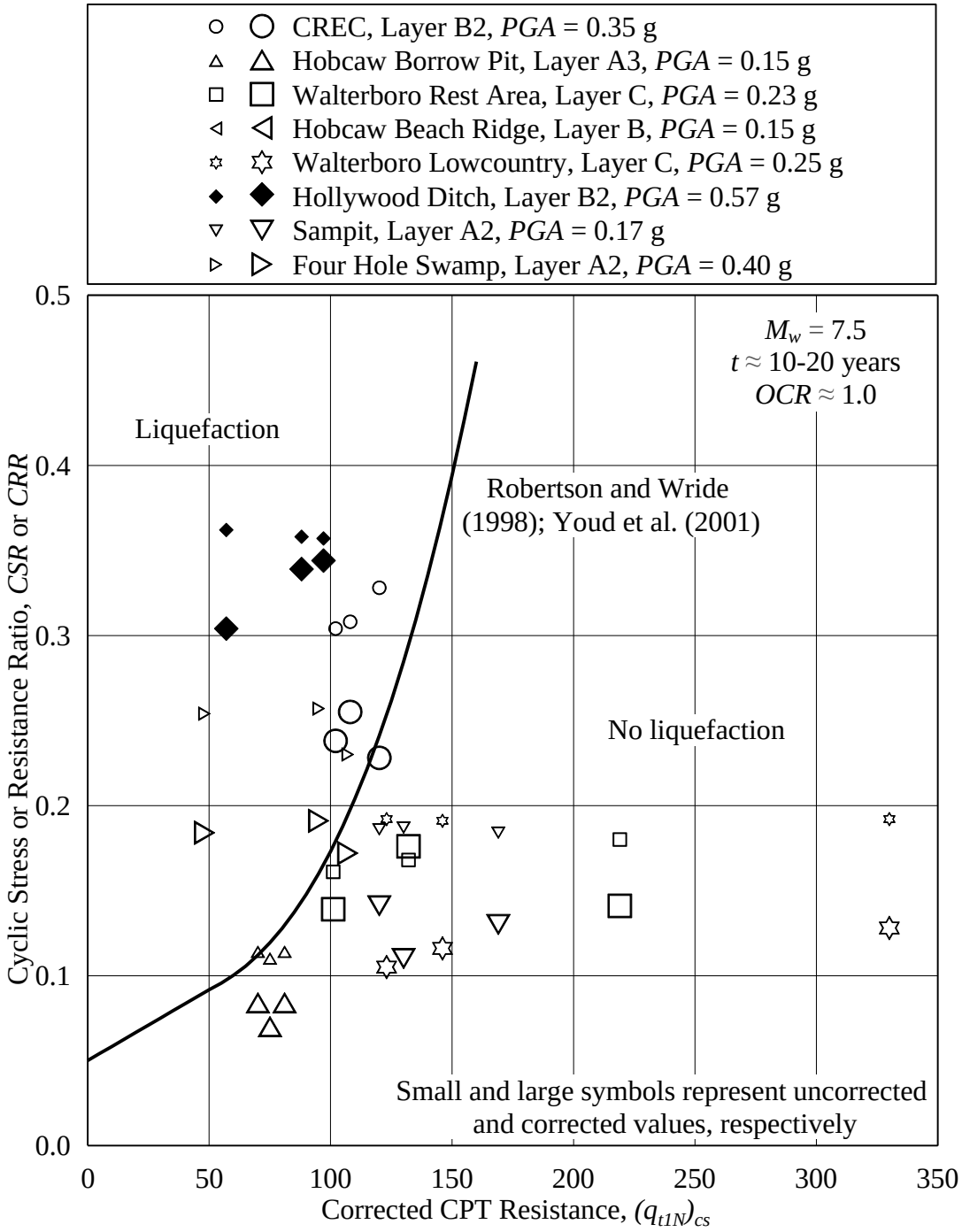

Figure 7.9: CPT-based liquefaction evaluation of the critical layers at the eight sites assuming the ground shaking during the 1886 Charleston earthquake.

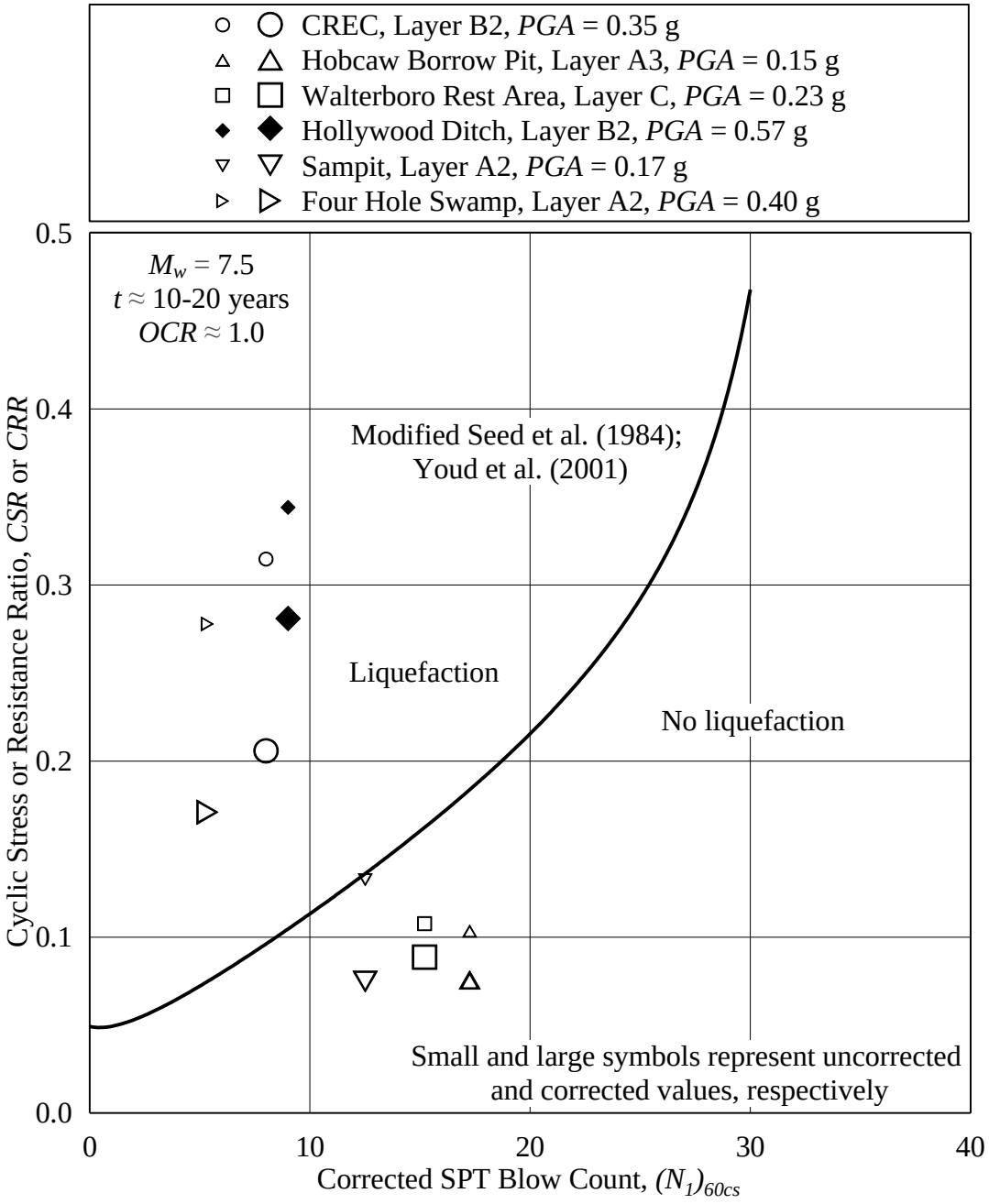

Figure 7.10: SPT-based liquefaction evaluation of the critical layers at six sites assuming the ground shaking during the 1886 Charleston earthquake.

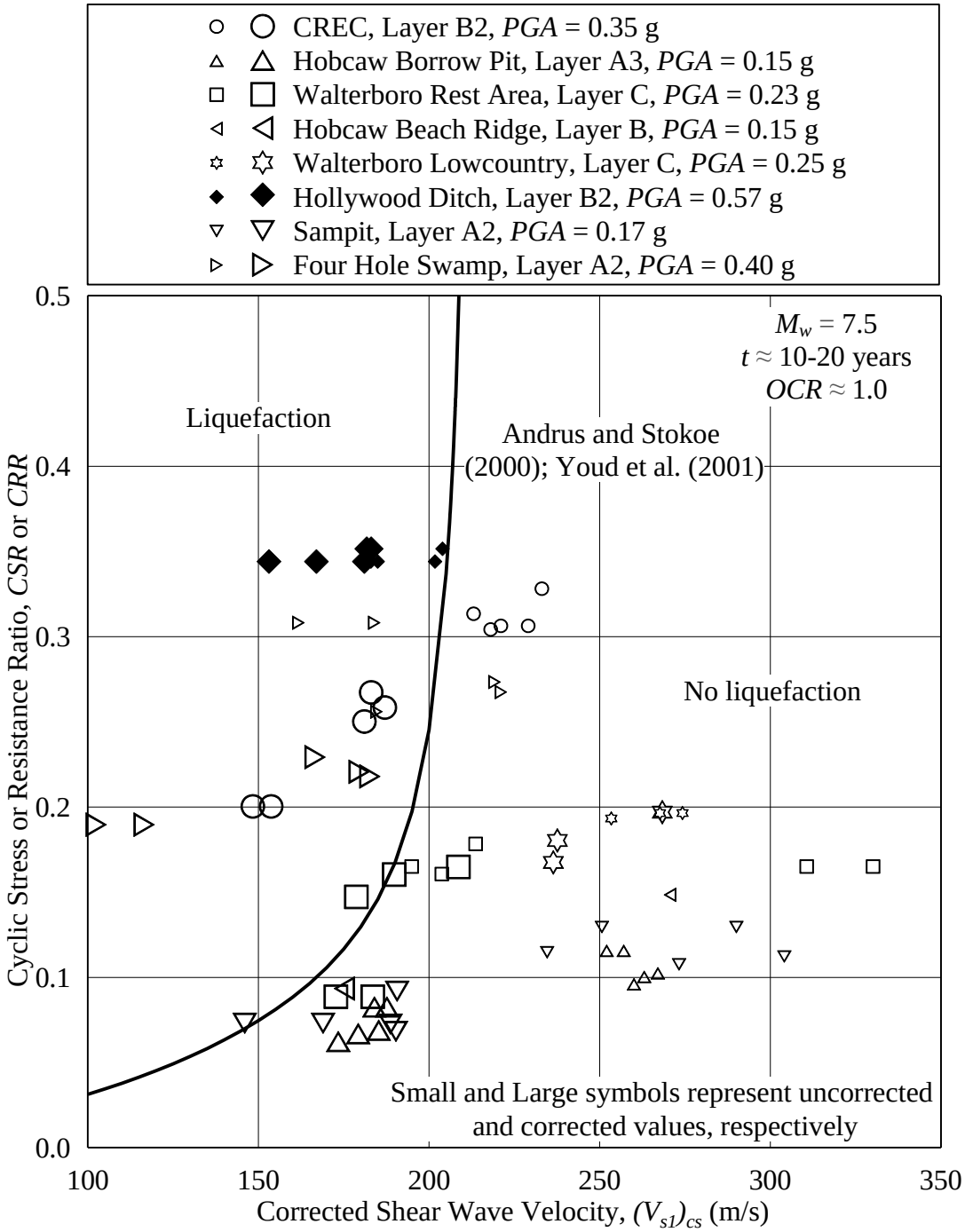

Figure 7.11: V_s-based liquefaction evaluation of the critical layers at the eight sites assuming the ground shaking during the 1886 Charleston earthquake.

CHAPTER 8

CONCLUSIONS AND RECOMMENDATIONS

8.1 Conclusions

This study considered the need for corrective procedures to account for anisotropic consolidations and overconsoildated conditions on liquefaction resistance of sands. The results from several laboratory studies were reviewed to better understand the influence of K_0 and *OCR* on liquefaction resistance and to recommend correction factors.

In Chapter 2, a new relationship was derived to estimate K_0 from DMT, CPT, and *OCR* information from previously published calibration chamber test data. The new relationship proved to be a better fit to the test data than the previously proposed relationship which did not consider *OCR*. Also in Chapter 2, methods for estimating K_0 based on V_{sHH}/V_{sHV} was reviewed and a relationship was derived assuming average values of the fabric anisotropic ratio and the stress exponent from published laboratory data.

Values of K_0 calculated from SBPMT, DMT-CPT-*OCR* and V_S test results in natural and man-made sand deposits were compiled and compared in Chapter 3. Estimates of K_0 based on SBPMT and DMT-CPT-*OCR* increased at about 4 to 5% per log cycle of time based on the geologic age. Estimates of K_0 based on SBPMT and DMT-CPT-*OCR* exhibited similar significant scatter. Scatter in the plotted K_0-time data appeared to increase more when time since last liquefaction event was used than when geologic age was used. Data compiled in Chapter 3 also provided independent support for

the time versus *MEVR* relationship proposed by Andrus et al. (2009). Estimates of K_0 based on SBPMT and DMT-CPT-*OCR* increased at a similar rate with *MEVR*, but exhibited just as much scatter as K_0 data plotted versus time since last liquefaction event. Estimates of K_0 for sites in North America were also plotted versus *PGA* for soft rock outcropping condition and 10% probability of exceedence in 50 years, but did not exhibit any increase with regional seismicity.

When plotted versus the geologic age or the time since the last liquefaction event, V_{sHH}/V_{sHV} did not exhibit an increasing trend, but a slight decreasing trend. The results suggested that both V_{sHH} and V_{sHV} increase at similar rates with time, and thus the influence of age is cancelled out in the ratio. Therefore, it was concluded that the relationship based on laboratory results derived in Chapter 2 give the estimates of K_0 of freshly deposited sands rather than aged sands. An improved relationship for estimating in situ K_0 from V_{sHH}/V_{sHV} was suggested by adding an age term.

Effects of fabric anisotropy and two contributing factors to stress-induced anisotropy namely, anisotropic consolidation and *OCR* on liquefaction resistance of sands were reviewed in Chapter 4. Laboratory test results indicate that liquefaction resistance of sands can change significantly with changes in the angles between the sliding and the microscopic shearing directions, and the angles between longest axes of particles and the vertical axis. Also, laboratory test results indicate that significant increase in liquefaction resistance occurs with increase in K_0 and/or *OCR*. The published laboratory studies suggested a unique relationship between liquefaction resistance of isotropic and anisotropic normally consolidated sands. Approximate relationships between liquefaction

resistance of overconsolidated sands and normally consolidated sands have also been shown in previous laboratory studies. Based on these previous studies, expressions for K_{K0} and K_{OCR} correction factors were suggested in Chapter 4.

Much of the effect of increased K_0 on liquefaction resistance of aged sands is captured by the K_{DR} factor. Hence, it was recommended that the K_{K0} factor not be used with the K_{DR} factor in field liquefaction evaluations of aged sands. However, *OCR* exhibits an additional effect on liquefaction resistance other than through its effect on K_0. To account for this additional effect, it was recommended to apply the K_{OCR} factor besides the K_{DR} factor in field liquefaction evaluations of overconsoildated aged sands. Both K_{K0} and K_{OCR} factors can be of particular significance while evaluating deposits where (1) ground improvement techniques have been applied which increase the lateral stress (2) laboratory shaking has induced lateral stress, both of which involve a mechanism different from the natural field aging processes.

Profiles of K_0 estimated from DMT-CPT-*OCR* measurements for eight sites in the SCCP were presented in Chapter 5. Estimates of K_0 for the sites were in the typical range for natural sands. A gentle increasing trend in K_0 with age was observed. No distinct trend was observed in K_0 with the time since initial deposition or the time since the last liquefaction event, indicating that K_0 decreases little, if any, because of liquefaction.

Profiles of seismic wave velocities from cone and crossohole testing at eight sites in the SCCP were presented in Chapter 6. Unsaturated (i.e., V_P < 1,400 m/s) zones extended from 0.2 to 1.3 m below the groundwater tables at five of the six crosshole sites. The V_{sHV} measurements from crosshole test and the V_{sVH} measurements from SCPT were

in good general agreement with each other. Ratios of V_{sHH} to V_{sHV} at the six crosshole sites indicated greater overall stress stiffness in the vertical direction than in the horizontal direction. At two of the six sites, the velocity-based K_0 estimates were in excellent agreement with the estimates based on DMT-CPT-*OCR* presented in Chapter 5. At the other four sites, the velocity-based K_0 estimates were lower than the estimates based on DMT-CPT-*OCR*.

In Chapter 7, the liquefaction potential of natural sand deposits at five no liquefaction sites and three paleoliquefaction sites in the SCCP was evaluated based on both penetration resistances and V_S, assuming the ground shaking during 1886 Charleston earthquake. Geological ages of the sand deposits at the eight sites ranged from 70,000 to over 1,000,000 years. Overconsoildation ratios ranged from 1.0 to 2.4 in the critical sand layers. The behavior at six of the eight sites during the 1886 Charleston earthquake was correctly predicted. However, one of the no liquefaction sites and one of the paleoliquefaction sites were incorrectly predicted to liquefy in 1886. It is possible that liquefaction, or at least pore pressure build up occurred at these two sites in 1886, but the capping non-liquefiable layer was thick enough to prevent noticeable surface manifestations in the two areas. The results confirmed the importance of diagenesis, unsaturation and *OCR* corrections, as well as the need to assess the capping layer and critical layer thickness in liquefaction assessment of aged sand deposits.

8.2 Recommendations

The following are recommendations for future works:

1. Additional data of in-situ K_0 in clean sand deposits from SBPMT, DMT-CPT-*OCR* and V_{sHH}/V_{sHV} are needed to further validate or refine the two K_0 relationships recommended in this study (Equations 2.11 and 3.5).

2. To obtain a better K_0-age relationship, SBPMT can be conducted in a calibration chamber to estimate K_0 in sands at different times after the specimen preparation. Also, SBPMT should be conducted at the SCCP sites. This work should also attempt to explain the scatters in K_0-age data by quantifying the influence of *OCR.*

3. The V_{sHH} measurements in the SCCP sites should be repeated using a stronger source to validate the measurements made with the solenoid.

APPENDICES

APPENDIX A

MAPS OF THE EIGHT SITES IN THE SOUTH CAROLINA COASTAL PLAIN

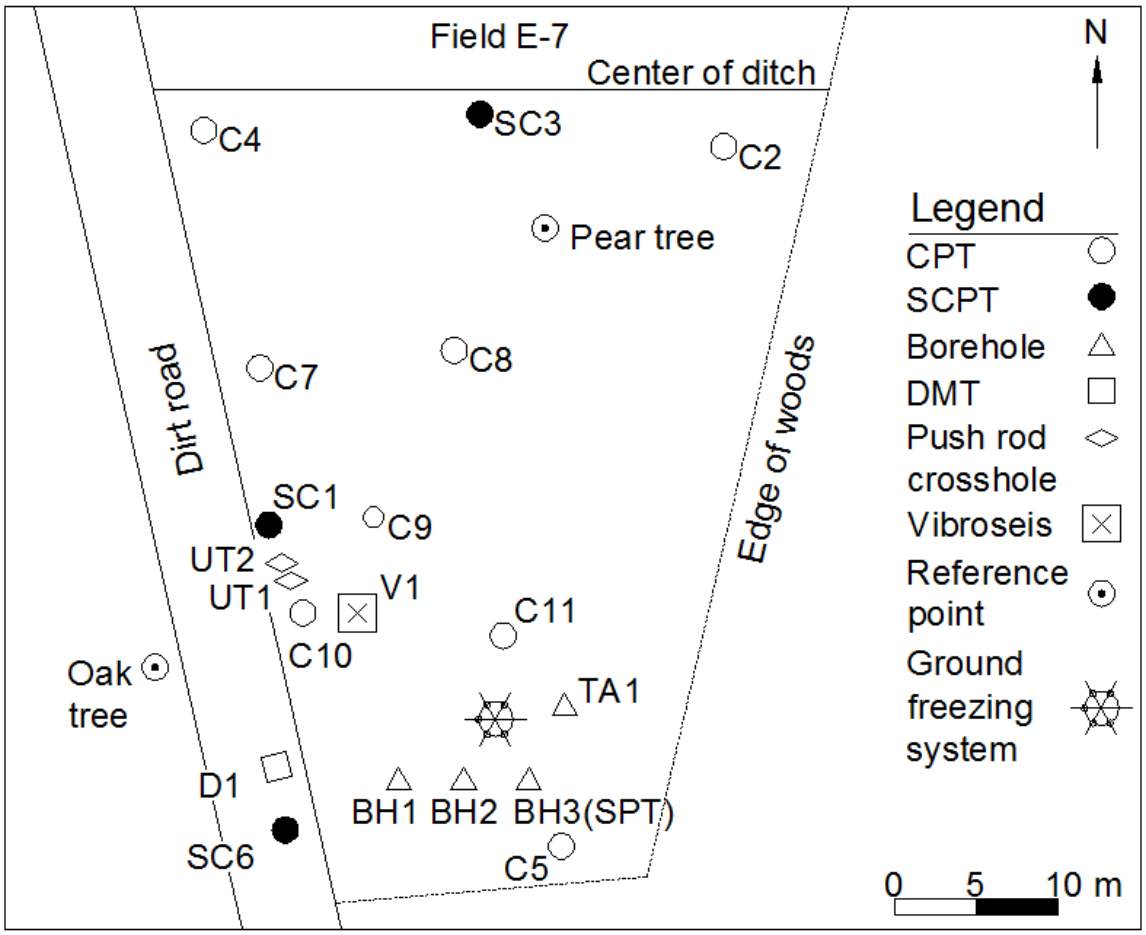

Figure A.1: Map showing test locations at the CREC site (Esposito et al. 2014).

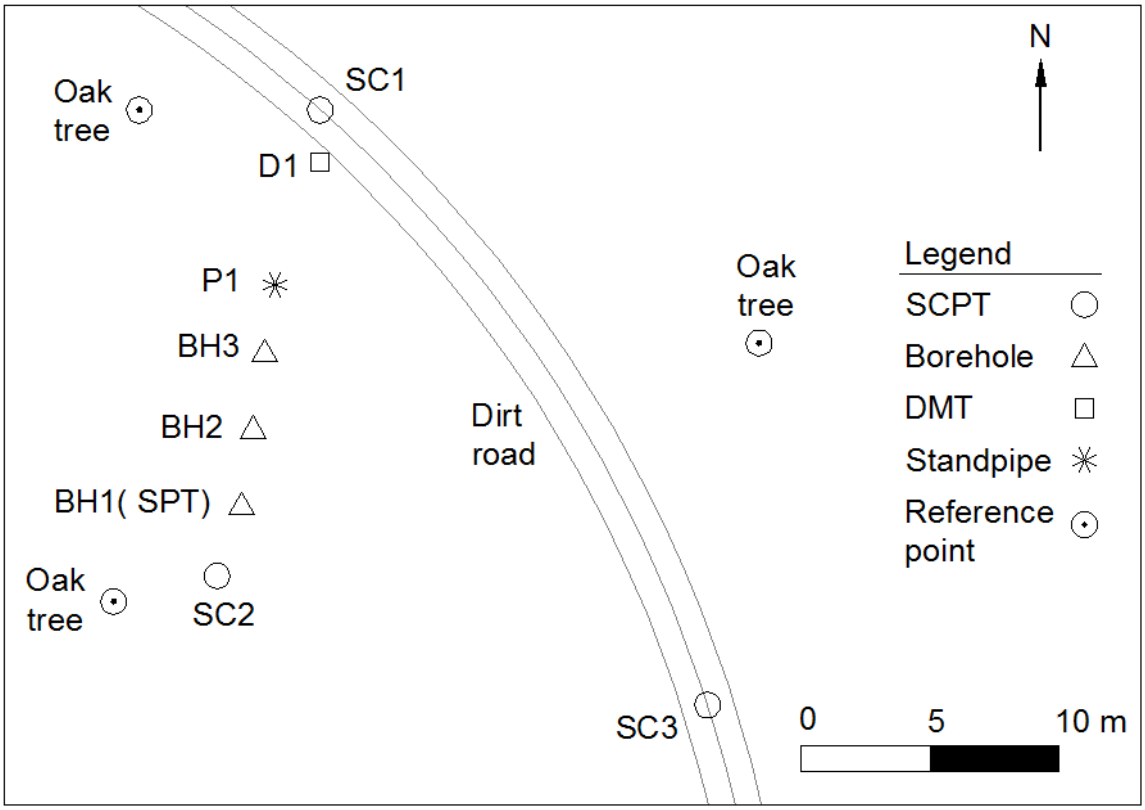

Figure A.2: Map showing test locations at the Hobcaw Borrow Pit site after Boller (2008) and Geiger (2010).

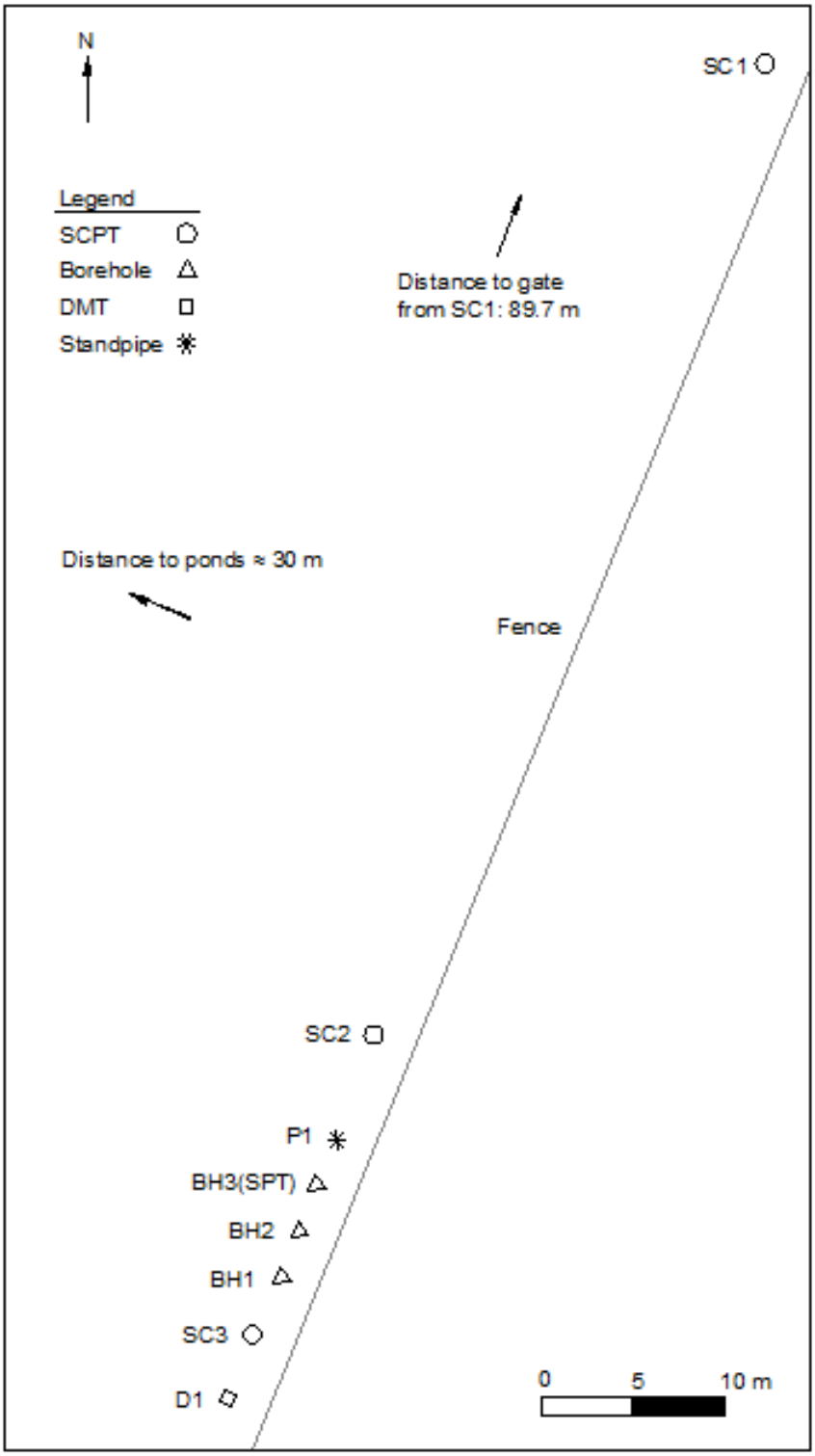

Figure A.3: Map showing test locations at the Walterboro Rest Area site after Geiger (2010).

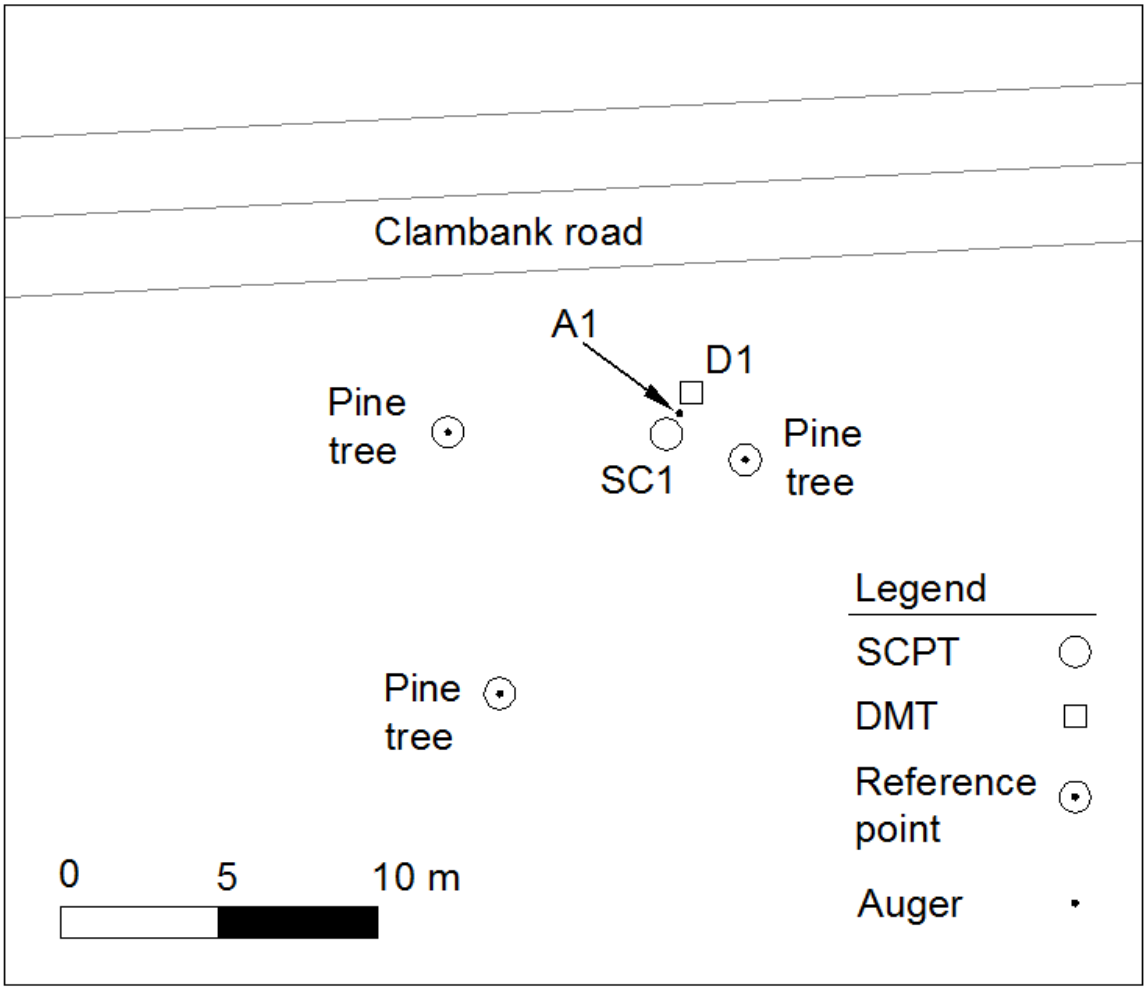

Figure A.4: Map showing test locations at the Hobcaw Beach Ridge site.

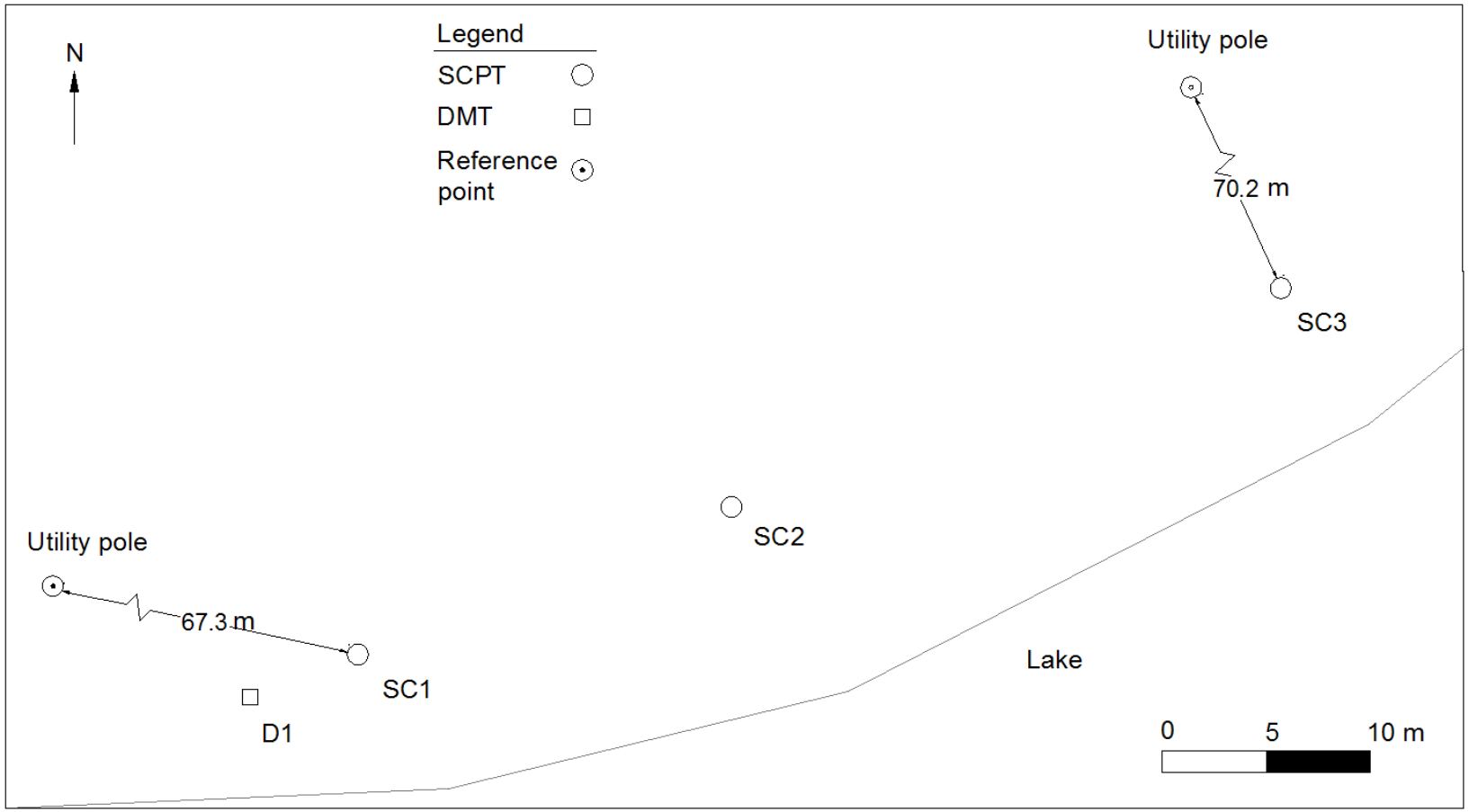

Figure A.5: Map showing test locations at the Walterboro Lowcountry site Geiger (2010).

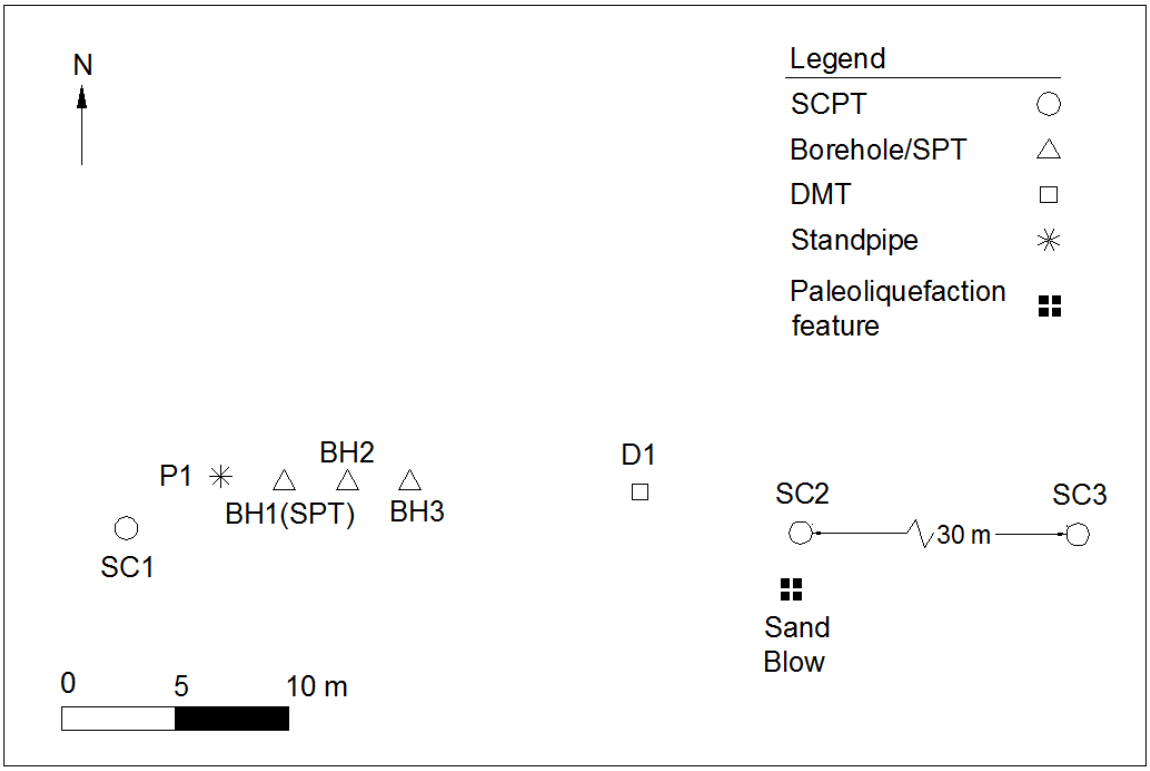

Figure A.6: Map showing test locations at the Hollywwod Ditch site after Williamson (2013).

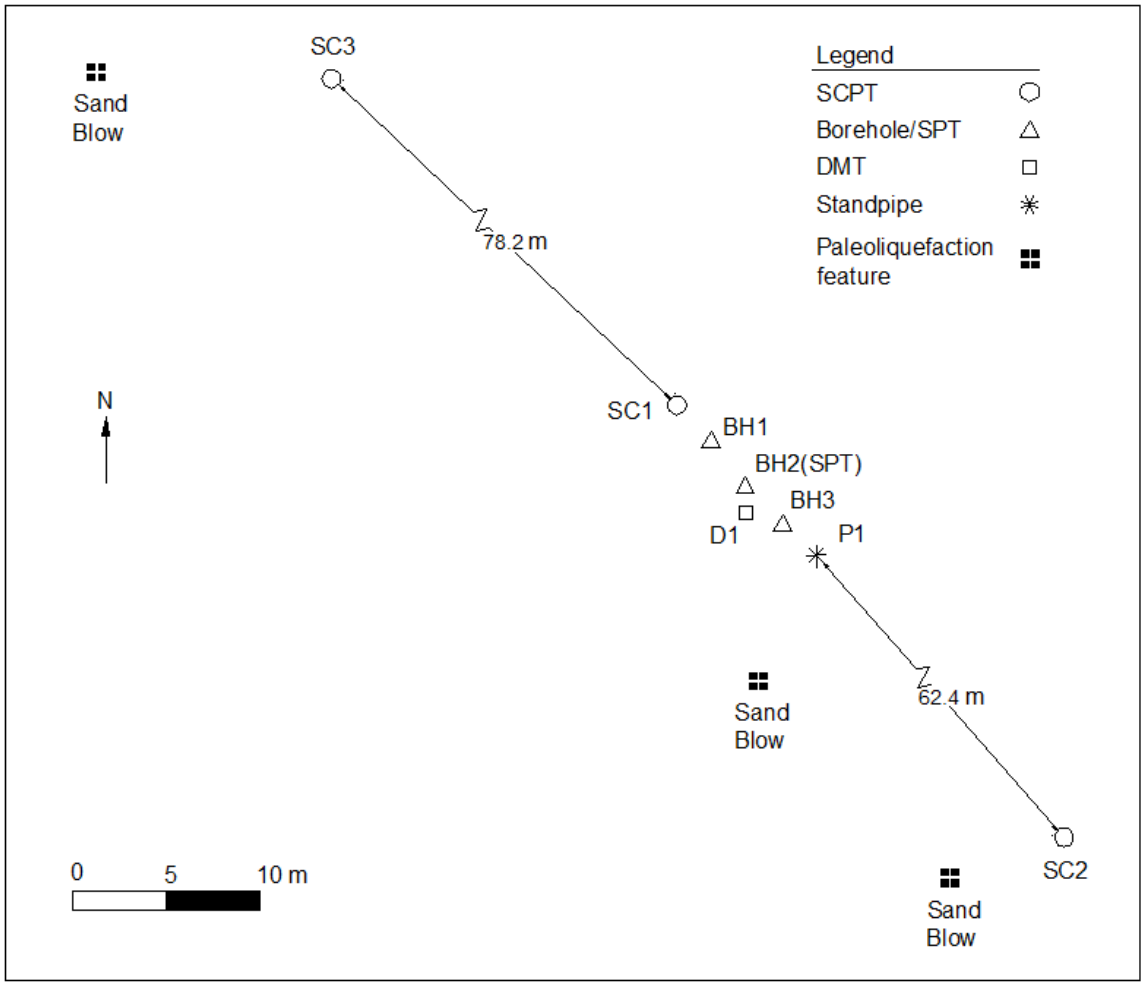

Figure A.7: Map showing test locations at the Sampit site after Williamson (2013).

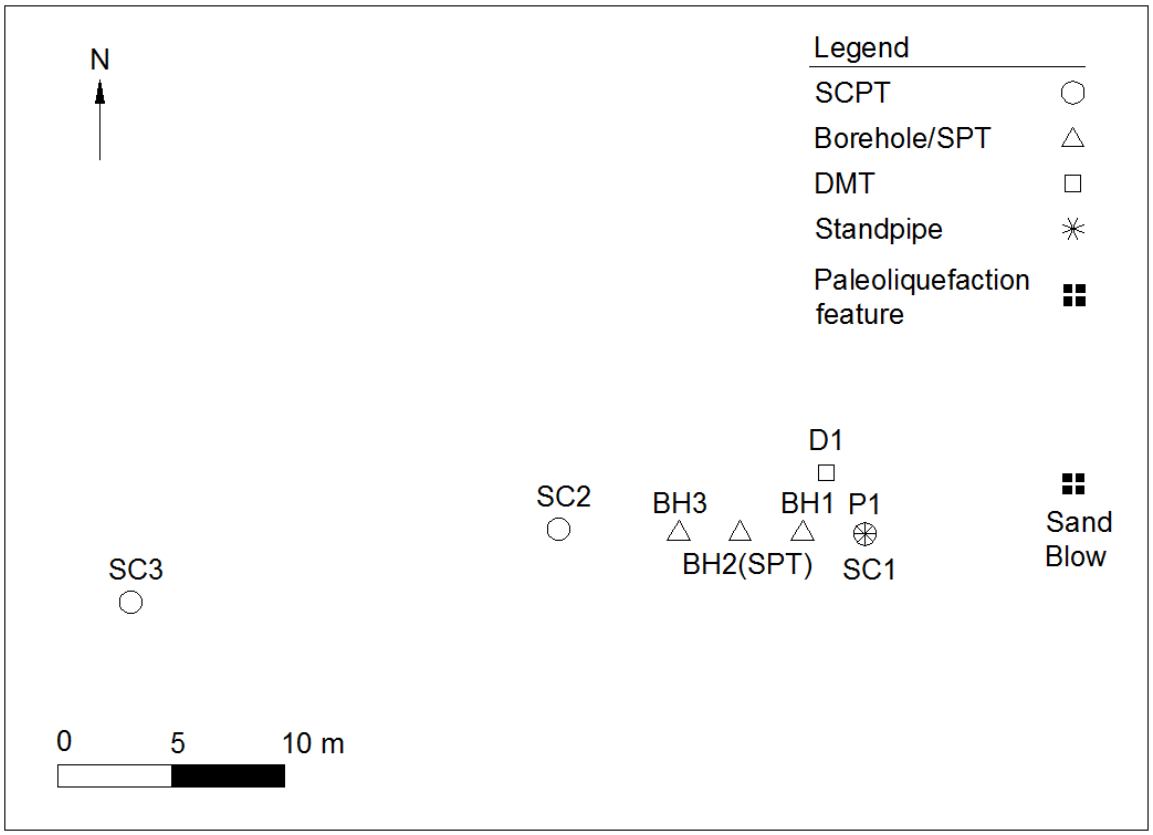

Figure A.8: Map showing test locations at the Four Hole Swamp site after Williamson (2013).

APPENDIX B

BOREHOLE TILTINGS AT THE SIX CROSSHOLE SITES IN THE SOUTH CAROLINA COASTAL PLAIN

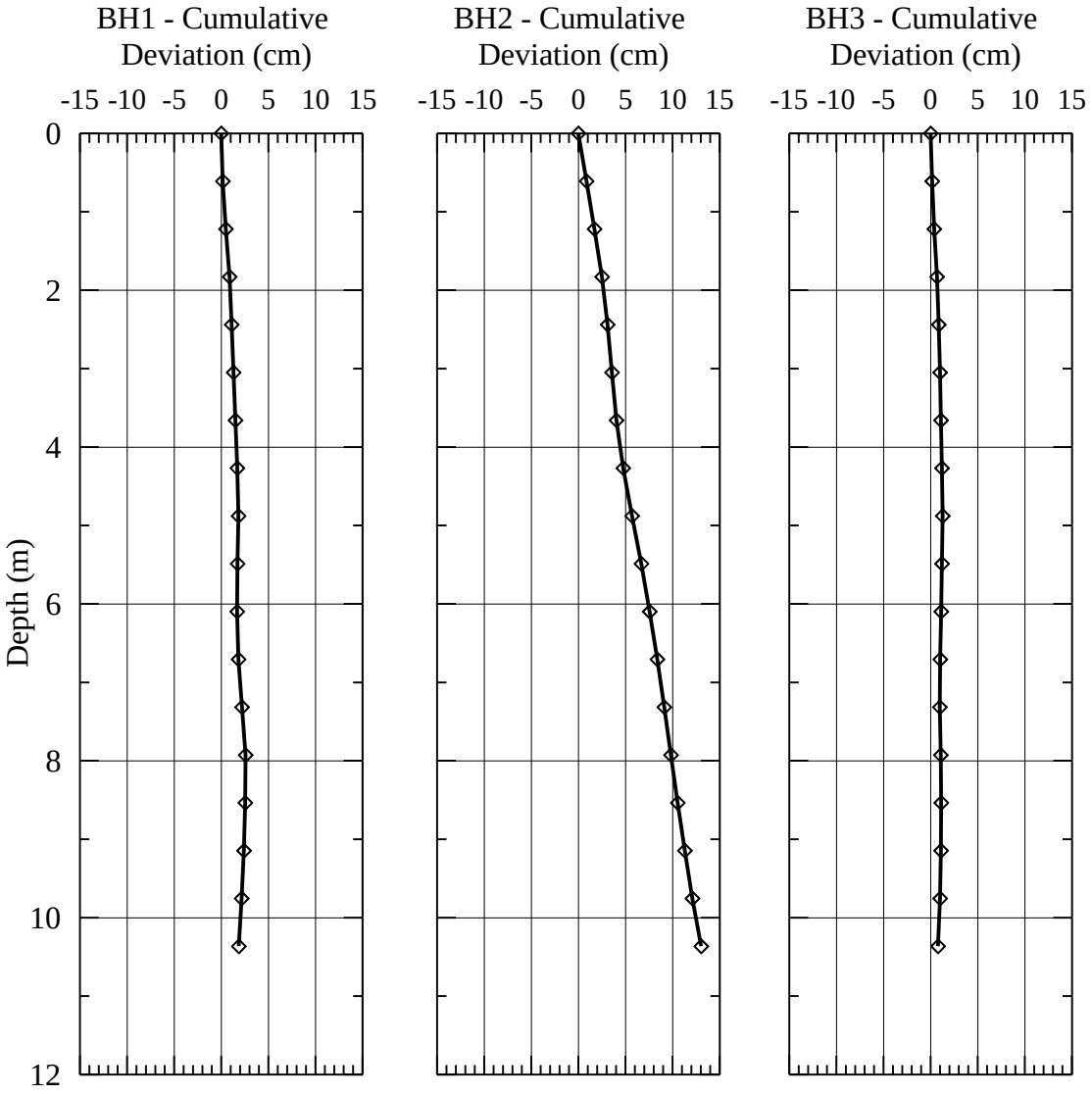

Figure B.1: Borehole displacements in the A_0A_{180} direction at the CREC site after Hayati (2009).

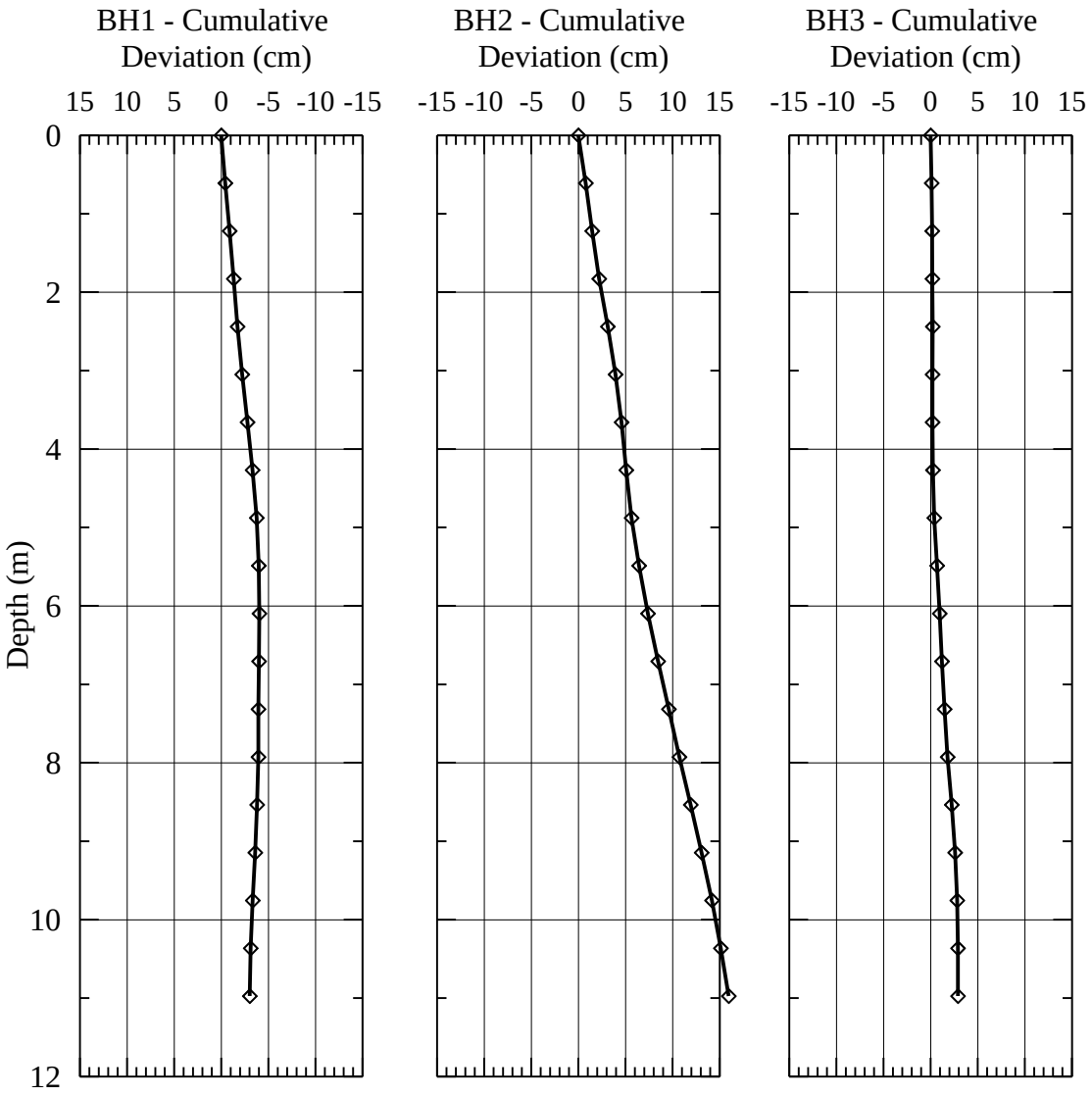

Figure B.2: Borehole displacements in the A_0A_{180} direction at the Hobcaw Borrow Pit site after Hossain (2010).

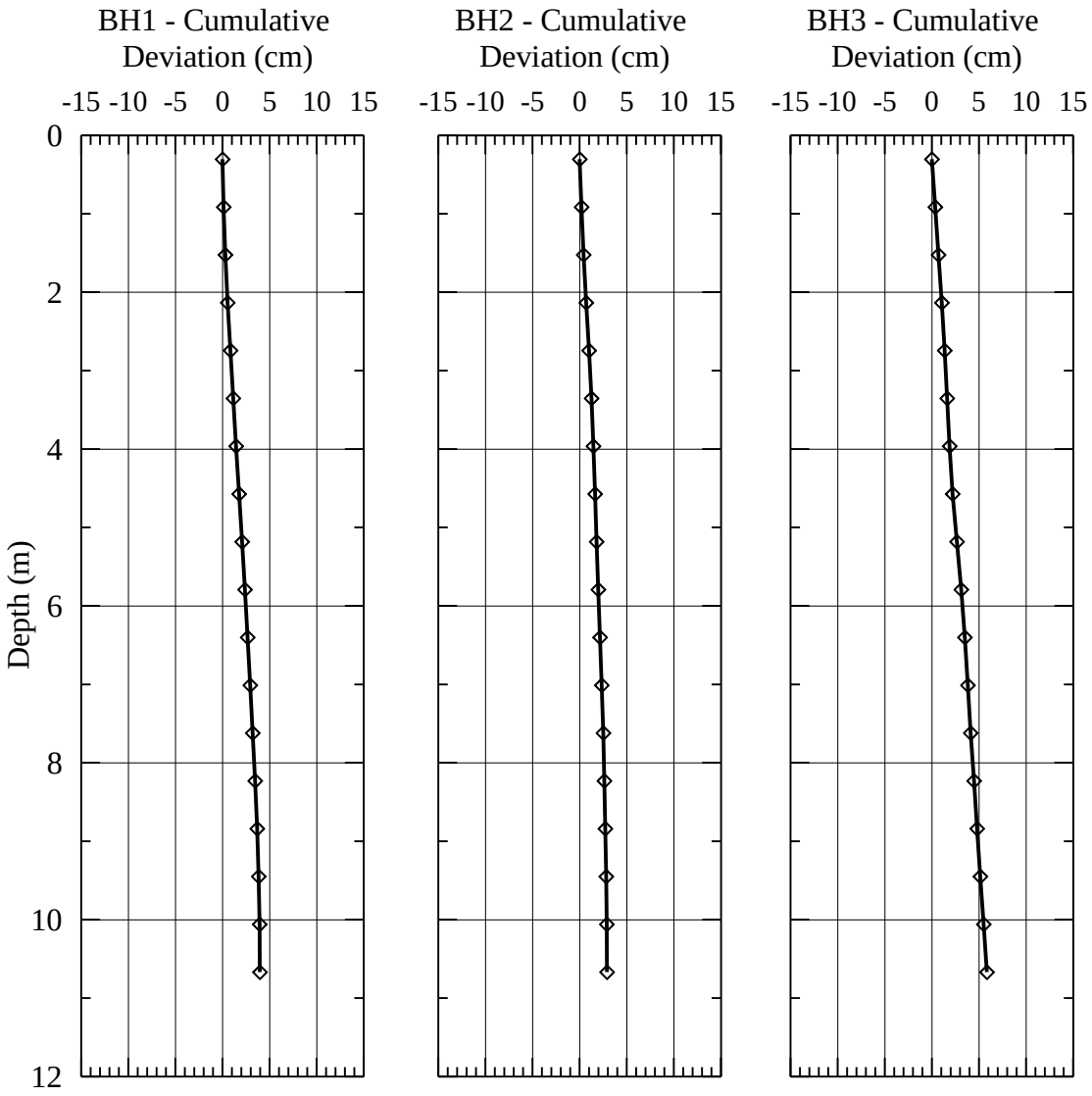

Figure B.3: Borehole displacements in the A_0A_{180} direction at the Walterboro Rest Area site after Hossain (2010).

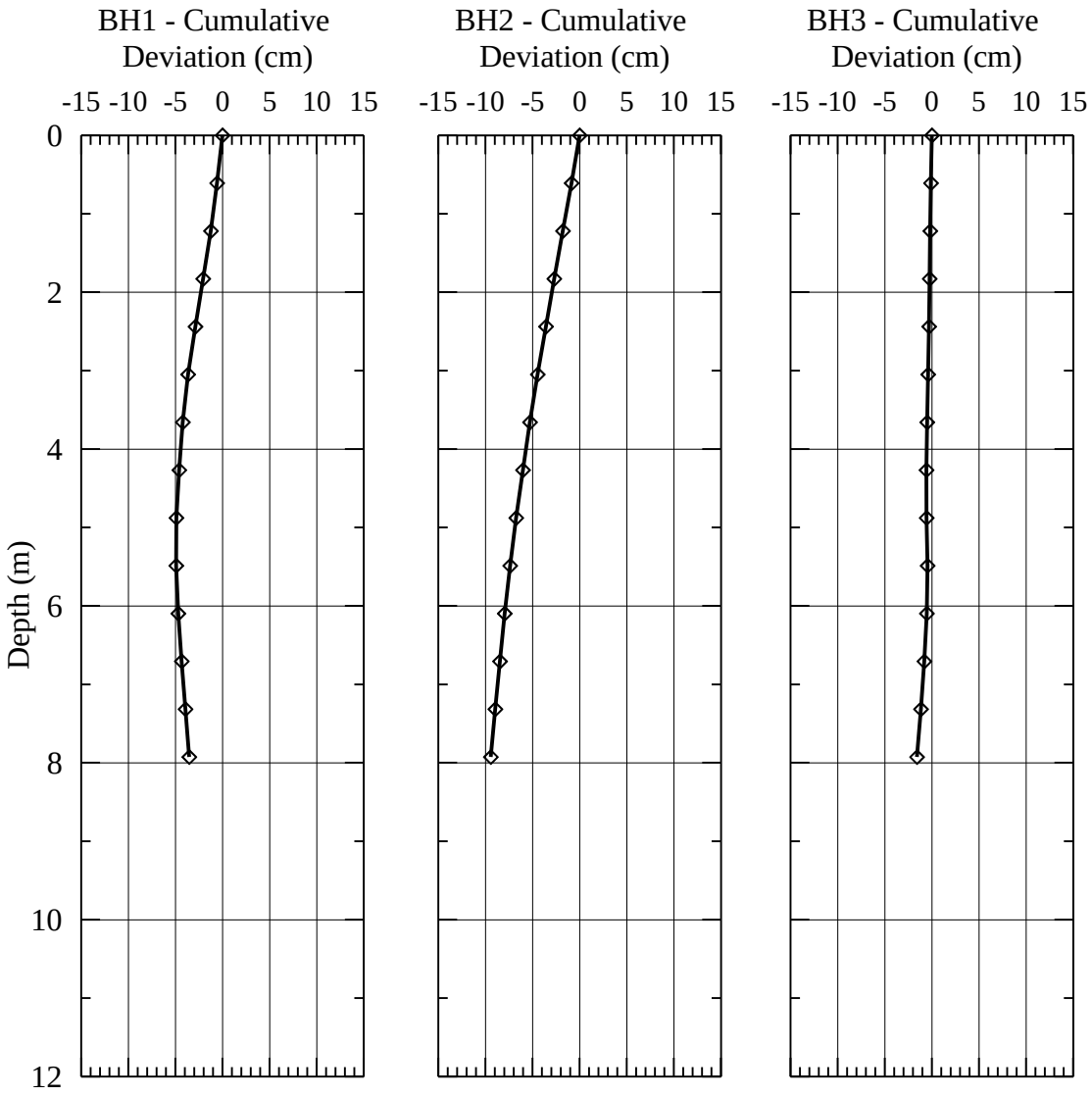

Figure B.4: Borehole displacements in the A_0A_{180} direction at the Hollywood Ditch site after Hossain (2010).

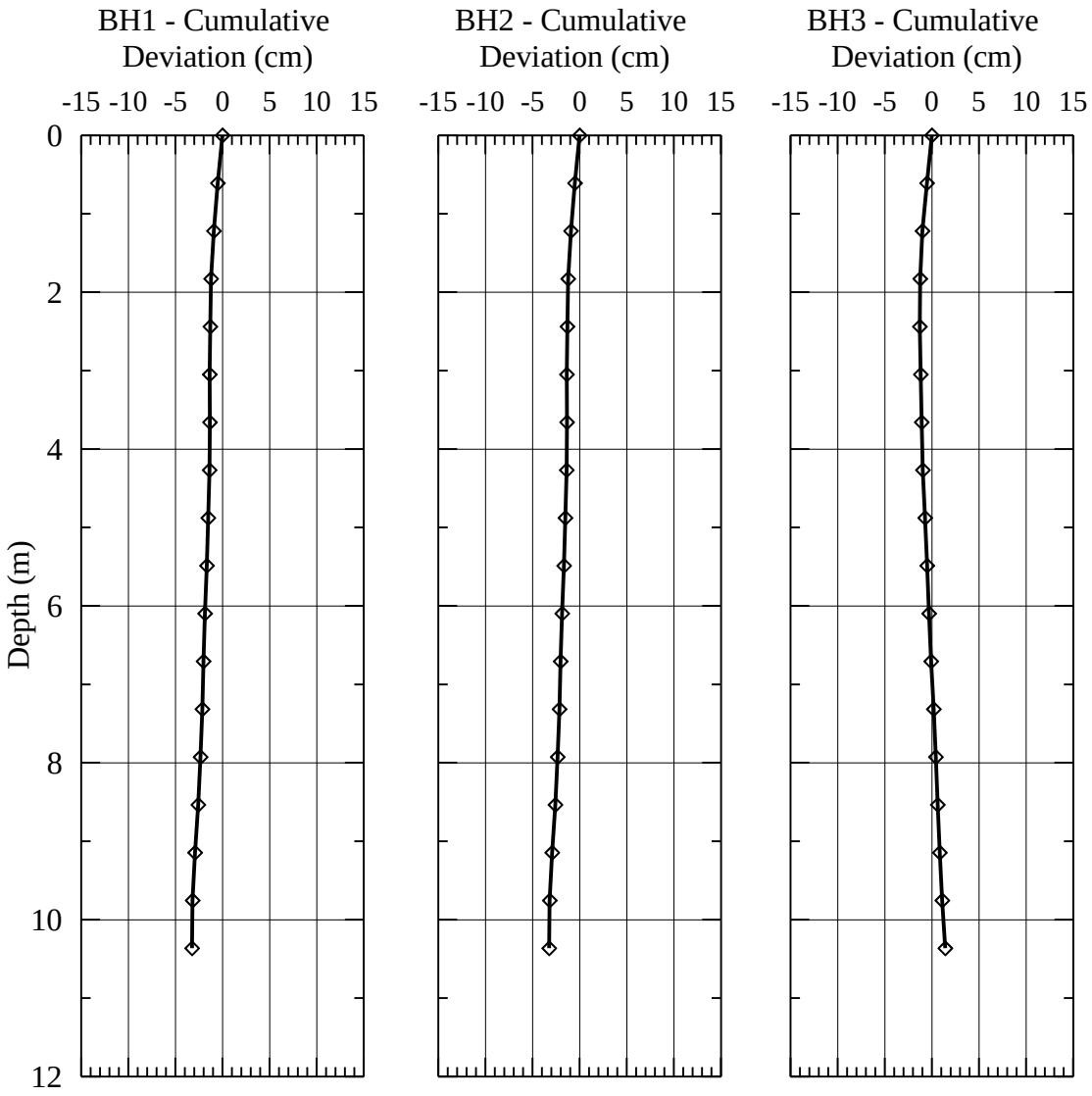

Figure B.5: Borehole displacements in the A_0A_{180} direction at the Sampit site after Hossain (2010).

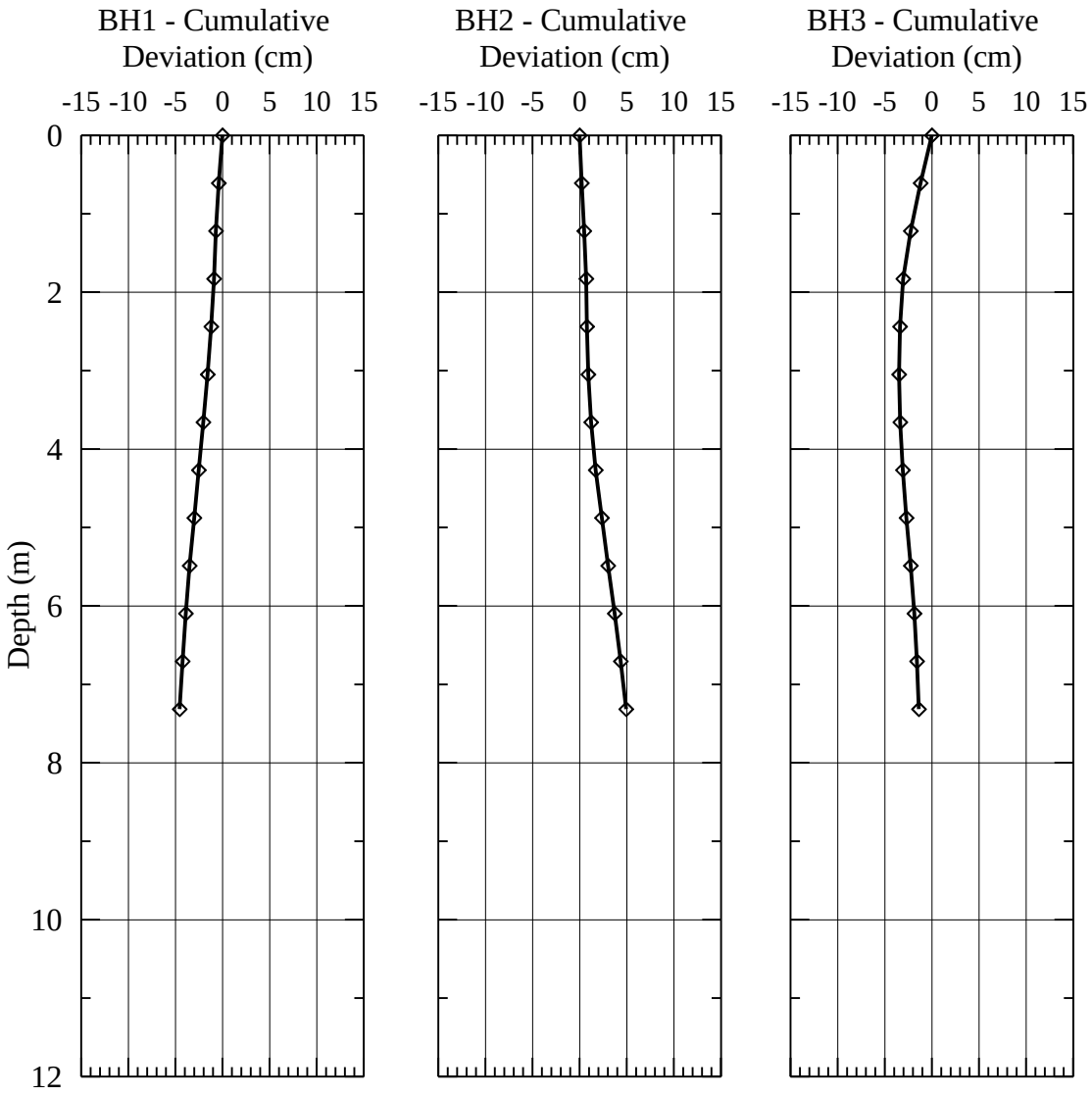

Figure B.6: Borehole displacements in the A_0A_{180} direction at the Four Hole Swamp site after Hossain (2010).

APPENDIX C

SUMMARY OF COMPRESSION WAVE VELOCITIES FROM THE SIX CROSSHOLE SITES IN THE SOUTH CAROLINA COASTAL PLAIN

Table C.1: Direct measurements of P-wave velocity in crosshole testing with solenoid source in BH1 and receiver in BH2 at CREC site adapted from Hayati (2009). Measurements were conducted in March 2008.

Depth (ft)	Corrected[a] edge to edge distance (ft)	Travel time (ms)	Adjusted[b] time (ms)	Record quality[c]	P-wave velocity (ft/s)
2	9.97	12.33	12.24	F to P	815
8	10.01	2.01	1.92	F	5218
10	10.02	1.98	1.89	F	5306
12	10.03	1.95	1.86	F	5397
16	10.07	2.08	1.99	F	5064

[a]Corrected for inclination.
[b]Correction of -0.0915 ms as calibration factor.
[c]F = Fair, P = Poor.

Table C.2: Direct measurements of P-wave velocity in crosshole testing with solenoid source in BH3 and receiver in BH2 at CREC site adapted from Hayati (2009). Measurements were conducted in March 2008.

Depth (ft)	Corrected[a] edge to edge distance (ft)	Travel time (ms)	Adjusted[b] time (ms)	Record quality[c]	P-wave velocity (ft/s)
10	10.45	2.05	1.96	F	5336
12	10.44	1.98	1.89	F	5528
16	10.39	2.11	2.02	F to P	5147
34	10.14	2.01	1.92	F to P	5064

[a]Corrected for inclination.
[b]Correction of -0.0915 ms as calibration factor.
[c]F = Fair, P = Poor.

Table C.3: Interval measurements of P-wave velocity in crosshole testing using dynamic cone source with first receiver in BH1 and second receiver in BH2 at the CREC site. Measurements were conducted in April 2011.

Depth (ft)	Corrected[a] center to center distance (ft)	Travel time (ms)	Record quality[b]	P-wave velocity (ft/s)
1	10.30	10.06	G	1024
2	10.30	9.40	G	1095
3	10.30	9.77	G	1055
4	10.31	8.42	G	1224
5	10.32	9.52	G	1084
6	10.33	5.62	G	1839
7	10.33	2.08	E	4979
8	10.34	2.08	E	4982
9	10.34	2.08	VG	4984
10	10.35	2.01	E	5136
11	10.35	2.01	E	5138
12	10.35	2.01	E	5141
13	10.36	2.01	E	5145
14	10.37	2.01	VG	5150
15	10.39	2.01	E	5155
16	10.40	2.01	E	5163
17	10.42	2.01	E	5171
18	10.43	2.01	E	5180
19	10.43	1.89	E	5514

[a]Corrected for inclination.
[b]G = Good, VG = Very Good, E = Excellent.

Table C.4: Interval measurements of P-wave velocity in crosshole testing using dynamic cone source with first receiver in BH2 and second receiver in BH3 at the CREC site. Measurements were conducted in April 2011.

Depth (ft)	Corrected[a] center to center distance (ft)	Travel time (ms)	Record quality[b]	P-wave velocity (ft/s)
2	10.77	9.09	G	1184
3	10.76	9.46	G	1137
4	10.75	8.42	G	1276
5	10.74	4.64	G	2315
7	10.72	2.20	E	4881
8	10.72	2.20	E	4877
9	10.71	2.14	E	5015
10	10.71	2.14	E	5012
11	10.70	2.08	E	5156
12	10.70	2.08	E	5153
13	10.69	2.08	E	5148
14	10.68	2.08	E	5142
15	10.66	2.08	E	5136
16	10.65	2.08	E	5130
17	10.63	2.08	E	5123
18	10.61	2.01	E	5268

[a]Corrected for inclination.
[b]G = Good, E = Excellent.

Table C.5: Direct measurements of P-wave velocity in crosshole testing with solenoid source in BH1 and receiver in BH2 at the Hobcaw Borrow Pit site adapted from Geiger (2010). Measurements were conducted in November 2008.

Depth (ft)	Corrected[a] edge to edge distance (ft)	Travel time (ms)	Adjusted[b] time (ms)	Record quality[c]	P-wave velocity (ft/s)
2	9.55	10.254	10.1236	F	943
4	9.54	16.113	15.9826	F	597
6	9.53	11.352	11.2216	F	850
8	9.52	9.948	9.8176	F	969
10	9.51	2.075	1.9446	F	4889
12	9.50	2.106	1.9756	G	4810
14	9.50	1.953	1.8226	F	5215
16	9.50	2.075	1.9446	F	4886
18	9.48	2.044	1.9136	G	4955
20	9.45	1.983	1.8526	G	5103
22	9.42	2.045	1.9146	F	4918
24	9.38	2.075	1.9446	F	4822
26	9.34	2.075	1.9446	F	4803
28	9.30	2.075	1.9446	F	4781
30	9.25	2.136	2.0056	G	4613
32	9.21	2.045	1.9146	G	4809
34	9.17	2.014	1.8836	G	4868
36	9.14	1.892	1.7616	G	5187

[a]Corrected for inclination and thickness of grout.
[b]Correction of -0.0915 ms as calibration factor and -0.0389 ms for travel time through grout.
[c]F = Fair, G = Good.

Table C.6: Interval measurements of P-wave velocity in crosshole testing using solenoid source with first receiver in BH2 and second receiver in BH3 at the Hobcaw Borrow Pit site adapted from Geiger (2010). Measurements were conducted in November 2008.

Depth (ft)	Corrected[a] center to center distance (ft)	Travel time (ms)	Record quality[b]	P-wave velocity (ft/sec)
2	9.75	9.643	F	1011
4	9.77	15.259	G	640
6	9.80	10.681	F	917
14	9.89	1.967	G	5027
16	9.90	1.906	F	5195
20	9.94	1.967	F	5054
22	9.97	1.906	F	5230

[a]Corrected for inclination.
[b]F = Fair, G = Good.

Table C.7: Direct measurements of P-wave velocity in crosshole testing with solenoid source in BH3 and receiver in BH1 at the Hobcaw Borrow Pit site adapted from Geiger (2010). Measurements were conducted in November 2008.

Depth (ft)	Corrected[a] edge to edge distance (ft)	Travel time (ms)	Adjusted[b] time (ms)	Record quality[c]	P-wave velocity (ft/s)
4	19.32	26.855	26.725	G	723
12	19.38	4.059	3.929	G	4932
36	19.30	4.059	3.929	F	4912

[a]Corrected for inclination and thickness of grout.
[b]Correction of -0.0915 ms as calibration factor and -0.0389 ms for travel time through grout.
[c]F = Fair, G = Good.

Table C.8: Interval measurements of P-wave velocity in crosshole testing using dynamic cone source with first receiver in BH1 and second receiver in BH2 at the Hobcaw Borrow Pit site adapted from Hossain (2010). Measurements were conducted in June 2010.

Depth (ft)	Corrected[a] center to center distance (ft)	Travel time (ms)	Record quality[b]	P-wave velocity (ft/s)
2	9.93	7.629	E	1301
4	9.92	7.812	E	1270
6	9.91	7.934	E	1249
8	9.89	3.723	VG	2657
9	9.89	3.235	G	3056
10	9.88	1.892	E	5222
11	9.88	1.831	E	5395
12	9.88	1.770	E	5581
13	9.88	1.770	E	5582
14	9.88	1.740	E	5678
15	9.88	1.709	E	5779
16	9.88	1.709	E	5779
17	9.87	1.709	E	5774
18	9.86	1.709	E	5768

[a]Corrected for inclination.

[b]G = Good, VG = Very Good, E = Excellent.

Table C.9: Interval measurements of P-wave velocity in crosshole testing using dynamic cone source with first receiver in BH2 and second receiver in BH3 at the Hobcaw Borrow Pit site adapted from Hossain (2010). Measurements were conducted in June 2010.

Depth (ft)	Corrected[a] center to center distance (ft)	Travel time (ms)	Record quality[b]	P-wave velocity (ft/s)
2	9.75	7.873	E	1239
4	9.77	7.935	VG	1232
6	9.80	7.995	G	1225
8	9.82	11.289	G	870
9	9.84	1.953	G	5038
10	9.85	1.892	E	5206
11	9.86	1.892	E	5212
12	9.87	1.892	E	5218
13	9.88	1.892	E	5221
14	9.89	1.831	E	5399
15	9.90	1.892	E	5230
16	9.90	1.831	E	5407
17	9.91	1.831	E	5412
18	9.92	1.831	E	5416

[a]Corrected for inclination.

[b]G = Good, VG = Very Good, E = Excellent.

Table C.10: Direct measurements of P-wave velocity in crosshole testing with solenoid source in BH1 and receiver in BH2 at the Walterboro Rest Area site adapted from Hossain (2010). Measurements were conducted in January 2010.

Depth (ft)	Corrected[a] edge to edge distance (ft)	Travel time (ms)	Adjusted[b] time (ms)	Record quality[c]	P-wave velocity (ft/s)
3	8.43	9.522	9.392	G	898
5	8.43	8.423	8.293	G	1016
11	8.43	1.693	1.563	G	5393
13	8.44	1.724	1.594	G	5293
15	8.45	1.693	1.563	G	5405
17	8.46	1.693	1.563	G	5414
19	8.47	1.709	1.579	G	5366
21	8.48	1.785	1.655	G	5124
23	8.49	1.740	1.609	G	5274
25	8.49	1.709	1.579	VG	5381
27	8.51	1.739	1.609	G	5288
29	8.52	1.770	1.640	G	5194
31	8.52	1.740	1.609	VG	5297
33	8.53	1.709	1.578	VG	5402

[a]Corrected for inclination and thickness of grout.
[b]Correction of -0.0915 ms as calibration factor and -0.0389 ms for travel time through grout.
[c]G = Good, VG = Very Good.

Table C.11: Interval measurements of P-wave velocity in crosshole testing using solenoid source with first receiver in BH2 and second receiver in BH3 at the Walterboro Rest Area site adapted from Hossain (2010). Measurements were conducted in January 2010.

Depth (ft)	Corrected[a] center to center distance (ft)	Travel time (ms)	Record quality[b]	P-wave velocity (ft/sec)
15	8.97	1.725	F	5203
23	8.90	1.701	F	5231
27	8.87	1.729	F	5127
29	8.85	1.816	G	4874
31	8.83	1.831	F	4821

[a]Corrected for inclination.
[b]F = Fair, G = Good.

Table C.12: Direct measurements of P-wave velocity in crosshole testing with solenoid source in BH3 and receiver in BH2 at the Walterboro Rest Area site adapted from Hossain (2010). Measurements were conducted in January 2010.

Depth (ft)	Corrected[a] edge to edge distance (ft)	Travel time (ms)	Adjusted[b] time (ms)	Record quality[c]	P-wave velocity (ft/s)
13	8.61	1.72	1.59	G	5402
17	8.57	1.69	1.56	G	5484
21	8.54	1.72	1.59	VG	5356
29	8.47	1.72	1.59	VG	5317

[a]Corrected for inclination and thickness of grout.
[b]Correction of -0.0915 ms as calibration factor and -0.0389 ms for travel time through grout.
[c]G = Good, VG = Very Good.

Table C.13: Interval measurements of P-wave velocity in crosshole testing using solenoid source with first receiver in BH2 and second receiver in BH1 at the Walterboro Rest Area site adapted from Hossain (2010). Measurements were conducted in January 2010.

Depth (ft)	Corrected[a] center to center distance (ft)	Travel time (ms)	Record quality[b]	P-wave velocity (ft/sec)
15	8.84	1.632	F	5415
23	8.85	1.694	F	5227
27	8.89	1.725	G	5155

[a]Corrected for inclination.
[b]F = Fair, G = Good.

Table C.14: Interval measurements of P-wave velocity in crosshole testing using dynamic cone source with first receiver in BH1 and second receiver in BH2 at the Walterboro Rest Ares site adapted from Hossain (2010). Measurements were conducted in June 2010.

Depth (ft)	Corrected[a] center to center distance (ft)	Travel time (ms)	Record quality[b]	P-wave velocity (ft/s)
2	8.81	7.141	E	1234
4	8.81	7.385	E	1192
6	8.80	7.446	E	1182
8	8.80	2.441	G	3605
9	8.80	2.380	G	3697
10	8.80	1.770	E	4973
11	8.80	1.709	E	5152
12	8.81	1.709	E	5154
13	8.81	1.648	E	5347
14	8.82	1.709	E	5160
15	8.82	1.678	E	5257
16	8.83	1.648	E	5357
17	8.84	1.663	E	5314
18	8.84	1.618	E	5466

[a]Corrected for inclination.
[b]G = Good, E = Excellent.

Table C.15: Interval measurements of P-wave velocity in crosshole testing using dynamic cone source with first receiver in BH2 and second receiver in BH3 at the Walterboro Rest Ares site adapted from Hossain (2010). Measurements were conducted in June 2010.

Depth (ft)	Corrected[a] center to center distance (ft)	Travel time (ms)	Record quality[b]	P-wave velocity (ft/s)
2	9.01	7.568	VG	1191
4	9.00	7.874	E	1143
8	8.99	8.606	G	1045
9	8.99	2.319	F	3878
10	8.99	1.831	E	4911
11	8.99	1.709	E	5260
12	8.99	1.709	E	5260
13	8.99	1.648	E	5453
14	8.98	1.709	E	5254
15	8.97	1.709	E	5252
16	8.96	1.648	E	5439
17	8.95	1.618	E	5533
18	8.94	1.602	E	5580

[a]Corrected for inclination.
[b]G = Good, VG = Very Good, E = Excellent.

Table C.16: Direct measurements of P-wave velocity in crosshole testing with solenoid source in BH3 and receiver in BH2 at the Hollywood Ditch site adapted from Hossain (2010). Measurements were conducted in June 2010.

Depth (ft)	Corrected[a] edge to edge distance (ft)	Travel time (ms)	Adjusted[b] time (ms)	Record quality[c]	P-wave velocity (ft/s)
2	9.00	12.391	12.212	G	737
4	8.97	8.789	8.610	F	1042
12	8.86	1.862	1.683	VG	5269
14	8.84	1.892	1.713	VG	5163
16	8.82	1.862	1.683	F	5242
18	8.79	1.953	1.774	G	4958
20	8.78	1.770	1.591	VG	5518
22	8.77	1.831	1.652	G	5310
24	8.77	1.739	1.560	VG	5621

[a]Corrected for inclination and thickness of grout.
[b]Correction of -0.0915 ms as calibration factor and -0.0879 ms for travel time through grout.
[c]F = Fair, G = Good, VG = Very Good.

Table C.17: Interval measurements of P-wave velocity in crosshole testing using dynamic cone source with first receiver in BH3 and second receiver in BH2 at the Hollywood Ditch site adapted from Hossain (2010). Measurements were conducted in June 2010.

Depth (ft)	Corrected[a] center to center distance (ft)	Travel time (ms)	Record quality[b]	P-wave velocity (ft/s)
2	9.37	10.620	G	883
4	9.34	8.118	G	1151
6	9.32	13.244	G	703
8	9.29	2.259	F	4112
10	9.26	1.922	E	4818
12	9.24	1.861	E	4964
14	9.22	1.831	E	5035
16	9.19	1.801	E	5106

[a]Corrected for inclination.
[b]F = Fair, G = Good, E = Excellent.

Table C.18: Direct measurements of P-wave velocity in crosshole testing with solenoid source in BH1 and receiver in BH2 at the Sampit site adapted from Hossain (2010). Measurements were conducted in June 2010.

Depth (ft)	Corrected[a] edge to edge distance (ft)	Travel time (ms)	Adjusted[b] time (ms)	Record quality[c]	P-wave velocity (ft/s)
24	8.50	1.770	1.481	G	5743
30	8.54	1.801	1.512	F	5649
32	8.56	1.770	1.481	F	5780
34	8.57	1.709	1.420	F	6037

[a]Corrected for inclination and thickness of grout.
[b]Correction of -0.0915 ms as calibration factor and -0.1977 ms for travel time through grout.
[c]F = Fair, G = Good.

Table C.19: Interval measurements of P-wave velocity in crosshole testing using dynamic cone source with first receiver in BH1 and second receiver in BH2 at the Sampit site adapted from Hossain (2010). Measurements were conducted in June 2010.

Depth (ft)	Corrected[a] center to center distance (ft)	Travel time (ms)	Record quality[b]	P-wave velocity (ft/s)
2	8.91	9.216	VG	967
4	8.92	10.132	VG	880
6	8.92	3.082	E	2892
8	8.91	1.770	E	5033
9	8.90	1.557	E	5717
10	8.90	1.617	E	5504
11	8.90	1.617	E	5504
12	8.89	1.633	E	5442
13	8.90	1.648	E	5400
14	8.87	1.602	E	5539
15	8.90	1.633	E	5450
16	8.87	1.587	E	5586
17	8.90	1.602	E	5556
18	8.87	1.541	E	5755

[a]Corrected for inclination.
[b]VG = Very Good, E = Excellent.

Table C.20: Direct measurements of P-wave velocity in crosshole testing with solenoid source in BH3 and receiver in BH2 at the Four Hole Swamp site adapted from Hossain (2010). Measurements were conducted in June 2010.

Depth (ft)	Corrected[a] edge to edge distance (ft)	Travel time (ms)	Adjusted[b] time (ms)	Record quality[c]	P-wave velocity (ft/s)
6	8.96	6.23	6.13	F	1460
8	8.97	12.88	12.79	F	701
10	8.98	1.68	1.59	VG	5658
12	8.98	1.68	1.59	VG	5660
14	8.99	1.65	1.56	VG	5778
16	9.00	1.74	1.65	VG	5462
18	9.01	1.43	1.34	G	6708
20	9.02	1.46	1.37	VG	6567
22	9.03	1.47	1.37	VG	6573
24	9.04	1.47	1.37	VG	6581

[a]Corrected for inclination. No grout correction was made because of very soft grout.
[b]Correction of -0.0915 ms as calibration factor.
[c]F = Fair, G = Good, VG = Very Good.

Table C.21: Interval measurements of P-wave velocity in crosshole testing using solenoid source with first receiver in BH2 and second receiver in BH1 at the Four Hole Swamp site adapted from Hossain (2010). Measurements were conducted in June 2010.

Depth (ft)	Corrected[a] center to center distance (ft)	Travel time (ms)	Record quality[b]	P-wave velocity (ft/sec)
10	9.15	1.83	G	4996
12	9.12	1.80	VG	5069
14	9.09	1.71	F	5320
16	9.05	1.74	VG	5204
20	8.98	1.47	F	6130
22	8.95	1.43	G	6240
24	8.92	1.43	G	6219

[a]Corrected for inclination.
[b]F = Fair, G = Good, VG = Very Good.

Table C.22: Interval measurements of P-wave velocity in crosshole testing using dynamic cone source with first receiver in BH1 and second receiver in BH2 at the Four Hole Swamp site adapted from Hossain (2010). Measurements were conducted in June 2010.

Depth (ft)	Corrected[a] center to center distance (ft)	Travel time (ms)	Record quality[b]	P-wave velocity (ft/s)
5	9.18	4.883	G	1881
6	9.18	4.944	VG	1856
7	9.17	4.975	G	1843
8	9.17	1.709	VG	5363
9	9.16	1.770	E	5173
10	9.15	1.800	E	5081
11	9.14	1.815	E	5032
12	9.12	1.739	E	5245
13	9.11	1.678	E	5428
14	9.09	1.678	E	5417
15	9.07	1.587	E	5718

[a]Corrected for inclination.

[b]G = Good, VG = Very Good, E = Excellent.

Table C.23: Interval measurements of P-wave velocity in crosshole testing using dynamic cone source with first receiver in BH3 and second receiver in BH2 at the Four Hole Swamp site adapted from Hossain (2010). Measurements were conducted on June 2010.

Depth (ft)	Corrected[a] center to center distance (ft)	Travel time (ms)	Record quality[b]	P-wave velocity (ft/s)
2	9.11	5.738	G	1588
4	9.15	5.920	G	1546
6	9.19	7.202	G	1275
7	9.19	8.178	G	1124
8	9.20	1.953	G	4711
9	9.20	1.831	E	5026
10	9.21	1.800	E	5114
11	9.21	1.804	E	5106
12	9.21	1.740	E	5296
13	9.22	1.739	E	5300
14	9.22	1.709	E	5396
15	9.22	1.587	E	5812
16	9.23	1.587	E	5814

[a]Corrected for inclination.
[b]G = Good, E = Excellent.

APPENDIX D

SUMMARY OF CROSSHOLE SHEAR WAVE VELOCITIES FROM THE SIX CROSSHOLE SITES IN THE SOUTH CAROLINA COASTAL PLAIN

Table D.1: Direct measurements of sHV-wave velocity in crosshole testing with solenoid source in BH1 and receiver in BH2 at the CREC site adapted from Hayati (2009). Measurements were conducted on March 2008.

Depth (ft)	Corrected[a] edge to edge distance (ft)	Up travel time (ms)	Up adjusted[b] time (ms)	Down travel time (ms)	Down adjusted[c] time (ms)	Record quality[d]	sHV-wave velocity (ft/s)
2	9.98	17.95	17.89	19.29	19.17	G to F	539
4	10.00	17.40	17.34	No or poor record		F	698
6	10.01	15.56	15.50	15.93	15.81	F	639
8	10.02	16.79	16.73	17.09	16.97	G to F	595
10	10.03	19.10	19.04	18.8	18.68	G	532
12	10.04	14.47	14.41	15.56	15.44	VG	673
14	10.06	18.37	18.31	15.69	15.57	G	594
16	10.08	21.36	21.30	16.05	15.93	G	542
24	10.18	6.59	6.53	6.53	6.41	F to P	1574
26	10.19	6.29	6.23	6.53	6.41	G to F	1613
28	10.22	6.59	6.53	No or poor record		G to F	586
30	10.25	6.23	6.17	7.75	7.63	F to P	1485
31	10.27	8.42	8.36	8	7.88	F to P	1264
32	10.28	7.02	6.96	No or poor record		F to P	658
34	10.32	10.74	10.68	No or poor record		F to P	650
35	10.34	10.80	10.74	9.58	9.46	G to F	1024

[a]Corrected for inclination.
[b]Correction of -0.061 ms as calibration factor.
[c]Correction of -0.1221 ms as calibration factor.
[d]P = Poor, F = Fair, G = Good, VG = Very Good.

Table D.2: Direct measurements of sHV-wave velocity in crosshole testing with solenoid source in BH3 and receiver in BH2 at the CREC site adapted from Hayati (2009). Measurements were conducted on March 2008.

Depth (ft)	Corrected[a] edge to edge distance (ft)	Up travel time (ms)	Up adjusted[b] time (ms)	Down travel time (ms)	Down adjusted[c] time (ms)	Record quality[d]	sHV-wave velocity (ft/s)
2	10.50	30.40	30.34	30.64	30.52	F to P	345
6	10.46	14.40	14.34	14.95	14.83	F to P	717
8	10.45	14.04	13.98	15.26	15.14	G	718
10	10.44	14.53	14.47	15.75	15.63	VG to G	694
12	10.43	14.65	14.59	15.99	15.87	VG to G	685
14	10.41	16.11	16.05	17.58	17.46	VG	621
16	10.38	17.21	17.15	18.92	18.80	VG to G	577
18	10.34	18.49	18.43	19.1	18.98	G to F	553
20	10.31	18.19	18.13	18.31	18.19	F to P	568
30	10.19	7.51	7.45	No or poor record		F to P	1368
34	10.12	12.94	12.88	7.14	7.02	F to P	1017

[a]Corrected for inclination.
[b]Correction of -0.061 ms as calibration factor.
[c]Correction of -0.1221 ms as calibration factor.
[d]P = Poor F = Fair, G = Good, VG = Very Good.

Table D.3: Interval measurements of sHV-wave velocity in crosshole testing using dynamic cone source with first receiver in BH1 and second receiver in BH2 at the CREC site. Measurements were conducted on April 2011.

Depth (ft)	Corrected[a] center to center distance (ft)	Travel time (ms)	Record quality[b]	sHV-wave velocity (ft/s)
2	10.30	23.437	F	439
3	10.30	20.996	G	491
4	10.31	16.724	G	617
5	10.32	15.748	VG	655
6	10.33	14.892	E	693
7	10.33	14.892	E	694
8	10.34	15.381	E	672
9	10.34	14.770	E	700
10	10.35	14.893	VG	695
11	10.35	18.310	E	565
12	10.35	19.165	E	540
13	10.36	20.263	E	511
14	10.37	19.775	E	524
15	10.39	20.019	E	519
16	10.40	20.264	E	513
17	10.42	8.667	F	1202
18	10.43	7.447	F	1401
19	10.43	6.347	VG	1644

[a]Corrected for inclination.

[b]F = Fair, G = Good, VG = Very Good, E = Excellent.

Table D.4: Interval measurements of sHV-wave velocity in crosshole testing using dynamic cone source with first receiver in BH2 and second receiver in BH3 at the CREC site. Measurements were conducted on April 2011.

Depth (ft)	Corrected[a] center to center distance (ft)	Travel time (ms)	Record quality[b]	sHV-wave velocity (ft/s)
2	10.77	20.263	F	531
3	10.76	17.944	G	600
4	10.75	16.358	G	657
5	10.74	15.015	G	715
6	10.73	16.543	G	649
7	10.72	13.672	VG	784
8	10.72	14.160	VG	757
9	10.71	14.038	E	763
10	10.71	14.649	G	731
11	10.70	18.921	G	566
12	10.70	19.410	VG	551
13	10.69	18.921	E	565
14	10.68	19.897	E	537
15	10.66	19.775	E	539
16	10.65	22.094	E	482
17	10.63	7.874	G	1350
19	10.61	7.362	F	1441

[a]Corrected for inclination.

[b]F = Fair, G = Good, VG = Very Good, E = Excellent.

Table D.5: Direct measurement of sHH-wave velocity in crosshole testing with solenoid source in BH3 and receiver in BH2 at the CREC site adapted from Hayati (2009). Measurements were conducted in March 2008.

Depth (ft)	Corrected[a] edge to edge distance (ft)	Up travel time (ms)	Up adjusted[b] time (ms)	Down travel time (ms)	Down adjusted[b] time (ms)	Record quality[c]	sHH-wave velocity (ft/s)
10	10.44	20.32	20.23	20.45	20.36	G	514
12	10.43	20.45	20.36	20.20	20.11	G to F	515
14	10.41	21.55	21.46	21.79	21.70	G to F	482
16	10.38	25.67	25.58	27.53	27.44	G to F	391
24	10.26	No or poor record		6.41	6.32	F to P	495
28	10.21	5.31	5.22	5.19	5.10	F to P	604
34	10.12	No or poor record		8.00	7.91	F	390

[a]Corrected for inclination.
[b]Correction of -0.0915 ms as calibration factor.
[c]P = Poor, F = Fair, G = Good.

Table D.6: Direct measurement of sHH-wave velocity in crosshole testing with solenoid source in BH1 and receiver in BH2 at the CREC site. Measurements were conducted in April 2011.

Depth (ft)	Corrected[a] edge to edge distance (ft)	Up travel time (ms)	Up adjusted[b] time (ms)	Down travel time (ms)	Down adjusted[b] time (ms)	Record quality[c]	sHH-wave velocity (ft/s)
8	10.02	18.189	18.097	17.212	17.120	G	567
9	10.03	16.235	16.143	16.113	16.021	G	620
10	10.03	17.334	17.242	19.287	19.195	F	549
11	10.03	19.287	19.195	18.921	18.829	VG	525
12	10.04	19.287	19.195	18.921	18.829	VG	526
13	10.05	19.165	19.073	18.799	18.707	E	529
14	10.06	21.973	21.881	21.729	21.637	VG	460
15	10.07	20.874	20.782	20.264	20.172	VG	490
16	10.08	21.972	21.881	20.020	19.928	VG	481

[a]Corrected for inclination.
[b]Correction of -0.0915 ms as calibration factor.
[c]F = Fair, G = Good, VG = Very Good, E = Excellent.

Table D.7: Direct measurements of sHV-wave velocity in crosshole testing with solenoid source in BH1 and receiver in BH2 at the Hobcaw Borrow Pit site adapted from Geiger (2010). Measurements were conducted on November 2008.

Depth (ft)	Corrected[a] edge to edge distance (ft)	Up travel time (ms)	Up adjusted[b] time (ms)	Down travel time (ms)	Down adjusted[c] time (ms)	Record quality[d]	sHV-wave velocity (ft/s)
2	9.55	17.456	17.312	17.456	17.2509	F	553
4	9.54	15.747	15.603	11.962	11.7569	G	698
6	9.53	16.113	15.969	16.723	16.5179	F/G	587
8	9.52	16.357	16.213	16.479	16.2739	F	586
10	9.51	18.067	17.923	18.066	17.8609	G/VG	531
12	9.50	16.48	16.336	16.723	16.5179	F	579
14	9.50	15.493	15.349	15.625	15.4199	G	618
16	9.50	15.371	15.227	15.991	15.7859	G	613
18	9.48	14.038	13.894	14.404	14.1989	G	675
20	9.45	14.038	13.894	13.916	13.7109	G	685
22	9.42	17.334	17.19	19.287	19.0819	G	519
24	9.38	16.724	16.58	17.028	16.8229	VG	561
26	9.34	16.846	16.702	16.601	16.3959	G	564
28	9.30	15.93	15.786	16.174	15.9689	G	586
30	9.25	16.419	16.275	16.174	15.9689	G	574
32	9.21	15.503	15.359	15.197	14.9919	G/F	607
34	9.17	14.526	14.382	13.671	13.4659	F	658
36	9.14	14.312	14.168	14.16	13.9549	G	650

[a]Corrected for inclination and thickness of grout.
[b]Correction of -0.061 ms as calibration factor and -0.0835 ms for travel time through grout.
[c]Correction of -0.1221 ms as calibration factor and -0.0835 ms for travel time through grout.
[d]F = Fair, G = Good, VG = Very Good.

Table D.8: Interval measurements of sHV-wave velocity in crosshole using solenoid source with first receiver in BH2 and second receiver in BH3 at the Hobcaw Borrow Pit site adapted from Geiger (2010). Measurements were conducted on November 2008.

Depth (ft)	Corrected[a] center to center distance (ft)	Up travel time (ms)	Down travel time (ms)	Record quality[b]	sHV-wave velocity (ft/s)
2	9.75	16.846	18.799	G	547
4	9.77	16.602	21.119	G	518
6	9.80	16.846	16.602	G	586
8	9.82	17.579	17.945	G	553
10	9.85	15.869	16.235	G	614
14	9.89	14.282	14.648	G	684
16	9.90	14.038	13.55	G	718
18	9.92	13.184	13.428	G	745
20	9.94	13.55	14.16	G	718
22	9.97	17.456	17.334	G	573

[a]Corrected for inclination.
[b]G = Good.

Table D.9: Direct measurements of sHV-wave velocity in crosshole testing with solenoid source in BH3 and receiver in BH1 at the Hobcaw Borrow Pit site Adapted from Geiger (2010). Measurements were conducted on November 2008.

Depth (ft)	Corrected[a] edge to edge distance (ft)	Up travel time (ms)	Up adjusted[b] time (ms)	Down travel time (ms)	Down adjusted[c] time (ms)	Record quality[d]	sHV-wave velocity (ft/s)
4	19.32	33.039	32.895	32.956	32.754	G	588
12	19.38	30.395	30.251	30.761	30.556	G	637
16	19.40	30.274	30.130	29.785	29.580	F	650
26	19.36	38.086	37.942	30.639	30.434	F	566
36	19.30	30.640	30.496	30.517	30.312	G	635

[a]Corrected for inclination and thickness of grout.
[b]Correction of -0.061 ms as calibration factor and -0.0835 ms for travel time through grout.
[c]Correction of -0.1221 ms as calibration factor and -0.0835 ms for travel time through grout.
[d]F = Fair, G = Good.

Table D.10: Interval measurements of sHV-wave velocity in crosshole testing using dynamic cone source with first receiver in BH1 and second receiver in BH2 at the Hobcaw Borrow Pit site. Measurements were conducted on June 2010.

Depth (ft)	Corrected[a] center to center distance (ft)	Travel time (ms)	Record quality[b]	sHV-wave velocity (ft/s)
2	9.93	15.747	VG	630
4	9.92	12.329	VG	805
6	9.91	12.818	E	773
8	9.89	14.526	E	681
9	9.89	15.075	VG	656
10	9.88	14.771	VG	669
11	9.88	14.160	E	698
12	9.88	14.038	E	704
13	9.88	13.672	E	723
14	9.88	14.649	E	674
15	9.88	14.160	E	698
16	9.88	14.648	E	674
17	9.87	13.062	E	755
18	9.86	12.817	E	769

[a]Corrected for inclination.
[b]VG = Very Good, E = Excellent.

Table D.11: Interval measurements of sHV-wave velocity in crosshole testing using dynamic cone source with first receiver in BH2 and second receiver in BH3 at the Hobcaw Borrow Pit site. Measurements were conducted on June 2010.

Depth (ft)	Corrected[a] center to center distance (ft)	Travel time (ms)	Record quality[b]	sHV-wave velocity (ft/s)
2	9.75	15.625	VG	624
4	9.77	15.625	VG	625
6	9.80	16.357	E	599
8	9.82	19.653	G	500
9	9.84	15.625	VG	630
10	9.85	14.648	VG	673
11	9.86	14.160	E	697
12	9.87	14.892	E	663
13	9.88	13.672	E	723
14	9.89	14.160	E	698
15	9.90	13.916	E	711
16	9.90	13.184	E	751
17	9.91	12.817	E	773
18	9.92	12.817	E	774

[a]Corrected for inclination.
[b]VG = Very Good, E = Excellent.

Table D.12: Direct measurements of sHH-wave velocity in crosshole testing with solenoid source in BH1 and receiver in BH2 at the Hobcaw Borrow Pit site adapted from Geiger (2010). Measurements were conducted on November 2008.

Depth (ft)	Corrected[a] edge to edge distance (ft)	Up travel time (ms)	Up adjusted[b] time (ms)	Down travel time (ms)	Down adjusted[c] time (ms)	Record quality[d]	sHH-wave velocity (ft/s)
2	9.55	18.188	18.014	17.944	17.769	VG/E	534
4	9.54	21.362	21.188	20.264	20.089	G	462
6	9.53	18.433	18.259	19.287	19.112	E/VG	510
8	9.52	18.310	18.136	18.554	18.379	G	521
10	9.51	20.996	20.822	21.118	20.943	E	455
12	9.50	18.799	18.625	18.677	18.502	E/F	512
14	9.50	18.066	17.892	No or poor record		F	531
16	9.50	18.677	18.503	18.677	18.502	E	514
20	9.45	20.508	20.334	21.728	21.553	F	451
22	9.42	19.531	19.357	19.775	19.600	VG/E	483
24	9.38	20.874	20.700	20.508	20.333	VG/G	457
26	9.34	17.578	17.404	18.066	17.891	F	529
28	9.30	No or poor record		19.409	19.234	F	483
30	9.25	19.043	18.869	19.531	19.356	G/VG	484
32	9.21	17.456	17.282	19.409	19.234	G/VG	504
34	9.17	15.747	15.573	15.381	15.206	F	596
36	9.14	15.015	14.841	15.015	14.840	VG/G	616

[a]Corrected for inclination and thickness of grout.
[b]Correction of -0.0915 ms as calibration factor and -0.0835 ms for travel time through grout.
[c]Correction of -0.0915 ms as calibration factor and -0.0835 ms for travel time through grout.
[d]F = Fair, G = Good, VG = Very Good, E = Excellent.

Table D.13: Interval measurements of sHH-wave velocity in crosshole using solenoid source with first receiver in BH2 and second receiver in BH3 at the Hobcaw Borrow Pit site adapted from Geiger (2010). Measurements were conducted on November 2008.

Depth (ft)	Corrected[a] center to center distance (ft)	Up travel time (ms)	Down travel time (ms)	Record quality[b]	sHH-wave velocity (ft/s)
2	9.75	No or poor record	20.264	G	481
4	9.77	No or poor record	18.31	F	534
6	9.80	17.089	16.602	G/F	582
8	9.82	No or poor record	17.457	F	563
10	9.85	18.188	18.921	G	531
22	9.97	21.240	No or poor	F	469
24	10.00	17.700	No or poor	F	565
30	10.07	17.578	No or poor	G	573
32	10.10	19.165	18.799	F/G	532
36	10.16	14.648	15.014	F/G	685

[a]Corrected for inclination.
[b]F = Fair, G = Good.

Table D.14: Direct measurements of sHV-wave velocity in crosshole testing with solenoid source in BH1 and receiver in BH2 at the Walterboro Rest Area site. Measurements were conducted in January 2010.

Depth (ft)	Corrected[a] edge to edge distance (ft)	Up travel time (ms)	Up adjusted[b] time (ms)	Down travel time (ms)	Down adjusted[c] time (ms)	Record quality[d]	sHV-wave velocity (ft/s)
1	8.44	16.357	16.212	17.578	17.372	VG	503
3	8.43	16.357	16.212	16.357	16.151	G	521
5	8.43	15.015	14.871	14.343	14.137	G	581
7	8.42	16.052	15.908	14.710	14.504	F	555
15	8.45	10.864	10.720	9.155	8.949	F	866
17	8.46	9.583	9.439	9.827	9.621	VG	888
19	8.47	9.522	9.378	10.010	9.804	G	884
21	8.48	10.437	10.293	10.376	10.170	F	829
23	8.49	12.817	12.673	7.263	7.057	F	936
25	8.49	13.245	13.101	No or poor record		G	645
27	8.51	14.404	14.260	14.282	14.076	F	600
29	8.52	15.137	14.992	15.198	14.993	VG	568
31	8.52	17.822	17.678	21.179	20.973	F	444
33	8.53	14.099	13.955	14.038	13.832	VG	614

[a]Corrected for inclination and thickness of grout.
[b]Correction of -0.061 ms as calibration factor and -0.0835 ms for travel time through grout.
[c]Correction of -0.1221 ms as calibration factor and -0.0835 ms for travel time through grout.
[d]F = Fair, G = Good, VG = Very Good.

Table D.15: Interval measurements of sHV-wave velocity in crosshole using solenoid source with first receiver in BH2 and second receiver in BH3 at the Walterboro Rest area site. Measurements were conducted in January 2010.

Depth (ft)	Corrected[a] center to center distance (ft)	Up travel time (ms)	Down travel time (ms)	Record quality[b]	sHV-wave velocity (ft/s)
1	9.02	21.362	19.776	F	439
3	9.01	21.850	21.118	F	419
17	8.95	9.338	9.948	F	929
19	8.93	9.162	11.657	F	870
21	8.91	9.644	9.644	F	924
27	8.87	15.503	14.039	F	602
29	8.85	17.578	No or poor record	F	503
31	8.83	16.053	17.761	F	523
33	8.80	14.526	13.367	G	632

[a]Corrected for inclination.
[b]F = Fair, G = Good.

Table D.16: Direct measurements of sHV-wave velocity in crosshole testing with solenoid source in BH3 and receiver in BH2 at the Walterboro Rest Area site. Measurements were conducted in January 2010.

Depth (ft)	Corrected[a] edge to edge distance (ft)	Up travel time (ms)	Up adjusted[b] time (ms)	Down travel time (ms)	Down adjusted[c] time (ms)	Record quality[d]	sHV-wave velocity (ft/s)
13	8.61	10.864	10.254	10.781	10.171	VG	823
17	8.57	9.521	9.338	9.438	9.255	VG	917
21	8.54	10.010	10.254	9.927	10.171	G	850
25	8.51	13.855	12.696	13.772	12.613	F	647
29	8.47	15.198	15.686	15.115	15.603	F	552

[a]Corrected for inclination and thickness of grout.
[b]Correction of -0.061 ms as calibration factor and -0.0835 ms for travel time through grout.
[c]Correction of -0.1221 ms as calibration factor and -0.0835 ms for travel time through grout.
[d]F = Fair, G = Good, VG = Very Good.

Table D.17: Interval measurements of sHV-wave velocity in crosshole using solenoid source with first receiver in BH2 and second receiver in BH1 at the Walterboro Rest area site. Measurements were conducted in January 2010.

Depth (ft)	Corrected[a] center to center distance (ft)	Up travel time (ms)	Down travel time (ms)	Record quality[b]	sHV-wave velocity (ft/s)
13	8.81	9.705	9.461	F	920
17	8.84	8.850	9.644	F	957
21	8.85	10.071	No or poor record	F	842
25	8.87	12.634	13.000	F	692
29	8.89	14.710	15.625	F	587

[a]Corrected for inclination.
[b]F = Fair.

Table D.18: Interval measurements of sHV-wave velocity in crosshole testing using dynamic cone source with first receiver in BH1 and second receiver in BH2 at the Walterboro Rest Ares site. Measurements were conducted in June 2010.

Depth (ft)	Corrected[a] center to center distance (ft)	Travel time (ms)	Record quality[b]	sHV-wave velocity (ft/s)
2	8.81	14.709	G	599
4	8.81	12.939	VG	681
6	8.80	11.963	G	736
8	8.80	10.864	VG	810
10	8.80	11.474	G	767
11	8.80	10.38	VG	848
12	8.81	9.4	G	937
13	8.81	10.009	F	880
14	8.82	9.887	VG	892
15	8.82	10.071	G	876
16	8.83	8.911	VG	991
17	8.84	8.911	G	992
18	8.84	9.216	VG	959

[a]Corrected for inclination.
[b]F = Fair, G = Good, VG = Very Good.

Table D.19: Interval measurements of sHV-wave velocity in crosshole testing using dynamic cone source with first receiver in BH2 and second receiver in BH3 at the Walterboro Rest Area site. Measurements were conducted in June 2010.

Depth (ft)	Corrected[a] center to center distance (ft)	Travel time (ms)	Record quality[b]	sHV-wave velocity (ft/s)
2	9.01	18.066	F	499
4	9.00	14.283	G	630
6	8.99	20.874	G	431
8	8.99	11.475	G	784
9	8.99	10.987	VG	818
10	8.99	11.597	G	775
11	8.99	11.474	G	784
12	8.99	12.695	G	708
13	8.99	12.940	G	694
14	8.98	9.644	VG	931
15	8.97	10.193	VG	880
16	8.96	9.765	G	918
17	8.95	9.400	G	952
18	8.94	9.155	VG	976

[a]Corrected for inclination.
[b]F = Fair, G = Good, VG = Very Good.

Table D.20: Direct measurement of sHH-wave velocity in crosshole testing with solenoid source in BH1 and receiver in BH2 at the Walterboro Rest Area site. Measurements were conducted in January 2010.

Depth (ft)	Corrected[a] edge to edge distance (ft)	Up travel time (ms)	Up adjusted[b] time (ms)	Down travel time (ms)	Down adjusted[b] time (ms)	Record quality[c]	sHH-wave velocity (ft/s)
1	8.44	18.371	18.196	18.616	18.441	VG	461
3	8.43	15.869	15.694	15.686	15.511	VG	541
5	8.43	15.442	15.267	15.503	15.328	VG	551
7	8.42	20.020	19.845	19.287	19.112	F	433
11	8.43	11.718	11.543	11.902	11.727	G	724
13	8.44	16.235	16.060	16.785	16.610	F	517
15	8.45	14.648	14.473	10.804	10.629	F	689
17	8.46	8.789	8.614	8.484	8.309	F	1000
21	8.48	7.202	7.027	7.385	7.210	F	1116
23	8.49	12.451	12.276	12.451	12.276	VG	691
25	8.49	14.099	13.924	14.038	13.863	VG	611
27	8.51	15.747	15.572	15.198	15.023	VG	556
29	8.52	16.052	15.877	16.052	15.877	VG	536
31	8.52	16.351	16.176	16.113	15.938	VG	531
33	8.53	15.076	14.901	14.953	14.778	VG	575

[a]Corrected for inclination and thickness of grout.
[b]Correction of -0.0915 ms as calibration factor and -0.0389 ms for travel time through grout.
[c]F = Fair, G = Good, VG = Very Good.

Table D.21: Interval measurements of sHH-wave velocity in crosshole using solenoid source with first receiver in BH2 and second receiver in BH3 at the Walterboro Rest Area site. Measurements were conducted in January 2010.

Depth (ft)	Corrected[a] center to center distance (ft)	Up travel time (ms)	Down travel time (ms)	Record quality[b]	sHH-wave velocity (ft/s)
1	9.02	16.601	17.273	F	533
3	9.01	23.254	23.621	F	384
5	9.00	16.907	16.846	G	533
7	8.99	23.986	24.902	F	368
11	8.99	20.753	19.897	F	443
13	8.99	16.480	16.113	F	551
15	8.97		15.075	F	595
23	8.90	14.099	13.306	F	650
27	8.87	15.503	15.808	VG	566
29	8.85	16.235	15.991	G	549
31	8.83	16.120	16.297	G	545
33	8.80	15.686	No or poor	G	561

[a]Corrected for inclination.
[b]F = Fair, G = Good, VG = Very Good.

Table D.22: Direct measurements of sHV-wave velocity in crosshole testing with solenoid source in BH3 and receiver in BH2 at the Hollywood Ditch site. Measurements were conducted in June 2010.

Depth (ft)	Corrected[a] edge to edge distance (ft)	Up travel time (ms)	Up adjusted[b] time (ms)	Down travel time (ms)	Down adjusted[c] time (ms)	Record quality[d]	sHV-wave velocity (ft/s)
2	9.00	25.268	25.068	24.170	23.909	G	368
4	8.97	No or poor record		16.601	16.340	G	549
6	8.94	15.991	15.791	15.503	15.242	VG	576
8	8.91	17.212	17.012	16.968	16.707	G	529
10	8.89	15.137	14.937	16.236	15.975	VG	576
12	8.86	NA	NA	16.846	16.585	G	535
14	8.84	21.607	21.407	20.752	20.491	G	422
16	8.82	13.916	13.716	14.771	14.510	G	625
20	8.78	14.893	14.693	13.672	13.411	G	626
22	8.77	13.183	12.983	13.245	12.984	G	676
24	8.77	13.183	12.983	No or poor record		G	675

[a]Corrected for inclination and thickness of grout.
[b]Correction of -0.061 ms as calibration factor and -0.1389 ms for travel time through grout.
[c]Correction of -0.1221 ms as calibration factor and -0.1389 ms for travel time through grout.
[d]G = Good, VG = Very Good.

Table D.23: Direct measurements of sHV-wave velocity in crosshole testing with solenoid source in BH1 and receiver in BH2 at the Hollywood Ditch site. Measurements were conducted in June 2010.

Depth (ft)	Corrected[a] edge to edge distance (ft)	Up travel time (ms)	Up adjusted[b] time (ms)	Down travel time (ms)	Down adjusted[c] time (ms)	Record quality[d]	sHV-wave velocity (ft/s)
4	8.71	26.978	26.778	25.512	25.251	F	335
8	8.71	16.601	16.401	16.968	16.707	G	526
12	8.72	17.090	16.890	17.944	17.683	G	505
16	8.75	22.827	22.627	22.339	22.078	F	391
20	8.79	NA[d]	NA	14.771	14.510	G	606
24	8.85	14.443	14.243	14.771	14.510	G	616

[a]Corrected for inclination and thickness of grout.
[b]Correction of -0.061 ms as calibration factor and -0.1389 ms for travel time through grout.
[c]Correction of -0.1221 ms as calibration factor and -0.1389 ms for travel time through grout.
[d]F = Fair, G = Good.

Table D.24: Interval measurements of sHV-wave velocity in crosshole using solenoid source with first receiver in BH2 and second receiver in BH1 at the Hollywood Ditch site. Measurements were conducted in June 2010.

Depth (ft)	Corrected[a] center to center distance (ft)	Up travel time (ms)	Down travel time (ms)	Record quality[b]	sHV-wave velocity (ft/s)
2	9.07	27.710	25.268	F	343
4	9.08	No or poor record	16.724	F	543
12	9.10	20.875	20.630	F	438
14	9.11	21.606	17.822	F	466
16	9.12	26.733	18.066	F	423

[a]Corrected for inclination.
[b]F = Fair.

Table D.25: Interval measurements of sHV-wave velocity in crosshole testing using dynamic cone source with first receiver in BH3 and second receiver in BH2 at the Hollywood Ditch site. Measurements were conducted in June 2010.

Depth (ft)	Corrected[a] center to center distance (ft)	Travel time (ms)	Record quality[b]	sHV-wave velocity (ft/s)
2	9.37	14.892	F	629
4	9.34	9.888	G	948
6	9.32	21.729	G	430
8	9.29	16.235	E	574
10	9.26	15.259	E	609
12	9.24	16.968	E	549
14	9.22	20.630	E	453
16	9.19	20.386	E	460

[a]Corrected for inclination.

[b]F = Fair, G = Good, E = Excellent.

Table D.26: Direct measurement of sHH-wave velocity in crosshole testing with solenoid source in BH3 and receiver in BH2 at the Hollywood Ditch site. Measurements were conducted in June 2010.

Depth (ft)	Corrected[a] edge to edge distance (ft)	Up travel time (ms)	Up adjusted[b] time (ms)	Down travel time (ms)	Down adjusted[b] time (ms)	Record quality[c]	sHH-wave velocity (ft/s)
2	8.997	19.775	19.545	21.240	21.009	F	444
4	8.969	20.508	20.278	18.676	18.446	F	464
6	8.941	14.892	14.662	14.770	14.540	G	612
8	8.914	16.601	16.371	15.991	15.761	F	555
10	8.888	22.094	21.864	22.705	22.475	VG	401
12	8.865	21.118	20.888	22.217	21.987	VG	414
14	8.843	19.165	18.935	19.409	19.179	G	464
16	8.819	18.188	17.958	19.043	18.813	VG	480
18	8.794	18.005	17.775	17.456	17.226	VG	503
20	8.778	14.587	14.357	No or poor record		F	611
22	8.771	12.451	12.221	12.268	12.038	F/G	723
24	8.766	12.939	12.709	13.732	13.502	G	669

[a]Corrected for inclination and thickness of grout.
[b]Correction of -0.0915 ms as calibration factor and -0.1389 ms for travel time through grout.
[c]F = Fair, G = Good, VG = Very Good.

Table D.27: Interval measurements of sHH-wave velocity in crosshole using solenoid source with first receiver in BH2 and second receiver in BH1 at the Hollywood Ditch site. Measurements were conducted in June 2010.

Depth (ft)	Corrected[a] center to center distance (ft)	Up travel time (ms)	Down travel time (ms)	Record quality[b]	sHH-wave velocity (ft/s)
10	9.09	22.339	22.461	F	406
12	9.10	21.973	22.217	F	412
16	9.12	20.264	19.897	F	454
18	9.14	No or poor record	20.752	F	441

[a]Corrected for inclination.
[b]F = Fair.

Table D.28: Direct measurements of sHV-wave velocity in crosshole testing with solenoid source in BH1 and receiver in BH2 at the Sampit site. Measurements were conducted in June 2010.

Depth (ft)	Corrected[a] edge to edge distance (ft)	Up travel time (ms)	Up adjusted[b] time (ms)	Down travel time (ms)	Down adjusted[c] time (ms)	Record quality[d]	sHV-wave velocity (ft/s)
2	8.54	19.043	18.668	19.531	19.095	F/G	452
4	8.54	22.583	22.208	21.850	21.414	F/G	392
6	8.54	15.381	15.006	15.503	15.067	F	568
8	8.53	14.282	13.907	15.137	14.701	G	597
10	8.53	10.254	9.879	10.681	10.245	G	848
12	8.51	10.132	9.757	10.376	9.940	G	864
14	8.50	10.010	9.635	10.498	10.062	G	863
16	8.49	9.888	9.513	10.620	10.184	G	863
18	8.49	10.742	10.367	11.474	11.038	F/G	794
20	8.50	13.794	13.419	14.282	13.846	G	623
22	8.50	14.282	13.907	14.526	14.090	G	607
24	8.50	15.991	15.616	15.625	15.189	G	552
26	8.51	15.259	14.884	15.869	15.433	G	562
28	8.52	14.404	14.029	15.015	14.579	G	596
30	8.54	19.165	18.790	19.775	19.339	G	448
32	8.56	12.695	12.320	12.817	12.381	G	693
34	8.57	11.230	10.855	12.207	11.771	G	759

[a]Corrected for inclination and thickness of grout.
[b]Correction of -0.061 ms as calibration factor and -0.3139 ms for travel time through grout.
[c]Correction of -0.1221 ms as calibration factor and -0.3139 ms for travel time through grout.
[d]F = Fair, G = Good.

Table D.29 Interval measurements of sHV-wave velocity in crosshole using solenoid source with first receiver in BH2 and second receiver in BH3 at the Sampit site. Measurements were conducted in Jun. 2010.

Depth (ft)	Corrected[a] center to center distance (ft)	Up travel time (ms)	Down travel time (ms)	Record quality[b]	sHV-wave velocity (ft/s)
2	8.97	21.973	23.560	F	395
6	8.97	13.428	13.672	F	662
8	8.97	12.451	12.756	F/G	712
10	8.96	12.146	12.329	F/G	733
12	8.96	12.207	12.329	F	730
14	8.96	12.329	12.085	F	734
16	8.94	11.352	15.259	F	687
18	8.93	15.747	14.527	F	591
20	8.92	11.108	9.924	F	851
34	8.89	22.828	17.700	F	442

[a]Corrected for inclination.
[b]F = Fair, G = Good.

Table D.30 Interval measurements of sHV-wave velocity in crosshole testing using dynamic cone source with first receiver in BH1 and second receiver in BH2 at the Sampit site. Measurements were conducted in June 2010.

Depth (ft)	Corrected[a] center to center distance (ft)	Travel time (ms)	Record quality[b]	sHV-wave velocity (ft/s)
2	8.91	18.493	G	482
4	8.92	21.728	G	410
6	8.92	13.183	G	676
8	8.91	13.751	VG	648
9	8.90	13.000	E	685
10	8.90	11.352	E	784
11	8.90	10.132	E	878
12	8.89	9.888	E	899
13	8.90	10.132	E	878
14	8.87	9.583	E	926
15	8.90	9.766	E	911
16	8.87	10.315	E	860
17	8.90	10.865	E	819
18	8.87	11.841	E	749

[a]Corrected for inclination.
[b]G = Good, VG = Very Good, E = Excellent.

Table D.31 Direct measurements of sHH-wave velocity in crosshole testing with solenoid source in BH1 and receiver in BH2 at the Sampit site. Measurements were conducted in June 2010.

Depth (ft)	Corrected[a] edge to edge distance (ft)	Up travel time (ms)	Up adjusted[b] time (ms)	Down travel time (ms)	Down adjusted[b] time (ms)	Record quality[c]	sHH-wave velocity (ft/s)
2	8.54	16.968	16.563	17.090	16.685	F	508
4	8.54	18.433	18.028	19.898	19.493	F	452
6	8.54	No or poor record		18.433	18.028	F	474
8	8.53	17.213	16.807	17.334	16.928	G	501
10	8.53	13.672	13.266	13.916	13.511	G	628
12	8.51	11.719	11.313	11.597	11.191	G	744
14	8.50	11.231	10.825	11.108	10.702	G	776
16	8.49	13.184	12.778	12.940	12.534	G	661
18	8.49	11.963	11.557	12.329	11.923	G	712
20	8.50	12.085	11.679	12.940	12.534	G/F	692
22	8.50	14.160	13.754	16.113	15.707	G/F	572
24	8.50	15.869	15.464	18.311	17.906	G/F	507
26	8.51	16.968	16.563	17.945	17.539	G/F	494
28	8.52	16.968	16.562	17.212	16.806	G	505
30	8.54	17.334	16.929	17.700	17.295	G	494
32	8.56	15.381	14.976	15.381	14.976	G	565
34	8.57	16.968	16.563	17.090	16.685	F	508

[a]Corrected for inclination and thickness of grout.
[b]Correction of -0.0915 ms as calibration factor and -0.3139 ms for travel time through grout.
[d]F = Fair, G = Good.

Table D.32 Interval measurements of sHH-wave velocity in crosshole using solenoid source with first receiver in BH2 and second receiver in BH3 at the Sampit site. Measurements were conducted in June 2010.

Depth (ft)	Corrected[a] center to center distance (ft)	Up travel time (ms)	Down travel time (ms)	Record quality[b]	sHH-wave velocity (ft/s)
8	8.97	17.455	17.822	F	509
10	8.96	14.893	15.015	F	599
16	8.94	13.794	12.085	G	694
24	8.89	18.555	16.235	G/F	514
26	8.88	18.554	18.188	F	483
28	8.87	17.700	17.578	F	503
30	8.85	17.334	17.456	G/F	509
32	8.83	19.653	20.020	F	445
34	8.82	18.555	16.235	G/F	514

[a]Corrected for inclination.
[b]F = Fair, G = Good.

Table D.33 Direct measurements of sHV-wave velocity in crosshole testing with solenoid source in BH3 and receiver in BH2 at the Four Hole Swamp site. Measurements were conducted in June 2010.

Depth (ft)	Corrected[a] edge to edge distance (ft)	Up travel time (ms)	Up adjusted[b] time (ms)	Down travel time (ms)	Down adjusted[c] time (ms)	Record quality[d]	sHV-wave velocity (ft/s)
6	8.81	21.240	21.095	11.718	11.513	F	585
8	8.82	No or poor record		15.503	15.298	F	567
10	8.83	20.386	20.241	20.874	20.669	G	428
12	8.84	20.020	19.875	15.381	15.175	G	509
14	8.84	17.456	17.311	17.212	17.007	G	511
16	8.85	16.052	15.907	22.522	22.317	F	473
18	8.86	4.822	4.677	5.188	4.983	F	1894

[a]Corrected for inclination and thickness of grout.
[b]Correction of -0.061 ms as calibration factor and -0.0835 ms for travel time through grout.
[c]Correction of -0.1221 ms as calibration factor and -0.0835 ms for travel time through grout.
[d]F = Fair, G = Good.

Table D.34 Interval measurements of sHV-wave velocity in crosshole testing using dynamic cone source with first receiver in BH1 and second receiver in BH2 at the Four Hole Swamp site. Measurements were conducted in June 2010.

Depth (ft)	Corrected[a] center to center distance (ft)	Travel time (ms)	Record quality[b]	sHV-wave velocity (ft/s)
5	9.18	11.719	G	784
6	9.18	11.108	G	826
7	9.17	11.597	G	791
8	9.17	10.681	VG	858
9	9.16	11.536	G	794
10	9.15	20.874	G	438
11	9.14	20.996	VG	435
13	9.11	19.043	VG	478
14	9.09	16.968	VG	536
15	9.07	25.391	G	357

[a]Corrected for inclination.
[b]G = Good, VG = Very Good.

Table D.35 Interval measurements of sHV-wave velocity in crosshole testing using dynamic cone source with first receiver in BH3 and second receiver in BH2 at the Four Hole Swamp site. Measurements were conducted in June 2010.

Depth (ft)	Corrected[a] center to center distance (ft)	Travel time (ms)	Record quality[b]	sHV-wave velocity (ft/s)
2	9.11	10.376	F	878
4	9.15	11.352	F	806
7	9.19	11.475	F	801
8	9.20	10.375	G	887
9	9.20	22.949	F	401
10	9.21	17.578	F	524
11	9.21	20.038	G	460
12	9.21	16.968	G	543
13	9.22	19.531	VG	472
14	9.22	18.066	G	510
15	9.22	15.381	VG	600
16	9.23	5.798	G	1592

[a]Corrected for inclination.
[b]F = Fair, G = Good, VG = Very Good.

Table D.36 Direct measurement of sHH-wave velocity in crosshole testing with solenoid source in BH3 and receiver in BH2 at the Four Hole Swamp site. Measurements were conducted in June 2010.

Depth (ft)	Corrected[a] edge to edge distance (ft)	Up travel time (ms)	Up adjusted[b] time (ms)	Down travel time (ms)	Down adjusted[b] time (ms)	Record quality[c]	sHH-wave velocity (ft/s)
6	8.81	10.010	9.835	10.742	10.567	F	865
8	8.82	14.282	14.107	14.404	14.229	G	623
10	8.83	19.653	19.478	18.738	18.563	G	465
12	8.84	20.386	20.211	18.738	18.563	F	457
14	8.84	20.630	20.455	20.569	20.394	G	433
16	8.85	14.831	14.656	14.648	14.473	G	608

[a]Corrected for inclination and thickness of grout.
[b]Correction of -0.0915 ms as calibration factor and -0.0835 ms for travel time through grout.
[c]F = Fair, G = Good.

APPENDIX E

SUMMARY OF SCPT SHEAR WAVE VELOCITIES FROM THE EIGHT SITES IN THE SOUTH CAROLINA COASTAL PLAIN

Table E.1: Measurements of sVH-wave velocity using direct ray path from seismic cone SC1 at the CREC site modified from Boller (2008). Measurements were conducted in March 2007.

Depth to top geophone (ft)	Depth to bottom geophone (ft)	Average measurement depth (ft)	Average sVH-wave velocity (ft/sec)	Record quality[a]
0	4.35	6.0	596	P
4.35	7.57	9.2	613	P
7.57	10.78	12.4	621	F
10.78	13.98	15.6	571	P
13.98	17.19	18.8	615	F
17.19	20.38	22.0	747	P
20.38	23.58	25.2	1418	F
23.58	26.78	28.4	1448	F
26.78	29.98	31.6	1292	F
29.98	30.04	34.8	1415	F
30.04	34.35	38.1	1827	F

[a]P = Poor, F = Fair.

Table E.2: Measurements of sVH-wave velocity using direct ray path from seismic cone SC3 at the CREC site modified from Boller (2008). Measurements were conducted in March 2007.

Depth to top geophone (ft)	Depth to bottom geophone (ft)	Average measurement depth (ft)	Average sVH-wave velocity (ft/sec)	Record quality[a]
0	4.23	2.12	532	P
4.23	7.45	5.84	605	P
7.45	10.66	9.06	520	P
10.66	13.88	12.27	619	F
13.88	17.06	15.47	468	F
17.06	20.28	18.67	1428	G
20.28	23.48	21.88	1354	G
23.48	26.49	24.99	1660	G
26.49	30.04	28.27	2216	F
30.04	33.24	31.64	1302	G

[a]P = Poor, F = Fair, G = Good.

Table E.3: Measurements of sVH-wave velocity from using direct ray path seismic cone SC6 at the CREC site modified from Boller (2008). Measurements were conducted in March 2007.

Depth to top geophone (ft)	Depth to bottom geophone (ft)	Average measurement depth (ft)	Average sVH-wave velocity (ft/sec)	Record quality[a]
0	1.36	0.68	505	P
1.36	4.59	2.98	578	P
4.59	7.82	6.21	529	P
7.82	11.05	9.44	616	F
11.05	14.28	12.67	512	F
14.28	17.50	15.89	582	F
17.50	20.72	19.11	918	G
20.72	23.93	22.33	2038	G
23.93	27.10	25.52	2231	G
27.10	30.32	28.71	1804	G
30.32	33.54	31.93	1425	P
33.54	36.76	35.15	1373	G

[a]P = Poor, F = Fair, G = Good.

Table E.4: Measurements of shear sVH-velocity from seismic cone SC1 at the Hobcaw Borrow Pit site adapted from Boller (2008). Measurements were conducted in July 2007.

Depth to top geophone (ft)	Depth to bottom geophone (ft)	Average measurement depth (ft)	Average sVH-wave velocity (ft/sec)	Record quality[a]
1.1	4.4	2.7	357	F
4.4	7.6	6.0	802	G
7.6	10.9	9.3	602	G
10.9	14.3	12.6	700	G
14.3	17.5	15.8	756	G
17.5	20.8	19.2	799	F
20.8	24.1	22.4	747	G
24.1	27.4	25.8	616	G
27.4	30.8	29.2	559	G
30.8	34.2	32.5	644	VG
34.2	37.5	35.8	746	VG
37.5	40.8	39.1	827	G
40.8	44.8	42.4	641	G
44.8	47.4	45.7	995	G
47.4	50.7	49.1	1037	E

[a]F = Fair, G = Good, VG = Very Good, E = Excellent .

Table E.5: Measurements of sVH-wave velocity from seismic cone SC2 at the Hobcaw Borrow Pit site adapted from Boller (2008). Measurements were conducted in July 2007.

Depth to top geophone (ft)	Depth to bottom geophone (ft)	Average measurement depth (ft)	Average sVH-wave velocity (ft/sec)	Record quality[a]
4.0	7.4	5.8	683	G
7.4	10.8	9.2	669	G
10.8	14.1	12.5	703	VG
14.1	17.4	15.8	797	VG
17.4	20.7	19.1	792	VG
20.7	24.1	22.4	555	F
24.1	27.4	25.8	670	G
27.4	30.7	29.1	614	VG
30.7	34.0	32.4	801	G
34.0	37.4	35.7	781	G
37.4	39.4	38.4	838	G

[a]F = Fair, G = Good, VG = Very Good.

Table E.6: Measurements of sVH-wave velocity from seismic cone SC3 at the Hobcaw Borrow Pit site adapted from Boller (2008). Measurements were conducted in July 2007.

Depth to top geophone (ft)	Depth to bottom geophone (ft)	Average measurement depth (ft)	Average sVH-wave velocity (ft/sec)	Record quality[a]
1.3	4.6	2.9	858	F
4.6	7.8	6.2	769	F
7.8	11.2	9.6	621	G
11.2	14.6	12.9	718	F
14.6	17.9	16.2	878	F
17.9	21.2	19.5	660	G
21.2	24.5	23.2	639	G
24.5	27.8	26.2	502	G
27.8	31.1	29.5	553	G
31.1	34.4	32.8	721	G
34.4	37.7	36.1	704	VG
37.7	41.2	39.4	844	G
41.2	42.1	40.4	905	G

[a]F = Fair, G = Good, VG = Very Good.

Table E.7: Measurements of sVH-wave velocity from seismic cone SC1 at the Walterboro Rest Area site adapted from Geiger (2010). Measurements were conducted in June 2009.

Depth to top geophone (ft)	Depth to bottom geophone (ft)	Average measurement depth (ft)	Average sVH-wave velocity (ft/sec)	Standard deviation[a]	Record quality[b]
0.75	4.03	2.39	300	16	VG
4.75	8.03	6.39	511	62	G
7.75	11.03	9.39	546	52	VG
10.75	14.03	12.39	572	37	VG
13.75	17.03	15.39	620	50	VG
16.75	20.03	18.39	596	78	G
19.75	23.03	21.39	695	99	G
23.75	27.03	25.39	580	54	VG
26.75	30.03	28.39	629	67	G
29.75	33.03	31.39	616	84	G
32.75	36.03	34.39	604	49	VG
35.75	39.03	37.39	634	137	F
38.75	42.03	40.39	598	82	G
41.75	45.03	43.39	630	57	VG
44.75	48.03	46.39	534	39	VG
48.75	52.03	50.39	590	25	E
51.75	55.03	53.39	715	168	F to P
61.75	65.03	63.39	754	109	F to P
67.75	71.03	69.39	997	236	F to P

[a]Standard deviation based on four estimates of velocity determined from first crossovers and first peaks for two hits with opposite polarity.
[b]P = Poor, F = Fair, G = Good, VG = Very Good, E = Excellent.

Table E.8: Measurements of sVH-wave velocity from seismic cone SC2 at the Walterboro Rest Area site adapted from Geiger (2010). Measurements were conducted in June 2009.

Depth to top geophone (ft)	Depth to bottom geophone (ft)	Average measurement depth (ft)	Average sVH-wave velocity (ft/sec)	Standard deviation[a]	Record quality[b]
1.75	5.03	3.39	331	39	G
4.75	8.03	6.39	624	31	VG
7.75	11.03	9.39	647	138	F
10.75	14.03	12.39	471	109	F
14.75	18.03	16.39	479	70	G
17.75	21.03	19.39	586	124	F
20.75	24.03	22.39	581	84	G
23.75	27.03	25.39	512	80	F
26.75	30.03	28.39	754	35	E
30.75	34.03	32.39	665	93	G
33.75	37.03	35.39	717	49	VG
35.75	39.03	37.39	764	18	E

[a]Standard deviation based on four estimates of velocity determined from first crossovers and first peaks for two hits with opposite polarity.
[b]F = Fair, G = Good, VG = Very Good, E = Excellent.

Table E.9: Measurements of sVH-wave velocity from seismic cone SC3 at the Walterboro Rest Area site adapted from Geiger (2010). Measurements were conducted in June 2009.

Depth to top geophone (ft)	Depth to bottom geophone (ft)	Average measurement depth (ft)	Average sVH-wave velocity (ft/sec)	Standard deviation[a]	Record quality[b]
1.75	5.03	3.39	360	80	F
7.75	11.03	9.39	635	37	VG
10.75	14.03	12.39	554	34	VG
14.75	18.03	16.39	592	79	G
17.75	21.03	19.39	719	71	VG
20.75	24.03	22.39	767	188	F
24.75	28.03	26.39	740	192	F
27.75	31.03	29.39	775	333	F to P
30.75	34.03	32.39	669	163	F
33.75	37.03	35.39	846	319	F to P
35.75	39.03	37.39	806	241	F to P

[a]Standard deviation based on four estimates of velocity determined from first crossovers and first peaks for two hits with opposite polarity.
[b]P = Poor, F = Fair, G = Good, VG = Very Good.

Table E.10: Measurements of sVH-wave velocity from seismic cone at the Hobcaw Beach Ridge site. Measurements were conducted in March 2012.

Depth to top geophone (ft)	Depth to bottom geophone (ft)	Average measurement depth (ft)	Average sVH-wave velocity (ft/sec)	Record quality[a]
0.00	4.35	2.18	525	G to VG
4.35	8.35	6.35	838	VG to E
8.35	10.65	9.50	668	E
10.65	13.85	12.25	632	VG to E
13.85	17.05	15.45	442	VG to E
17.05	20.25	18.65	398	G to VG
20.25	23.75	22.00	626	G to VG
23.75	26.85	25.30	926	G to VG
26.85	30.05	28.45	661	F to G
30.05	33.45	31.75	885	F to G
33.45	35.15	34.30	833	VG

[a]F = Fair, G = Good, VG = Very Good, E = Excellent.

Table E.11: Measurements of sVH-wave velocity from seismic cone SC1 at the Walterboro Lowcountry site adapted from Geiger (2010). Measurements were conducted in June 2009.

Depth to top geophone (ft)	Depth to bottom geophone (ft)	Average measurement depth (ft)	Average sVH-wave velocity (ft/sec)	Standard deviation[a]	Record quality[b]
0.75	4.03	2.39	237	28	F
4.75	8.03	6.39	568	64	G
7.75	11.03	9.39	576	23	E
10.75	14.03	12.39	721	273	F
14.75	18.03	16.39	757	165	F
17.75	21.03	19.39	766	175	F
20.75	24.03	22.39	810	165	F
23.75	27.03	25.39	719	161	F
26.75	30.03	28.39	612	57	VG
30.75	34.03	32.39	592	78	G
33.75	37.03	35.39	652	56	VG
36.75	40.03	38.39	671	27	E
40.75	44.03	42.39	633	38	VG
43.75	47.03	45.39	630	42	VG
46.75	50.03	48.39	619	50	VG
49.75	53.03	51.39	556	39	VG
52.75	56.03	54.39	613	34	VG
56.75	60.03	58.39	643	64	G
59.75	63.03	61.39	620	74	G
62.75	66.03	64.39	642	55	VG
65.75	69.03	67.39	650	99	F to G

[a]Standard deviation based on four estimates of velocity determined from first crossovers and first peaks for two hits with opposite polarity.
[b]F = Fair, G = Good, VG = Very Good, E = Excellent.

Table E.12: Measurements of sVH-wave velocity from seismic cone SC2 at the Walterboro Lowcountry site adapted from Geiger (2010). Measurements were conducted in June 2009.

Depth to Top geophone (ft)	Depth to bottom geophone (ft)	Average measurement depth (ft)	Average sVH-wave velocity (ft/sec)	Standard deviation[a]	Record quality[b]
4.75	8.03	6.39	660	47	VG
7.75	11.03	9.39	687	93	G
10.75	14.03	12.39	754	51	VG
13.75	17.03	15.39	797	93	G
16.75	20.03	18.39	747	33	E
20.75	24.03	22.39	683	41	VG
23.75	27.03	25.39	691	44	VG
26.75	30.03	28.39	663	47	VG

[a]Standard deviation based on four estimates of velocity determined from first crossovers and first peaks for two hits with opposite polarity.
[b]G = Good, VG = Very Good, E = Excellent.

Table E.13: Measurements of sVH-wave velocity from seismic cone SC3 at the Walterboro Lowcountry site adapted from Geiger (2010). Measurements were conducted in June 2009.

Depth to top geophone (ft)	Depth to bottom geophone (ft)	Average measurement depth (ft)	Average sVH-wave velocity (ft/sec)	Standard deviation[a]	Record quality[b]
1.75	5.03	3.39	397	104	F
4.75	8.03	6.39	519	36	VG
7.75	11.03	9.39	642	57	VG
10.75	14.03	12.39	689	25	E
14.75	18.03	16.39	671	33	E
17.75	21.03	19.39	602	48	VG
20.75	24.03	22.39	608	53	VG
23.75	27.03	25.39	558	48	VG
26.75	30.03	28.39	657	94	G

[a]Standard deviation based on four estimates of velocity determined from first crossovers and first peaks for two hits with opposite polarity.
[b]F = Fair, G = Good, VG = Very Good, E = Excellent.

Table E.14: Measurements of sVH-wave velocity from seismic cone SC1 at the Hollywood Ditch site. Measurements were conducted in July 2007.

Depth to top geophone (ft)	Depth to bottom geophone (ft)	Average measurement depth (ft)	Average sVH-wave velocity (ft/sec)	Record quality[a]
1.46	4.73	3.10	1520	F
4.72	7.99	6.36	2130	P
7.98	11.25	9.62	494	VG
11.24	14.51	12.88	506	VG
14.50	17.77	16.14	506	VG
17.76	21.03	19.40	587	G
21.02	24.29	22.66	728	G to F
24.28	27.55	25.92	634	VG to G
27.54	30.81	29.17	670	VG
29.33	32.60	30.97	809	VG

[a]P = Poor, F = Fair, G = Good, VG = Very Good.

Table E.15: Measurements of sVH-wave velocity from seismic cone SC2 at the Hollywood Ditch site. Measurements were conducted in July 2007.

Depth to top geophone (ft)	Depth to bottom geophone (ft)	Average measurement depth (ft)	Average sVH-wave velocity (ft/sec)	Record quality[a]
1.42	4.69	3.06	1394	P
4.68	7.95	6.32	1156	F
7.93	11.20	9.57	499	G
11.19	14.46	12.83	503	G
14.44	17.71	16.08	524	G
17.69	20.96	19.33	533	G
20.94	24.21	22.58	798	G
24.19	27.46	25.83	605	VG to E
27.44	30.71	29.08	678	VG to E
30.69	33.96	32.33	736	VG to E
33.94	37.21	35.58	838	E
37.19	40.46	38.83	1028	V
40.44	43.71	42.08	754	E
43.69	46.96	45.33	769	VG to E
46.94	50.21	48.58	1097	VG to E
50.19	53.46	51.83	971	VG to E
53.44	56.71	55.08	988	VG to E
56.69	59.96	58.33	972	E

[a]P = Poor, F = Fair, G = Good, VG = Very Good, E = Excellent.

Table E.16: Measurements of sVH-wave velocity from seismic cone SC3 at the Hollywood Ditch site. Measurements were conducted in July 2007.

Depth to top geophone (ft)	Depth to bottom geophone (ft)	Average measurement depth (ft)	Average sVH-wave velocity (ft/sec)	Record quality[a]
1.73	5.00	3.37	533	F
4.99	8.26	6.63	568	F
8.26	11.53	9.90	571	G
11.51	14.78	13.15	542	VG
14.77	18.04	16.41	494	VG
18.03	21.30	19.67	569	VG
21.29	24.56	22.93	823	G
24.55	27.82	26.19	724	VG
27.80	31.07	29.44	618	VG
31.05	34.32	32.69	759	VG
34.31	37.58	35.95	823	VG
37.56	40.83	39.20	895	VG
40.82	44.09	42.46	980	VG
44.07	47.34	45.71	1064	VG
47.32	50.59	48.96	1110	VG
50.58	53.85	52.22	955	VG
53.82	57.09	55.46	953	VG
57.07	60.34	58.71	961	VG
58.98	62.25	60.62	933	G

[a]F = Fair, G = Good, V = Very Good.

Table E.17: Measurements of sVH-wave velocity from seismic cone SC1 at the Sampit site. Measurements were conducted in July 2007.

Depth to top geophone (ft)	Depth to bottom geophone (ft)	Average measurement Depth (ft)	Average sVH-wave velocity (ft/sec)	Record quality[a]
4.1	7.3	5.7	1387	G
7.5	10.8	9.1	967	VG
10.9	14.2	12.6	964	G
13.8	17.0	15.4	786	VG
17.3	20.6	18.9	840	G
20.6	23.9	22.2	574	VG
23.9	27.1	25.5	453	VG
27.2	30.5	28.9	480	VG
30.5	33.8	32.2	574	VG
34.0	37.2	35.6	518	VG
37.1	40.4	38.8	508	VG
40.4	43.7	42.0	686	VG
43.7	46.9	45.3	889	E
47.1	50.3	48.7	963	G
50.3	53.5	51.9	915	G

[a]G = Good, V = Very Good, E = Excellent.

Table E.18: Measurements of sVH-wave velocity from seismic cone SC2 at the Sampit site. Measurements were conducted in July 2007.

Depth to top geophone (ft)	Depth to bottom geophone (ft)	Average measurement depth (ft)	Average sVH-wave velocity (ft/sec)	Record quality[a]
4.4	7.6	6.0	816	F
7.6	10.9	9.3	990	VG
10.9	14.2	12.5	677	G
14.2	17.5	15.9	697	VG
17.5	20.8	19.1	757	G
20.9	24.1	22.5	606	G
24.2	27.4	25.8	475	G
27.5	30.7	29.1	543	G
30.8	34.7	32.8	573	G
34.0	37.3	35.7	484	G
37.4	40.7	39.0	493	G
40.7	43.9	42.3	563	G
44.0	47.3	45.6	825	G
47.3	50.6	49.0	1071	G

[a]F = Fair, G = Good, V = Very Good.

Table E.19: Measurements of sVH-wave velocity from seismic cone SC3 at the Sampit site. Measurements were conducted in July 2007.

Depth to top geophone (ft)	Depth to bottom geophone (ft)	Average measurement depth (ft)	Average sVH-wave velocity (ft/sec)	Record quality[a]
1.0	4.3	2.7	424	F
4.2	7.5	5.9	1260	F
7.7	10.9	9.3	744	G
11.0	14.2	12.6	888	G
14.3	17.6	15.9	998	G
17.7	20.9	19.3	852	G
21.0	24.3	22.6	810	G
24.3	27.5	25.9	753	G
27.6	30.9	29.2	510	G
30.9	34.1	32.5	639	VG
34.2	37.5	35.8	610	VG
37.5	40.7	39.1	513	VG
40.8	44.0	42.4	487	G
44.1	47.4	45.7	550	VG
47.5	50.7	49.1	730	E
50.2	53.5	51.9	809	E

[a]F = Fair, G = Good, VG = Very Good, E = Excellent.

Table E.20: Measurements of sVH-wave velocity from seismic cone SC1 at the Four Hole Swamp site. Measurements were conducted in December 2007.

Depth to top geophone (ft)	Depth to bottom geophone (ft)	Average measurement depth (ft)	Average sVH-wave velocity (ft/sec)	Record quality[a]
0.6	3.8	2.2	1170	F
7.2	10.5	8.8	485	VG
10.6	13.9	12.3	544	E
15.8	19.1	17.4	1922	VG
20.6	23.9	22.2	1987	E

[a]F = Fair, VG = Very Good, E = Excellent.

Table E.21: Measurements of sVH-wave velocity from seismic cone SC2 at the Four Hole Swamp site. Measurements were conducted in December 2007.

Depth to top geophone (ft)	Depth to bottom geophone (ft)	Average measurement depth (ft)	Average sVH-wave velocity (ft/sec)	Record quality[a]
0.6	3.9	2.2	1352[b]	F
6.6	9.9	8.3	654	F
10.7	14.0	12.3	609	F
15.8	19.1	17.4	1896	F

[a]F = Fair.
[b]Records suggest at least a portion of the plank source was below the ground surface elevation at the cone hole.

Table E.22: Measurements of sVH-wave velocity from seismic cone SC3 at the Four Hole Swamp site. Measurements were conducted in December 2007.

Depth to top geophone (ft)	Depth to bottom geophone (ft)	Average measurement depth (ft)	Average sVH-wave velocity (ft/sec)	Record quality[a]
3.7	7.9	3.7	1234	F
8.2	11.5	9.8	593	G
12.8	16.1	14.4	799	G
17.1	20.4	18.8	2489	F

[a]F = Fair, G = Good.

APPENDIX F

LIQUEFACTION ASSESSMENT OF THE EIGHT SITES IN THE SOUTH CAROLINA COASTAL PLAIN

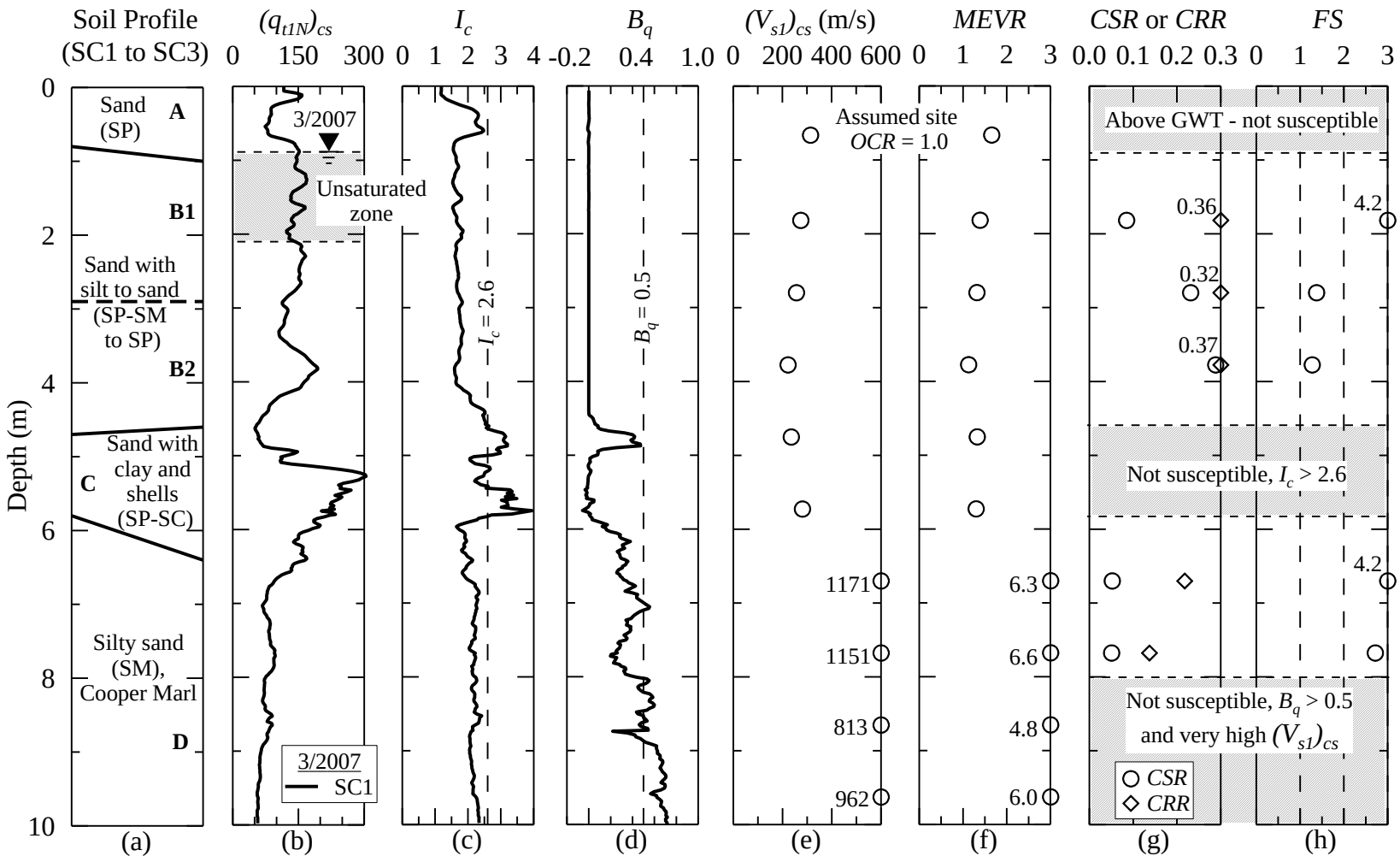

Figure F.1: Liquefaction assessment of the CREC site based on seismic cone SC1 data reported in Boller (2008) and general CPT-based procedure recommended by Youd et al. (2001).

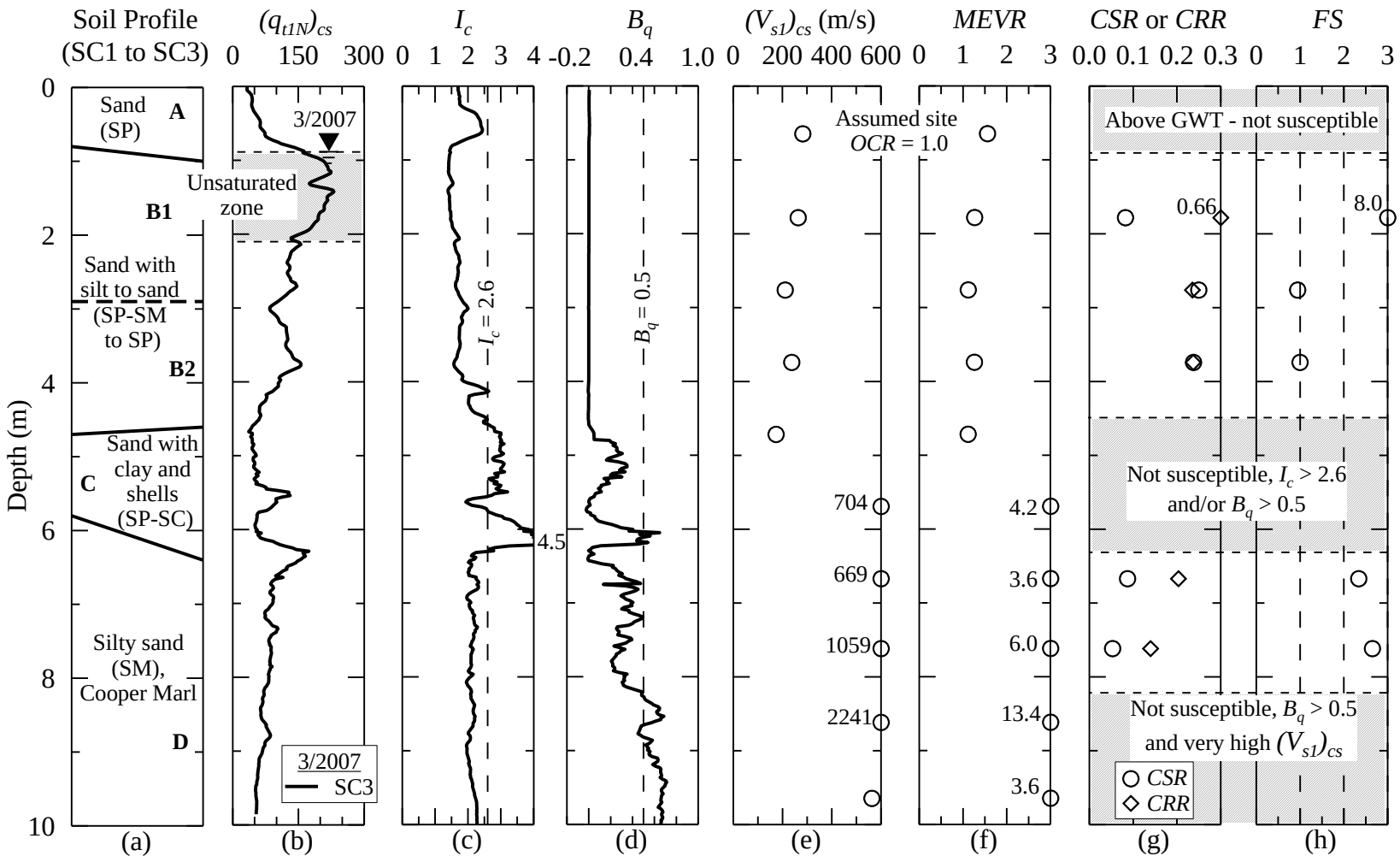

Figure F.2: Liquefaction assessment of the CREC site based on seismic cone SC3 data reported in Boller (2008) and general CPT-based procedure recommended by Youd et al. (2001).

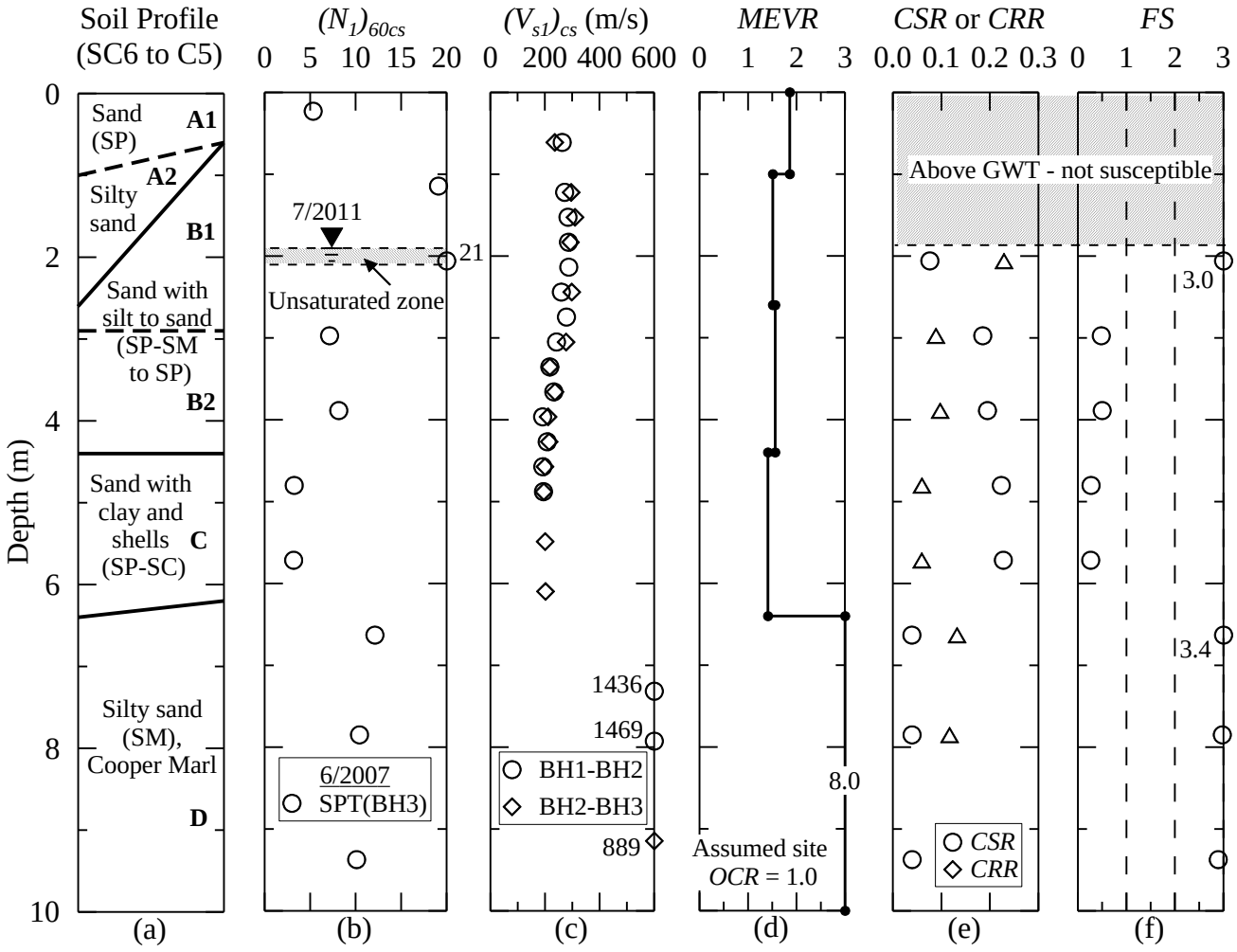

Figure F.3: Liquefaction assessment of the CREC site based on SPT data reported in Boller (2008) and general SPT-based procedure recommended by Youd et al. (2001).

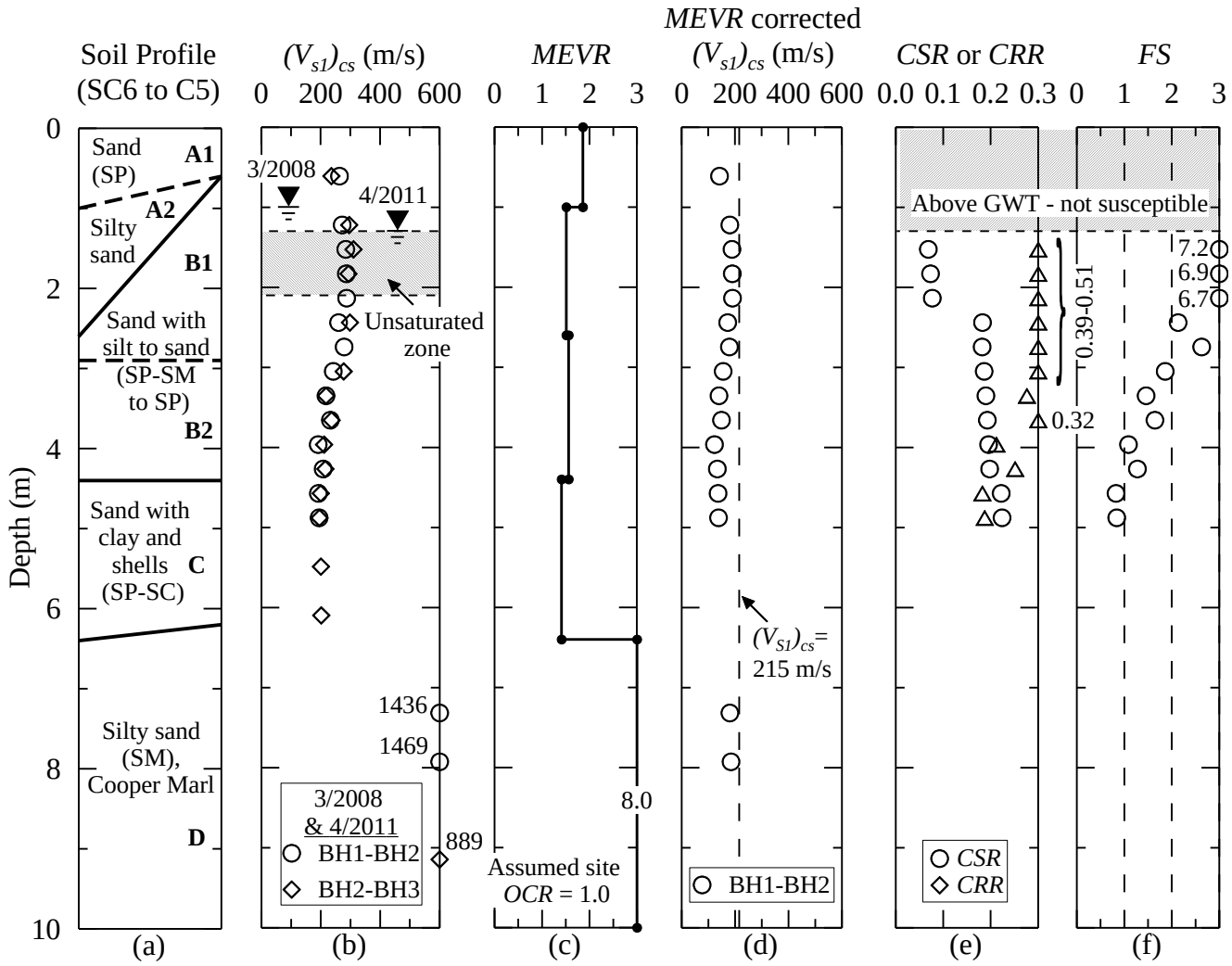

Figure F.4: Liquefaction assessment of the CREC site based on crosshole profile BH1-BH2 and general V_S-based procedure recommended by Youd et al. (2001).

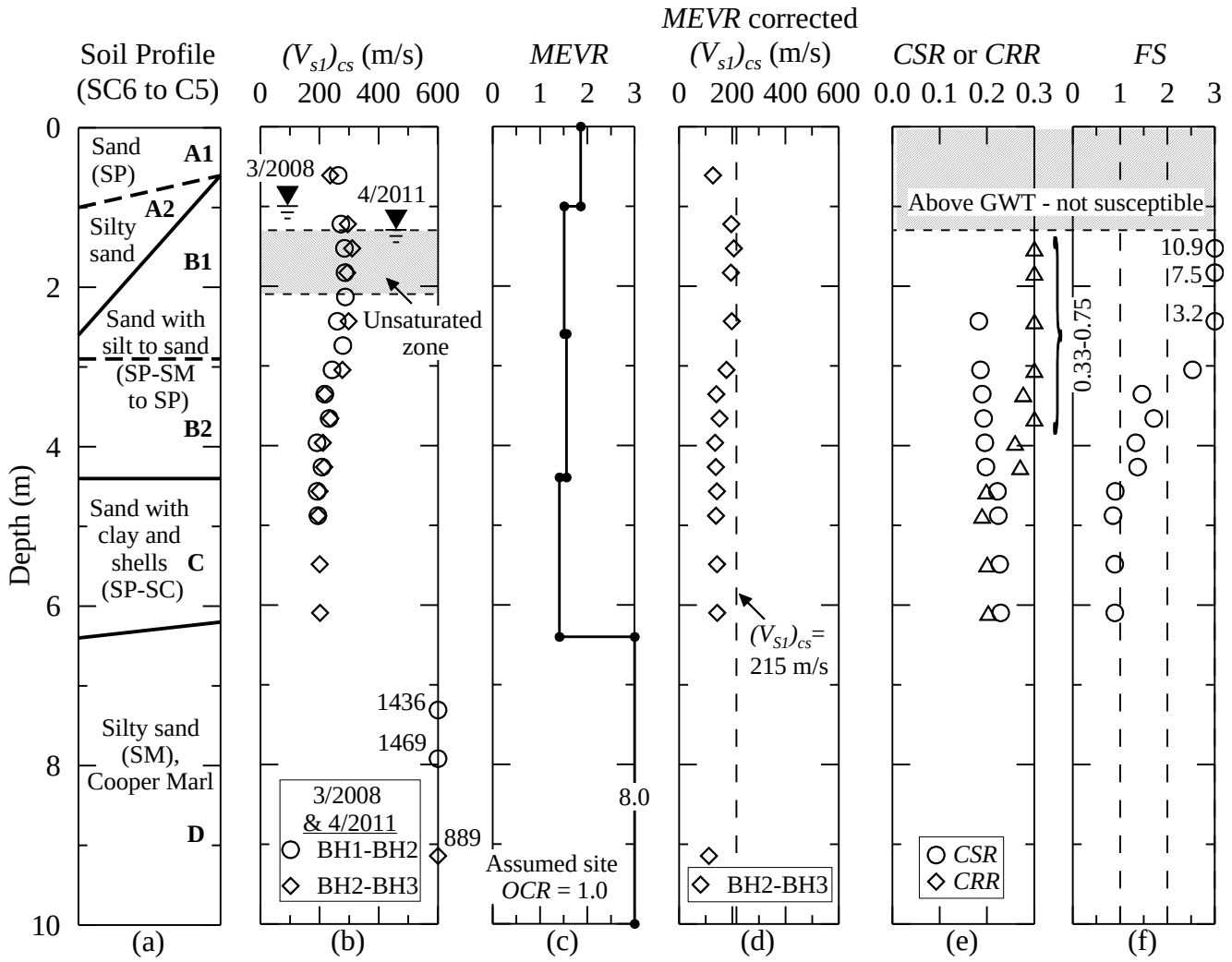

Figure F.5: Liquefaction assessment of the CREC site based on crosshole profile BH2-BH3 and general V_S-based procedure recommended by Youd et al. (2001).

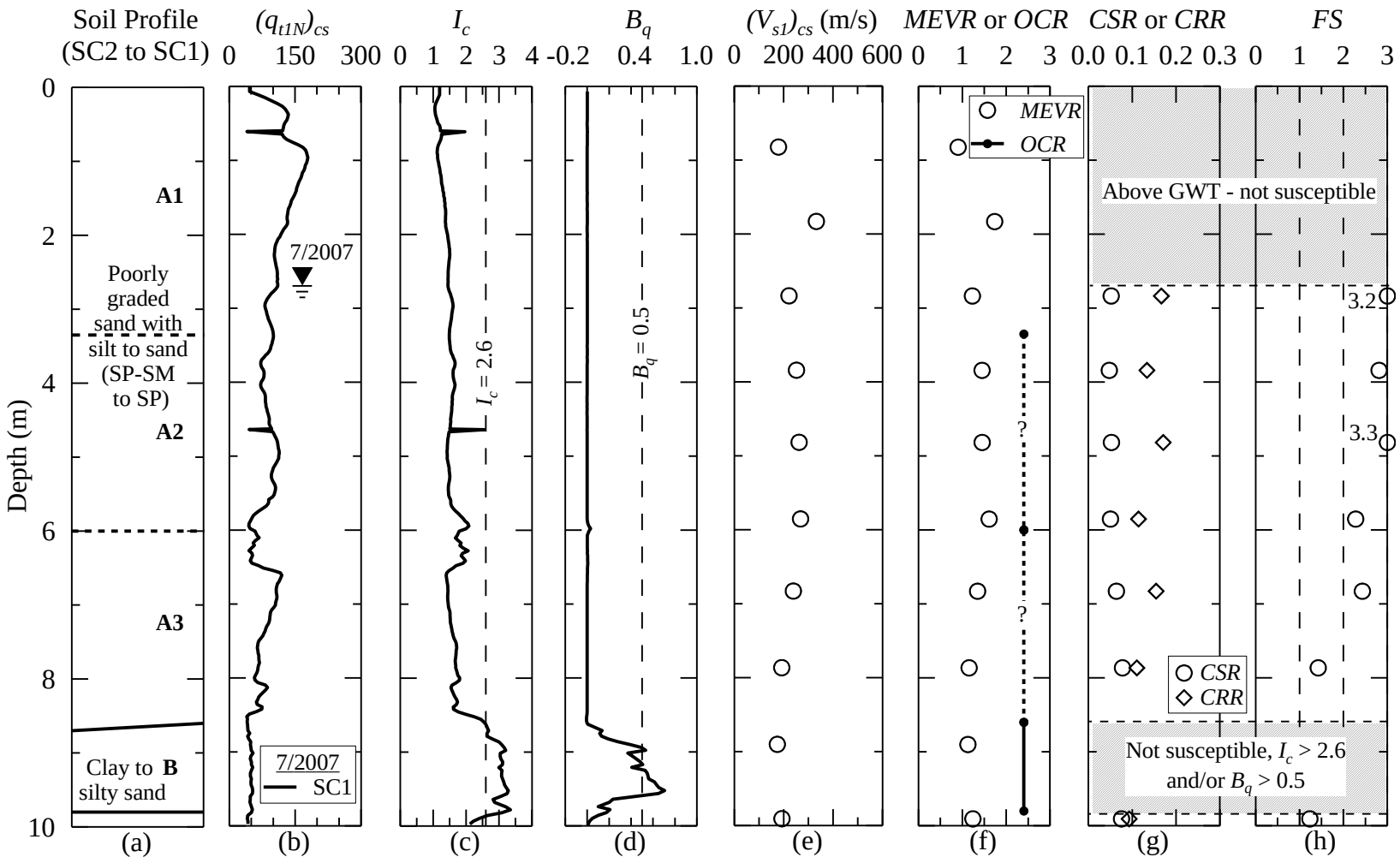

Figure F.6: Liquefaction assessment of the Hobcaw Borrow Pit site based on seismic cone SC1 data reported in Boller (2008) and general CPT-based procedure recommended by Youd et al. (2001).

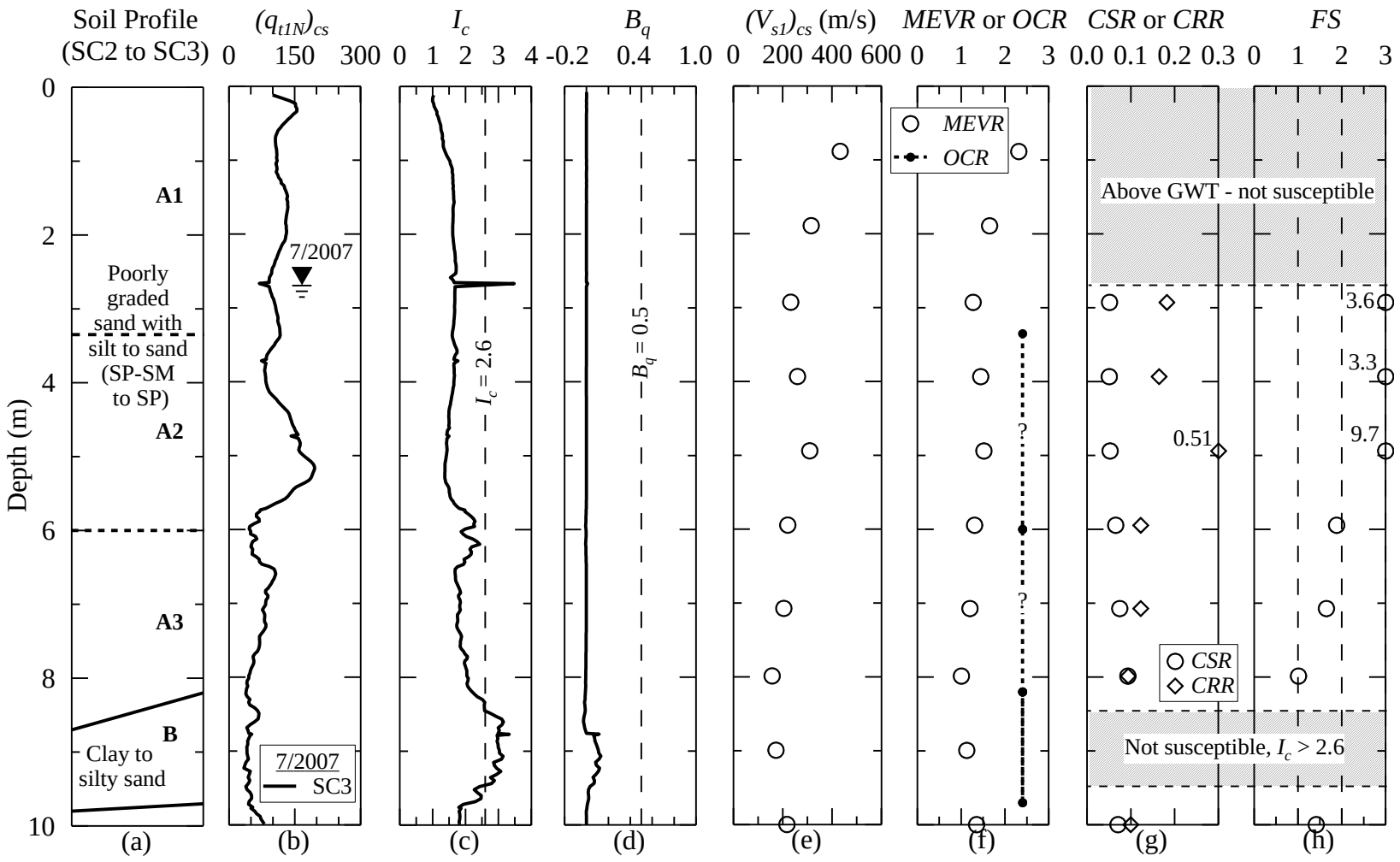

Figure F.7: Liquefaction assessment of the Hobcaw Borrow Pit site based on seismic cone SC3 data reported in Boller (2008) and general CPT-based procedure recommended by Youd et al. (2001).

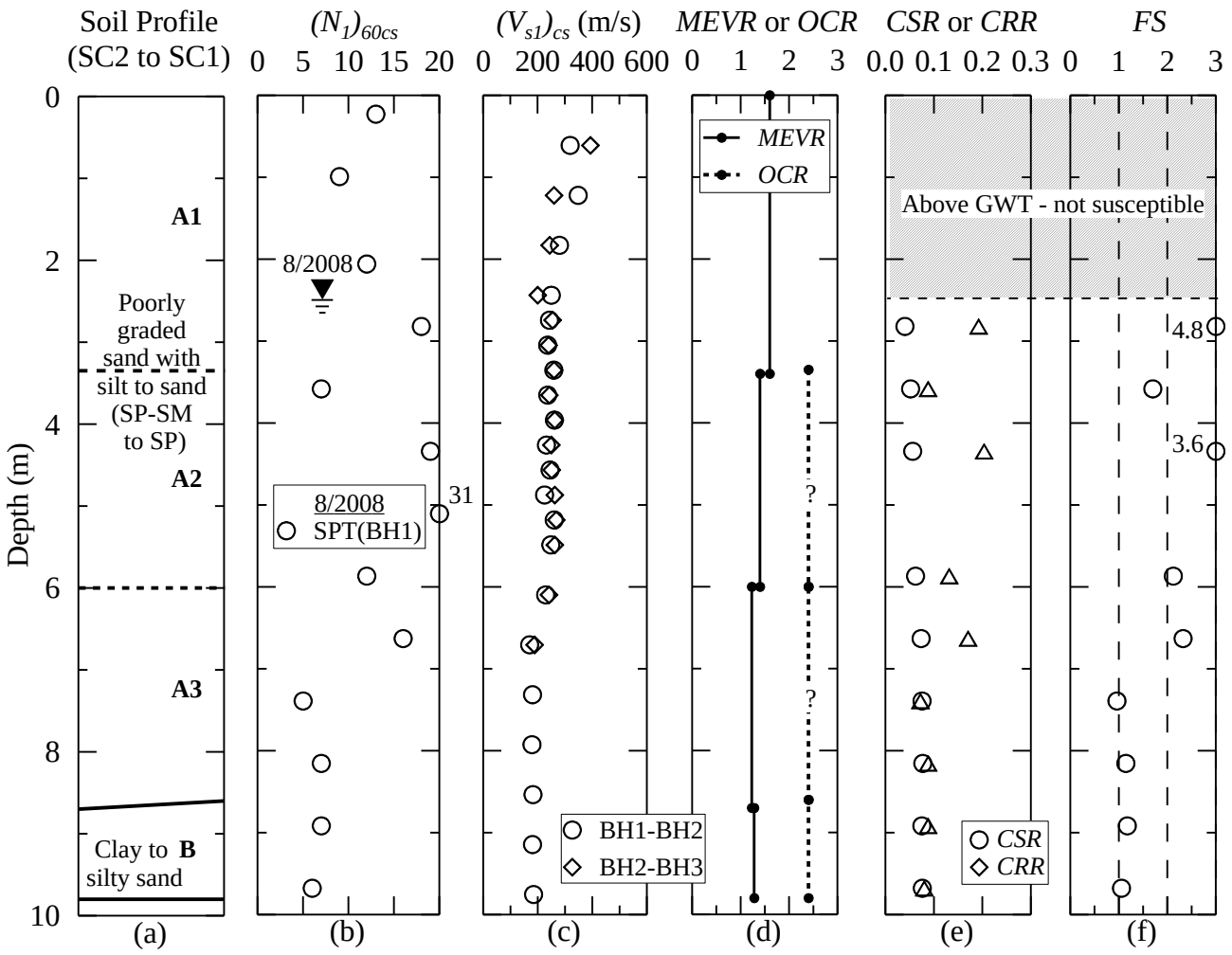

Figure F.8: Liquefaction assessment of the Hobcaw Borrow Pit site based on SPT data reported in Geiger (2010) and general SPT-based procedure recommended by Youd et al. (2001).

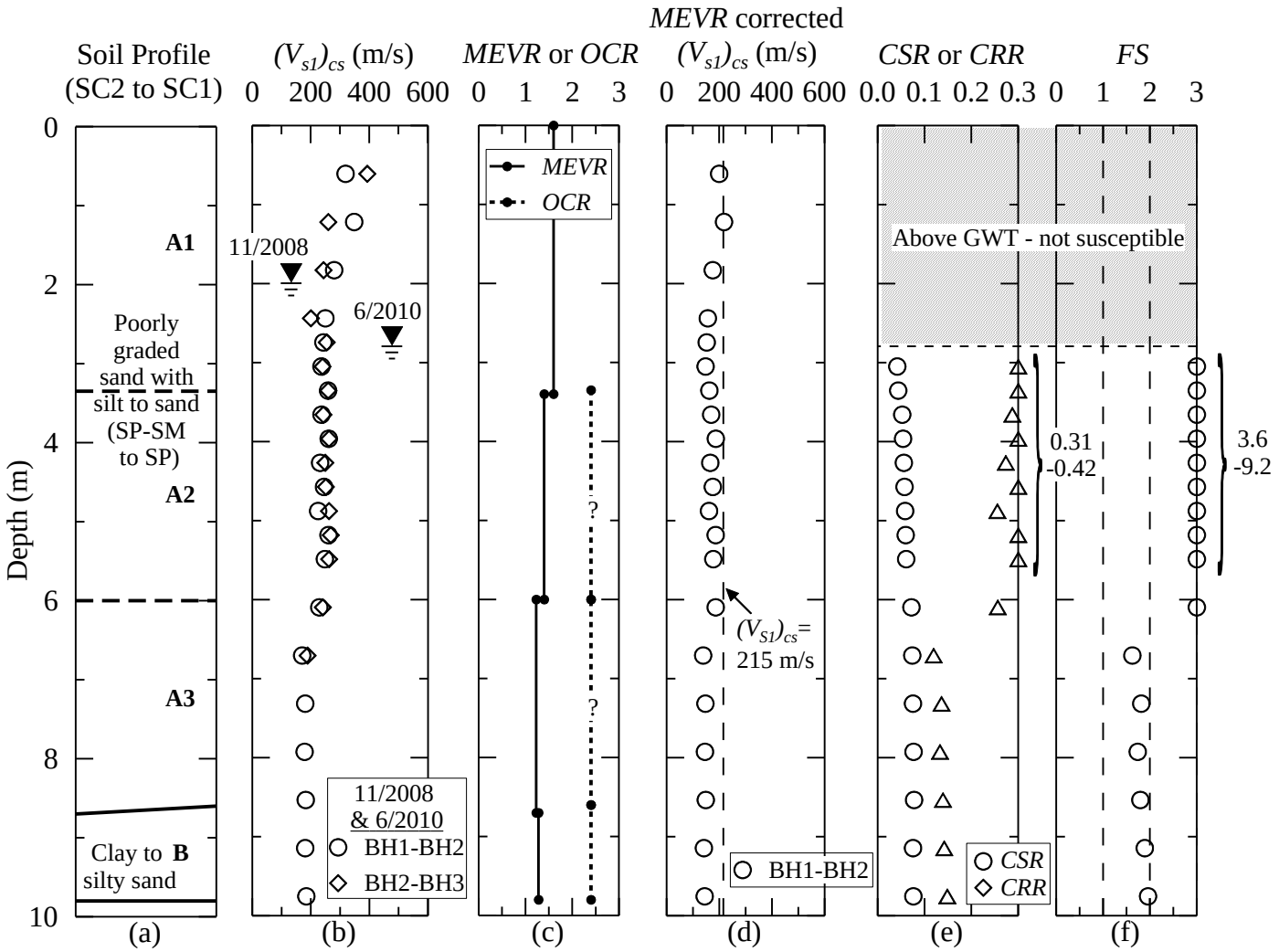

Figure F.9: Liquefaction assessment of the Hobcaw Borrow Pit site based on crosshole profile BH1-BH2 and general V_S-based procedure recommended by Youd et al. (2001).

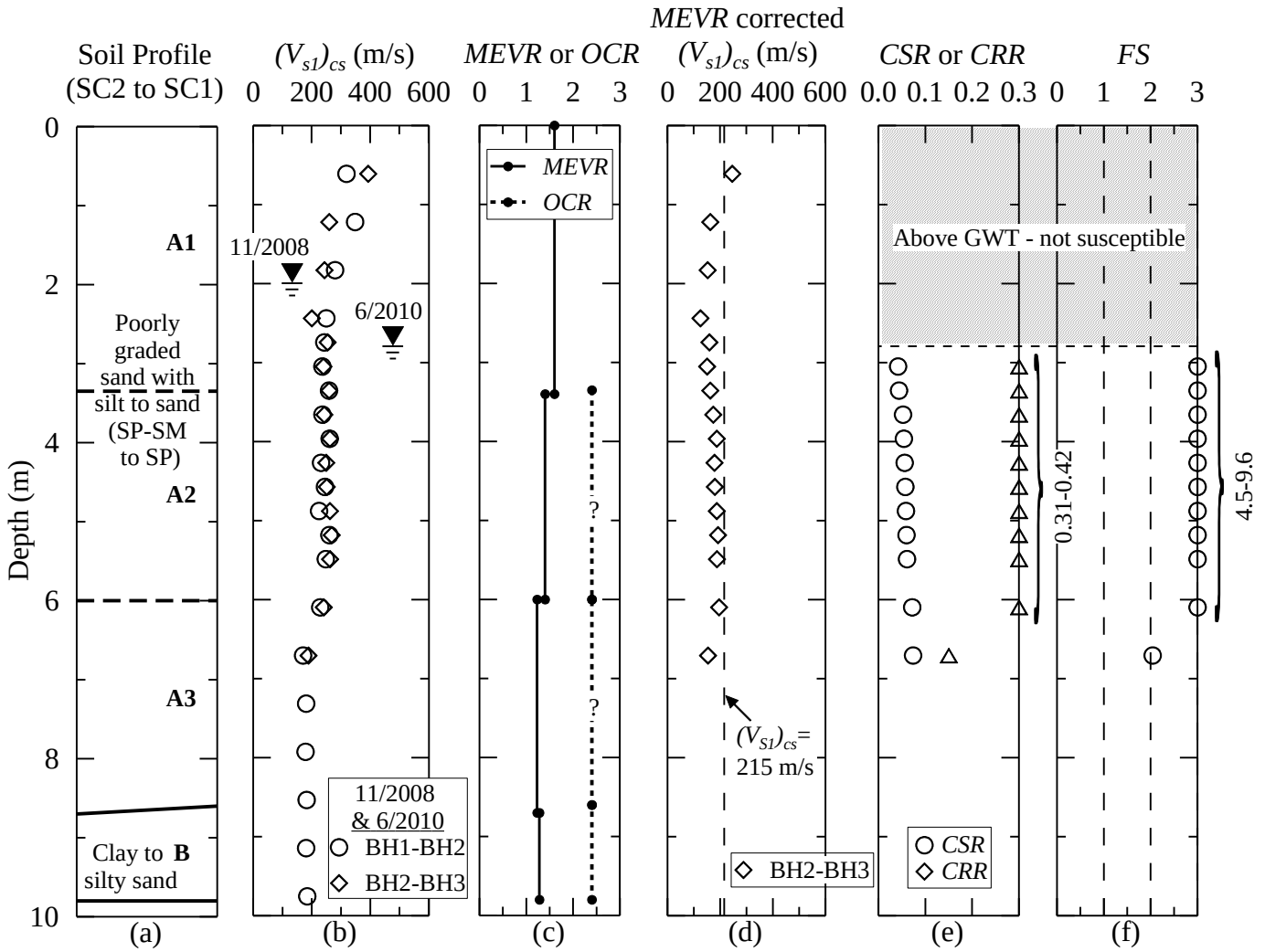

Figure F.10: Liquefaction assessment of the Hobcaw Borrow Pit site based on crosshole profile BH2-BH3 and general V_S-based procedure recommended by Youd et al. (2001).

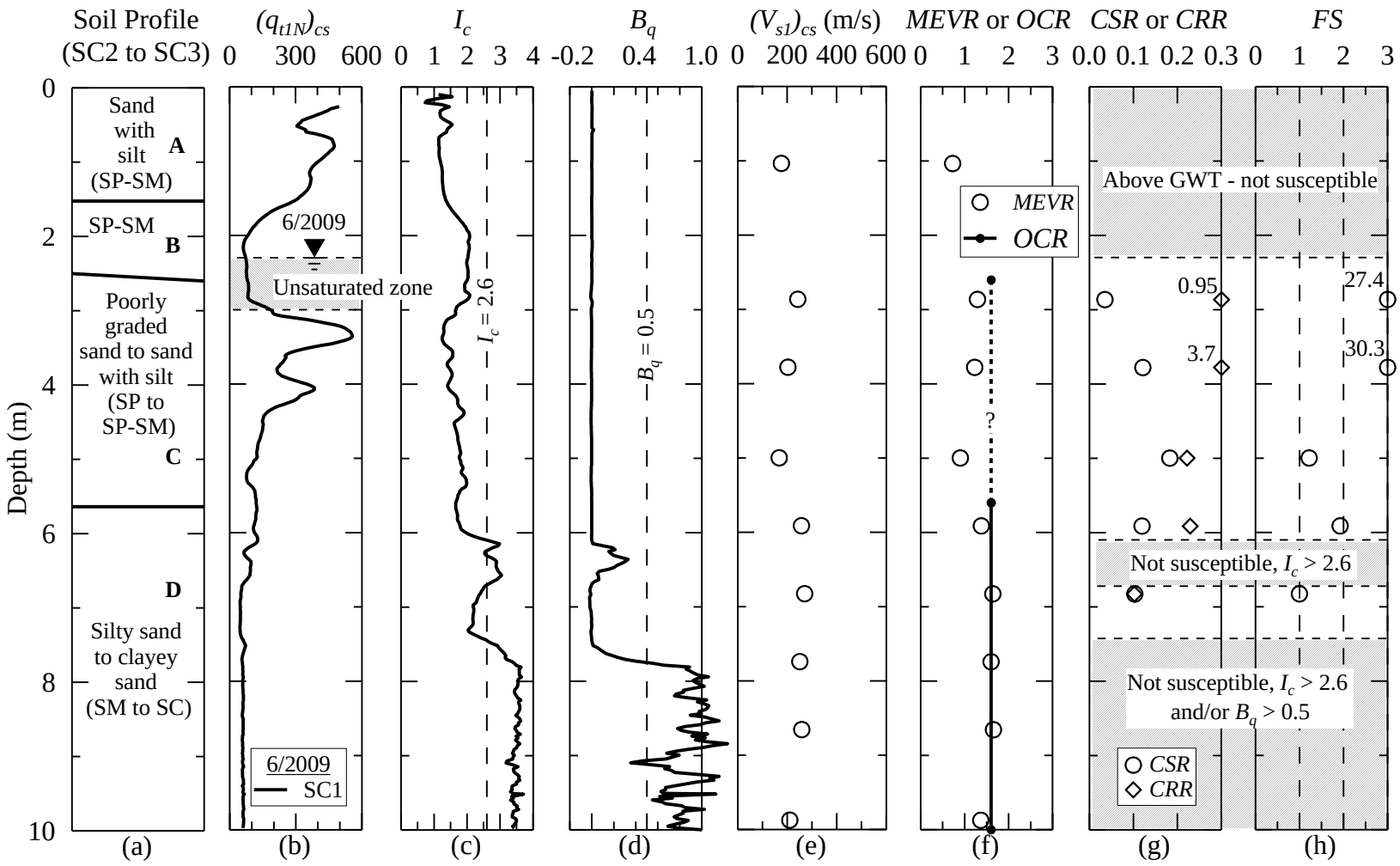

Figure F.11: Liquefaction assessment of the Walterboro Rest Area site based on seismic cone SC1 data reported in Geiger (2010) and general CPT-based procedure recommended by Youd et al. (2001).

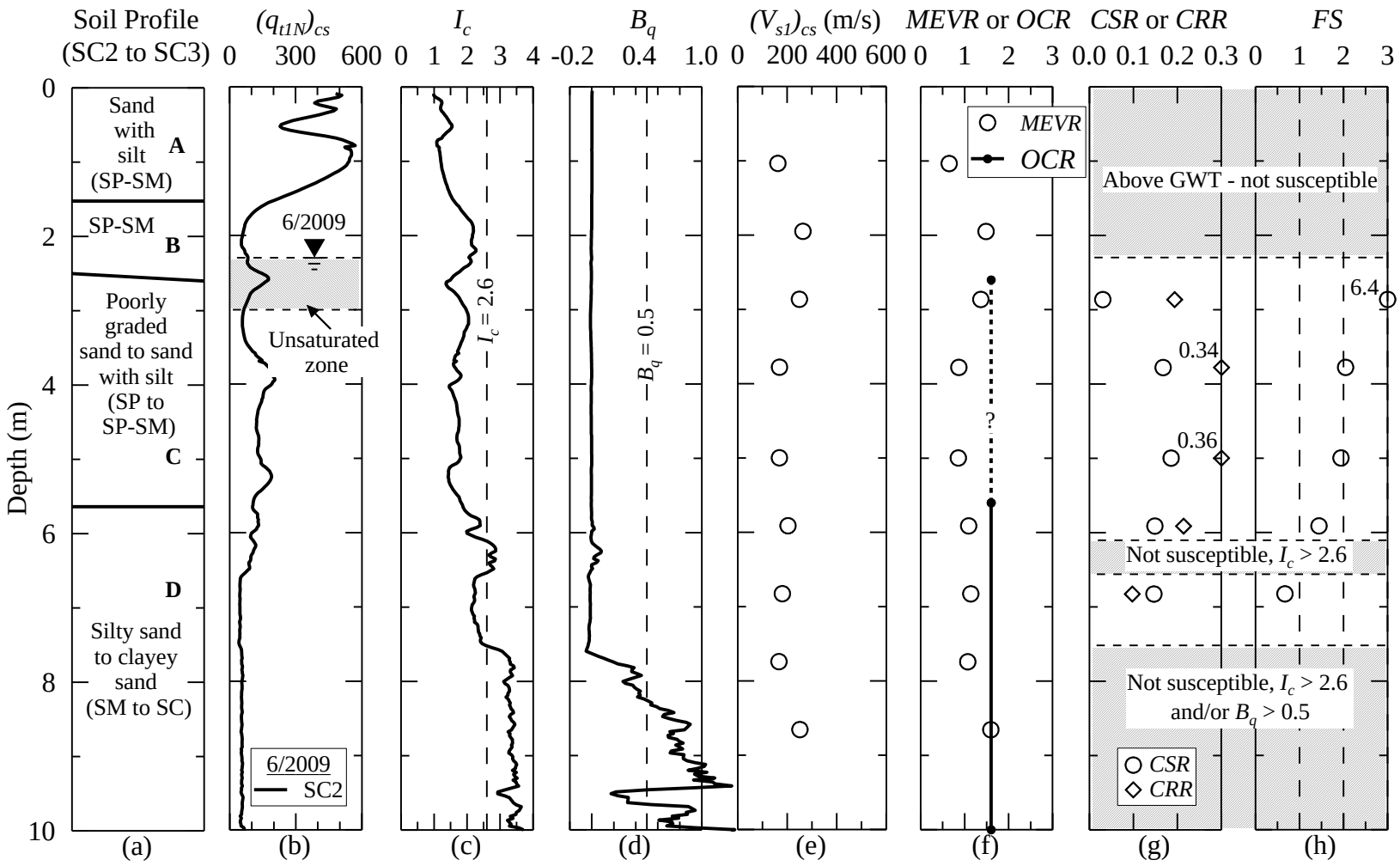

Figure F.12: Liquefaction assessment of the Walterboro Rest Area site based on seismic cone SC2 data reported in Geiger (2010) and general CPT-based procedure recommended by Youd et al. (2001).

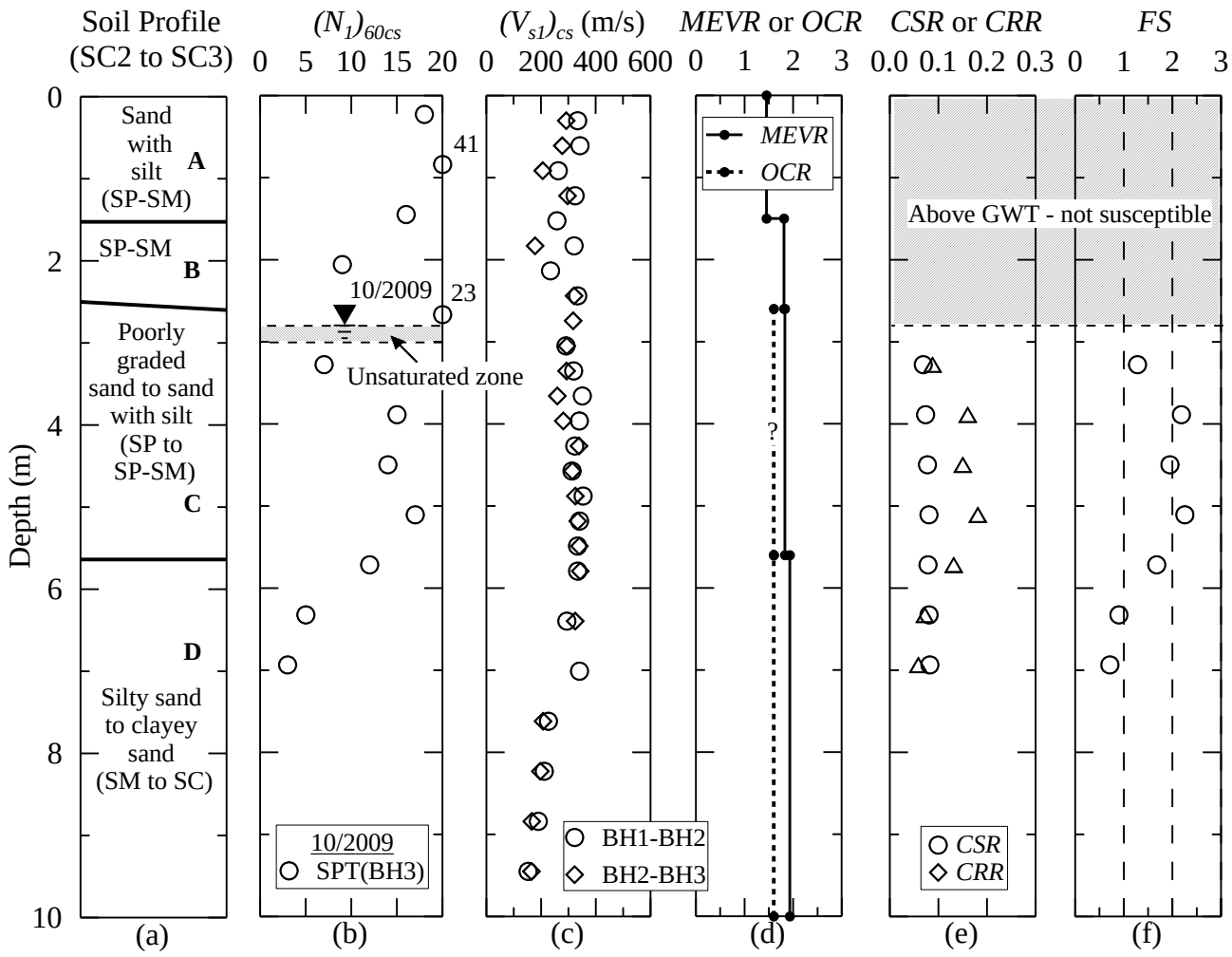

Figure F.13: Liquefaction assessment of the Walterboro Rest Area site based on SPT data reported in Geiger (2010) and general SPT-based procedure recommended by Youd et al. (2001).

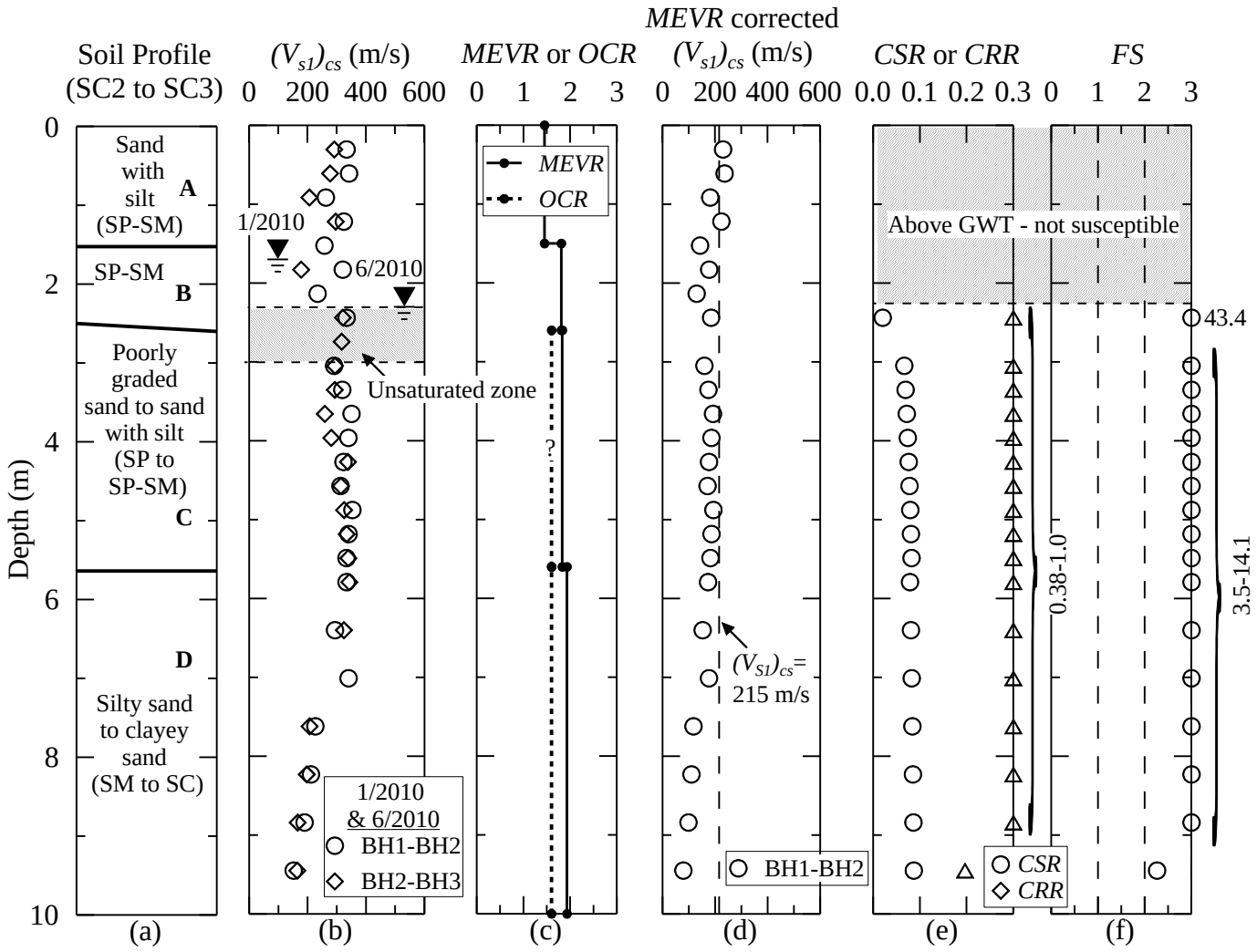

Figure F.14: Liquefaction assessment of the Walterboro Rest Area site based on crosshole profile BH1-BH2 and general V_S-based procedure recommended by Youd et al. (2001).

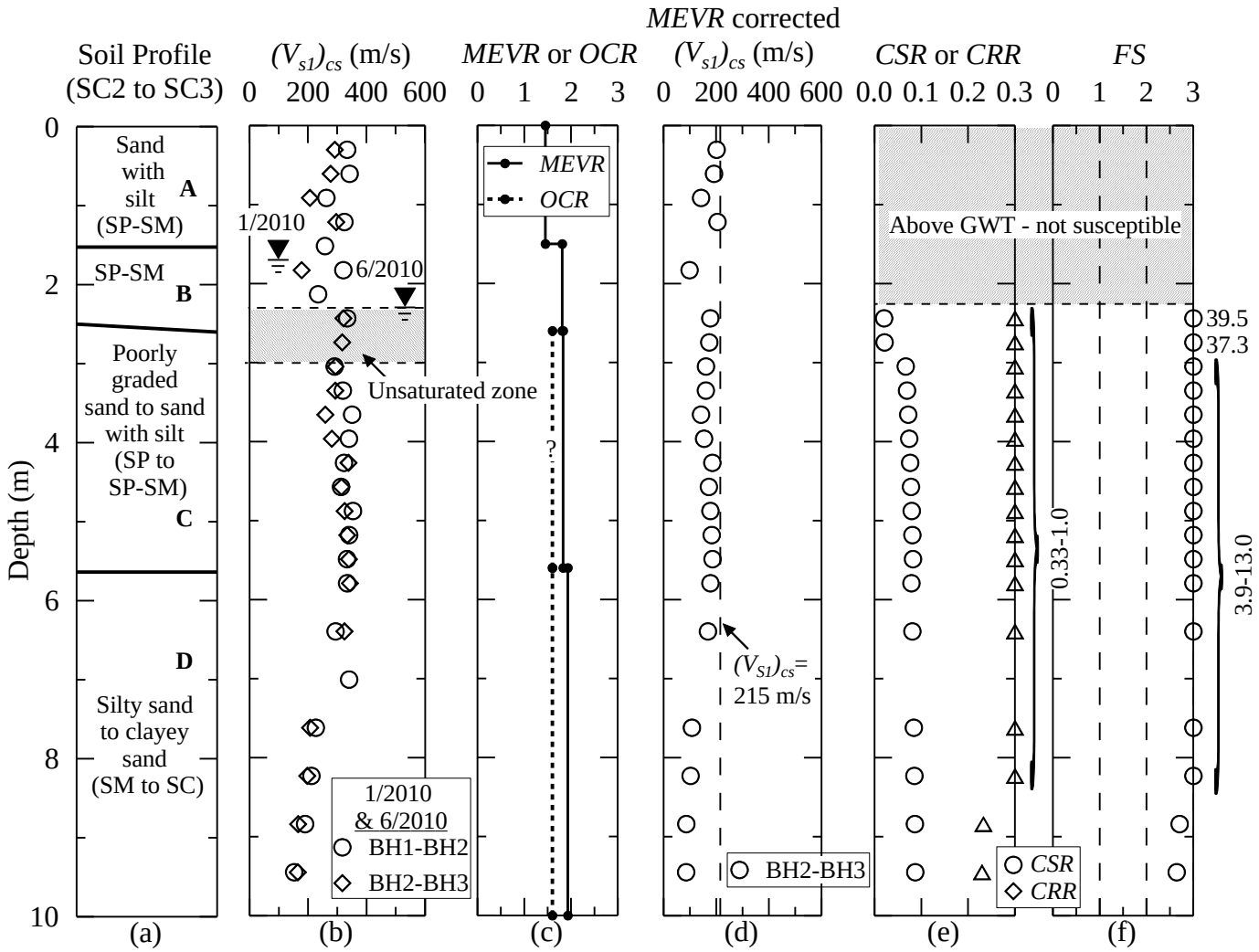

Figure F.15: Liquefaction assessment of the Walterboro Rest Area site based on crosshole profile BH2-BH3 and general V_S-based procedure recommended by Youd et al. (2001).

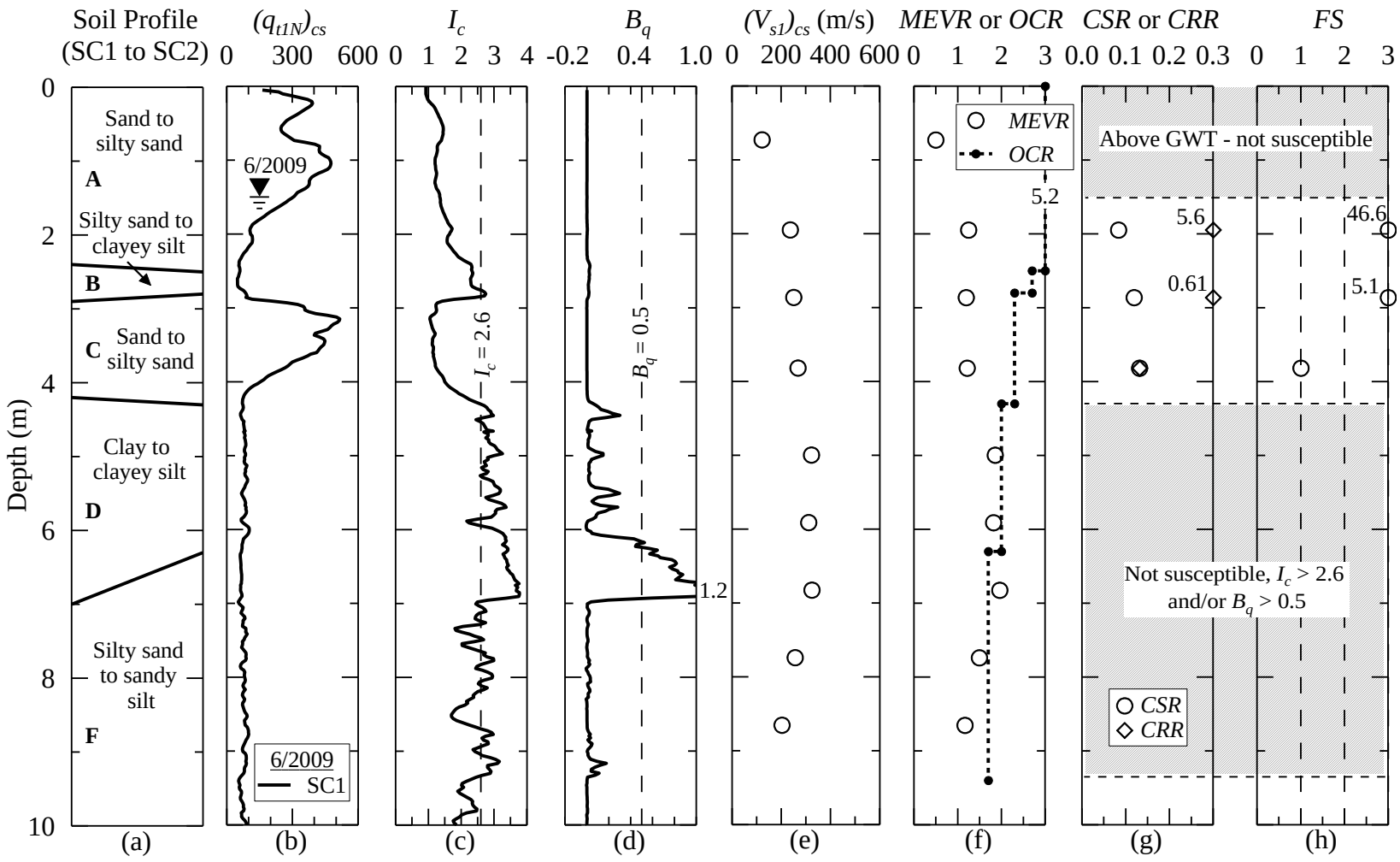

Figure F.16: Liquefaction assessment of the Walterboro Lowcountry site based on seismic cone SC1 data reported in Geiger (2010) and general CPT-based procedure recommended by Youd et al. (2001).

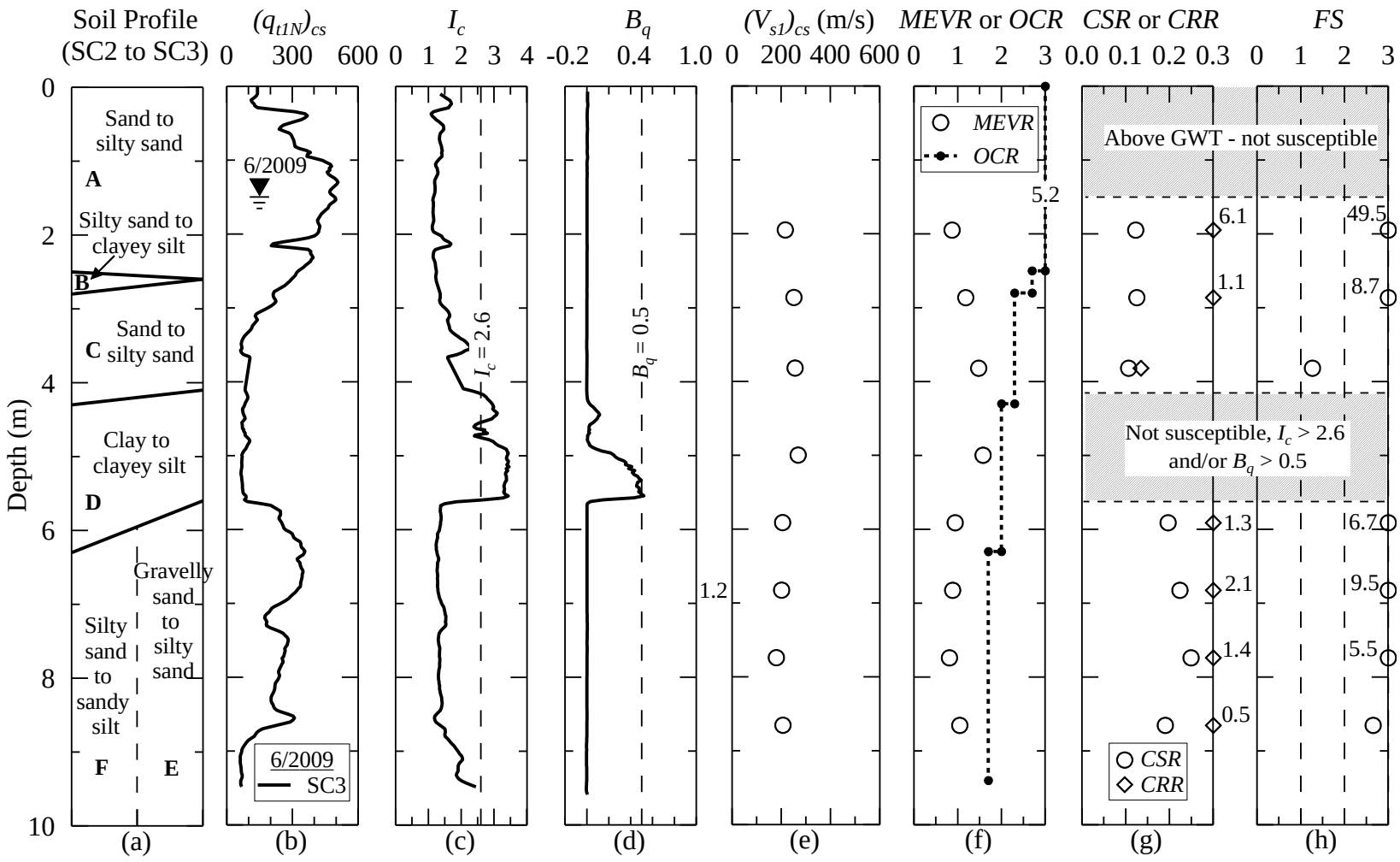

Figure F.17: Liquefaction assessment of the Walterboro Lowcountry site based on seismic cone SC3 data reported in Geiger (2010) and general CPT-based procedure recommended by Youd et al. (2001).

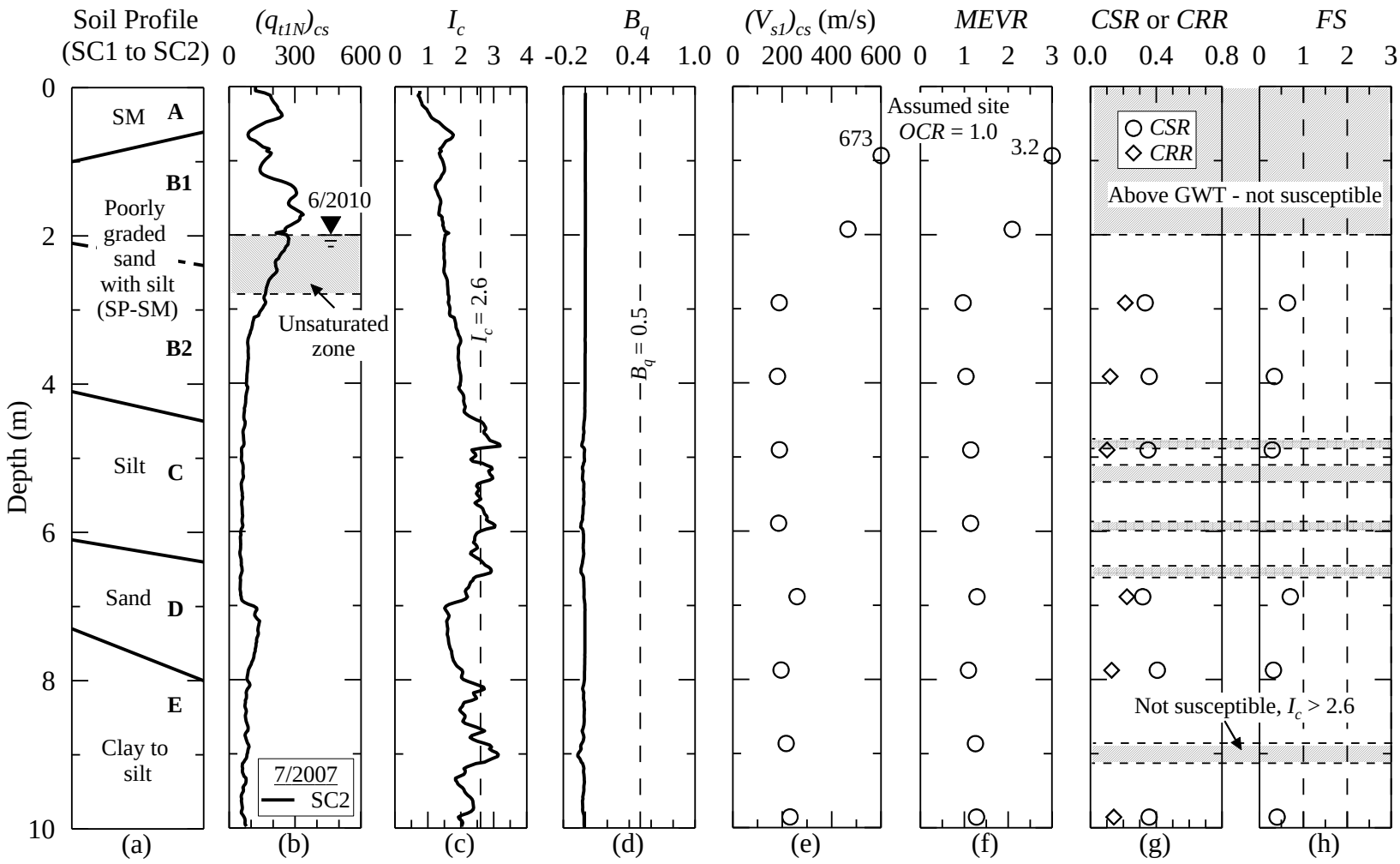

Figure F.18: Liquefaction assessment of the Hollywood Ditch site based on seismic cone SC2 data and general CPT-based procedure recommended by Youd et al. (2001).

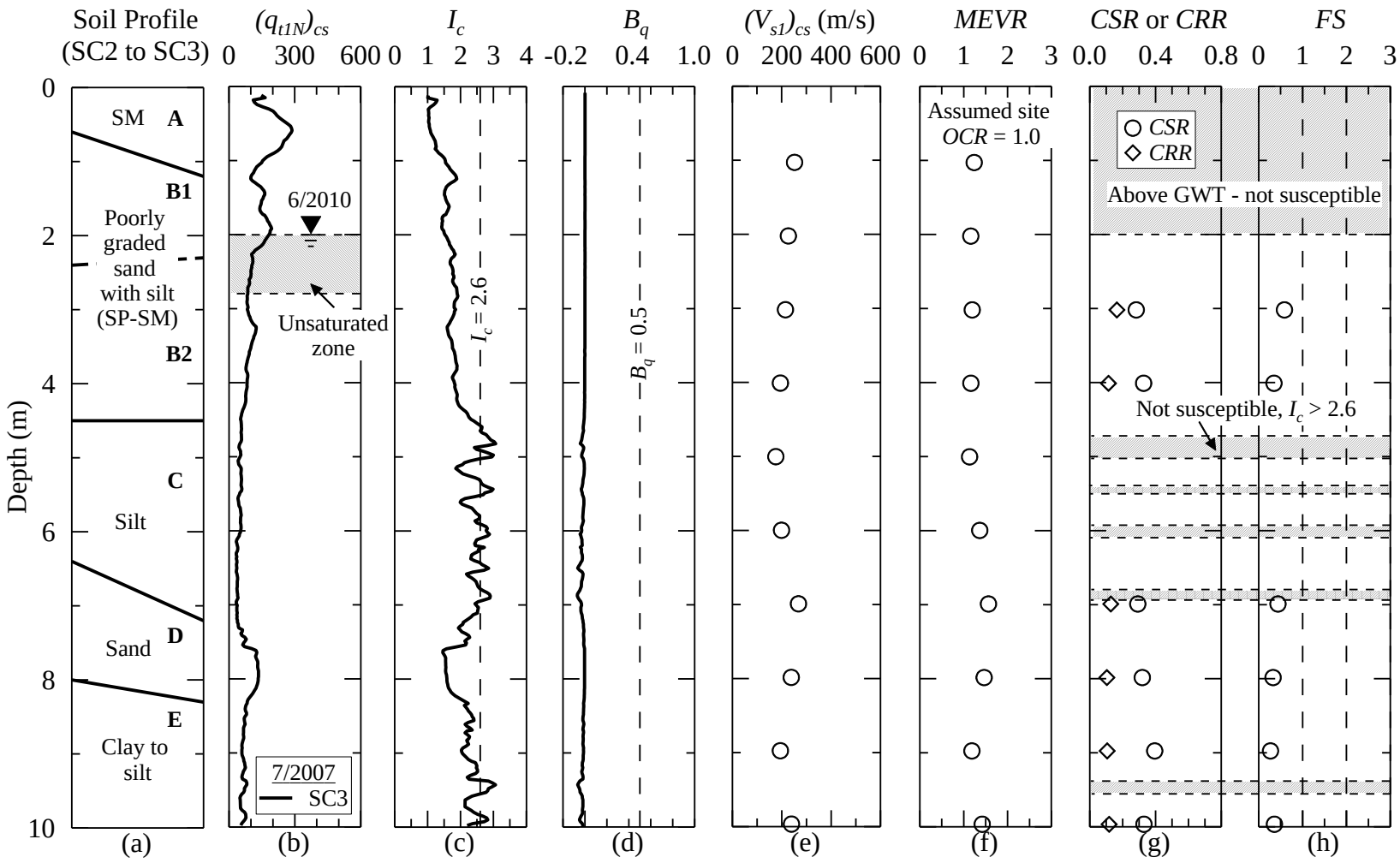

Figure F.19: Liquefaction assessment of the Hollywood Ditch site based on seismic cone SC3 data and general CPT-based procedure recommended by Youd et al. (2001).

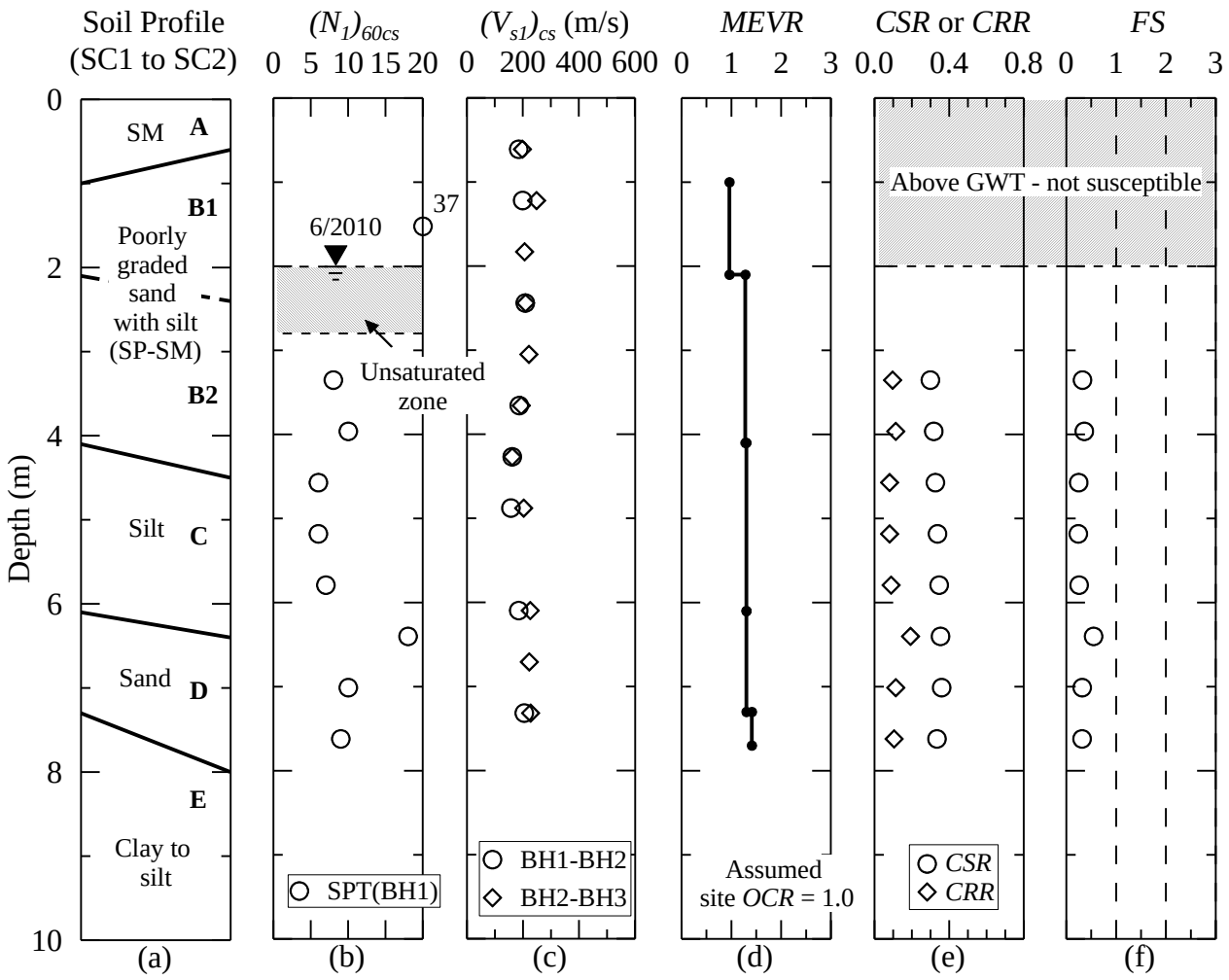

Figure F.20: Liquefaction assessment of the Hollywood Ditch site based on SPT data reported in Williamson and Gassman (2014) and general SPT-based procedure recommended by Youd et al. (2001).

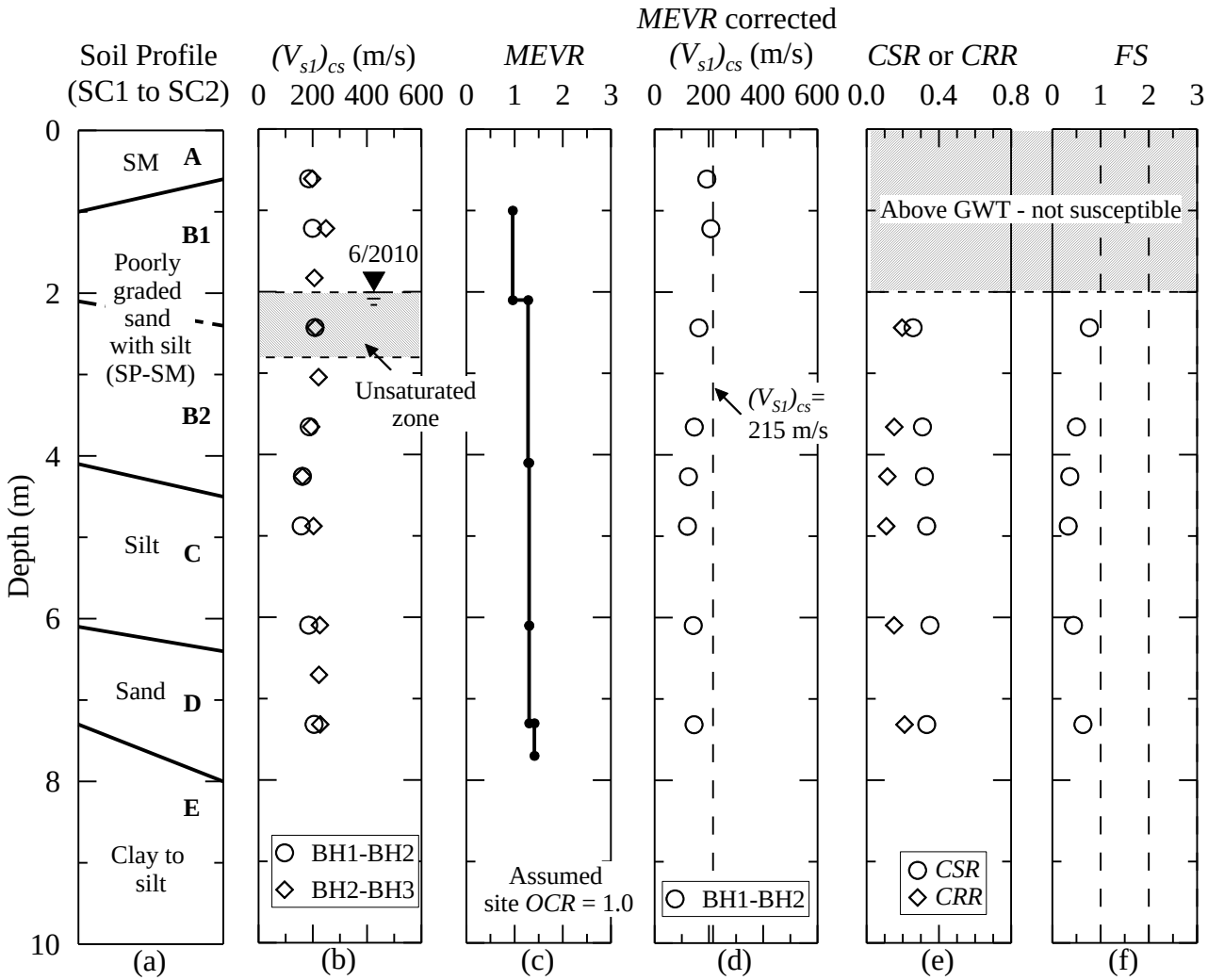

Figure F.21: Liquefaction assessment of the Hollywood Ditch site based on crosshole profile BH1-BH2 and general V_S-based procedure recommended by Youd et al. (2001).

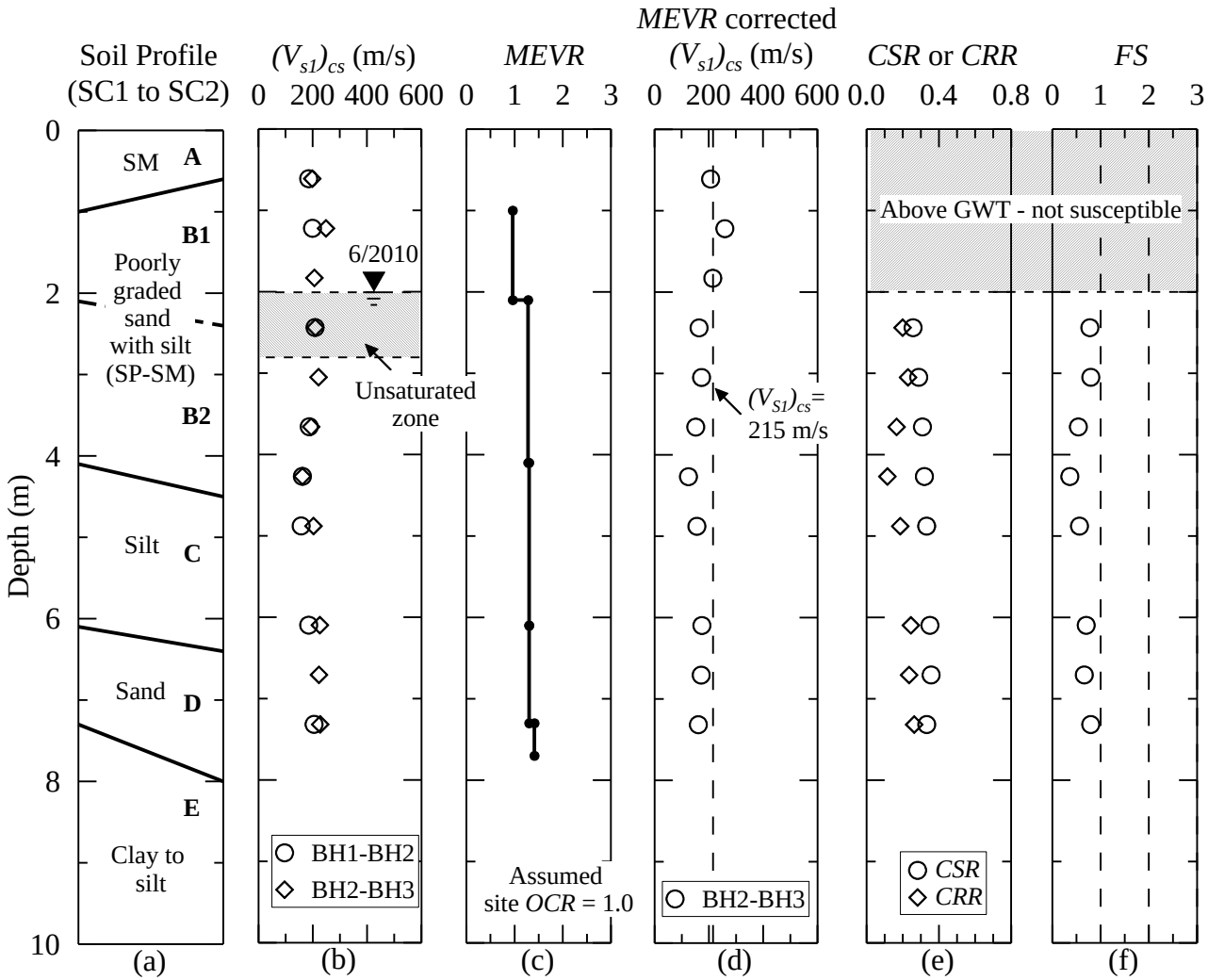

Figure F.22: Liquefaction assessment of the Hollywood Ditch site based on crosshole profile BH2-BH3 and general V_S-based procedure recommended by Youd et al. (2001).

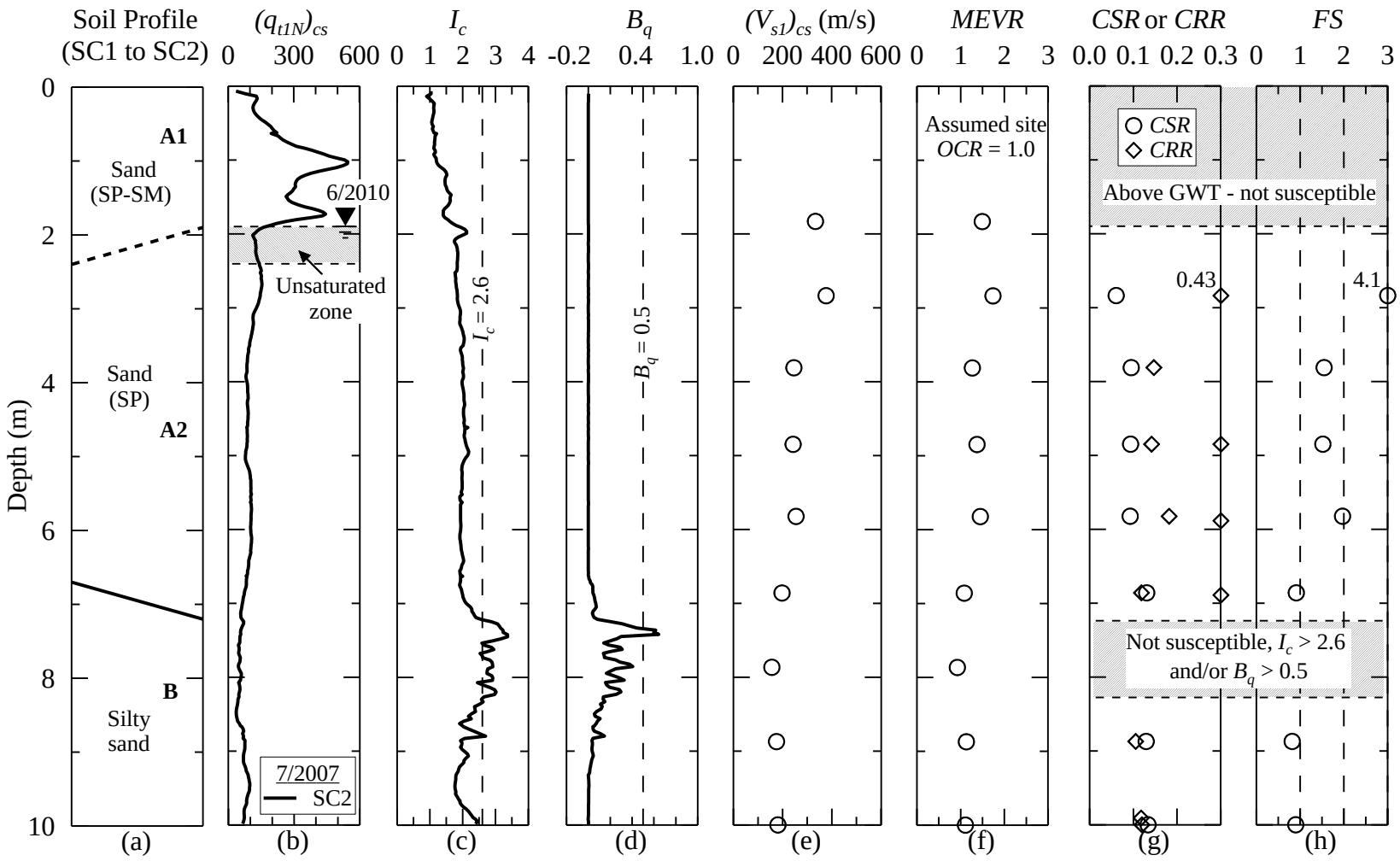

Figure F.23: Liquefaction assessment of the Sampit site based on seismic cone SC2 data and general CPT-based procedure recommended by Youd et al. (2001).

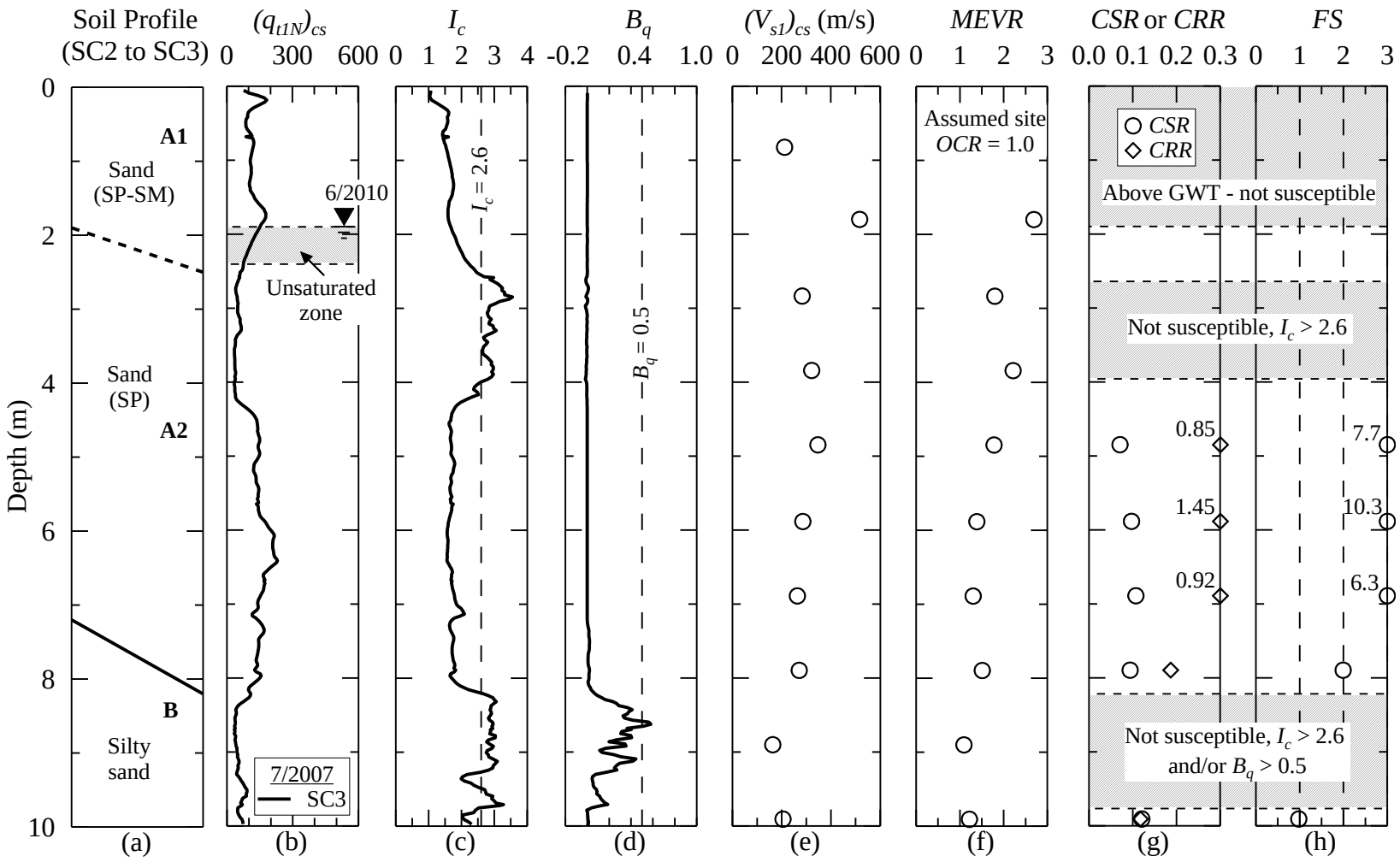

Figure F.24: Liquefaction assessment of the Sampit site based on seismic cone SC3 data and general CPT-based procedure recommended by Youd et al. (2001).

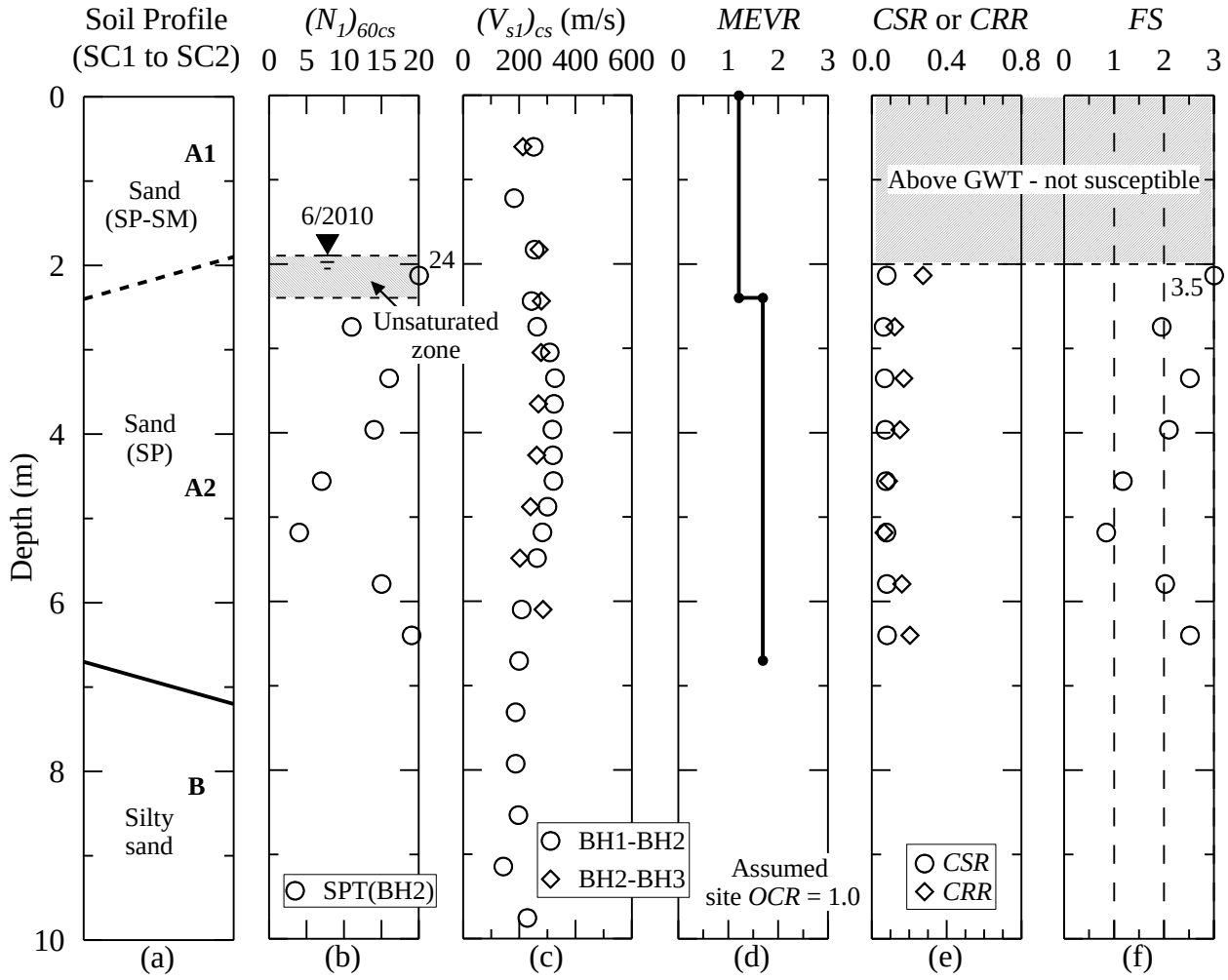

Figure F.25: Liquefaction assessment of the Sampit site based on SPT data reported in Williamson and Gassman (2014) and general SPT-based procedure recommended by Youd et al. (2001).

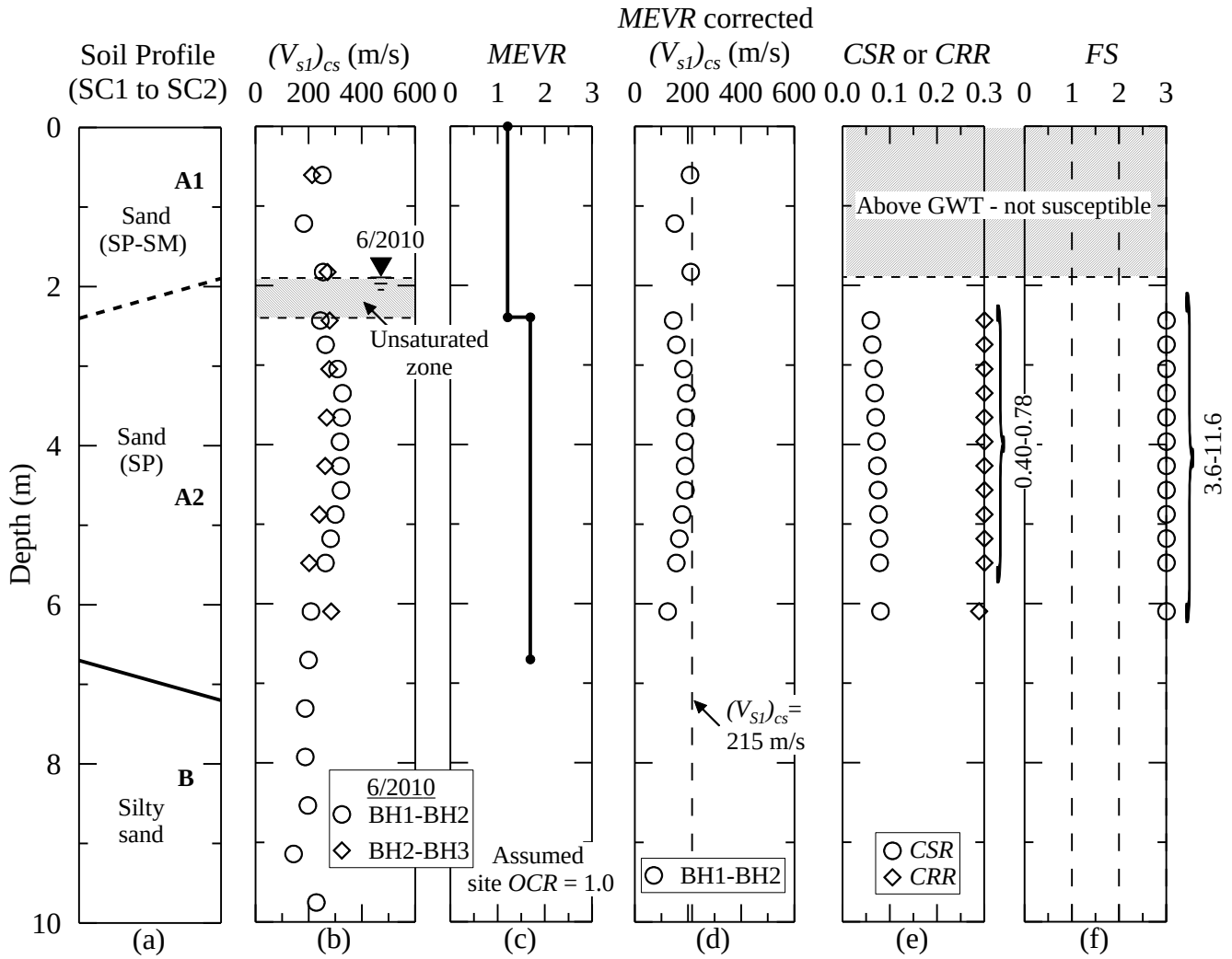

Figure F.26: Liquefaction assessment of the Sampit site based on crosshole profile BH1-BH2 and general V_S-based procedure recommended by Youd et al. (2001).

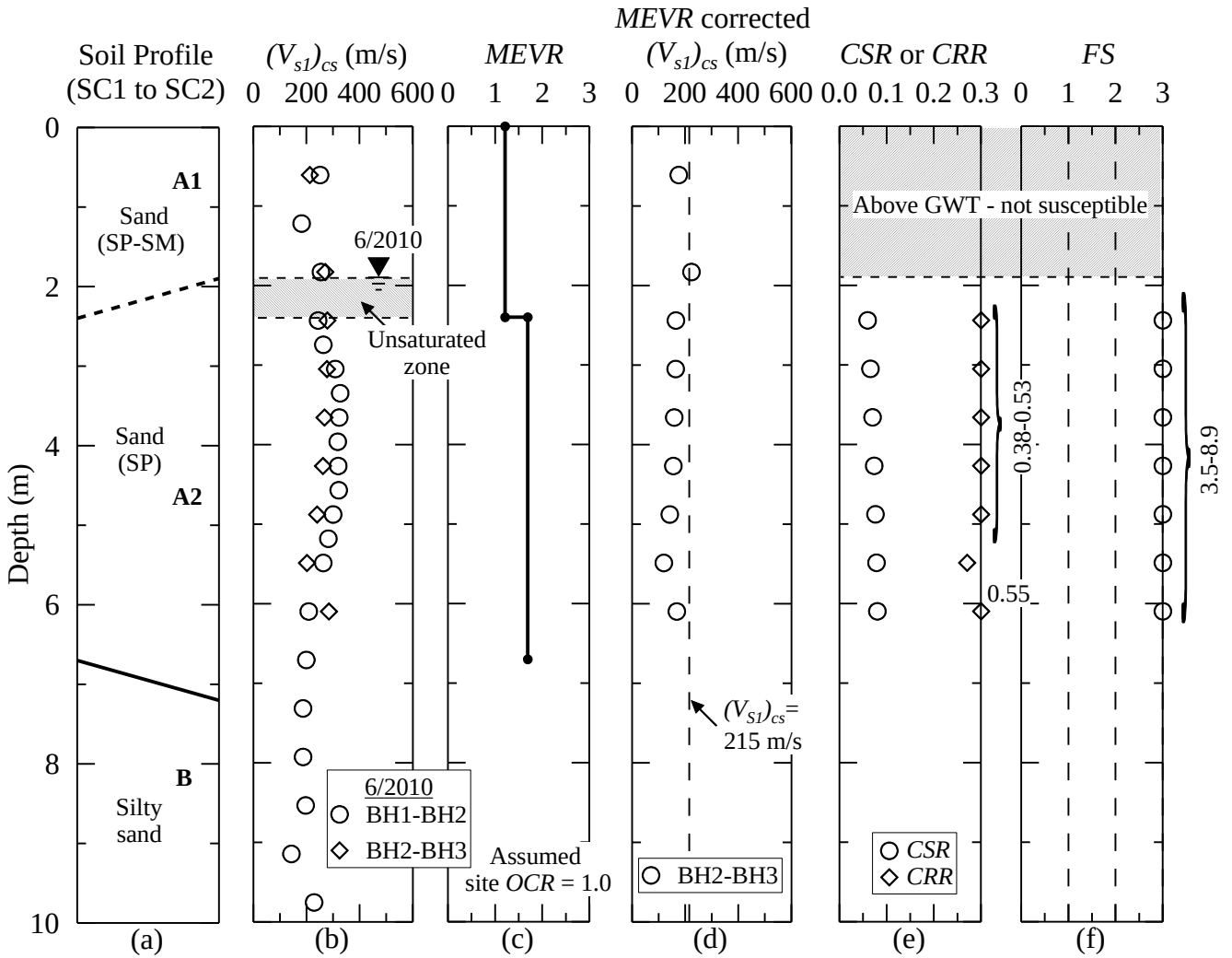

Figure F.27: Liquefaction assessment of the Sampit site based on crosshole profile BH2-BH3 and general V_S-based procedure recommended by Youd et al. (2001).

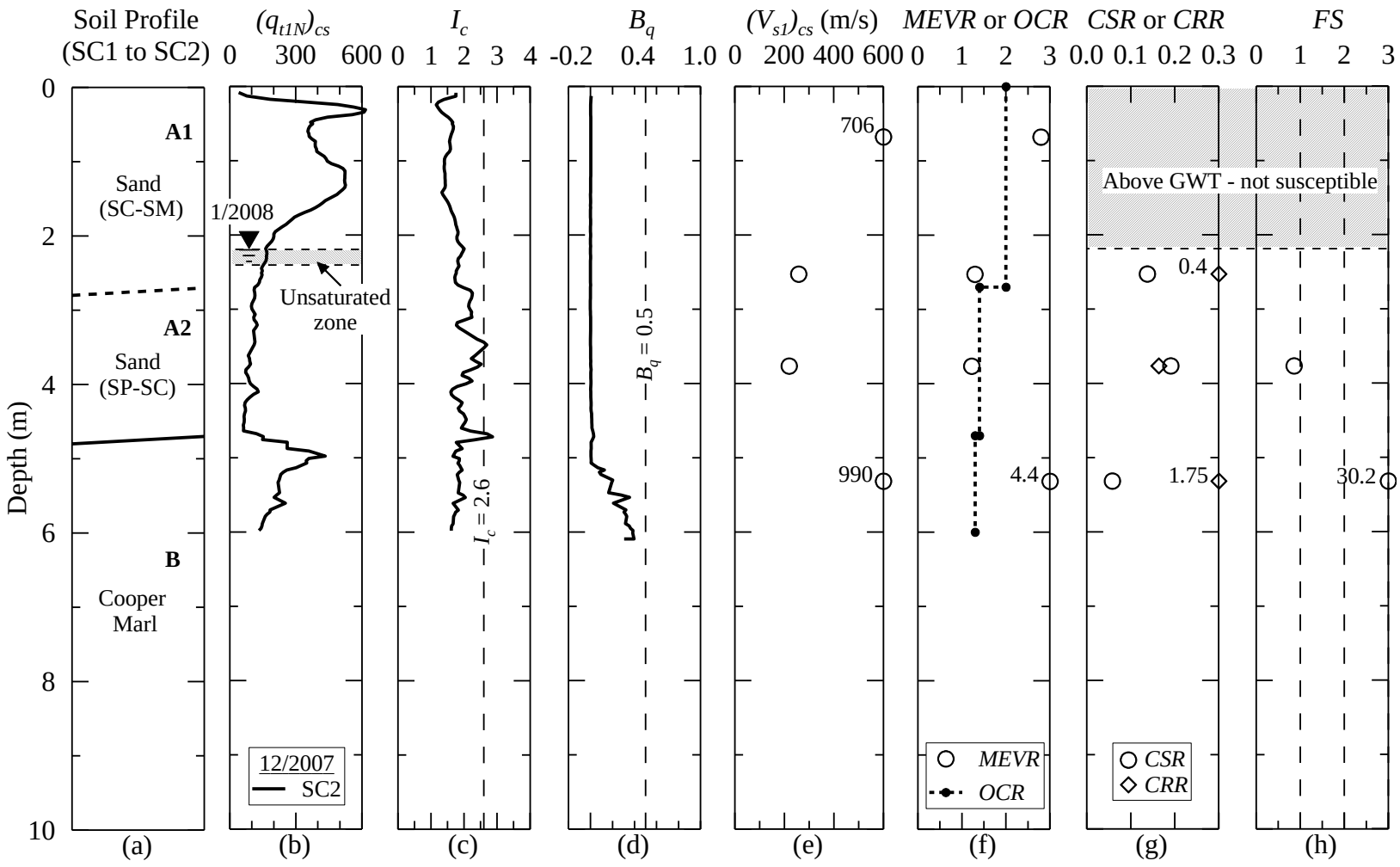

Figure F.28: Liquefaction assessment of the Four Hole Swamp site based on seismic cone SC2 data and general CPT-based procedure recommended by Youd et al. (2001).

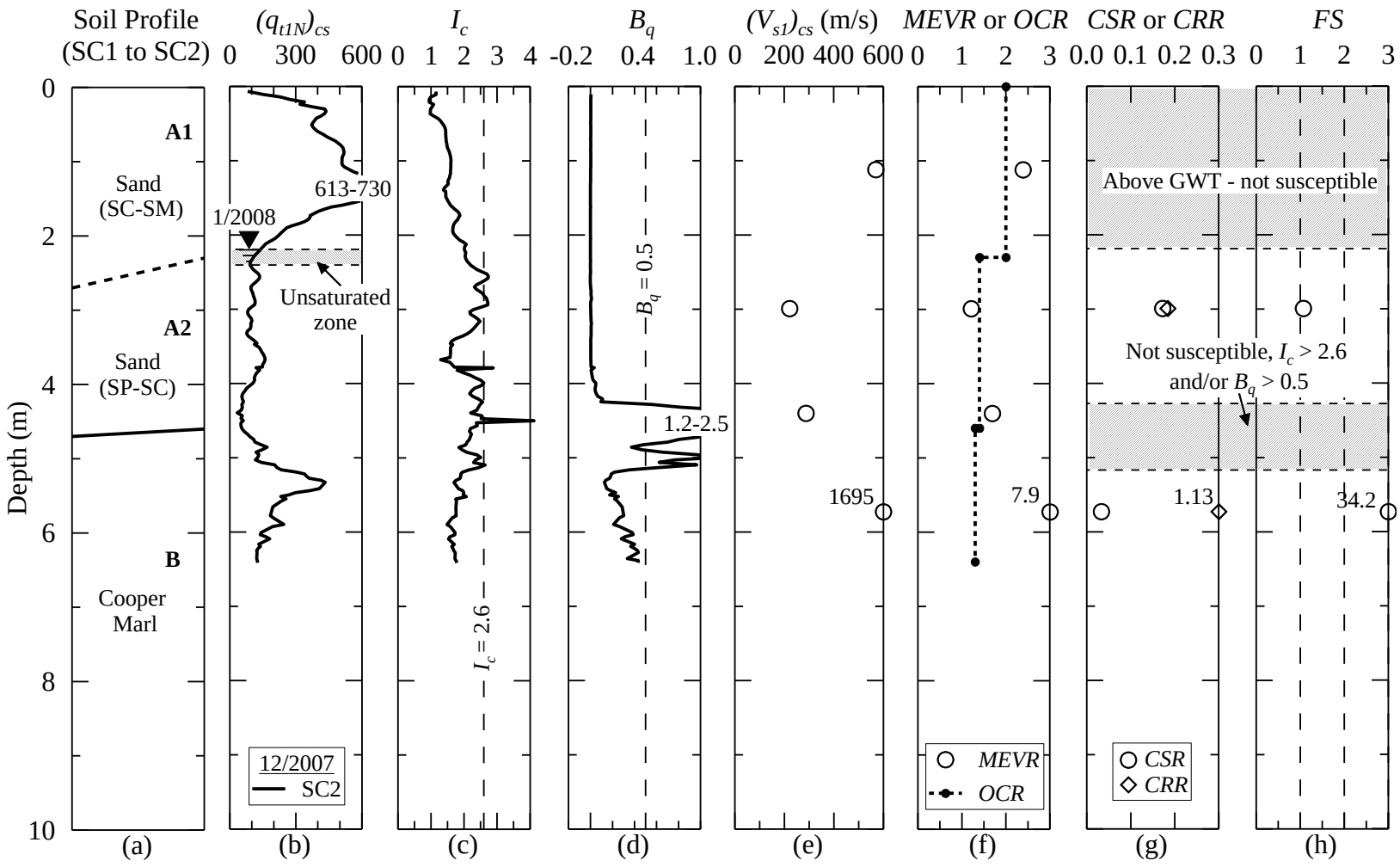

Figure F.29: Liquefaction assessment of the Four Hole Swamp site based on seismic cone SC3 data and general CPT-based procedure recommended by Youd et al. (2001).

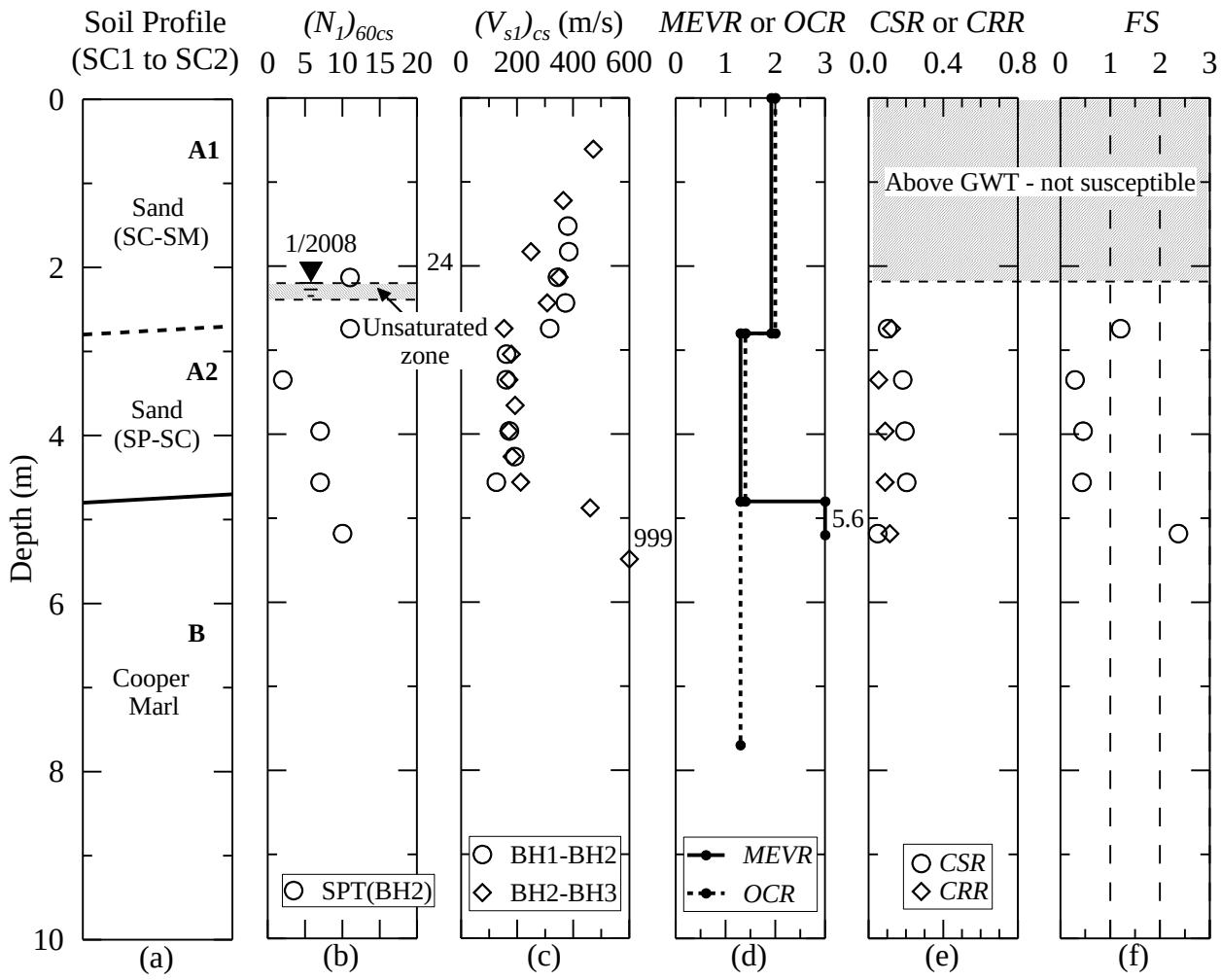

Figure F.30: Liquefaction assessment of the Four Hole Swamp site based on SPT data reported in Williamson and Gassman (2014) and general SPT-based procedure recommended by Youd et al. (2001).

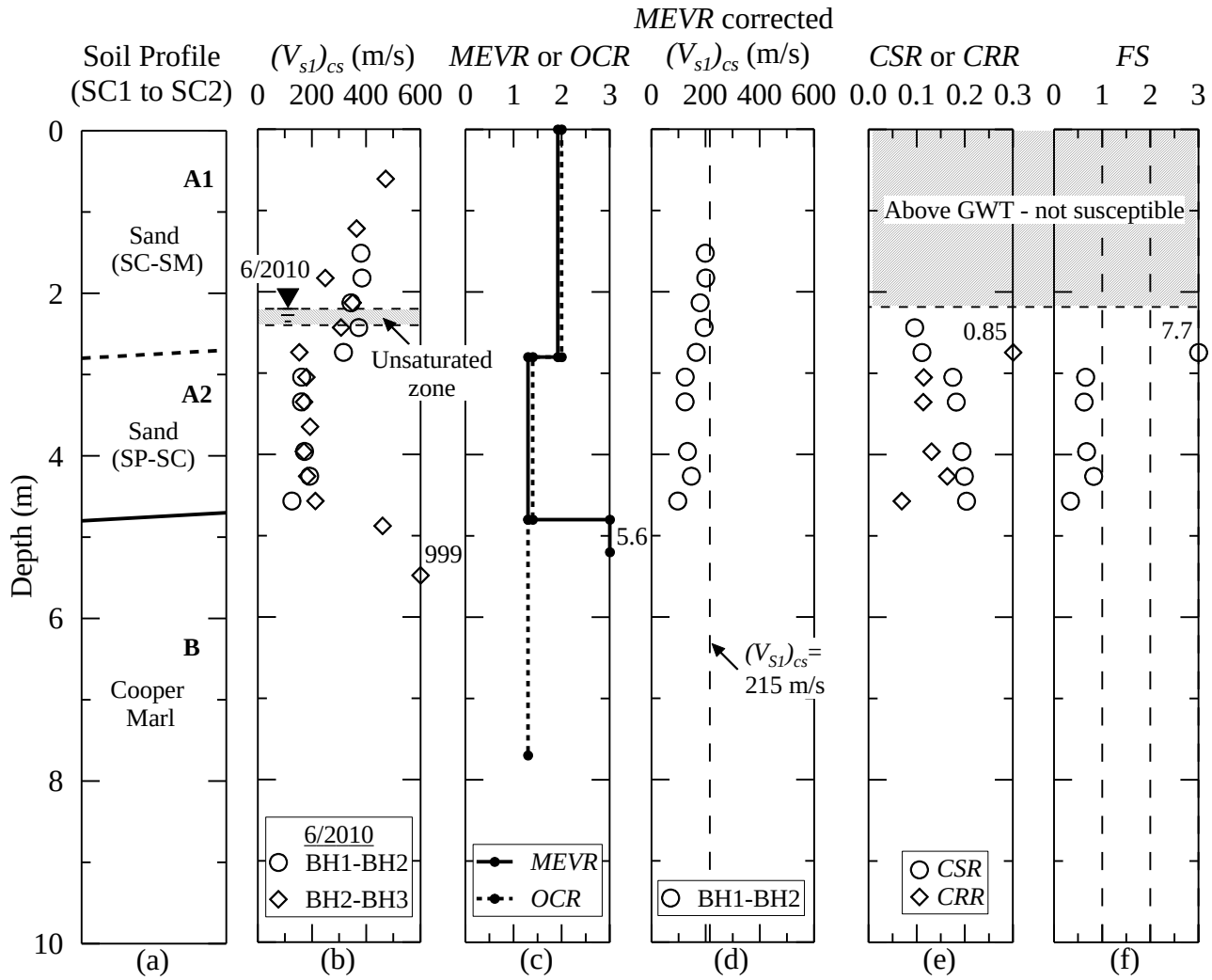

Figure F.31: Liquefaction assessment of the Four Hole Swamp site based on crosshole profile BH1-BH2 and general V_S-based procedure recommended by Youd et al. (2001).

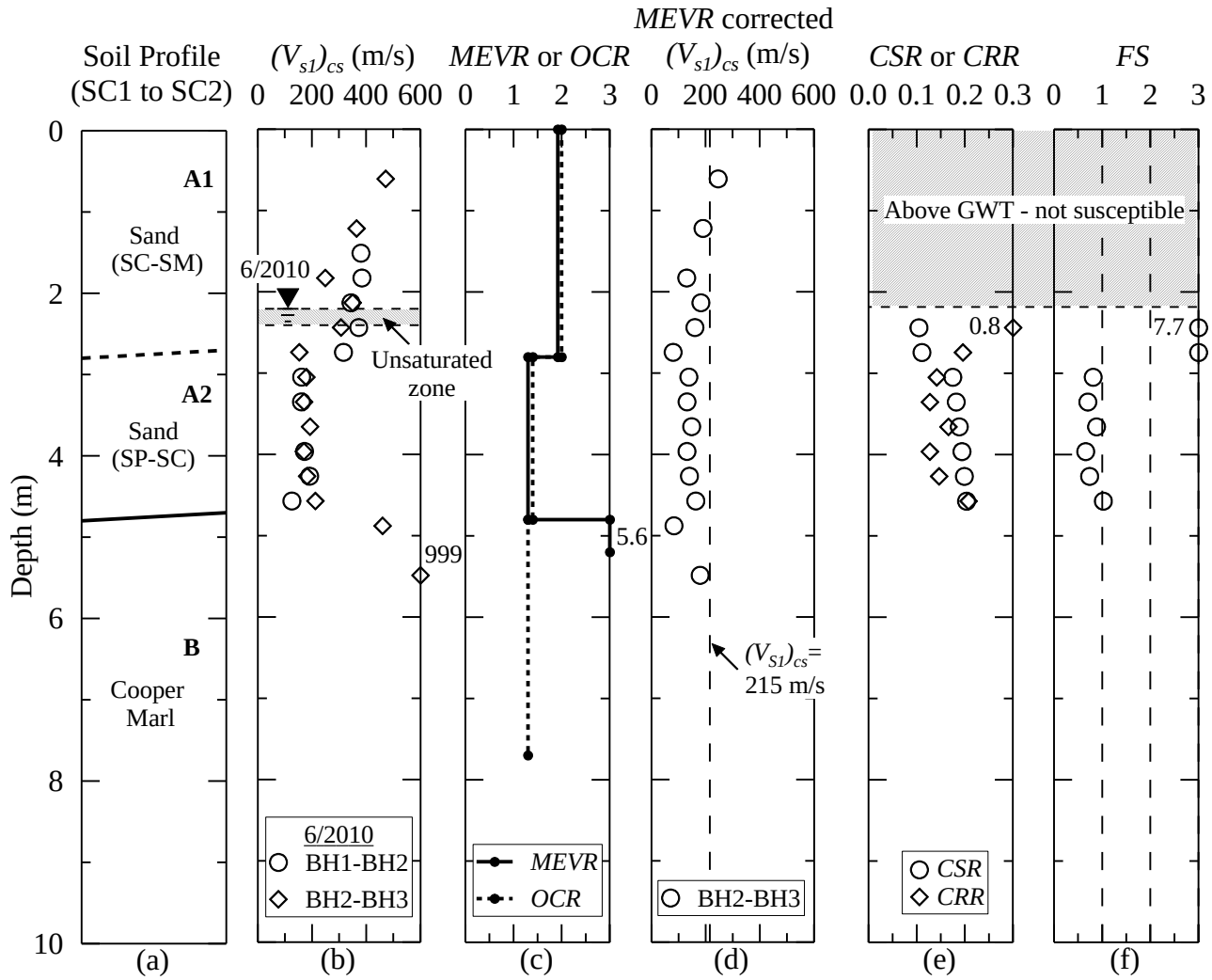

Figure F.32: Liquefaction assessment of the Four Hole Swamp site based on crosshole profile BH2-BH3 and general V_S-based procedure recommended by Youd et al. (2001).

BIBLIOGRAPHY

American Society for Testing and Materials, ASTM (2004). *Annual Book of ASTM Standards*, Philadelphia, PA, Vol. 4.08.

Allen, J.C., and Stokoe II, K.H. (1982). "Development of resonant column apparatus with anisotropic loading." *Geotechnical Engineering Report GR82-28*, University of Texas at Austin, Austin, TX.

Amick, D. C., Gelinas, R., Maurath, G., Cannon, R., Moore, D., Billington, E., and Kemppinen, H. (1990). "Paleoliquefaction features along the Atlantic Seaboard." *Tech. Rep. NUREG/CR-5613*, 146 p.

Andrus, R. D. (1994). "In situ characterization of gravelly soils that liquefied in the 1983 Borah Peak earthquake." *Ph.D. Dissertation*, University of Texas at Austin, Austin, TX.

Andrus, R. D., and Stokoe, K. H., II (2000). "Liquefaction resistance of soils from shear-wave velocity." *J. Geotech. and Geoenvir. Engrg.*, 24(9-10), 713-721.

Andrus, R. D., Hayati, H., and Mohanan, N. P. (2009). "Correcting liquefaction resistance for aged sands using measured to estimated velocity ratio." *J. Geotech. and Geoenvir. Engrg.*, 135(6): 735-744.

Andrus, R. D., Stokoe, K. H., II, Bay, J. A., and Youd, T. L. (1992). "In situ V_S of gravelly soils which liquefied." *Proc., 10th World Conf. on Earthquake Engrg.*, held in Madrid, Spain, Balkema, The Netherlands, 1447-1452.

Andrus, R. D., Stokoe, K. H. , II, and Juang, C. H. (2004). "Guide for shear-wave-based liquefaction potential evaluation." *Earthq. Spectra*, 20 (2), 285-308.

Arango, I., Lewis, M. R., and Kramer, C. (2000). "Updated liquefaction potential analysis eliminates foundation retrofitting of two critical structures." *Soil Dyn. Earthquake Eng.*, 20, 17-25.

Arango, I., and Migues, R. E. (1996). "Investigation of the seismic liquefaction of old sand deposits." *Rep. on Research*, Bechtel Corp., National Science Foundation Grant No. CMS-94-16169, San Francisco, CA.

Arthur, J. R. F., and Menzies, B. K. (1972). "Inherent anisotropy in a sand." *Géotechnique*, 22(1), 115-128.

Arthur, J. R. F., and Philips, A. B. (1975). "Homogeneous and layered sand in triaxial compression." *Géotechnique*, 25(2), 799-815.

Arthur, J. R. F., Chua, K. S., and Dunstan, T. (1977). "Induced anisotropy in a sand." *Géotechnique*, 27(1), 13-30.

Baldi, G., (1985). "Laboratory validation of in-situ tests." *AGI Golden Jubilee Volume for XI ICSMFE* , San Francisco, CA, 217-239.

Baldi, G., Bellotti, R., Ghionna, V., Jamiolkowski, M., Marchetti, S., and Pasqualini, E. (1986). "Flat dilatometer tests in calibration chambers." *Proc., Use of In Situ Tests in Geotechnical Engineering*, ASCE, 431-446.

Baldi, G., Bellotti, R., Ghionna, V. N., Jamiolkowski, M., and Pasqualini, E. (1983). "Prova penetrométrica stática e densitá relativa della sabbia – Atti del." *XV Congegno Nazionale di Geotecnica*, Spoleto, 4-6, Maggio, Vol. 1.

Baligh, M. M., Martin, R. T., Azzouz, A. S., and Morrison, M. J. (1985). "The piezo-lateral stress cell." *Proc., 11th Intl. Conf. on Soil Mechanics and Foundation Engineering*, San Francisco, CA, Vol. 2, 841-844.

Baguelin, F., Jezequel, J. F., LeMee, E., and LeMehaute, A. (1972). "Expansion of cylindrical probes in cohesive soils." *J. Soil Mech. and Found. Div.*, 98(11), 1129-1142.

Barrow, B. L. (1983). "Field investigations of liquefaction sites in Northern California." *M.S. Thesis*, University of Texas at Austin, TX.

Bellotti, R., Ghionna, V., Jamiolkowski, M., Robertson, P. K., and Peterson, R. W. (1989). "Interpretation of moduli from self-boring pressuremeter tests in sand." *Géotechnique*, 39(2), 269-292.

Bellotti, R., Jamiolkowski, M., Lo Presti, D.C.F., and O'Neill, D.A. (1996). "Anisotropy of small strain stiffness in Ticino sand," *Géotechnique*, 46(1), 115-131.

Benoît, J., and Lutenegger, A. J. (2000). *National geotechnical experimentation sites*. ASCE, Co-published with the GeoInstitute, Reston, VA, 397p.

Bhatia (1980). "The verification of relationships for effective stress method to evaluate liquefaction potential of saturated sands." *Ph.D. Dissertation*, University of British Columbia, Vancouver, Canada.

Bjerrum, L., and Anderson, K. H. (1972). "In-situ measurement of lateral pressures in clay." *Proc., 5th ECSMFE*, Madrid, Vol. 1, 11-20.

Boller, R. C. (2008). "Geotechnical investigations at three sites in the South Carolina Coastal Plain that did not liquefy during the 1886 Charleston earthquake." *M.S. Thesis*, Clemson University, Clemson, SC.

Boller, R., Andrus, R., Hayati, H., Camp, W., Gassman, S., and Talwani, P. (2008). "Liquefaction evaluation of the CREC geotechnical experimentation site near Charleston, South Carolina based on cone tests." *Proc., 6th National Seismic Conf. on Bridges and Highways*, Charleston, SC.

Bozozuk, M. (1974). "Minor principal stress measurements in marine clay with hydraulic fractures tests." *Proc., Conf. on Subsurface Exploration for Underground Excavation and Heavy Construction*, ASCE, 333-349.

Brambati, A., Carbognin, L., Quaia, T., Teatini, P., and Tosi, L. (2003). "The Lagoon of Venice: geological setting, evolution and land subsidence." *Episodes*, 26(3), 264-268.

Brewer, R. (1964). *Fabric and mineral analysis of soils*, Wiley, NY, 470p.

Bruzzi, D., Ghionna, V. N., Jamiolkowski, M., Lancellotta, R., and Manfredini, G. (1986). Self-boring pressuremeter in Po River sand. *Proc. 2nd Symp. on Pressuremeter and its Marine Applications*, Vol. 950, 57-73.

Cai, G., Liu, S., Puppala, A. J., and Tong, L. (2011). "Assessment of the coefficient of lateral earth pressure at rest (K_0) from in situ seismic tests." *ASTM Geotech. Test. J.*, 34(4), 1-11.

Campanella, R. G., and Robertson, P. K. (1983). "Flat plate dilatometer testing: research and development." *Soil Mechanics Series No. 68*, Dept. of Civil Engineering, University of British Columbia, Vancouver, Canada.

Caputo, R., Iordanidou, K., Minarelli, L., Papathanassiou, G., Poli, M. E., Rapti-Caputo, D., Sboras, S., Stefani, M. and Zanferrari, A. (2012). "Geological evidence of pre-2012 seismic events, Emilia-Romagna, Italy." *Annals of Geophysics*, 55(4).

Casagrande, A., and Carillo, N. (1944). "Shear failure of anisotropic materials." *Journal of Boston Society of Civil Engineers*, 31(4), 74-81.

Carminati, E., Enzi, S., and Camuffo, D. (2007). "A study on the effects of seismicity on subsidence in foreland basins: an application to the Venice area." *Global and Planetary Change*, 55(4), 237-250.

Clague, J. J., Naesgaard, E., and Sy, A. (1992). "Liquefaction features on the Fraser delta: evidence for prehistoric earthquakes?" *Canadian Journal of Earth Sciences*, 29(8), 1734-1745.

Clarke, B.G. (1995). *Pressuremeter in Geotechnical Design*. Blackie Academic and Professional, London, UK, 364p.

Cunha (1994). "Interpretation of selfboring pressuremeter tests in sand." *Ph.D. Thesis*, University of British Columbia, Vancouver, Canada, 279p.

Dalton, J. C. P., and Hawkins, P. G. (1982). "Fields of stress - some measurements of the in-situ stress in a meadow in the Cambridgeshire countryside." *Ground Engineering*, 15(4), 15-22.

Donath, A. (1891). "Untersuchengen über den Erddruck auf Stützwände." *Zeitschrift für Bauwesen.*, 41, 491-518.

Durgunoglu, H. T., and Mitchell, J. K. (1975). "Static penetration resistance of soils: I - Analysis, II – Evaluation of theory and implications for practice." *Proc., In Situ Measurement of Soil Properties*. ASCE, 151-189.

Dutton, C. E. (1889). "The Charleston earthquake of August 31, 1886." *U.S. Geological Survey Ninth Annual Report 1887-1888*, 203-528.

Egan, J. A., and Wang, Z. L. (1991). "Liquefaction related ground Deformation and effects on facilities at Treasure Island, San Francisco, during the 17 October 1989 Loma Prieta earthquake." *Proc., 3rd Japan-US Workshop on Earthquake Resistant Design of Lifeline Facilities and Countermeasures for Soil Liquefaction*, National Center for Earthquake Engineering Research, State University of New York at Buffalo, Buffalo, NY.

El-Sohby, M. A., and Andrawes, K. Z. (1973). "Experimental examination of sand anisotropy." *Proc., 8th Intl. Conf. on Soil Mechanics and Foundation Engineering*, Moscow, Russia, 6-11.

Esposito III, M. P., Andrus, R. D., and Camp III, W. M. (2014). "Ground freezing and sampling of a Pleistocene sand deposit near Charleston, South Carolina." *J. Geotech. Geoenvir. Engrg.*, 140(1), 185-193.

Fioravante, V., Jamiolkowski, M., and LoPresti, D. C. F. (1998). "Assessment of the coefficient of earth pressure at rest from shear wave velocity." *Géotechnique*, 48(5), 657–666.

Fourie, A. B., Hofmann, B. A., Mikula, R. J., Lord, E. R. F., and Robertson, P. K. (2001). "Partially saturated tailings sand below the phreatic level." *Géotechnique*, 51(7), 577-585.

Fuhriman, M. D. (1993). "Crosshole seismic tests at two Northern California sites affected by the 1989 Loma Prieta earthquake." *M.S. Thesis*, The University of Texas at Austin, Austin, TX.

Gao, Y., Wang, Y., and Su, J. (2013). "Mechanisms of aging-induced modulus changes in sand under isotropic and anisotropic loading." *J. Geotech. Geoenviron. Engrg.*, 139(3), 470-482.

Gardner, G. H. F., Wyllie, M. R. J., and Droschak, D. (1964). "Effects of pressure and fluid saturation on the attenuation of elastic waves in sands." *J. Petrol. Tec.*, 16(2), 189-198.

Geiger, A. (2010). "Liquefaction analysis of three Pleistocene sand deposits that did not liquefy during the 1886 Charleston, South Carolina earthquake based on shear wave velocity and penetration resistance." *M.S. Thesis*, Clemson University, Clemson, SC.

Geiger, A. J., Boller, R. C., Andrus, R. D., Heidari, T., Hayati, H., and Camp, W. M., III (2010). "Estimating liquefaction potential of a 200,000-year old sand deposit near Georgetown, South Carolina." *Proc., 5th Int. Conf. on Recent Advances in Geotech. Earthquake Eng. and Soil Dynamics*, San Diego, CA.

Grozic, J. L. H., Robertson, P. K., and Morgenstern, N. R. (2000). "Cyclic liquefaction of loose gassy sand." *Can. Geotech. J.*, 37(4), 843-856.

Guo, P. (2008). "Modified direct shear test for anisotropic strength of sand." *J. Geotech. Geoenvir. Engrg.*, 134(9), 1311-1318.

Handy, R. L., Remmes, B., Moldt, S., Lutenegger, A. J., and Trott, G. (1982). "In situ stress determination by Iowa stepped blade." *J. Geotech. Engrg. Div.*, 108(11), 1405-1422.

Hanna, A., and Ghaly, A. (1992). "Effects of K_0 and overconsoildation on uplift capacity." *J. Geotech. Engrg.*, 118(9), 1449-1469.

Hamouche, K. K., Leroueil, S., Roy, M., and Lutenegger, A. J. (1995). "In situ evaluation of K_0 in eastern Canada clays." *Can. Geotech. J.*, 32(4), 677-688.

Hardin, B. O. (1961). "Study of elastic wave propagation and damping in granular materials." *Ph.D. Dissertation*, University of Florida, FL, 207p.

Hardin, B. O., and Black, W. L. (1966). "Sand stiffness under various triaxial stresses." *J. Soil Mech. and Found. Div.*, 92(2), 27-43.

Hardin, B. O., and Drnevich, V. P. (1972). "Shear modulus and damping in soils: measurement and parameter effects." *J. Soil Mech. and Found. Div.*, 98(6), 603-642.

Hardin, B. O., and Richart Jr, F. E. (1963). "Elastic wave velocities in granular soils." *J. Soil Mech. and Found. Div.*, 89(1), 33-65.

Hatanaka, M., and Masuda, T. (2008). "Experimental study on the relationship between degree of saturation and P-wave velocity in sandy soils." *Proc., 2nd Intl. Conf. on Geotech. Engrg. for Disaster Mitigation and Rehabilitation*, held in Nanjing,

China, May 30 -June 2, H. Liu, A. Deng and J. Chu (eds.), Science Press, Beijing, and Springer-Verlag GmbH, Berlin, Heidelberg, 346-351.

Hayati, H., and Andrus, R. D. (2008). "Liquefaction potential map of Charleston, South Carolina based on the 1886 earthquake." *J. Geotech. Geoenvir. Eng.*, 134(6), 815-828.

Hayati, H. (2009). "Characterizing liquefaction resistance of aged sand deposits." *Ph.D. Dissertation*, Clemson University, Clemson, SC.

Heidari, T., and Andrus, R. D. (2012). "Liquefaction potential assessment of Pleistocene beach sands near Charleston, South Carolina." *J. Geotech. and Geoenvir. Engrg.*, 138(10), 1196-1208.

Holzer, T. L., and Bennett, M. J. (2003). "Unsaturation beneath a water table." *Envir. and Engrg. Geoscience*, 9(4), 379-385.

Hossain, M. A. (2010). "Correcting liquefaction resistance of partially saturated soil using compression wave velocity." *M.S. Thesis*, Clemson University, Clemson, SC.

Hossain, A. M., Andrus, R. D., and Camp, W. M., III (2013). "Correcting liquefaction resistance of unsaturated soil using wave velocity." *J. Geotech. and Geoenvir. Engrg.*, 139(2), 277-287.

Hossain, A. M., Geiger. A. J., Andrus, R. D., Hayati, H., Aboye, S. A., Esposito M. P. III, and Heidari, T. (2014). "In Situ Seismic Crosshole Testing of Six Natural Sand Deposits in the South Carolina Coastal Plain." *Proc., 2014 Geo-Congress: Geo-*

characterization and Modelling for Sustainability, ASCE, Atlanta, GA, February 23-26, 1142-1156.

Hu, K., Gassman, S. L., and Talwani, P. (2002). "In-situ properties of soils at paleoliquefaction sites in the South Carolina Coastal Plain." *Seismological Research Letters*, 73(6), 964-978.

Hu, M., O'Sullivan, C., Jardine, R. R., and Jiang, M. (2010). "Stress-induced anisotropy in sand under cyclic loading." *Granular Matter*, 12(5), 469-476.

Hughes, J. M. O., Wroth, C. P., and Windle, D. (1977). "Pressuremeter tests in sands." *Géotechnique*, 27(4), 455-477.

Ishibashi, I., and Sherif, M. A. (1974). "Soil liquefaction by torsional simple shear device." *J. Geotech. Engrg. Div.*, 100(8), 871-888.

Ishihara, K., Hung, Y., and Tsuchiya, H. (1998). "Liquefaction resistance of nearly saturated sand as correlated with longitudinal velocity." *Poromechanics*, Balkema, Rotterdam, Netherlands, 583-586.

Ishihara, K., Iwamoto S., Yasuda S., and Takatsu H. (1977). "Liquefaction of anisotropically consolidated sand." *Proc., 9th Int. Conf. on Soil Mechanics and Foundation Engineering*, Vol. 2, 261-264.

Ishihara, K., and Takatsu, H. (1979). "Effects of overconsolidation and K_0 conditions on the liquefaction characteristics of sands." *Soil Found.*, 19(4), 59-68.

Ishihara, K., Tsuchiya, H., Huang, Y., and Kamada, K. (2001). ''Recent studies on liquefaction resistance of sand: effect of saturation.'' *Proc., 4th Int. Conf. on Recent Advances in Geotech. Earthquake Engrg. and Soil Dynamics*, held in San

Diego, CA, March 26-31, S. Prakash (ed.), Missouri Univ. of Science and Technology, Rolla, MO.

Ishihara, K. (1985). "Stability of natural deposits during earthquakes." *Proc., 11th Int. Conf. on Soil Mechanics and Foundation Engineering*, Vol. 1, No. 1, 321-375.

Ishihara, K., Yamazaki, A., and Haga, K. (1985). "Liquefaction of K_0 consolidated sand under cyclic rotation of principal stress direction with lateral constraint." *Soil Found.*, 25(4), 63-74.

Iwasaki, T., Tatsuoka, F., and Takagi, Y. (1978). "Shear moduli of sands under cyclic torsional shear loading." *Soil Found.*, 18(1), 39-56.

Jaky, C. (1944). "The coefficient of earth pressure at-rest." *J. Soc. Hungarian Architects Eng.*, 78(22), 355-358.

Jamiolkowski, M. (1985). "New developments in field and laboratory testing of soils," *Proc., 11th Intl. Conf. on Soil Mechanics and Foundation Engineering*, San Francisco, Vol. 1, 57-153.

Juang, C. H., Jiang, T., and Andrus, R. D. (2002). "Assessing probability-based methods for liquefaction potential evaluations." *J. Geotech. and Geoenvir. Engrg.*, 128(7), 580-589.

Johansson, C. E. (1965). "Structural studies of sedimentary deposits." *Geol. Fören. Stockholm Forh.*, 87(1), 3-61.

Kjellman, W. (1936). "Report on an apparatus for consummate investigation of the mechanical properties of soils." *Proc., 1st Intl. Conf. on Soil Mechanics*, Graduate School of Engineering, Harvard University, Cambridge, MA, Vol. 2, 16-20.

Knox, D. P., Stokoe, K. H. II, and Copperman, S. E. (1982). "Effect of state of stress on velocity of low amplitude shear waves propagating along principal stress directions in dry sand." *Report No. GR 82-23*, University of Texas at Austin, Austin, TX.

Kokusho, T. (2000). "Correlation of pore-pressure B-value with P-wave velocity and Poisson's ratio for imperfectly saturated sand or gravel." *Soil Found.*, 40(4), 95-102.

Ku, T. and Mayne, P. (2013). "Evaluating the in situ lateral stress coefficient (K_0) of soils via paired shear wave velocity modes." *J. Geotech. Geoenviron. Eng.*, 139(5), 775-787.

Kulhawy, F. H., & Mayne, P. W. (1990). "*Manual on estimating soil properties for foundation design.*" *No. EPRI-EL-6800*, Electric Power Research Inst., Palo Alto, CA; Cornell University, Ithaca, NY.

Kuribayashi, E., Iwasaki, T., and Tatsuoka, F. (1975). "Effects of stress-strain conditions on dynamic properties of sands." *Proc. Jap. Soc. Civ. Engrgs*, No. 242, 105-114.

Lawrence Jr, F. V. (1965). "Ultrasonic shear wave velocities in sand and clay." *Research Rep. R65-05*. Massachusetts Institute of Technology, Cambridge, MA, 24p.

Lee, S. H., and Stokoe, K. H. II (1985). "Investigation of low amplitude shear wave velocity in anisotropic material." *Report No. GR 86-6*, University of Texas at Austin, Austin, TX.

Lee, N. J. (1993). "Experimental study of body wave velocities in sand under anisotropic conditions." *Ph.D. Dissertation*, University of Texas at Austin, Austin, TX.

Leon, E., Gassman, S. L., and Talwani, P. (2006). "Accounting for soil aging when assessing liquefaction potential." *J. Geotech. and Geoenvir. Eng.*, 132(3), 363-377.

Lewis, M. R., Arango. I., Kimball, J. K., and Ross, T. E. (1999). "Liquefaction resistance of old sand deposits." *Proc., 11th Panamerican Conf. on Soil Mech. and Geotech. Eng.*, Foz do Iguassu, Brazil, 821-829.

Lewis, M. R., McHood, M. D., and Arango, I. (2004). "Liquefaction evaluations at the Savannah River Site, a case history." *Proc., Fifth Int. Conf. on Case Histories in Geotechnical Engineering*, Paper No 3.21.

Lunne, T., and Mayne, P. W. (1998). "Offshore in-situ testing to determine horizontal stress." *NGI Rep. 521552-1*, Norwegian Geotechnical Institute, Oslo, Norway.

Mahmood, A., and Mitchell, J. K. (1974). "Fabric-property relationships in fine granular materials." *Clays and Clay minerals*, 22(5), 397-408.

Marchetti, S. (1980). "In situ tests by flat dilatometer." *J. Geotech. Engrg. Div.*, 106(3), 299-321.

Marchetti, S. (1985). "On the field determination of K_0 in sands." *Proc., 11th Intl. Conf. on Soil Mechanics and Foundation Engineering*, San Francisco, CA, 2667-2672.

Martin, J. R., and Clough, G. W. (1990). "Implications from a geotechnical investigation of liquefaction phenomena associated with seismic events in the Charleston, SC area." *Report to USGS Grant No. 14-08-001-G-1348*, Virginia Tech, Blacksburg, VA, 414 p.

Massarsch, K. R. (1975). “New method for measurement of lateral earth pressure in cohesive soils.” *Can. Geotech. J.*, 12(1), 142-146.

May, J. P. (1978). “Quaternary geology of Hobcaw Barony Georgetown, South Carolina.” *Report to the Belle W. Baruch Forest Science Institute*, The Citadel, Charleston, SC.

Mayne, P. W., and Kulhawy, F. H. (1982). “K_0-*OCR* relationships in soils.” *J. Geotech. Engrg. Div.*, 108(GT6), 851–872.

Mayne, P. W., and Kulhawy, F. H. (1990). “Direct and indirect measurements of in-situ K_0 in clays.” *Transportation Research Record 1278*, Transportation Research Board, Washington, DC, 141-149.

McCartan, L., Lemon, E. M., Jr., and Weems, R. E. (1984). “Geologic map of the area between Charleston and Orangeburg.” *Misc. Investigations Series Map I-1472, scale 1:250,000*, U.S. Geological Survey, Reston, VA.

Meegoda, N. J., and Arulanandan, K. (1986). “Electrical method of predicting in situ stress state of normally consolidated clays.” *Proc., Use of In Situ Tests in Geotechnical Engineering*, ASCE, 794-808.

Mesri, G., Feng, T. W., and Benak, J. M. (1990). "Postdensification penetration resistance of clean sands." *J. Geotech. Engrg.*, 116 (7), 1095-1115.

Mitchell, J. K., Frank, J. G., and Willem, C. B. (1978). “Fabric analysis of undisturbed sands from Niigata, Japan.” *Technical report No. S-78-11*, Univ. of California, Berkeley, CA.

Mitchell, J. K., and Solymar, Z. V. (1984). "Time-dependent strength gain in freshly deposited or densified sand." *J. Geotech. Engrg.*, 110(11), 1559-1576.

Mitchell, J. K., Lodge, A. L., Coutinho, R. Q., Kayen, R. E., Seed, R. B., Nishio, S., and Stokoe, K. H. II. (1994). "In situ test results from four Loma Prieta Earthquake liquefaction sites: SPT, CPT, DMT, and shear wave velocity." *Rep. UCB/EERC-94/04*, Earthquake Engrg. Res. Ctr., Univ. of California, Berkeley, CA, 179p.

Mulilis, J. P., Seed, H. B., Chan, C. K., Mitchell, J. K., and Arulanandan, K. (1977). "Effects of sample preparation on sand liquefaction." *J. Geotech. Engrg. Div.*, 103(2), 91-108.

Miyamori, K. (1976). "Shear strength and deformation characteristics of sand under three dimensional stress condition." *J. Japanese Soc. Civil Engineers*, 225, 81-91.

Nakazawa, H., Ishihara, K., Tsukamoto, Y., and Kamata, T. (2004). "Case studies on evaluation of liquefaction resistance of imperfectly saturated soil deposits." *Proc., Intl. Conf. on Cyclic Behavior of Soils and Liquefaction Phenomena*, held in Bochum, Germany, Taylor & Francis Group, London, 295-304.

Nemat-Nasser, S., and Tobita, Y. (1982). "Influence of fabric on liquefaction and densification potential of cohesionless sand." *Mech. Mater.*, 1(1), 43-62.

NRC Committee on Earthquake Engineering (1985). *Liquefaction of soils during earthquakes*, National Research Council, National Academy Press, Washington, DC.

Obermeier, S. F., Jacobson, R. B., Powars, D. S., Weems, R. E., Hallbick, D. C., Gohn, G. S., and Markewich, H. W. (1986). "Holocene and late Pleistocene earthquake-

induced sand blows in coastal South Carolina." *Proc., 3rd U.S. National Conf. on Earthquake Eng.*, 197-208.

Obermeier, S. F., Weems, R. E., Jacobson, R. B. (1987). "Earthquake-induced liquefaction features in the coastal South Carolina region." *U.S. Geological Survey Open-File-Report 87-504*, 17 p.

Oda, M. (1972a). "Initial fabrics and their relations to mechanical properties of granular material." *Soil Found.*, 12(1), 17-36.

Oda, M. (1972b). "The mechanism of fabric changes during compressional deformation of sand." *Soil Found.*, 12(2), 1-18.

Oda, M., and Koishikawa, I. (1977). "Anisotropic fabric of sands." *Proc., 9th Int. Conf. on Soil Mechanics and Foundation Engineering*, Japanese Geotechnical Society, Tokyo, Japan,Vol. 1, 235–38.

Oda, M., Nemat-Nasser, S., and Konishi, J. (1985). "Stress-induced anisotropy in granular masses." *Soil Found.*, 25(3), 85-97.

Okamura, M., and Soga, Y. (2006). "Effects of pore fluid compressibility on liquefaction resistance of partially saturated sand." *Soil Found.*, 46(5), 695-700.

Okamura, M., Ishihara, M., and Tamura, K. (2006). "Degree of saturation and liquefaction resistances of sand improved with sand compaction pile." *J. Geotech. and Geoenvir. Engrg.*, 132(2), 258-264.

Olson, S. M., Obermeier, S. F., and Stark, T. D. (2001). "Interpretation of penetration resistance for back-analysis at sites of previous liquefaction." *Seismological Research Letters*, 72(1), 46-59.

Owens, J. P. (1989). “Geologic map of the Cape Fear region, Florence $1^{\circ} \times 2^{\circ}$ quadrangle and northern half of the Georgetown $1^{\circ} \times 2^{\circ}$ quadrangle, North Carolina and South Carolina.” *Misc. Investigations Series I-1948-A, scale 1:250,000,* U.S. Geological Survey, Reston, VA.

Parkin, A. K., Gerrard, C. M., and Willoughby, D. R. (1968). “Discussion on deformation of sand in shear.” *J. Soil Mech. Found. Div.*, 94(1), 336-340.

Pass, D. G. (1994). “Soil characterization of the deep accelerometer site at Treasure Island, San Francisco, California.” *M.S. Thesis*, University of New Hampshire, Durham, NH.

Phillips, A. B., and May, P. H. (1967). “A form of anisotropy in granular media.” *Special Task Report*, Dept. of Civil and Municipal Engineering, Univ. College, London, UK.

Powell, J. J. M. (1990). “A comparison of four different pressuremeters and their methods of interpretation in a stiff heavily overconsolidated clay.” *Pressuremeters, Proc., ISP 3*, Telford, London, 287-298.

Ramamurthy, T. (1970). “A universal triaxial apparatus.” *J. Indian Nat. Soc. Soil Mech. Found. Engineering*, 9(3), 251–269.

Ricceri, G., and Simonini, P. (1998). “Geotechnical investigations to characterize the Upper Quaternary basin of Venice.” *Proc., 1st First International Conference on Site Characterization-ISC'98,* held in Atlanta, GA, April 19-22, 1229-1234.

Ricceri, G., Simonini, P., and Cola, S. (2002). "Applicability of piezocone and dilatometer to characterize the soils of the Venice Lagoon." *Geotechnical and Geological Engineering*, 20(2), 89-121.

Ridley, A. M., and Burland, J. B. (1993). "A new instrument for the measurement of soil moisture suction." *Géotechnique*, 43(2), 321–324.

Roesler, S. (1979). "Anisotropic shear modulus due to stress anisotropy." *J. Geotech. Engrg. Div.*, 105(GT7), 871–880.

Robertson, P. K., Campanella, R. G., Gillespie, D., and Greig, J. (1986). "Use of piezometer cone data." *Proc., Use of In Situ Tests in Geotechnical Engineering.*, ASCE, 1263-1280.

Robertson, P. K., and Wride, C. E. (1998). "Evaluating cyclic liquefaction potential using the cone penetration test." *Can. Geotech. J.*, 35(3), 442-459.

Robertson, P. K., Wride, C. E., List, B. R., Atukorala, U., Biggar, K. W., Byrne, P. M., Campanella, R. G., Cathro, D. C., Chan, D. H., Czajewski, K., Finn, W. D. L., Gu, W. H., Hammamji, Y., Hofmann, B. A., Howie, J. A., Hughes, J., Imrie, A. S., Konrad, J-M., Kupper, A., Law, K. T., Lord, E. R. F., Monahan, P. A., Morgenstern, N. R., Phillips, R., Piche, R., Plewes, H. D., Scott, D., Sego, D. C., Sobkowicz, J., Stewart, R. A., Watts, B. D., Woeller, D. J., Youd, T. L., Zavodni, Z. (2000). "The CANLEX project: Summary and conclusions." *Can. Geotech. J.*, 37(3), 563-591.

Salgado, R., Boulanger, R. W., and Mitchell, J. K. (1997). "Lateral stress effects on CPT liquefaction resistance correlations." *J. Geotech. and Geoenvir. Engrg.*, 123(8), 726-735.

Santamarina, J. C., and Cho, G. C. (2004). "Soil behavior: the role of particle shape." *Proc., Advances in Geotechnical Egineering: The Skempton Conference*, R. J. Jardine, D. M. Potts, and K. G. Higgins (eds.), Thomas Telford, London, UK, Vol. 1, 604-617.

Schmertmann, J. H. (1975). "Measurement of in situ shear strength." *Proc., In Situ Measurement of Soil Properties*, ASCE, 57-138.

Schmertman, J. H. (1978). "Guidelines for cone penetration test performance and design." *Rep. No. FHWA-TS-78-209*, Federal Highway Administration, Washington, DC.

Schmertmann, J. (1991). "The mechanical aging of soils." *J. Geotech. Engrg.*, 117(9), 1288-1330.

Seed, H. B. (1979). "Soil liquefaction and cyclic mobility evaluation for level ground during earthquakes." *J. Geotech. Engrg.*, 97(9), 201-255.

Seed, H. B., and Idriss, I. M. (1971). "Simplified procedure for evaluating soil liquefaction potential." *J. Geotech. Engrg. Div.*, ASCE, 97(9): 1249-1273.

Seed, H. B., Tokimatsu, K., Harder, L. F., Chung, R. M. (1984). "The influence of SPT procedures in soil liquefaction resistance evaluations." *Earthquake Engineering Research Center Report No. UCB/EERC-84/15*, Univ. of California at Berkeley, CA.

Seid-Karbasi, M. S., and Byrne, P. M. (2006). “Effects of partial saturation on liquefiable ground response.” *Proc., GeoCongress 2006: Geotechnical Engrg. in the Information Technology Age,* held in Atlanta, GA, February 26 - March 2, D. J. DeGroot, J. T. DeJong, D. Frost, and L. G. Baise, (eds.), ASCE, Reston, VA, Paper No. 11803.

Sherif, M. A., Ishibasi, I., and Tsuchiya, C. (1977). “Saturation effects on initial soil liquefaction.” *J. Geotech. Engrg. Div.*, ASCE, 103(GT8), 914-917.

Skempton, A. W. (1954). “The pore-pressure coefficients A and B.” *Géotechnique*, 4(4), 143-147.

Skempton, A. W. (1986). “Standard penetration test procedures and the effects in sands of overburden pressure, relative density, particle size, aging and overconsolidation.” *Géotechnique*, 36(3), 425-447.

Silva, W., Wong, I., Siegel, T., Gregor, N., Darragh, R., and Lee, R. (2003). “Ground motion and liquefaction simulation of the 1886 Charleston, South Carolina, earthquake.” *Bull. Seism. Soc. Am.*, 93(6), 2717-2736.

Sowers, G. F., and Hedges, C. S. (1966). "Dynamic cone for shallow in-situ penetration testing.", *5th Pacific Area National Meeting, ASTM Special Technical Publication No. 399*, American Society for Testing and Materials, 29-38.

Stokoe, K. H., Lee, S. H. H., and Knox, D. P. (1985). “Shear moduli under true triaxial stresses.” *Advances in the art of testing soil under cyclic conditions*, ASCE, Reston, VA, 166-185.

Stokoe, K. H., and Ni, S. H. (1985). "Effects of stress state and strain amplitude on shear modulus of dry sand." *Proc. Second Symp. on the Interaction of Non-Nuclear Munitions with Structures*, held in Panama City Beach, FL, 407-412.

Sully, J. P. (1991). "Measurement of in-situ lateral stress during full displacement penetration tests." *Ph.D. thesis*, Univ. of British Columbia, Vancouver, Canada.

Sully, J. P., and Campanella, R. G. (1990). "Measurement of lateral stress in cohesive soils by full-displacement in-situ test methods." *Transportation Research Record 1278*, National Research Council, Washington, DC, 164-171.

Sully, J. P., and Campanella, R. G. (1995). "Evaluation of in-situ anisotropy from crosshole and downhole shear wave velocity measurements." *Géotechnique*, 45(2), 267-282.

Talwani, P., and Schaeffer, W. T. (2001). "Recurrence rates of large earthquakes in the South Carolina Coastal Plain based on paleoliquefaction data." *J. of Geophysical Research: Solid Earth*, 106 (B4), 6621-6642.

Tanaka, H., and Tanaka, M. (1998). "Characterization of sandy soils using CPT and DMT." *Soil Found.*, 38(3), 55-66.

Tatsuoka, F., Iwasaki, T., Fukushima, S., and Sudo, H. (1979). "Stress conditions and stress histories affecting shear modulus and damping of sand under cyclic loading." *Soil Found.*, 19(2), 29-43.

Tavenas, F. A., Blanchette, G., Leroueil, S., Roy, M., and Rochelle, P. L. (1975). "Difficulties in the in situ determination of K_0 in soft sensitive clays." *Proc., In Situ Measurement of Soil Properties*, ASCE, 450-476.

Tedd, P., and Charles, J. A. (1983). "Evaluation of push-in pressure cell results in stiff clay." *Proc., Int. Symp. on Soil and Rock Investigation by in-situ Testing*, Vol. 2, 579-584.

Thomann, T. G. (1990). "Stiffness and strength changes in cohesionless soils due to stress history and dynamic disturbance." *Ph.D. Dissertation*, The University of Michigan, Ann Arbor, MI.

Thormann, G., and Hryciw, R. D. (1990). "Laboratory measurements of small strain shear modulus under K_0 conditions." *Geotech. Testing J.*, 2, 97-105.

Tong, L., Liu, L., Cai, G., and Du, G. (2013). "Assessing the coefficient of the earth pressure at rest from shear wave velocity and electrical resistivity measurements." *Engrg. Geol.*, 163, 122-131.

Troncoso, J., Ishihara, K., and Verdugo, R. (1988). "Aging effects on cyclic shear strength of tailing materials." *Proc., 9th World Conf. on Earthquake Engineering*, Vol. III, 121-126.

Tsukamoto, Y., Ishihara, K., Nakazawa, H., Kamada, K., and Huang, Y. (2002). "Resistance of partly saturated sand to liquefaction with references to longitudinal and shear wave velocities." *Soil Found.*, 42 (6): 93-104.

Uchida, K., Sawada, T., and Hasegawa, T. (1980). "Dynamic properties of sand subjected to initial shear stress." *Proc. Int. Symp. on Soils under Cyclic and Transient Loading*, Swansea, UK, Vol. 1, 121-133.

Weems, R. E., Obermeier, S. F., Pavich, M. J., Gohn, G. S., Rubin, M., Phipps, R. L., and Jacobson, R. B. (1986). "Evidence for three moderate to large prehistoric

Holocene earthquakes near Charleston, SC." *Proc., 3rd U.S. National Conf. on Earthquake Eng., EERI*, Vol. 1, 3-13.

Weems, R. E., and Lemon, E. M. Jr., (1993). "Geology of the Cainhoy, Charleston, Fort Moultrie, and North Charleston Quadrangles, Charleston and Berkley Counties, South Carolina," *USGS Misc. Investigation Map I- 1935, scale 1:24,000*, Department of the Interior, U.S. Geological Survey, Reston, VA.

Willaimson, J. R. (2013). "Liquefaction potential of South Carolina Coastal Plain soils using dilatometer data." *M.S. Thesis*, University of South Carolina, Columbia, SC.

Williamson, J. R., and Gassman, S. L. (2014). "Identification of liquefiable coastal plain soils using DMT, SPT, and CPT Profiles." *Proc., 2014 Geo-Congress: Geo-characterization and Modelling for Sustainability*, ASCE, Atlanta, GA, February 23-26, 2112-2121.

Wong, R. K. S., and Arthur, J. R. F. (1985). "Induced and inherent anisotropy in sand." *Géotechnique*, 35(4), 471-481.

Wride, C. E., Robertson, P. K., Biggar, K. W., Campanella, R. G., Hofmann, B. A., Hughes, J. M. O., Küpper, A., and Woeller D. J. (2000). "Interpretation of in situ test results from the CANLEX sites." *Can. Geotech. J.*, 37(3), 505-529.

Wroth, C. P., and Hughes, J. M. O. (1973). "An instrument for the in situ measurement of the properties of soft clay." *Proc, 7th Int. Conf. on SMFE*, Vol. 1, 487-494.

Yan, L., and Byrne, P. M. (1990). "Simulation of downhole and crosshole seismic tests on sand using the hydraulic gradient similitude method." *Can. Geotech. J.*, 27(4), 441-460.

Yamashita, K., and Toki, S. (1993). "Effects of fabric anisotropy of sand on cyclic undrained triaxial and torsional strengths." *Soil Found.*, 33(3), 92-104.

Yamashita, S., Hori, T. and Suzuki, T. (2005). "Effects of initial and induced anisotropy on initial stiffness of sand by triaxial and bender elements test." *Geomechnics, Testing, Modeling, and Simulation*, Yamamuro J. A., and Koseki, J. (eds.), ASCE, GSP No.143, 350-369.

Yoshimi, Y., Tanaka., K., and Tokimatsu., K. (1989). "Liquefaction resistance of a partially saturated sand." *Soil Found.*, 29(2), 157-162.

Youd, T. L., et al. (2001). "Liquefaction resistance of soils: summary report from the 1996 NCEER and 1998 NCEER/NSF workshops on evaluation of liquefaction resistance of soils." *J. Geotech. Geoenvir. Eng.*, 127(10): 817-833.

Youd, T. L., and Perkins, D. M. (1978). "Mapping of liquefaction induced ground failure potential." *J. Geotech. Engrg. Div.*, 104(4), 433-446.

Yu, P., and Richart, F. E., Jr. (1984). "Stress ratio effects on shear modulus of dry sands." *J. Geotech. Engrg.*, 110(3), 331-345.

Yu, H., Zeng, X., Li, B., and Ming, H. (2013). "Effect of Fabric Anisotropy on Liquefaction of Sand." *J. Geotech. Geoenviron. Engrg*., 139(5), 765-774.

Zeng, X., and Ni, B. (1999). "Stress-induced anisotropic G_{max} of sands and its measurement." *J. Geotech. Geoenvir. Engrg.*, 125(9), 741-749.